Response to Gabor Vali's comments on "The Fifth International Workshop .... " by DeMott and Co-authors

We thank Dr. Vali for his comprehensive and insightful comments, and his understanding of the complexities of such workshops.

Broad comment [1]: While it is clear that no classification can reflect perfectly the variety of instruments used, it is worth thinking about how useful is the one applied in this paper. No doubt, the online vs. offline designation has its origin in common references to the instruments in that some can be deployed in the field as a self-standing unit, while the others have essential work done in the laboratory. Thus, 'field' vs. 'laboratory' instruments could also be applied. The current designation has disadvantages. It doesn't inform people unfamiliar with the details of what the essential difference is. Is it the operating principle of the devices? Is it aerosol flow through the device versus samples captured and processed? Portable versus fixed in not necessarily applicable, as a filter processing unit is no larger and difficult to transport as a CFD chamber. A drop freezer can be the smallest of all the devices. Also, field deployment of a device impacting a flow of aerosol on water drops would be an online instrument for which much of the RH discussion about CFD's would be irrelevant. So, while the offline/online distinction isn't all bad, perhaps "direct sampling" versus "post-processing" would be more meaningful. Another useful direction would be to focus on variable RH instruments versus those with liquid water. What characteristics is the most important? Tables 1 and 2 do a pretty good job in listing the main features of the various devices. But the titles of subsections 2.1 and 2.2, and the headings in the Tables could be improved by removing the hesitation in the designations and, preferably before 2.1, explain the reason for the classification. Dry versus wet in the table headings is not the best. My recommendation is to use 'direct sampling' versus 'post-processing' and define in the Introduction how these terms are applied. This is also appears to be the intention with lines 30-32 on page 7. These designations would allow the AIDA chamber to be in the group of instruments with clouds forming on the sampled aerosol, just like in the CFD's. Omit 'portable' as part of the definition. (Apologies for this rambling paragraph.)

Authors' response to Broad Comment [1]:

It was a most difficult decision, in considering how to separate the discussion pre-submission. However, the workshop was separated in a distinct manner that the discussion mimics. The samplers for offline immersion freezing measurements required the largest particle loadings and so sampled first each day. This sometimes included two separate fills of the APC. At the end of this period, online instruments would collect particles for a period from the APC, over a period that extended a couple of hours beyond the period of sampling for post-processing. Finally, an aerosol fill was done directly into the AIDA chamber and this accommodated the few of the post-processing samples for devices that did not desire quite as high particle loadings (e.g., FRIDGE-STD and DFPC), and then other online samplers that would sample from AIDA just prior to the AIDA expansion. The concentrations were never the same in the APC period and in AIDA. Importantly, the aerosol fill to the AIDA chamber was not always the same INP type used in the morning sampling period from the APC. This was a conscious (and deemed necessary) decision to accommodate the ability of all instruments to sample all aerosols, and for the direct sampling

instruments to be able to do so over a range of temperatures (e.g., only limited temperatures could be assessed by flow chambers in the two hours after the collections from the APC into liquid or onto filters were done, and before the AIDA expansion had to begin). We mention this here to preface our responses to later comments. Nevertheless, understanding this may help to explain a lot about how the paper is organized, and hence we have decided to add such discussion to the Methods section. We hope that this discussion helps all readers to understand why we use concentration comparisons in some plots and then revert to active fraction and/or active site density in later figures that include data from both APC and AIDA experiments.

As for the exact description of device types, field versus laboratory would not work, because some of the immersion freezing methods are being taken to field facilities for immediate processing, mitigating in some cases the need for freezing samples. Direct sampling versus post-processing is more or less what we intended as the meaning for online versus offline, so we accept Dr. Vali's suggestion on using this terminology.

Changes in manuscript re: Broad Comment [1]:

This discussion will appear as follows as the 4th paragraph in revised Section 2.3, with the new title, "*Generation of varied INP types and general study procedures*". We write, "*The daily protocol determined for aerosol generation and measurements is an aspect of these studies that bears strongly on the organization and discussion of results in this manuscript. Especially, sampling periods were organized to optimize the opportunities and conditions for all instruments to sample the variety of aerosols. Each day over the three-week workshop period typically began with fills of one INP type into the APC, and sampling of that aerosol into liquid and onto filters over a two-hour period for later assessment by the post-processing devices, as detailed below. This was followed by the direct samplers processing the same INP type from the APC over another two-hour period. This typically permitted direct measurement at a couple specific temperatures, with data at other temperatures being acquired on another day for the same INP type (from the APC or AIDA). Then, at midday, the AIDA chamber would be filled, typically with a different INP type than used in the morning APC experiments. Direct sampling from AIDA by the flow chambers would occur over a period of time just prior to the start of expansion cooling experiments. As well, collections onto filters or wafers used by the DFPC and FRIDGE device (standard method) would be made only from the AIDA aerosol fill on each day, since these methods required very short sampling times in order to limit particle loading. For example, the DFPC-ISAC filters were collected for periods of 10's of seconds. Other collections into liquid or onto filters for immersion freezing post-processing would not occur from the AIDA chamber prior to expansions. A consequence of these procedures is that we will find it convenient to present results on different bases when discussing sampling from the APC and from AIDA. While we might ideally wish to present all data on the same basis as measurements are reported for atmospheric sampling, as number concentrations, we choose to do so only for the APC experiment period that offers the opportunity for comparing the most measurement systems. We describe how that is done next. For AIDA sampling, we will display results as active fractions and ice active site density, which then allows integrating APC results along with AIDA results for the same INP types over the course of the workshop.*"

Additionally, we widely employ the terminology of direct sampling and post-processing for the different methods used. We introduce this in Section 2 with the statement, "*These categories are, firstly, instruments operating online or for direct processing of aerosol particles and, secondly, those utilizing collections of particles for subsequent offline or post-processing*." We also revise section headings, table titles, and consolidate the AIDA chamber description into the direct sampling category discussion in Section 2.1 and remove the original Section 2.3.

Broad comment [2]: I am somewhat reluctant to raise this issue, but this paper needs special scrutiny in this regard because it weighs heavily on the principal results of the paper. Screening of data to be included or excluded is perhaps the trickiest and most sensitive part of the paper. There is a sense of some censoring of the data throughout Section 2. Undoubtedly some judgements had to be made about data validity by some criteria. One can see the attempt to do this, and the authors certainly deserve to be given the credit of proper judgement. However, the first question that comes to mind when looking at the degree of agreement shown in the results is how much screening of the data was done? How many discrepant cases were excluded due to errors or uncertainties? In other words, how much subjectivity entered into the analysis. Some comments on this issue would help the readers gauge the value of the results.

Authors' response to Broad Comment [2]:

It is disconcerting to hear the word censoring raised in regard to judgements on instrument operation and data submission. While full participation was encouraged, even for groups doing such a thing for the first time, there was no requirement for individual groups to submit data for every case covered in this paper. In fact, there was no requirement to collect data in every case, and it is the case that some groups collected much more data than others. We have tried to be upfront about the fact that this workshop had both formal and informal parts, and this paper deals with the latter. Investigators who recognized a certain issue in a given experiment that was not part of the formal intercomparison (a separate paper) were free to remove the data pending their own investigations (some that are continuing). This was not a frequent occurrence. In at least one case, a temperature calibration issue was recognized by one team (M-AL) following the workshop, and all of their data were subsequently reanalyzed. The MIT SPIN group did not always extend RH scans to levels sufficient to express immersion freezing in all experiments during the informal workshop phase. Other groups chose to focus their efforts on the formal period of comparisons, and to use the other part of the workshop for development activities (PNNL-CIC). We do not wish to state all of these details in the paper. It should be clear by the volume of data shown in many of the figures that this allowance was not in any way an attempt to unify the data sets. The participation of different groups at different levels can also be recognized in the data table listing. We considered that if 15 measurements are used to demonstrate correspondence or not, that this is a reasonably sufficient examination.

Changes in manuscript re: Broad Comment [2]:

We re-emphasize at the end of the Introduction that this paper describes the informal component of FIN-02. We write, "*This paper is intended as an overview of the informal activities of the workshop while addressing the*

majority of these objectives. It is not intended to answer all of the goals and objectives that are better addressed in separate studies. It is not our intent to rigorously test the capabilities of different measurement systems, but rather to point to areas of success and areas for needed development or further research."

Broad comment [3]: It becomes gradually clear as one reads on in the paper, that the focus of the analyses was freezing nucleation, at least as much as it could be assumed to be the dominant mode of nucleation if sufficient supersaturation was achieved to ensure that INPs are in liquid droplets. Perhaps, I missed it, but if this is true, shouldn't it be clearly spelled out in the Introduction, and be part of the goals? Similarly, the size range covered (9/28-32) is a pre-defined constraint and would be best stated up front.

Authors' response to Broad Comment [3]:

We are thankful for this comment because it was not intended that this be a gradual realization. In the abstract, we had stated the different measurements with a focus on immersion freezing (modified here to account for the revised naming of the different methods: "The results presented here use data from the workshop to assess the comparability of immersion freezing measurement methods activating INPs in bulk suspensions, methods that activate INPs in condensation and/or immersion freezing modes as single particles on a substrate, continuous flow diffusion chambers (CFDCs) directly sampling and processing particles well above water saturation to maximize immersion and subsequent freezing of aerosol particles, and expansion cloud chamber simulations in which liquid cloud droplets were first activated on aerosol particles prior to freezing." In the first paragraph of the Methods section we state (again, slightly revised here in new form), "No measurements of contact freezing were included in this study, and neither will we discuss results herein from workshop measurements that were made in the regime associated with deposition nucleation (including at temperatures below the homogeneous freezing temperature or pure water droplets), but we will focus on inter-comparisons of particles acting via immersion freezing or proximal behaviors. By proximal behaviors, we follow the terminology of Vali et al. (2015),…" We simply could not pull all of the workshop studies into this overview paper, or it could have become unwieldy. We attempted to point out that the database remains for future papers by the participants, or inspection by any interested parties.

Changes in manuscript re: Broad Comment [3]:

In addition to the modest changes mentioned in our response above, we continue to add a direct statement at the end of the Introduction pointing out the emphasis decided for comparisons presented in this paper.

"For these reasons, and to include as many measurements as possible in comparisons, we focus primarily on measurements relevant to immersion freezing nucleation, as discussed further below. This allows for integrating the most possible measurements into comparisons made for assessing one important aspect of the state of the art of ice nucleation measurements."

Broad comment [4]: Unless I missed it, the promise made at 8/32 to describe the aerosol collection and transfer methods for testing as suspensions are missing from Section 2.4. Problems associated with the method used and the final efficiency of the capture are not found. See also 13/4-5.

Authors' response to Broad Comment [4]:

We thank Dr. Vali for pointing out that we indeed neglected to describe the details of particle collection into liquid.

Changes in manuscript re: Broad Comment [4]:

We have added this now to Section 2.3 (formerly 2.4). The segment below has been integrated into a revision of the overall discussion of experimental protocol for APC sampling. In doing so, some repetitive statements are now removed.

"Collection of particles into liquid suspensions for shared use by a suite of immersion freezing devices was performed by impinging a flow of particles from the APC into a glass bioaerosol sampler (SKC Inc.) (Hader et al., 2014; DeMott et al., 2017), referred to here as impinger samples. Two impinger samples were collected for ~120 min with a flow rate of 12.5 L min^{-1} from the APC. Flows were checked daily. Impingers were cleaned by wiping, rinsing with ultrapure water (18 MΩ-cm), and soaking in isopropyl alcohol overnight (2-propanol, ≥99.8%, ROTH). Before assembly the impingers were rinsed using ultrapure water once more. Following the sampling of Snomax® particles, the impingers were baked overnight at 200°C instead of soaking in alcohol. This was done to eliminate the possibility of carryover by ice active due to these biological samples. During sampling the water was replenished every ~30 minutes to keep the water level near 20 mL. Due to evaporation, the final bottled volume was typically about half of the added water. The two impinger suspensions were combined into one sample and topped off to a total of ~36 mL. The sample was divided into 4 ml aliquots, bottled in pre-cleaned DNA free cryovials and stored locally in a freezer at -20°C. The same procedure was applied to the handling of blanks. At the end of the campaign, blanks and samples were placed on dry ice and shipped overnight to participating groups. Shipment to Israel was delayed by customs, allowing the sample to thaw en-route. After receiving the sample, each group decided on their own sample storage and handling strategies. Again, we note that the University of Leeds group performed NIPI measurements of these suspensions on-site in Karlsruhe immediately after collection (i.e., without freezing)."

Broad comment [5]: Some re-phrasing of conclusions such as in lines 6 to 23 on page 13 should be considered. The degree of agreement in the data is remarkable and deserves to be celebrated. But to say that the agreement extends over 7 orders of magnitude over the whole temperature range is misleading. Except in the center of the temperature range only 4-5 data sets are represented. Thus, in a strict sense, the agreement among all data sets is not quantitative over the whole range. They all coincide in defining a common trend and agree in overlap regions. None of the data sets extend over the whole range. Also, there is a division of the types of instruments for which data are available at the upper and lower ends of the temperature regime. The main novelty in these results is the agreement between CFD type and drop freezing types of measurements in the overlap region. This is a real accomplishment and

demonstrates that the two types of measurements can be combined to yield atmospheric measurements over a wide temperature range. The extent to which that is a practical solution for low INP air samples is worth addressing.

Authors' response to Broad Comment [5]:

We have revised the statements accordingly, since indeed, the point was to show the meshing of results for this particular sample, as well as correspondence overall within groupings. We alter the 7 order of magnitude statement for this reason, to reflect the context of what direct overlap is captured.

Changes in manuscript re: Broad Comment [5]:

The paragraph now reads: "*The comparisons obtained for sampling Argentinian soil dust particles (Fig. 4) were among the best in this study. A striking feature of these results is the general correspondence between all methods and sampling techniques in ranges of overlap, as well as the apparent meshing of results from direct sampling and post-processing of immersion freezing to capture 7 or more orders of magnitude of INP activity in the temperature regime from -5 to -35°C. Direct overlap showing correspondence of the continuous flow methods with a minimum of four different bulk methods occurs over 3 orders of magnitude range at temperatures from -20 to -30°C. Good consistency is also seen amongst direct sampling methods as a group and post-processing methods taken together, for shared impinger samples, and whether post-processed samples were collected by impinger or separate polycarbonate filters (IS and FRIDGE-IMM) that were subsequently rinsed of particles. Recall that the IS filter was collected simultaneously with the impinger sample, while the FRIDGE-IMM filter was collected over a shorter time frame. The largest discrepancies, in consideration of measurement uncertainties (see Supplement for explanation of measurement uncertainties for each device) occur at the coldest temperatures. In this region, data from the PIMCA-PINC instrument, which activates individually-grown droplets on particles prior to cooling, falls at the upper end of measured INP concentrations in comparison to the few other immersion methods that extended to the heterogeneous ice nucleation limit, just warmer than homogeneous freezing temperatures. We note again here that some scatter may occur in the direct processing flow diffusion chambers due to investigators deciding in each case what RH_w above 100% to report data for as representing immersion freezing of the entire particle population.*"

Additionally, we have added a discussion point in the Conclusions on the issue of low INP sampling. This was mentioned in regard to the likely need to pre-concentration INPs for direct processing at >-20°C. This is also a prime topic of FIN-03 and its overview paper. We will not add the Conclusion revision here, as the entire new Conclusions are appended to the response to Reviewer 2.

Broad comment [6]: Only in S.2.1 is the method for calculations of the INP concentrations stated. How were the presented data derived for each device should be part of the description for each one. This also applies to how uncertainty ranges were determined.

Authors' response to Broad Comment [6]:

This comment was retracted in an updated note by the reviewer. As noted, this information is available in the extensive Supplemental material, repeating in most cases information that is already published.

Changes in manuscript re: Broad Comment [6]: None.

Broad comment [7]: A suggestion I make reluctantly, because of the amount of re-writing it implies, the authors should consider including a Discussion section, moving some material from Results there, and going a little further in some themes. Having a Discussion section would allow for better perspective on the various aspects of the results (e.g. 14/3-22), and give good opportunities for comparisons with previous publications (e.g. 18/2-28).

Authors' response to Broad Comment [7]:
We can see how this might work, and appreciate the suggestion. Nevertheless, we also believe that the flow of the paper, and the manner that the AIDA studies are used to continue the comparison of data and to then fold in APC results, favor the present structure. With the introduction of plots in n_s space, it is natural to add the parameterizations and discuss them in place. It would take major rewriting to extract discussion and have it stand alone in an organized manner. Expanded discussion may not have an advantage over a more concise description of results and reference to previous studies.

Changes in manuscript re: Broad Comment [7]: We have renamed the section as "Results and Discussion" and have chosen to expand the Summary and Conclusions.

Broad Comment [8]: Parts of the description of results refer to the sigmoid shapes and the central slopes of the INP vs. T curves. I mention here that similar considerations, and a definition for a slope parameter were given in Vali (ACP 14, 5171- 5194, 2014.). The rich material in this paper could very usefully add and expand on the analyses in that paper. That may go beyond the scope the authors set for this paper, but in reality it would not be a large step.

Authors' response to Broad Comment [8]:
We agree that such an exercise could be useful, but as a science focused and separate topic. However, we wish to limit the scope of this present paper to intercomparisons and issues that arose during this focused objective, in line with the previous comment.

Changes in manuscript re: Broad Comment [8]: None.

Broad Comment [9]: There are many references to the Supplement. It would be helpful if, in each case, the reference pointed to some specific part of the Supplement.

Authors' response to Broad Comment [9] and changes in manuscript re: Broad Comment [9]:
We have checked all references to the Supplement. Most of the references were already to specific sections of the supplement or to the tables. The rest were found to reference uncertainties, in which cases we have added the words "for each specific device". Each section describes the manner in which these were defined, and most of these are uniform.

Broad Comment [10]: It is regrettable that the ACP (3.1) and AIDA (3.2) sampling results are in different forms, i.e. per air volume and as site density. Was this unavoidable? Considered unimportant? It comes as a surprise to the reader. Having the two different aerosol processing paths provided some assurance of minimizing problems related to each one. Perhaps there were other operational advantages or limitations as well. Yet, one would have like to see the results in the same format. For inter-comparisons the two data sets provide additional support and that is the main goal of the Workshop. But it isn't clear why the results need to be given in different manner. More careful reading of the paper may reveal the reasons, but perhaps readers (like me) could be helped by a statement of those reasons up front.

Authors' response to Broad Comment [10]: This decision has been discussed in response to previous comments. We understand now that we needed to describe the manner of operations of the workshop that was jointly determined by the workshop leads in consult with participants. The operational protocol determined what we deem as the best means of comparing the different chamber results. It was not meant to leave unrevealed any particular thing about comparisons. Indeed, the decision made to show the AIDA results in terms of active fraction (identical in all respects to a number concentration intercomparison) and n_s was to permit explicit comparison of results from the two sampling periods for the same INP types (even though they were different aerosolization experiments, sometimes on different days). This led to the multi-panel figure comparing active fraction and n_s values from both the AIDA sampling and from the APC, using shading in one panel to underlay one type of data and hopefully not making the figures unreadable. We decided that nothing especially revealing would be lost by not repeating the active fraction plot in each example give in Figures 8 to 11. The timing of sampling largely drove this decision, already mentioned above. There was no way to sample the INP concentration by all samplers, including AIDA, for each aerosol generation experiment.

Changes in manuscript re: Broad Comment [10]: See response to Broad Comment [1]. We definitely want readers to be able to navigate the paper smoothly, so we have additionally added small statements in the Methods section and reminders in the Results section to assist understanding why different formats are used for APC and AIDA sampling results, and how these are brought together ultimately in the later figures.

Broad Comment [11]: The focus on measurements of atmospheric INPs in the recommendations on page 22 is well placed. But ice nucleation measurements are also needed for fundamental understanding of ice nucleation and of the nature of INPs. Another important direction that ice nucleation measurements should explore in future workshops is to perform tests with mono-disperse aerosols.

Authors' response to Broad Comment [11]:
We definitely agree. However, producing monodisperse aerosols for many investigators is yet another logistical challenge. Probably there will need to be a number of different and smaller workshop approaches with different teams.

Changes in manuscript re: Broad Comment [11]: Both recommended topics, and others are listed in an expanded Summary and Conclusions section, appended to the end of the response to Reviewer 2.

Specific items

Specific item 1. page/line 3/32: 'constrain' INP population???
Specific item 1 author response/manuscript change: Removed as superfluous.

Specific item 2. page/line 4/7: The fact that the more general aspects of the project are to be published later is a bit of a problem. A brief description of the three stages would help.
Specific item 2 author response: While we eliminated this material as a possible distraction, we add some words now about the different parts of FIN so that readers can understand the activity and the FIN-02 part of it. The overview article is in preparation.
Specific item 2 manuscript change: In the Introduction, we now add, *"Briefly, and distinct from most previous workshops in its comprehensive scope, FIN sought to perform comprehensive operational comparisons of ice nucleation instruments for sampling calibration type INPs (representative of different atmospheric classes) in a laboratory setting and for sampling ambient atmospheric aerosols in a natural setting. In addition, the component FIN-01 (first study in late 2014) sought to intercompare single particle mass spectrometer instruments that are sometimes used to assess the detailed chemical composition of INPs by sampling the residues of ice crystals nucleated in flow diffusion chambers or aerodynamically segregated from atmospheric clouds. FIN-01 tested these instruments for their determined reference mass spectra on some of the INPs also planned for use in comparing ice nucleation instruments, it compared the different clustering algorithms used by the aerosol mass spectral community, and it repeated testing on ice crystal residues. FIN-02, the workshop phase discussed herein, was the laboratory ice nucleation instrument intercomparison. FIN-03, the field phase, was conducted at Storm Peak Laboratory in Steamboat Springs, CO. A final aspect of both FIN-01 and FIN-02 was to provide a minor period within the overall informal gatherings for scientific study that would feature a formal intercomparison of measurements. FIN was a volunteer activity on the part of participants, who agreed to participate to their fullest extent in both the informal and formal components, but were also free to explore new developments. Referees were solicited for organizing and analyzing the results of formal comparisons in FIN-01 and FIN-02. These formal or so-called "blind" experiments were conducted to investigate the degree to which the informal results presented in papers such as this one could be independently reproduced."*

Specific item 3. Page/line 4/10-12: The order of these last two sentences of the paragraph should be reversed.

Specific item 3 author response/manuscript change: This section has been rewritten, as noted just above.

Specific item 4. *Page/line 4/22: What do you mean by 'align'?*

Specific item 4 author response/manuscript change: We meant "coordinate." Wording changed.

Specific item 5. Page/line 4/25-32: Goals are well defined. It would be nice if the conclusions responded clearly to each item.

Specific item 5 author response/manuscript change: We now explicitly focus our summary of results around the stated objectives in the new Summary and Conclusions section.

Specific item 6. Page/line 4/33: The intent to define a priori instrument characteristics is somewhat futile. Instruments that participated can be grouped as on-line and off-line but linking that too strongly to dry and wet is too much of a simplification. It would be more effective to describe the methods starting with Fig. 1 and then detail what the instruments do (above water saturation and immersion freezing) and do not do (deposition, condensation-freezing, contact). Indeed, reference to Vali et al, 2015 can help with the definitions.

Specific item 6 author response/manuscript change: The dry and wet designations have been used now in a number of prior published intercomparison studies. Nevertheless, we have refocused all discussion around direct and post-processed sampling systems. The noted sentence now reads, *"These categories are, firstly, instruments operating online or for direct processing of aerosol particles and, secondly, those utilizing collections of particles for subsequent offline or post-processing."* Additional small changes to the entire paragraph remove reference to wet and dry or online and offline, and clarifies what is measured in each case.

Specific item 7. Page/line 5/16: The operating principles are in in Tables 1. and 2 to some extent and are described in 2.1 and 2.2. The Supplement is to describe the detailed implementations of the basic idea in each device.

Specific item 7 author response/manuscript change: Wording is changed. The operating principles are already described in basic publications about most devices, so we attempted to reduce clutter. We write, *"Names, basic descriptions, and general operating principles are provided in Tables 1 and 2, and sections 2.1 and 2.2. Detailed implementations of the basic principles in each device are given in the Supplement sub-sections."*

Specific item 8. Fig. 1: The inclusion of X wt% designation here is unhelpful. The inclusion of this factor complicates interpretation. Indicated range may have been correct for the INPs chosen for test but have no general meaning. There are other materials that cover the whole temperature range with a single wt%. Adding the specific INP for which the graph is valid would add unnecessary detail. I suggest to leave those wt% indications off the graph. Of course, solute effects are ignored here.

Specific item 8 author response/manuscript change: We respectfully disagree, feeling that this point is useful for noting a fundamental difference in how the parameter space is covered by different instruments, even within the same general class. These values were indeed not intended to have a specific meaning except to indicate dilutions of samples to increase dynamic range, a general procedure that is needed for some sample types and droplet volumes. We write in the caption of Fig. 1, *"The blue arrow following the water saturation line in T-RH_w space shows the trajectory of subsequently diluted samples (generically and schematically referred to as X, 0.X an 0.0X weight percent suspensions) of collected aerosols measured by immersion freezing methods. Such dilution is required in many cases for the laboratory samples tested, but the need for dilution or not also depends on the droplet size/volume used."*

Specific item 9. Page/line 6/14: The definition of max RH_w practicable before 'breakthrough' is made difficult by the use of RH_w for many different aspects of the processes.

Specific item 9 author response/manuscript change: We have streamlined this discussion by removing so many references to water relative humidity. We write, *"When the temperature gradient in the growth section is adjusted to generate water supersaturated conditions that activate cloud droplets within the aerosol lamina, the lower relative humidity in the evaporation section shrinks droplets back toward haze particle sizes. This method works up to some high value of RH_w in the growth section whereupon activated cloud droplets survive through to detection, often referred to as the water droplet breakthrough RH_w. The breakthrough value varies with temperature, geometry and flow rate for different devices. Therefore, a single RH_w level in the growth region for breakthrough to occur is not noted in Fig. 1. Instead, results are stated as being associated with specific RH_w values (or % supersaturation values, which equal RH_w-100) that are simply a value that was lower than the droplet breakthrough condition. In some cases, this was the maximum RH_w achievable in the growth region prior to droplet breakthrough."*

Specific item 10. Page/line 6/18-20: Is this caveat not in conflict with the goals defined earlier? May be just say that experiments included in the evaluations all stayed below the breakthrough RH w.

Specific item 10 author response/manuscript change: This is a good suggestion, and one we implement. The sentence is eliminated in preference to the rewrite of the sentences in the comment above.

Specific item 11. Page/line 6/31-33: This sentence should start the paragraph to explain why the choice of 102% needs discussion.

Specific item 11 author response/manuscript change: There was no intention of focusing on 102%, as it was simply put out that as a value that one might not expect to be relevant in the atmosphere. It is relevant for CFDCs. We have removed this sentenced and reorganized/rewritten this paragraph. It was too wordy and somewhat repetitive. This entire paragraph now reads, *"The focus on reporting of flow chamber data at highly supersaturated conditions as best representing proximal immersion freezing behaviors is motivated by recent research and publications. Presently, continuous flow diffusion chamber instruments in general do not expose particles to uniform water supersaturations with the precision achieved by cloud condensation nuclei (CCN) instruments. Rather, the*

transition into the immersion freezing regime above water saturation does not occur sharply in line with the supersaturation calculated for the aerosol central lamina, but ensues completely only at higher RH_w as controlled by aerosol particle properties and instrument characteristics. For example, hygroscopicity and kinetic factors control water uptake, chambers have different flow rates and growth section lengths, there is a finite difference in RH_w across the aerosol lamina, and many devices appear (for as yet unclear reasons) often to induce a proportion of all particles to escape the defined aerosol lamina and expose these particles to lower RH_w outside of the intended central lamina (DeMott et al., 2015; Garimella et al., 2017). Hence, higher RH_w is used in these instruments to bypass limitations in achieving CCN activation on the entire particle population, and to increase the condensation rate and thus water content of the formed droplets. The justification is to make the measurement conditions (most particles placed in cloud droplets larger than a few μm prior to freezing) more similar to the cloud parcel simulations in the AIDA cloud chamber (see next section) with more typical cloud supersaturations and time scales. In practice, continuous flow instruments processed dry particle samples by slowly "scanning" RH_w from near ice saturation conditions to water supersaturated conditions (see DeMott et al., 2011 for discussion of these methods, and the Supplement Section S.1.2 for a few examples. Investigators were then asked to select those data they felt represented the highest (not necessarily maximum) immersion freezing activity possible to assess in their RH_w scans, and reported the INP concentrations and RH_w values selected."

Specific item 12. Page/line 6/37-7/1: This is problematic. How is this known? The fraction of aerosol activated as a measure of the RH achieved in an instrument? The nominal RH and actual volume-weighted one differ, as just described in earlier part of the paragraph.

Specific item 12 author response/manuscript change: We believe that the point may have been misunderstood. It was poorly stated. The point is that the instrument lamina RH cannot be interpreted as the exposure RH. As pointed out, this was somewhat repetitive, and so the paragraph has been rewritten. See above.

Specific item 13. Page/line 7/3-7/5: Recommendation here is out of place and heavy-handed.

Specific item 13 author response/manuscript change: We have removed this. It is a clear need for the field, but out of place for this section.

Specific item 14. Page/line 7/7: Shouldn't this 'primary comparison' be defined as a 'goal' up front?

Specific item 14 author response/manuscript change: We believe this was mentioned upfront, and only wish here to point out that additional data are available.

Specific item 15. Page/line 7/11: Quite unclear. Highest vs. maximum. Could the question be said to have been to select the RH point in the scans that the operators thought was most representative for freezing nucleation? Again, this objective should be stated before discussing details of RH variations in the instruments. All those variations are caveats on the validity of the values chosen/used for the comparisons. In any case, isn't it likely that the activated

INP were in drops, due to the high hygroscopicity of the aerosol? In that case, the INP's don't experience 102% or whatever supersaturation. Clearly, these considerations need to be addressed here.

Specific item 15 author response/manuscript change: All of the INPs are not in the drops in CFDCs up to some RH that exceeds the expectation, and that is the point of the discussion, that every group operating such instruments has noted this. The suggestion is well taken though, and this section has been rewritten, as noted above (specific item 11 response).

Specific item 16. Page/line 8/5: Is this because only ice crystals forming from frozen droplets on the surface are counted? How certain is that? Same issue as in previous point.

Specific item 16 author response/manuscript change: We are not sure that we fully understood this comment, but hopefully some added words and reorganized discussion help here. We were only remarking that data will be included from the substrate-based diffusion chambers up to reported values of 101-102% RH with respect to water, but acknowledging that the equivalence of INP response to immersion freezing remains under evaluation, especially as this may depend on particle loading. We did not wish to gloss over this issue, only to limit extensive discussion of it when we are referring to two particular instruments. We have added overall to this discussion, including some past references, at least ones that reference the substantial literature on this topic, as note by the reviewer. See next comment.

Specific item 17. Page/line 8/7: " ... limits reduction of ..." is unclear. The influence of vapor competition, and its dependence on INP density on the substrate has extensive literature, and perhaps should not be glossed over so easily. The operational definition used here for making the comparisons deserves more explanation. The concluding sentence on 8/13-15 is unclear - do you mean cases when vapor competition was only inferred to have been present but not evaluated?

Specific item 17 author response/manuscript change: Upon review, only one of the submitted cases was removed from consideration by the DFPC group, and this related to potential heating (of the paraffin) impacts on Snomax activation, still under investigation. Hence, we have revised this section to emphasize matter-of-fact discussion of the two devices, and to mention that we are including them in this intercomparison of immersion freezing despite a continuing need to evaluate their ability to represent immersion freezing. We write, *"The thermodynamic path of measurements using these instruments is the same as for the continuous flow diffusion chambers in Fig. 1 (red lines), but typically terminate 1-2% RH_w above water saturation. Both devices were designed with the intention to overcome the so-called "volume effect" on freezing (e.g., Bigg, 1990; Schrod et al., 2016 and references therein) which describes the underestimation of INPs that can occur when processing particles on a substrate in a diffusion chamber due to vapor pressure reduction by the first particles freezing, especially when larger volumes are collected that result in larger numbers of INPs per surface area of the substrate. The FRIDGE instrument seeks to limit this effect using a low-pressure diffusion chamber to enhance vapor deposition over particles collected onto silicon wafer substrates, while the DFPC instrument follows the methods of Langer and Rodgers (1975) to focus a flow of humid air over filter substrates, and using the best practices outlined by Bigg (1990). For both devices,*

attempts were made to limit particle collections to shorter times during FIN-02, in order to keep particle loading light on the substrates. An additional fundamental difference between FRIDGE and the DFPC is the use of the filter substrate in the latter case, which is placed on a paraffin layer that is heated to establish thermal contact with a cold plate prior to ice nucleation measurements. The uncertain difference between condensation freezing and immersion freezing mechanisms (Vali et al., 2015) argues for an evaluation of results obtained near water saturation in this intercomparison as representative of proximal immersion freezing, for both instruments."

Specific item 18. Page/line 8/8: '...were allowed to ..' inserts a hierarchical tone that is unnecessary. An objective tone would be more appropriate. The working arrangements of the workshop are not of interest to the reader. Else, make it clear and explain in the Introduction that there was some sort of checks and balances arrangement in order to improve the final result. I don't know if there was or not. See also comment on 7/3-5.

Specific item 18 author response/manuscript change: We have attempted to remove any hierarchical tone, and revise as noted above. Again, this was the informal component of the workshop, and the intent was to offer the best chances to compare instruments on a fair basis. We included as much of the data as was possible, and truly tried to limit and omissions.

Specific item 19. Page/line 8/14: "wet suspension" -- ?? wouldn't liquid suspension or water suspension be more direct? Actually, the first two words could well be omitted and the sentence say "Measurements of immersion freezing ...."

Specific item 19 author response/manuscript change: The latter suggestion would ignore that immersion freezing describes a process and not a stock measurement method, in our opinion. We here use *"immersion freezing measurements of collected particles suspended in water."* In other cases, we take the tip to simplify to *"water suspension*".

Specific item 20. Page/line 8/31: " ... wet suspension groups ...? -- one can deduce what is meant but it could be said better

Specific item 20 author response/manuscript change: We have revised simply *to "Most groups using liquid suspension freezing methods shared common samples…"*

Specific item 21. Page/line 9/1: "... basic methods ... " may need to be re-considered if changes are made in response to the first item in this review.

Specific item 21 author response/manuscript change: Done, as mentioned above.

Specific item 22. *Page/line 9/29: suggest leaving out the word 'mode'*

Specific item 22 author response/manuscript change: Done.

Specific item 23. Page/line 10/3: suggest replacing 'wet dispersion of particles' by something like "aerosol generation from aqueous suspensions" or "particle dispersion from aqueous suspensions" or "dispersion of particles via spraying and drying"

Specific item 23 author response/manuscript change: We use, *"Aerosol generation from aqueous suspensions..."*

Specific item 24. Page/line 10/32: Was the depletion of aerosol in the APC by sample withdrawal avoided or neglected? Also, how justified was it to assume the decrease in concentration to be valid for all sizes?

Specific item 24 author response/manuscript change: Depletion of aerosol by sample withdrawal was in fact the primary mechanism for reduction in concentrations. The fits encapsulate this primary mechanism and wall losses. Brownian diffusional losses to the walls was of course limited due to particle mode size being typically a few to several tenths of a micron in diameter. Hence, particle sizes were in the range where large differences in reductions as a function of size over time were not expected. This was a reason for showing a figure to include two different size ranges. We found that using total particle numbers versus using the concentration of particles > 0.5 μm led to no more than a 30% difference in the fractional losses of particles over time during the initial fills with higher total aerosols. This is evident in Fig. 3. During the time period of direct particle sampling, the particle losses losing the same size ranges differed by no more than 10%, also evident in the figure. Hence, we assume a similar range of uncertainties on correction factors to bring the direct sampler INP concentrations into line with the period of sampling by post-processing devices. We have added statements in these regards. *"These loss processes were dominated by the drawing of air from the APC by samplers, replenished in all cases by clean synthetic air. Curves are shown for total particle numbers, numbers of particles larger than 0.5 μm, and total particle surface area (spherical equivalency assumed for measured particle diameters). By integrating the exponential fit functions during sampling periods (blue shading), the integrated number concentrations and surface areas were determined for the combination of sample periods for post-processing. While we focus in the following discussion on quantifying the decay of total (CPC) particle numbers in order to correct INP number concentration data during the direct sampling periods ("online" used as shorthand in equations) for equivalency with the prior post-processing collection periods ("offline" used as shorthand in equations), we noted (not shown) differences ranging from only 10-30% in fractional loss rates when instead using particle numbers in the larger size range (>500 nm) to characterize particle number decay over time in the APC. These relatively minor differences, evident in Fig. 3, are consistent with the limited physical loss mechanisms existing for particles with mode sizes as shown in Fig. 2, and with limited numbers of supermicron particles that might be subject to sedimentation."*

Specific item 25. Page/line 12/30: perhaps the intention was to put the words 'basis for" in the sentence, to read : .... primary basis for the comparison of ...

Specific item 25 author response/manuscript change: Done.

Specific item 26. Page/line 12/31: replace 'most' by 'largest number' ??

Specific item 26 author response/manuscript change: Done

Specific item 27. Page/line 13/18-20: The sentence is somewhat garbled.

Specific item 27 author response/manuscript change: Given the extended earlier discussion, we have removed some discussion here and have revised this sentence to read, *"We note again here that some scatter may occur in the direct processing flow diffusion chambers due to investigators deciding in each case what RH_w above 100% to report data for as representing immersion freezing of the entire particle population."* We may note to the reviewer that this topic will be featured within the referee paper on the formal workshop component of FIN-02.

Specific item 28. Page/line 14/3-22: These comments would be better placed in a Discussion, not in the Results section.

Specific item 28 author response/manuscript change: We have renamed the section to account for the inclusion of discussion.

Specific item 29. Page/line 15/12-14: I think it is too uncertain to explain results in terms of the numbers of proteins. Snomax contains full cells and evidence for separation of the INP material (protein) from the cell wall is unclear. Leveling off the INP curves shows a limit in the number of INPs as a fraction of the total number of cells. This is a matter of expression of the INP protein under induced conditions and of the processing of the bacterial culture. Again, the emphasis here should be on the agreement among measurement systems. Interpretation of the shape of the INP curves is a matter for Discussion (see Broad comments 7 and 8).

Specific item 29 author response/manuscript change: We were attempting to explain the behaviors in terms of discussion present already in past literature, but understand the point here and agree that we should omit this statement as tangential to the overall comparison.

Specific item 30. Page/line 15/25: Reference here to first-freezers etc. is confusing without more detailed knowledge of what is being discussed. This type of error analysis for specific devices should be part of the apparatus description (cf. Broad comment 6).

Specific item 30 author response/manuscript change: We were not discussing an error analysis in this section, but pointing to the fact that in some experiments, at least two of the freezing methods detected discrepancies in freezing conditions of their samples. We were also pointing out that such a result is consistent with the impact of handling on the first freezers detected on the basis of other published work.

Specific item 31. Page/line 15/32: Supporting Information =? Supplement. Where is the material referred to in this line?

Specific item 31 author response/manuscript change: Section S.2.2, stated now, to point specifically to the CMU methods.

Specific item 32. Page/line 16/10: Why wasn't the fraction expressed as active INP versus total number of potential INP particles introduced? Maybe that is what is meant, but I am not sure from the wording given here.
Specific item 32 author response/manuscript change: That is what was intended. The fraction was INP over potential INP for each type, representing a different experiment in each case. Reworded for clarity as, *"These data were first analyzed as active fractions, which is the number fraction of all particles freezing when normalized to the total number concentrations of particles (potential INP) present at the onset of expansions."*

Specific item 33. Page/line 16/16-17: The conversion to active site density is the same for all measurements, provided particle sizes are known. Why is this introduced here? (cf. Broad comment 10)
Specific item 33 author response/manuscript change: The active site density approach was introduced in Methods. It is mentioned here because we are about to present figures including it. The reasoning for this was provided in response to Broad comment 10. It was not possible to compare AIDA and APC experiments in any manner except on the basis of active fraction or n_s. We choose to show one active fraction plot and then proceed to reduce figures by showing only n_s. By overlaying the AIDA experiment n_s data on n_s calculated from the APC experiments, we seek to tie the two series together.

Specific item 34. Page/line 20/28-31: Do these two sentences refer to the same or two separate findings?
Specific item 34 author response/manuscript change: Rewritten for clarity. There are two points. The steep activation behavior with temperature exacerbates discrepancies. It was also the steep slope of the FS02 activation versus temperature that led to the finding that CFDC cooling in the evaporation region can express "late" activation of ice crystals that remain at small sizes and should not be attributed to the set point temperature of the lamina in the instrument. We write, *"The steep activation behavior of the FS02 also led to the finding that when sampling such INPs, cooling to achieve evaporation in the exit section of a CFDC (CFDC-CSU, CFDC-TAMU and INKA in this study) can express "late" activation of ice crystals that remain at small sizes and should not be attributed to the set point temperature of the instrument growth region. This may be an issue primarily for laboratory measurements of such INPs, since most natural INP T-spectral slopes…"*

Specific item 35. Page/line 21/21: Some numerical values for the errors discussed would be useful.
Specific item 35 author response/manuscript change: We are not sure how to answer this request, since it deals with a topic that was not investigated. Namely, we did not purposely attempt to create size distributions of INPs that would challenge instruments with size cuts. Furthermore, to suggest a range of errors that would occur in the atmospheric scenario, we would need to know a typical size distribution of atmospheric INPs. This could vary tremendously. The topic is appropriate for an ambient measurement intercomparison. It could be explored in a laboratory setting, but as mentioned, we did not explore it during FIN-02. Hence, we make no changes here.

Specific item 36. Page/line 21/23: 'de-agglomeration' has a simpler alternative: 'breakup' and removes the implication that all large INPs are aggregates of many smaller ones

Specific item 36 author response/manuscript change: Very good point, and accepted.

Specific item 37. Page/line 21/28: " ... full immersion of all particles in the same liquid volume .." is too vague to focus on, as other factors like time in suspension may also come into play. Also, are the differences beyond the error bars of the PIMCA-PINC and cold-plate methods?

Specific item 37 author response/manuscript change: We have added on breakup, sedimentation and active site alteration in bulk suspension as possible impacts on freezing spectra compared to PIMCA-PINC single droplet results. As for the last question, error bars are shown on all plots, so the answer is yes at the level of the experiments performed. If referring to the overall uncertainty evident in experimental results, it is harder to say. This topic would benefit from more overlap in the measurement regimes of the two methods for more instruments, but we have noted that PIMCA-PINC is restricted to assessing higher fractions freezing. We write, *"Reasons why the bulk immersion freezing methods do not always agree with PIMCA-PINC may relate in some unresolved manners to factors at play during extended bulk immersion, such as breakup, sedimentation, and alteration of active sites."*

Specific item 38. Page/line 21/32: why is that need artificial?

Agreed. It is artefactual, as in, not fundamental to the original operating principle.

Specific item 38 author response/manuscript change: We drop the artefactual part of that statement.

Specific item 39. Page/line 22/4: '…uniformly capture activation ...' is awkward wording

Specific item 39 author response/manuscript change: We have changed the word to *"equivalently"*.

Response to anonymous Reviewer 2 comments on "The Fifth International Workshop on Ice Nucleation phase 2 (FIN-02): Laboratory intercomparison of ice nucleation measurements"

We thank the reviewer for both the positive comments as well as detailed additional comments and corrections.

General Comment: As a general comment, I do think the Summary and Conclusion section could have expanded the "do's and don't's" a bit. The authorship represents a large number of those active in the field and I do not think it would be giving away any secrets if they discussed a bit what failed, or was discovered not to have worked during the campaign. Also, they do make a few suggestions for the future, but I am left wondering if the community came no closer to formulating certain experiments that could be done side-by-side anytime two or more instruments are co-sampling. In other words, does any suggested minimum protocol emerge to assess the agreement between instruments? Perhaps a complete picture and set of recommendations emerging from FIN-02 will be detailed in another publication?

Authors' response to General Comment: While the goal of the workshop was not necessarily to fashion protocol for all future such instrumental comparisons, nor to be judgmental, we agree with the reviewer that we could expand our recommendations, and point to things that could/should be done in a comparison involving any particular number of participants. At the same time, it is clear to those involved that the composite results of all three phases of the workshop will be needed to provide a complete picture and set of recommendations. Additional papers in that regard are forthcoming. We have completely reorganized and added to the Summary and Conclusions of this paper on the basis of the requests of both reviewers.

Changes in manuscript re: General Comment:
The Conclusions have been reorganized, first by summarizing and augmenting the initial discussion within the structure of the objectives listed in the Introduction of the paper, and secondly by adding a list of topics recommended for further research. As this section amounts to nearly 6 pages, we append it specially to the end of this response after first completing responses to itemized editorial comments.

Itemized Editorial Comments (page/line):

Comment 1. *Page/line* 1/38 item b only has a departmental affiliation it is missing an institutional affiliation.
Comment 1 author response/manuscript change: Thanks, corrected.

Comment 2. Page/line 6/16-18 What comes after the comma at: "...Fig. 1, and why..." does not make sense as written. The why results are given at certain RH is not noted? I think the clause needs to be rewritten.
Comment 2 author response/manuscript change: We have rewritten this section for clarity: *"Therefore, a single RH_w level in the growth region for breakthrough to occur is not noted in Fig. 1. Instead, results are stated as being associated with specific RH_w values (or % supersaturation values, which equal RH_w-100) that are simply a value that was lower than the droplet breakthrough condition. In some cases, this was the maximum RH_w achievable in the growth region prior to droplet breakthrough."*

Comment 3. Page/line 7/28 I recommend you change "in this manuscript" to 'presented here'.
Comment 3 author response/manuscript change: Changed as requested.

Comment 4: Page/line 7/30 This first sentence of the section is long and awkward. I recommend it is changed. It can be split into 2 sentences.
Comment 4 author response/manuscript change: Done

Comment 5: Page/line 8/4-5 thermodynamic paths not path • 8/10 would limit particle loading
Comment 5 author response/manuscript change: Changed as requested.

Comment 6: Page/line 8/18 activation temperatures instead of "temperatures of activation". Also, add 'and referenced' after "...are listed". I was looking for the instrument references as I was reading and did not realize they were in the table until getting there. Finally, I suggest striking "Details on all of" rather begin the next sentence with "The specific ..."

Comment 6 author response/manuscript change: Changed as requested. Reference to Table 1 was also added on Page 5.

Comment 7*:* Page/line 9/1 I recommend "besides" is changed to 'in addition to'

Comment 7 author response/manuscript change: Changed as suggested.

Comment 8: Page/line 9/3-5 The sentence beginning "In this regard..." is awkward and should be rephrased. Is it the recommendation of the 2007 workshop, or previous workshops and it was followed in 2007?

Comment 8 author response/manuscript change: Rewritten as, *"In this regard, we follow the example of the 2007 workshop, and a key recommendation from ice nucleation workshops prior to that time that an expansion cloud chamber be utilized to provide a simulation of cloud activation (DeMott et al., 2011)."* This is discussed in the 2011 paper and references to prior workshops are provided.

Comment 9: Page/line 9/5 recommend change to 'Schematic thermodynamic paths of the AIDA chamber experiments are shown by the ....'

Comment 9 author response/manuscript change: Changed as suggested.

Comment 10: Page/line 9/20 suggest '....cloud regime (i.e., 0 to -36 C). Thus they provide....'

Comment 10 author response/manuscript change: Changed as suggested.

Comment 11: Page/line 10/12 suggest wording is changed to 'However, in some experiments larger particles were present ...'

Comment 11 author response/manuscript change: Changed as suggested.

Comment 12: Page/line 10/13 should "some cases" be 'those cases'

Comment 12 author response/manuscript change: Corrected.

Comment 13: Page/line 12/2 I suggest that when ns,geo(T) is defined the units [m−2] are included.

Comment 13 author response/manuscript change: Done.

Comment 14: Page/line 13/6 suggest wording is changed to 'A striking feature of these results is the general correspondence between all methods ...'

Comment 14 author response/manuscript change: Changed as suggested.

Comment 15: Page/line 13 /14 suggest 'The greatest discrepancies' replace "Greatest discrepancies..."
Comment 15 author response/manuscript change: Changed to "The largest…"

Comment 16: Page/line 13/15 "Supplemental" should be 'Supplement'
Comment 16 author response/manuscript change: Done.

Comment 17: Page/line 13/19 suggest wording is changed to '...understanding of what RHw value might...."
Comment 17 author response/manuscript change: Changed as requested.

Comment 18: Page/line 13/23 The final sentence of the paragraph ending, "... Fig. 4 is encouraging" is oddly placed in a results section. I think it is extraneous.
Comment 18 author response/manuscript change: Removed.

Comment 19: Page/line 14/15 replace "at the same time" with 'simultaneously'
Comment 19 author response/manuscript change: Changed.

Comment 20: Page/line 14/27 replace "Comparison" with 'A comparison'
Comment 20 author response/manuscript change: Done.

Comment 21: Page/line 15/17-20 This is a very long and confusing sentence, I suggest rewording.
Comment 20 author response/manuscript change: This section is rewritten as, *"All immersion freezing methods capture the strong rise in activation due to the presence of the most active biological ice nucleators, those within the realm of the Groups I and II as defined by Yankofsky et al. (1981). This is expressed as a pronounced shoulder in all freezing spectra at temperatures warmer than -8°C in Fig. 7. We may note here that all bulk freezing methods shared the same impinger sample in this case, including the IS. This warm shoulder of ice nucleation activity has also been demonstrated by Wex et al. (2015), Budke and Koop (2015), and Polen et al. (2016)."*

Comment 22: Page/line 15/29 Should it not be CMU-CS?
Comment 20 author response/manuscript change: Yes, corrected.

Comment 23: Page/line 15/33 awkward wording. The source of variations question?
Comment 23 author response/manuscript change: Rewritten as, *"In summary, the strong variability in activity seen at the warmest activation temperature regime for Snomax® particles brings into question the ability to utilize the warmest temperature (> -10°C) freezing behavior of Snomax® reliably for calibration purposes. This has been*

noted previously by Polen et al. (2016), and attributed to batch-to-batch variability and the loss of activity during storage."

Comment 24: Page/line 22/1 "provide the decision" is awkwardly worded.

Comment 24 author response/manuscript change: Replaced with "…provide guidance…"

Comment 25: Figure 3 caption – The caption fails to define what the differently colored points indicate. Furthermore, I suggest the 2 light blue shadings be somehow differentiated. If my understanding is correct then I think the 2nd sentence would read, "An initial impinger and filter sampling period is highlighted in light blue 1 and is followed by an APC refill and subsequent sampling period (light blue 2). In any case I think the caption should be carefully reread and reworded for clarity.

Comment 25 author response/manuscript change: We had hoped for the colored scales to direct eyes to the appropriate axes, but for clarity we have rewritten it all as, *". Data from the first half of a daily experimental series, after an initial fill of Tunisian soil dust (Experiment 11 and 12 of the FIN-02 APC series on March 18, 2015) into the APC at a time (time 0) taken to be the experimental start time. Impinger and filter sample periods after two separate chamber fills are highlighted in light blue shading. To obtain a reference aerosol concentration (cm^{-3}) via the CPC (total particles) (blue points, left scale) or optical particle counter at sizes larger than 500 nm (n_500; brown points, right scale), as well as surface area ($\mu m^2\ cm^{-3}$) (black points, left scale) for the impinger/filter sampling period, the time-weighted average of the two sampling periods was determined. This period-integrated concentration value could then be used to ratio versus the concentrations of particles present at later sampling times during the direct processing instrument sampling of aerosols from the APC (green shaded region) in order to back-correct the directly-sampled INP number concentrations to those derived for the collections for post-processed samples."* The text section describing the procedure is already quite detailed, and does mention the fact that there were sometimes two sample chamber fills, and sampling periods for which the integrated particle number values and surface areas are determined.

Comment 26*:* Figure 4 caption – Suggestions: (1) strike "on some points" (2) replace "buried within" with 'subsumed by' (3) add '...errors) or alternatively the binned...'

Comment 26 author response/manuscript change: Changed as suggested.

Comment 27: Figure 7 caption – bring "in this case" to beginning of sentence

Comment 27 author response/manuscript change:

Done.

Comment 28: Figure 8 may be better presented vertically for such a 2-column journal? Perhaps the authors intend to stretch this over the entire page? Currently the text seems somewhat small. (also Figures 9-11).

Comment 28 author response/manuscript change: Due to the length of the caption, we will suggest to place these figures across the entire page, unless the editors suggest otherwise. And although the text is somewhat small, there were many different instruments to indicate, and it should be possible for most to expand the figures in PDF format. But again, we will go with the decision of the copy editors in this case.

Comment 29: General figure comments: Can the chosen color schemes for the instruments remain consistent between those figures that represent APC and AIDA data? Also, I think making many of the figures box plots with at least the major tick marks represented on the minor axis would be more reader friendly.

Comment 29 author response/manuscript change: It was indeed the intent to maintain color schemes for different data across figures. We will recheck that this is done. Once we began to introduce AIDA data at Figure 8 and beyond, and when we desired to show both soil dusts together in Figure 10, it complicated matters, so we simply made all of the online instruments black (or green and black in the case of Fig. 10). This also assisted with shading the APC versus AIDA sampling points in the later figures. We revise now to use black symbols for flow chambers all the way through the figure series, and we distinguish IS and FRIDGE-IMM series as blue in the APC figures now. The exception to this overall scheme will continue to occur in Figure 10, where green is used to distinguish the two dusts amongst the direct sampling instruments. As for the scaling on box plots, it would be too difficult to add the extra scale in the AIDA figures and simultaneously keep the long legends that are perhaps for important for easily distinguishing instruments. For that reason, we do not add the secondary scales on any of the figures.

New Conclusions section:

4 Summary and Conclusions

Through careful coordination and collaboration in a laboratory setting, most of the objectives of the second phase of the Fifth Ice Nucleation Workshop were strongly advanced if not fully achieved, and the existence of the data set should continue to serve explorations of measurement consistencies and issues for applying different techniques in isolation or in tandem for making atmospheric ice nucleation measurements. Extensive comparisons involving a large number of teams and using multiple INP types were made within just a three-week workshop. Some operational issues occurred for investigators at times (obvious errors, measurement biases, inability to achieve comparative conditions for proximal immersion freezing) and where these were recognized, data were either not entered into comparisons or in a few cases were revised. Some issues were investigated, such as the appearance of small ice in the CSU CFDC data for INPs with steep activation functions. Others remain the subject of active investigation.

We may summarize the workshop results generally around the stated objectives as follows:

1) *Compare ice nucleation measurement systems for conditions considered to be equivalent as much as possible, across a wide dynamic temperature range, including temperatures warmer than -15°C.*

To simplify this first analysis of FIN-02 data, a focus was placed in this paper on immersion freezing nucleation and activation within continuous flow chambers in the water supersaturated regime, across a wide temperature range including temperatures warmer than -15°C through the use of bacterial INPs in selected experiments. The proximal behavior model for comparing immersion freezing by direct processing instruments versus bulk immersion freezing

methods worked reasonably well, excepting cases noted later in this summary. Very good correspondence was obtained between many measurements for soil dusts and bacterial INPs, both amongst instruments that directly-processed single particles and those that post-processed bulk aerosol collections for assessing immersion freezing INP concentrations (Figures 4, 5, 7). Agreement of INP number concentrations and geometric active site density within less than about 1 order of magnitude was achieved under most circumstances analyzed herein for these three materials. This was strictly demonstrated for both direct and post-processed samples over a more limited temperature range, approximately -20 to -30°C for the soil dusts and -10 to -30°C for the bacterial INPs. For these atmospherically-relevant particle types, no strong biases between the two basic types of measurement systems were evident in this range of overlap.

The fact that agreements were quite good overall in this study may have been strongly assisted by the combination of co-sampling the same aerosol particle sources in the same laboratory, sharing similar collected aerosol samples, and limiting the largest particle sizes assessed in workshop experiments to those that could readily be measured by all techniques. The nature of active sites for the various INPs examined may also have influenced comparability of direct particle sampling versus post-processed bulk collection. Consequently, it appears that soil dust particles are much more equally assessed for INP content than some minerals and mineral mixtures, and may better serve as potential calibration INPs. This was supported by the worst agreement between methods, up to three orders of magnitude, for illite NX and the FS02 samples that have a very steep activation spectra versus temperature, which exacerbates disagreements that otherwise represent only a few degrees of temperature change. In the case of illite NX, discrepancies seen in Hiranuma et al. (2015) were reproduced at temperatures warmer than -25°C. The steep activation behavior of the FS02 also led to the finding that when sampling such INP types, cooling to achieve evaporation in the exit section of a CFDC (CFDC-CSU, CFDC-TAMU and INKA in this study) can express "late" activation of ice crystals that remain at small sizes and should not be attributed to the set point temperature of the instrument growth. This may be an issue primarily for laboratory measurements of such INPs, since most natural INP T-spectral slopes are lower than for many of the samples tested, often only approximately 2 orders of magnitude per 10°C, rather than 5 orders or more per 10°C (DeMott et al., 2017; Price et al., 2018).

Assessment of agreement between direct processing of single particles and post-processing measurement systems was mostly only possible below -20°C since flow chamber devices have a limit of detection which restricts measurements at warmer temperatures. The exception is in cases where the higher concentrations of bacterial INPs were assessed. Since biological/biogenic INPs are the most likely contributors to freezing at modest supercooling (e.g., Murray et al., 2012; Hoose and Möhler, 2012), it would seem valid that combining bulk aerosol sampling measurements to capture INPs at very modest supercooling with direct measurements extending to colder temperatures within the same atmospheric study will lead to a reasonably valid representation of immersion freezing INPs (e.g., DeMott et al., 2017; Welti et al., 2018).

2) *Gain insights into how detection of ice nucleation is influenced by the specific configuration of similar measurement systems.*

Among measurements on samples collected for post-processing, there was no particular or consistent bias between different approaches to bulk suspension measurements. Furthermore, there appears to be little discrepancy between

measurements made with particles collected directly into liquid versus collection onto filters followed by resuspension into liquid. There also appear to be no discernable impacts of freezing samples versus processing them immediately, on the basis of the μl-NIPI versus other methods apart from impacts on the warmest temperature freezing of bacterial particles (e.g., results from Snomax® experiments). Factors affecting reproducibility, such as accuracy of temperature attributed to sample freezing and instability of the warmest bacterial INPs, are the most important factors affecting the agreement between methods, which often spans an order of magnitude overall. Most measurement groups have likely performed careful assessments of their temperature measurements attributed to droplet volumes, but there is evidence that errors may occur due to the inability to perfectly assess temperature at the point of freezing (Beall et al., 2017).

For diffusion chamber measurements of collected particles, the need for awareness of volume effects on processed INPs remains as a requirement. Results in a few cases showed these measurements to fall to the low side in assessing immersion freezing nucleation. It may be necessary to collect varied volumes to assure that particle loading in different cases is not influencing accurate assessment of INP number concentrations.

Differences between INP measurements in the water-supersaturated regime by continuous flow chambers were seen, and these differences likely relate to the need of these systems to achieve higher than expected RH_w in order to fully activate aerosols to facilitate their subsequent immersion freezing on the full particle population within the diffusion chambers (DeMott et al., 2015; Garimella et al., 2017; Burkert-Kohn et al., 2017). These instruments may universally have an issue in focusing aerosol particles reliably into the center of the imposed RH_w field, among other factors that depend on particle types, including their hygroscopicity and ability to activate ice nucleation already in the sub-water saturated regime (not discussed in this paper). Solving the issue(s) involved could provide the guidance on correcting these data for the RH_w-sensitivity factor present in the water supersaturated regime for all of these devices. Different systems have varied ability to achieve higher RH_w, depending on the different water breakthrough RH_w as imposed by device design (see Section 3 and Section S.1.2). For example, it was noted that the PINC instrument more commonly measured INP concentrations at the lower range of the flow chamber devices, which may be attributable to its shorter residence time. These systems will continue to be used in this manner to measure atmospheric INP activation, but will struggle to equivalently capture activation to the same degree until issues are solved. Such solutions could involve redesign of how samples are introduced to the chambers. This is clearly deserving of a special study, which was beyond the scope of this workshop. Study of the use of different evaporation region temperatures also merits attention as it may impact detection of ice formation at higher RH_w. Limitations on assessing the impacts of larger aerosols as INPs in continuous flow instruments will remain, unless special inlets are developed.

Of note in this study is the agreement between most direct sampling and post-processing measurements at the colder temperatures in comparison to the large discrepancies found in a recent study comparing measurements of ambient particles (DeMott et al., 2017). We believe that this is attributable to assuring comparability of measurement methods in FIN-02 by restricting particle sizes, as mentioned above. This likewise implies that discrepancies between direct and post-processing methods can be expected to occur in ambient sampling when larger particles are present, although the source of those discrepancies as true impacts (i.e., of larger particles acting as individual INPs versus breakup of INPs after time in bulk suspensions) must remain a topic of future research. Both bulk sample immersion

freezing and proximal immersion freezing in the flow diffusion chambers sometimes underestimate freezing in comparison to the PIMCA-PINC single particle immersion freezing method. For CFDC type instruments, this is partly understood as the need to achieve much higher RH_w, sometimes practically unachievable, to effectively simulate and capture immersion freezing (previous paragraph), requiring corrections that were not applied in this study. Whether such corrections are the only reason for discrepancies with PIMCA-PINC require further investigations. Reasons why the bulk immersion freezing methods do not always agree with PIMCA-PINC may relate in some unresolved manners to factors at play during extended bulk immersion, such as breakup, sedimentation, and alteration of active sites. It would be helpful if the PIMCA-PINC method could be extended to lower active fractions and INP concentrations, but this appears to be a fundamental limitation of the phase discrimination technique.

3) Utilize different INP types to investigate if differences between instruments occur with these different types.

The use of varied INP types was clearly vital in achieving the first two objectives summarized above. For example, the use of a highly active biological INP type clearly helped to demonstrate that there is no fundamental limit on INP detection by any method if limits of detection are met. It is not known if this conclusion is peculiar to the biological INPs, although these may be the most common and important type to detect in the warmer supercooled temperature regime. While the utility of Snomax® as a calibration INP was again demonstrated here, issues in achieving well-defined active fractions at temperatures above -9°C via post-processing of bulk collections for immersion freezing found in previous studies were repeated herein. Comparisons with direct processing methods was not obtained in this temperature regime, making this an important topic for future studies.

The use of both natural soils and mineral samples as INPs allowed for seeing that the soil INPs were more consistently measured within and across measurement methods compared to the mineral component K-feldspar and a material representing key mineral compounds of desert dust aerosols (illite NX). The steeper nucleation rate functions of the minerals were key to identifying the potential bias in production of ice nucleation in the evaporation sections of the CSU and INKA CFDC's, likely due to the additional cooling occurring there. Other devices that warm the airflow while reducing the relative humidity toward ice saturation to evaporate activated cloud droplets did not see small ice crystal production. Detection of the small ice crystals produced in this manner can be largely biased against through adjustment of the channel size used for ice detection in the optical particle counter, although mitigation through redesign may provide a more satisfactory long term solution. Further investigation of this issue is merited.

Through the use of multiple INP types, results from this workshop could also be compared versus previously published parameterizations. These comparisons were very encouraging for demonstrating reproducibility of laboratory study results in general, further supporting the picture of general consistency of present INP measurements within identified uncertainties.

The FIN-02 archive will remain for additional scientific investigations, such as at least limited comparisons in the ice nucleation regime below water saturation (see below), analysis of experiments regarding homogeneous freezing and the role of particle pre-activation for ice formation. While the FIN-02 workshop objectives were generally achieved, a number of topical research needs remain and some recommendations are suggested.

- Although the coordinated sampling protocols during FIN-02 worked very well, and the possibility of establishing certain calibration standards was suggested, it is not practical for the majority of members of the

international INP measurement community to gather with high frequency for such activities. It may be possible that similar correspondence of measurements can be obtained through the distribution of some standards and the use of defined aerosol generation protocol. A basic attempt at such an exercise that restricts sample types to a natural dust and bacterial INPs is worth exploring, as a wide distribution exercise has only thus far occurred for illite NX. The general correspondence of present workshop data with n_s parameterizations derived in previous laboratory studies provides a positive outlook.

- Special investigation of detection of ice formation in the regime below water saturation remains as a need that will be only partially addressable with FIN-02 data due to somewhat limited range of temperatures assessed by most direct processing instruments. While the number of instruments involved in such an assessment is more limited, it is no less important for evaluation in regard to the use of ice nucleation instruments in the colder regions of the troposphere. For example, are similar results obtained or is there a wider discrepancy between shorter residence time diffusion chamber, substrate-based processing devices, and controlled expansion cloud chambers in this regime?
- Ice nucleation measurements are also needed for fundamental understanding of ice nucleation and of the nature of INPs, which an array of measurement devices can address better than a single technique. Questions remain on differences between condensation and immersion freezing (Vali et al., 2015; Burkert-Kohn et al., 2017), the nature of ice nucleation in the regime below water saturation (Higuchi and Fukuta, 1966; Marcolli, 2014), connecting practical measurements with molecular scale understanding and many other topics.
- Other focused studies involving instruments within direct and post-processing communities are recommended for addressing needs specific to these communities. For direct sampling, examples are a careful comparison of the operational characteristics of continuous flow instruments as a function of RH_w, and a rigorous comparison of use of optical size for detecting ice in CFDC-style instruments versus use of depolarization and machine learning methods. For post-processing methods, the role of sample storage aggregation and breakup as a function of particle loading and size in bulk immersion freezing studies deserves study.
- Establishing best practices for handling of bulk immersion freezing samples, and for limiting and correcting for the background freezing counts introduced in the water used for collection (for impingers) or for rinsing (of filters) is a topic that was not covered directly in FIN-02. Improvement and standardization of protocol would only help to improve the good results obtained across these methods in this study. This is a topic of a separate paper published in this special issue (Polen et al., 2018).
- The role of INP size and more careful quantification of biases involved in assessing this factor deserves more focused attention. The use of monodisperse aerosols in a workshop like FIN-02 would present logistical challenges, but would add an important dimension for study and greatly assist interpretation of results.
- The low INP concentration regime still presents a strong challenge for the measurement community, one that becomes critically important in atmospheric studies. Low INP concentrations are ubiquitous at modest supercooling, but can also occur at lower temperatures in the atmosphere. For existing direct sampling devices like flow chambers, no current comparisons have focused on their abilities to control and correct for

background frost artifacts. While ambient measurement campaigns such as FIN-03 allow some focus on this topic, a laboratory campaign could do the same. Only post-processing methods for immersion freezing can access the regime at modest supercooling. This limits temporal and spatial resolution, especially when sampling on aircraft. Can new methods be developed for directly assessing INP concentrations in larger sample volumes? Even modest improvement to direct methods to provide more overlap of measurement methods in the regime > -20°C would help to further evaluate the validity of meshing direct and post-processing methods to characterize INPs over the full mixed-phase temperature regime. Aerosol pre-concentration has been applied to extend the dynamic range of direct INP measurements in atmospheric studies (e.g., Tobo et al., 2013; Boose et al., 2016), but aerodynamic concentration methods bias against particle sizes much below 1 μm. Hence, it is worth investigating the possible use of other concentration methods applicable to the full aerosol size distribution, such as pre-condensation. Novel ideas are needed.

- Further comparisons for which the sampling groups are "blind" to the nature and concentrations of INPs being sampled could be useful toward giving confidence to the wider community that the INP measurement community is capable of recognizing issues and properly interpreting data. This will assist confidence and utility of larger global data sets. Such a comparison from FIN-02 will be reported on in a separate publication in preparation.
- Similar exercises as FIN-02 are also needed in sampling under ambient atmospheric conditions. This is the subject of the FIN-03 campaign that will be reported on separately.

Workshops such as FIN-02 will continue to play a large role in assessing measurement biases and ultimately improving the comparability of INP measurements made by a large community of researchers sampling on a global scale. The shared experience of these workshops is irreplaceable in providing special insights into the status of and issues involved in obtaining INP data in different scenarios that may be dominated by certain aerosol types. FIN-02 demonstrates that the INP measurement community remains on a progressive track towards assessing convergence between different methods used for INP quantification.

The Fifth International Workshop on Ice Nucleation phase 2 (FIN-02): Laboratory intercomparison of ice nucleation measurements

DeMott, Paul J.[1], Ottmar Möhler[2], Daniel J. Cziczo[3,4], Naruki Hiranuma[2,a], Markus D. Petters[5], Sarah S. Petters[5,b], Franco Belosi[6], Heinz G. Bingemer[7], Sarah D. Brooks[8], Carsten Budke[9], Monika Burkert-Kohn[10], Kristen N. Collier[8], Anja Danielczok[7,c], Oliver Eppers[11], Laura Felgitsch[12], Sarvesh Garimella[3,d], Hinrich Grothe[12], Paul Herenz[13], Thomas C. J. Hill[1], Kristina Höhler[2], Zamin A. Kanji[10], Alexei Kiselev[2], Thomas Koop[9], Thomas B. Kristensen[13,e], Konstantin Krüger[7,2], Gourihar Kulkarni[14], Ezra J. T. Levin[1], Benjamin J. Murray[15], Alessia Nicosia[6,f], Daniel O'Sullivan[15], Andreas Peckaus[2,g], Michael J. Polen[16], Hannah C. Price[15,h], Naama Reicher[17], Daniel A. Rothenberg[3], Yinon Rudich[17], Gianni Santachiara[6], Thea Schiebel[2], Jann Schrod[7], Teresa M. Seifried[12], Frank Stratmann[13], Ryan C. Sullivan[16], Kaitlyn J. Suski[1,i], Miklós Szakáll[11], Hans P. Taylor[5], Romy Ullrich[2], Jesus Vergara-Temprado[15,10], Robert Wagner[2], Thomas F. Whale[15], Daniel Weber[7], André Welti[13,j], Theodore W. Wilson[15,k], Martin J. Wolf[3], and Jake Zenker[8]

[1]Department of Atmospheric Science, Colorado State University, Fort Collins, CO 80523-1371, USA
[2]Karlsruhe Institute of Technology (KIT), Institute of Meteorology and Climate Research (IMK-AAF), Eggenstein-Leopoldshafen, Germany
[3] Department of Earth, Atmospheric and Planetary Sciences, Massachusetts Institute of Technology, Cambridge, MA, USA
[4]Department of Civil and Environmental Engineering, Massachusetts Institute of Technology, Cambridge, MA, USA
[5]Department of Marine, Earth and Atmospheric Sciences, North Carolina State University, Raleigh, NC, USA
[6]Institute of Atmospheric Sciences and Climate (ISAC-CNR), Bologna, Italy
[7]Institute for Atmospheric and Environmental Sciences, Goethe-University Frankfurt, 60438 Frankfurt am Main, Germany
[8]Department of Atmospheric Sciences, Texas A&M University, College Station, TX, USA
[9]Faculty of Chemistry, Bielefeld University, Bielefeld, Germany
[10]Institute for Atmospheric and Climate Science, ETH Zurich, Zurich, Switzerland
[11]Institute for Atmospheric Physics, Johannes Gutenberg University, Mainz, Germany
[12]Institute of Materials Chemistry, TU Wien, Vienna, Austria
[13]Leibniz Institute for Tropospheric Research, 04318 Leipzig, Germany
[14]Atmospheric Sciences and Global Change Division, Pacific Northwest National Laboratory, Richland, WA, USA
[15]Institute for Climate and Atmospheric Science, School of Earth and Environment, University of Leeds, Woodhouse Lane, Leeds, LS2 9JT, UK
[16]Center for Atmospheric Particle Studies, Carnegie Mellon University, Pittsburgh, PA, USA
[17]Department of Earth and Planetary Sciences, Weizmann Institute, Rehovot 76100, Israel
[a]now at: Department of Life, Earth and Environmental Sciences, West Texas A&M University, Canyon, TX, USA
[b]now at: Department of Environmental Sciences and Engineering, University of North Carolina, Chapel Hill, NC, USA
[c]now at: German Weather Service, Satellite-based Climate Monitoring, 63067 Offenbach am Main, Germany
[d]now at: ACME AtronOmatic, LLC, Portland, OR, USA
[e]now at: Division of Nuclear Physics, Lund University, Box 118, Lund SE-22100, Sweden
[f]now at: Laboratoire de Météorologie Physique (Lamp-CNRS), Aubière, France
[g]now at German Aerospace Center (DLR), Institute of Technical Physics, 70569 Stuttgart, Germany
[h]now at Facility for Airborne Atmospheric Measurements, Cranfield, MK43 0AL, UK
[i]now at: Pacific Northwest National Laboratory, Richland, WA, USA
[j]now at: Finnish Meteorological Institute, FI-00101 Helsinki, Finland
[k]now at Owlstone Medical Ltd., 162 Cambridge Science Park, Milton Road, Cambridge, CB4 0GH, UK

Correspondence to: Paul J. DeMott (Paul.Demott@colostate.edu)

Abstract. The second phase of the Fifth International Ice Nucleation Workshop (FIN-02) involved the gathering of a large number of researchers at the Karlsruhe Institute of Technology's Aerosol Interactions and Dynamics of the Atmosphere (AIDA) facility to promote characterization and understanding of ice nucleation measurements made by the variety of methods used worldwide. Compared to the previous workshop in 2007, participation was doubled, reflecting a vibrant research area. Experimental methods involved sampling of aerosol particles by ~~online~~direct processing ice nucleation measuring systems from the same volume of air in separate experiments using different ice nucleating particle (INP) types, and collections of aerosol particle samples onto filters or into liquid for sharing amongst ~~offline~~ measurement techniques that post-process these samples. In this manner, any errors introduced by differences in generation methods when samples are shared across laboratories were mitigated. Furthermore, as much as possible, aerosol particle size distribution was controlled so that the size limitations of different methods were minimized. The results presented here use data from the workshop to assess the comparability of ~~offline~~ immersion freezing measurement methods activating INPs in bulk suspensions, ~~offline~~ methods that activate INPs in condensation and/or immersion freezing modes as single particles on a substrate, ~~online~~ continuous flow diffusion chambers (CFDCs) ~~operating~~ directly sampling and processing particles well above water saturation to maximize immersion and subsequent freezing of aerosol particles, and expansion cloud chamber simulations in which liquid cloud droplets were first activated on aerosol particles prior to freezing. The AIDA expansion chamber measurements are expected to be the closest representation to INP activation in atmospheric cloud parcels in these comparisons, due to exposing particles freely to adiabatic cooling.

The different particle types used as INPs included the minerals illite NX and K-feldspar, two natural soil dusts representative of arable sandy loam (Argentina) and highly erodible sandy dryland (Tunisia) soils, respectively, and a bacterial INP (Snomax®). Considered together, the agreement among ~~offline~~ post-processed immersion freezing measurements of the numbers and fractions of particles active at different temperatures following bulk collection of particles into liquid was excellent, with possible temperature uncertainties inferred to be a key factor in determining INP uncertainties. Collection onto filters for rinsing versus directly into liquid in impingers made little difference. For ~~offline~~ methods that activated collected single particles on a substrate at a controlled humidity at or above water saturation, agreement with immersion freezing methods was good in most cases, but was biased low in a few others for reasons that have not been resolved, but could relate to water vapor competition effects. Amongst CFDC-style instruments, various factors requiring (variable) higher supersaturations to achieve equivalent immersion freezing activation dominate the uncertainty between these measurements, and for comparison with bulk immersion freezing methods. When operated above water saturation to include assessment of immersion freezing, CFDC measurements often measured at or above the upper bound of immersion freezing device measurements, but often underestimated INP concentration in comparison to an immersion freezing method that first activates all particles into liquid droplets prior to cooling (the PIMCA-PINC device), and typically slightly underestimated INP number concentrations in comparison to cloud parcel expansions in the AIDA chamber; this can be largely mitigated when it is possible to raise the relative humidity to sufficiently high values in the CFDCs, although this is not always possible operationally.

Correspondence of measurements of INPs among direct sampling and post-processing ~~online and offline~~ systems varied depending on the INP type. Agreement was best for Snomax® particles in the temperature regime colder than

-10°C, where their ice nucleation activity is nearly maximized and changes very little with temperature. At warmer than -10°C, Snomax® INP measurements (all via freezing of suspensions) demonstrated discrepancies consistent with previous reports of the instability of its protein aggregates that appear to make it less suitable as a calibration INP at these temperatures. For Argentinian soil dust particles, there was excellent agreement across all measurement ~~online and offline~~ methods; measures ranged within one order of magnitude for INP number concentrations, active fractions and calculated active site densities over a 25 to 30°C range and 5 to 8 orders of corresponding magnitude change in number concentrations. This was also the case for all temperatures warmer than -25°C in Tunisian dust experiments. In contrast, discrepancies in measurements of INP concentrations or active site densities exceeded two orders of magnitude across a broad temperature range for illite NX, and divergent activation spectra between directly sampled versus post-processing ~~online and offline~~ measurements found at warmer than -25°C in a previous study were replicated. Discrepancies also exceeded two orders of magnitude at temperatures of -20 to -25°C for K-feldspar, but these coincided with the range of temperatures where INP concentrations increase rapidly at approximately an order of magnitude per 2°C cooling for K-feldspar.

These few discrepancies did not outweigh the overall positive outcomes of the workshop activity, nor the future utility of this data set or future similar efforts for resolving remaining measurement issues. Measurements of the same materials were repeatable over the time of the workshop and demonstrated strong consistency with prior studies, as reflected by agreement of data broadly with parameterizations of different specific or general (e.g., soil dust) aerosol types. The divergent measurements of the INP activity of illite NX by direct versus post-processing ~~online and offline~~ methods was not repeated for other particle types, and the Snomax® data demonstrated that, at least for a biological INP type, there is no expected measurement bias between bulk collection~~offline~~ versus ~~online~~ immediately processed freezing methods to as warm as -10°C. Since particle size ranges were limited for this workshop, it can be expected that for atmospheric populations of INPs, measurement discrepancies will appear due to the different capabilities of methods for sampling the full aerosol size distribution, or due to limitations on achieving sufficient water supersaturations to fully capture immersion freezing in ~~online~~ direct processing instruments. Overall, this workshop presents an improved picture of present capabilities for measuring INPs than in past workshops, and provides direction toward addressing remaining measurement issues.

1 Introduction

Ice nucleating particles (INPs) are relatively rare atmospheric particles that play a large role in affecting cold cloud properties and precipitation processes. Their presence is needed to initiate ice crystal formation in the absence of conditions that would favor homogeneous freezing nucleation. They are needed as a trigger even in cases where secondary ice formation may be expected to occur. Their varied loading may influence cloud lifetime positively or negatively, as well as impact precipitation rates in mixed phase clouds (e.g., Tan et al., 2016; Fan et al., 2017). Furthermore, the efficacy of different aerosol types as INPs varies greatly, and this is not well resolved for major or minor atmospheric aerosol populations. There is a tremendous need to measure ~~and constrain~~ atmospheric INP populations, and to parameterize these for use in numerical models of all scales, where greatly simplified assumptions on ice phase transitions in clouds are presently used or are thought to be necessary for computational reasons. Studies

of INPs occur in laboratory settings where high aerosol loadings are possible, but also in field scenarios where the low number concentrations of INPs challenge near real-time samplers and require larger bulk collections to attempt to quantify INPs at modest supercooling. Consequently, a variety of devices exists, and the development and use of different instruments continues to expand during a period of great growth in research on mixed phase and ice cloud processes (DeMott et al., 2011). For these reasons, a series of workshops was convened over the course of a year in 2014 to 2015, continuing the historical efforts of the international ice nucleation community to compare and contrast measurements, both to advance understanding within the community and to offer an assessment to the user communities of capabilities and present uncertainties of measurements being published independently.

The philosophy, three-phase nature, and general overview of the Fifth International Ice Nucleation Workshop, dubbed FIN will be provided in a separate publication in preparation. Briefly, and distinct from most previous workshops in its comprehensive scope, FIN sought to perform comprehensive operational comparisons of ice nucleation instruments for sampling calibration type INPs (representative of different atmospheric classes) in a laboratory setting and for sampling ambient atmospheric aerosols in a natural setting. In addition, the component FIN-01 (first study in late 2014) sought to intercompare single particle mass spectrometer instruments that are sometimes used to assess the detailed chemical composition of INPs by sampling the residues of ice crystals nucleated in flow diffusion chambers or aerodynamically segregated from atmospheric clouds. FIN-01 tested these instruments for their determined reference mass spectra on some of the INPs also planned for use in comparing ice nucleation instruments, it compared the different clustering algorithms used by the aerosol mass spectral community, and it repeated testing on ice crystal residues. FIN-02, the workshop phase discussed herein, was the laboratory ice nucleation instrument intercomparison. FIN-03, the field phase, was conducted at Storm Peak Laboratory in Steamboat Springs, CO. A final aspect of both FIN-01 and FIN-02 was to provide a minor period within the overall informal gatherings for scientific study that would feature a formal intercomparison of measurements. FIN was a volunteer activity on the part of participants, who agreed to participate to their fullest extent in both the informal and formal components, but were also free to explore new developments. Referees were solicited for organizing and analyzing the results of formal comparisons in FIN-01 and FIN-02. These formal or so-called "blind" experiments were conducted to investigate the degree to which the informal results presented in papers such as this one could be independently reproduced.

This paper describes the goals and objectives, and some detailed results from the second phase of FIN, known as FIN-02, focused around comparing ice nucleation measurement systems in laboratory studies of known INPs. A related paper in preparation will describe the separate but integrated activity of comparing these same instrument systems in ~~so-called "blind" experiments,~~ the formal comparison period during FIN-02. ~~We will describe herein the justification for and distinction of those studies only.~~ The FIN-02 workshop was held at the Aerosol Interactions and Dynamics in the Atmosphere (AIDA) facility at Karlsruhe Institute of Technology, Eggenstein-Leopoldshafen, Germany during March 2015. This facility was also the site for the FIN-01 workshop. FIN-02 was designed to be in the classical form of an ice nucleation workshop, from the standpoint of having a legacy in similar workshops dating back to the late 1960s, as discussed in relation to the 2007 International Workshop on Comparing Ice Nucleation Measuring Systems (ICIS-2007) (unofficially the Fourth International Workshop on Ice Nuclei) by DeMott et al. (2011). The impetus for continuation of the ice nucleation workshop concept was given in that paper. Significant

additional developments have occurred in the field of ice nucleation measurements since the time of the 4th workshop, including widespread participation from a global community of researchers and commercialization development of INP measurement systems that directly process aerosols. The FIN-02 workshop was held at the AIDA facility to take advantage of the 4th workshop experience, also held there, and to once again coordinate ~~align~~ other measurements with experiments in the AIDA cloud chamber as a mimic of ice nucleation within atmospheric adiabatic cloud parcels.

The goals and objectives of FIN-02 were to:

1) Compare ice nucleation measurement systems for conditions considered to be equivalent as much as possible, across a wide dynamic temperature range, including temperatures warmer than -15°C.

2) Gain insights into how detection of ice nucleation is influenced by the specific configuration of similar measurement systems.

3) Gain insights into the strengths and weaknesses, limits of detection, potential artifacts and other peculiarities of different INP detection systems.

4) Utilize different INP types to investigate if differences between instruments occur ~~vary~~ with these different types.

This paper is intended as an overview of the informal activities of the workshop while addressing the majority of these objectives. It is not intended to answer all of the goals and objectives that are better addressed in separate studies. It is not our intent to rigorously test the capabilities of different measurement systems, but rather to point to areas of success and areas for needed development or further research. For these reasons, and to include as many measurements as possible in comparisons, we focus primarily on measurements relevant to immersion freezing nucleation, as discussed further below. This allows for integrating the most possible measurements into comparisons made for assessing one important aspect of the state of the art of ice nucleation measurements.

2 Methods

Guided by the objectives of FIN-02 and the variety of current systems available for measuring INPs, two broad categories of ~~portable~~ ice nucleation instruments were defined for studies. These categories are, firstly, instruments operating online or for direct processing of aerosol particles and, secondly, those utilizing collections of particles for subsequent offline or post-processing. This categorization to a large extent also separates methods that sample "dry" particles and those that utilize "wet" suspensions of particles in liquid for assessing freezing properties, with a few exceptions ~~we will note~~. Methods for sampling particles from a dry state permit assessment of the action of a variety of ice nucleation mechanisms that occur in different water relative humidity (RH_w) regimes: deposition nucleation primarily occurring below water saturation, and condensation and immersion freezing on approaching or exceeding water saturation, where cloud droplet activation occurs. ~~Wet suspension e~~Experiments wherein particles are suspended in water isolate the action of immersion freezing nucleation direction, and certain methods allow for isolating immersion freezing for single aerosol particles (Burkert-Kohn et al., 2017). No measurements of contact freezing were included in this study, and neither will we discuss results herein from workshop measurements that were made in the regime associated with deposition nucleation (including at temperatures below the homogeneous freezing temperature of pure water droplets ~~temperatures~~). Instead, we will focus on inter-comparisons of particles acting via immersion

freezing or proximal behaviors. By proximal behaviors, we follow the terminology of Vali et al. (2015), wherein condensation freezing is not necessarily considered as distinguishable from immersion freezing, and, hence, ~~offline~~direct processing of particles in diffusion chambers measuring in the regime well above water saturation are considered to be able to approximate more direct measurements of immersion freezing.

The number of ice nucleation measurement systems participating in FIN-02 was slightly more than twice the number that participated in the 4th workshop in 2007, reflecting a similar increase in the number of researchers now operating in this field. There were 21 total systems represented in FIN-02, 9 ~~online~~directly processing and 11 post-processing~~offline~~, plus the AIDA chamber. Names~~, and~~ basic descriptions, and general operating principles are provided in Tables 1 and 2, and sections 2.1 and 2.2. Detailed implementations of the basic principles in each device are given in the Supplement sub-sections. Shorthand names of instruments are defined in the manuscript at first introduction. The thermodynamic trajectories used by the primary instrument types used in FIN-02 are shown in Fig. 1 and their basic manners of operation are discussed in the two following sections. These sections are followed by a section describing the general manner of conduct of the workshop, including aerosol generation procedures. This becomes important for shaping the progression of how results are discussed in this paper.

2.1 ~~Online (portable)~~ Direct sampling systems

~~Online or~~ Direct sampling systems used in FIN-02 included continuous flow systems and the AIDA controlled expansion cloud chamber (see Table 1). ~~were represented primarily in the form of~~ Continuous flow ice-thermal diffusion chambers ~~that~~ sample initially dry particles and expose these to conditions leading to ice nucleation. Amongst these were portable chambers with cylindrical (e.g., Rogers et al., 1988) and parallel plate (e.g., Stetzer et al., 2008) wall systems. The former included the Colorado State University continuous flow diffusion chamber (CFDC-CSU) and systems descendant from this design: the Texas A&M continuous flow diffusion chamber (CFDC-TAMU) and the Ice Nucleation Instrument of the Karlsruhe Institute of Technology (INKA). In all of these, a cylindrical aerosol lamina representing a minor portion of the total flow is constrained within particle-free sheath flows (top to bottom) between two cylindrical walls that are ice-coated and can be independently temperature-controlled to determine the RH_w and temperature at the center of the aerosol lamina in upper "growth" regions of the chambers. Parallel plate systems insert the downward-flowing aerosol lamina between sheath flows inside two parallel rectangular ice-coated plates to similarly expose particles to controlled temperature and humidity conditions in their growth sections. Parallel plate devices of quite common design included in FIN-02 were the ETH-Zurich Portable Ice Nucleation Chamber (PINC), the Pacific Northwest National Laboratory Compact Ice Chamber (CIC-PNNL), and the Droplet Measurement Technologies SPectrometer for Ice Nucleation (SPIN) devices operated by groups from the Massachusetts Institute of Technology (SPIN-MIT) and the Leibniz Institute for Tropospheric Research (SPIN-TROPOS).

Measurements from continuous flow diffusion chambers are represented by the red lines in Fig. 1. All of the continuous flow diffusion chambers have the ability to raise the RH_w above the water saturation line in order to investigate ice nucleation during or following condensation of water droplets. Once water droplets have formed, a means is required to discriminate ice particles from water droplets. The most common method used for phase

discrimination in continuous flow chambers is to selectively shrink activated liquid droplets to accentuate ice crystals by their larger optical size. Some instruments use laser light depolarization for phase discrimination, but this is typically a suitable method only for higher signal to noise situations and ice active fractions that exceed several percent of particles (Nicolet et al., 2010; Garimella et al., 2016; Zenker et al., 2017). For these reasons, all such devices in FIN-02 include an "evaporation" section as a shorter column length below their growth sections, where the RH_w is lowered toward ice saturation conditions by setting the two wall temperatures to be equivalent at either the warmest wall, coldest wall, or lamina temperature in the growth sections (see Supplement). When the temperature gradient in the growth section is adjusted to generate water supersaturated conditions that activate cloud droplets within the aerosol lamina, the lower relative humidity ~~RH_w~~ in the evaporation section shrinks droplets back toward haze particle sizes. This method works up to some high value of RH_w in the growth section whereupon activated cloud droplets survive through to detection, often referred to as the water droplet breakthrough RH_w. The ~~RH_w at which this~~ breakthrough value ~~occurs~~ varies with temperature, geometry and flow rate for different devices. Therefore, a single RH_w level in the growth region for ~~this condition~~ breakthrough to occur is not noted in Fig. 1. Instead, results are stated as being associated with specific RH_w values (or % supersaturation values, which equal RH_w-100) that are simply a value that was lower than the droplet breakthrough condition. In some cases, this was the maximum RH_w achievable in the growth region prior to droplet breakthrough. ~~We did not seek to fully document this behavior during FIN-02, and will not seek to understand differences amongst the different continuous flow chambers in this regard within this paper.~~

~~While one might be inclined to dismiss RH_w in excess of 102% as irrelevant for most atmospheric situations, there are a number of reasons why higher values are often referenced for continuous flow diffusion chambers. Primarily, continuous flow diffusion chamber instruments in general do not presently expose particles to uniform water supersaturations with the precision currently achieved by cloud condensation nuclei (CCN) instruments. The transition into the immersion freezing regime above water saturation does not occur sharply in line with the supersaturation calculated for the aerosol central lamina, but rather ensues completely only at higher RH_w as controlled by aerosol particle properties and instrument characteristics. For example, hygroscopicity and kinetic factors control water uptake, chambers have different flow rates and growth section lengths, there is a finite difference in RH_w across the aerosol lamina, and many devices appear (for as yet unclear reasons) often to induce a proportion of all particles to escape the defined aerosol lamina and expose these particles to lower RH_w (DeMott et al., 2015; Garimella et al., 2017). Some additional discussion of this point is given later in this paper. The consequence is that when one seeks to represent complete immersion of all particles into liquid water and subsequent freezing, then an RH_w nominally greater than 100% is used, sometimes up to the limit before water droplet breakthrough occurs (DeMott et al., 2015). Hence, higher RH_w is used in these instruments to bypass limitations in achieving CCN activation on the entire particle population, and to increase the condensation rate and thus water content of the formed droplets. In this context, instrument RH_w is not used to simulate the cloud supersaturations and time scales that parcels would experience in ascending air masses (as is simulated in the AIDA cloud chamber – see next section). It is also the case that a single RH_w value may not lead to the same activation fraction of particles in different instruments. This leads to inherent uncertainty in comparing results from these chambers, an issue that we will only acknowledge here, but did not plan~~

~~as a special focus of study in FIN-02. We suggest that individual instrument teams need to understand these behaviors of their instruments sufficiently and that they be accounted for when performing measurements in the ambient atmosphere. Consequently, decisions on the RH_w value reported for comparison of immersion freezing or proximal behaviors of these instrument systems to other immersion freezing devices was up to each instrument team. While these are the primary comparisons made in this paper, we note that the continuous flow instruments processed dry particle samples by slowly "scanning" RH_w from near ice saturation conditions to water supersaturated conditions (see DeMott et al., 2011 for discussion of these methods, and the Supplement section S.1.2 for a few examples), and these data have been archived from FIN-02. Investigators were then asked to select those data they felt represented the highest (not necessarily maximum) immersion freezing activity it was deemed possible to assess in their RH_w scans, and reported the INP concentrations and RH_w values selected.~~

The focus on reporting of flow chamber data at highly supersaturated conditions as best representing proximal immersion freezing behaviors is motivated by recent research and publications. Presently, continuous flow diffusion chamber instruments in general do not expose particles to uniform water supersaturations with the precision achieved by cloud condensation nuclei (CCN) instruments. Rather, the transition into the immersion freezing regime above water saturation does not occur sharply in line with the supersaturation calculated for the aerosol central lamina, but ensues completely only at higher RH_w as controlled by aerosol particle properties and instrument characteristics. For example, hygroscopicity and kinetic factors control water uptake, chambers have different flow rates and growth section lengths, there is a finite difference in RH_w across the aerosol lamina, and many devices appear (for as yet unclear reasons) often to induce a proportion of all particles to escape the defined aerosol lamina and expose these particles to lower RH_w outside of the intended central lamina (DeMott et al., 2015; Garimella et al., 2017). Hence, higher RH_w is used in these instruments to bypass limitations in achieving CCN activation on the entire particle population, and to increase the condensation rate and thus water content of the formed droplets. The justification is to make the measurement conditions (most particles placed in cloud droplets larger than a few μm prior to freezing) more similar to the cloud parcel simulations in the AIDA cloud chamber (see next section) with more typical cloud supersaturations and time scales. In practice, continuous flow instruments processed dry particle samples by slowly "scanning" RH_w from near ice saturation conditions to water supersaturated conditions (see DeMott et al., 2011 for discussion of these methods, and the Supplement Section S.1.2 for a few examples. Investigators were then asked to select those data they felt represented the highest (not necessarily maximum) immersion freezing activity possible to assess in their RH_w scans, and reported the INP concentrations and RH_w values selected.

For continuous flow diffusion chambers in FIN-02, no additional corrections besides internal losses (if known) were applied. In other words, correction factors to account for the inability to assess maximum activation in the supersaturated regime, as discussed by DeMott et al. (2015), Garimella et al. (2017), and Burkert-Kohn et al. (2017) were not applied. We discuss particle losses in lines feeding various instruments in section 2.4.

Unique among the continuous flow chambers in FIN-02 was the combination of the PIMCA (Portable Immersion Mode Cooling chamber) device in series with the PINC instrument, referred to herein as PIMCA-PINC, wherein droplets are first activated on individual dry particles at temperatures above 0°C prior to cooling during flow into the colder temperature PINC to observe immersion freezing (See Supplement Section S.1.6). This is intended to provide

the most explicit simulation of immersion freezing. Experimental trajectories for PIMCA-PINC essentially follow those of ~~offline~~ post-processing immersion freezing devices (see below), but activation is on single, immersed particles. We note that either PINC or PIMCA-PINC operations were exclusive for a given INP type on a given day.

The CIC-PNNL flow diffusion chamber instrument was also operated at times in a non-standard manner to activate droplets at high supersaturation under modest supercooling in its upper chamber region and cool them to immersion freezing in the lower chamber region during FIN-02 studies (Kulkarni et al., 2018), but only data collected in the standard manner of generating near steady-state supersaturation at a single lamina temperature were included in the comparison presented herein.

The 84 m^3 AIDA controlled expansion cloud chamber was used to perform experiments serving as cloud parcel comparison to other measurements. In this regard, we follow the example of the 2007 workshop, and a key recommendation from ice nucleation workshops prior to that time that an expansion cloud chamber be utilized to provide a simulation of cloud activation (DeMott et al., 2011). Schematic thermodynamic paths of the AIDA chamber experiments are shown by the yellow curves in Fig. 1. Of note in this regard is the fact that small supersaturations occur prior to cloud formation in AIDA, but once droplets are activated on all particles, the cooling follows at water saturation until a point where evacuation can no longer sustain cooling against the surrounding warmer volume, and clouds begin to dissipate. In this regime at water saturation, a comparison to continuous flow chambers should not be made at water saturation, but only for the higher supersaturations that assure more complete droplet activation within the sample lamina of CFDCs. For comparison to immersion freezing results by other methods, we have omitted AIDA experiments for which high ice nucleation rates were achieved at below water saturation (e.g., deposition nucleation regime), and wherein full subsequent activation of particles as CCN was not achieved due to rapid ice growth.

2.2 ~~Offline~~ Post-processing systems

~~Among~~ Two types of instruments ~~that~~ post-processed particle collections. ~~in different experiments~~ These were diffusion chamber devices that processed particles collected onto substrates and devices that recorded freezing by particles within liquid droplets or confined liquid volumes. Thermal diffusion chamber devices that processed particles on substrates during FIN-02 were the FRIDGE (FRankfurt Ice nucleation Deposition freezinG Experiment) instrument operated to above water saturation in its standard mode (Klein et al., 2010; Schrod et al., 2016), referred to here as FRIDGE-STD (see Supplement section S.2.10), and the DFPC-ISAC (Dynamic Filter Processing Chamber - Institute of Atmospheric Sciences and Climate, National Research Council of Italy) instrument (Santachiara et al., 2010; Belosi et al., 2014; see Supplement Section S.2.11). These two methods were ~~originally designed~~ developed to ~~address the~~ measure condensation freezing and deposition ice nucleation modes from below to slightly above ~~at~~ water saturation ~~and below~~. ~~However, the uncertain difference between condensation freezing and immersion freezing mechanisms (Vali et al., 2015) argues for an evaluation of both methods by including their results obtained at near water saturation in this intercomparison.~~ The thermodynamic path of measurements using these instruments is the same as for the continuous flow diffusion chambers in Fig. 1 (red lines), but typically terminate ~~close to~~ 1-2% RH_w above water saturation. Both devices were designed with the intention to overcome the so-called "volume effect" on freezing (e.g.,

Bigg, 1990; Schrod et al., 2016 and references therein) which describes the underestimation of INPs that can occur when processing particles on a substrate in a diffusion chamber due to vapor pressure reduction by the first particles freezing, especially when larger volumes are collected that result in larger numbers of INPs per surface area of the substrate. The FRIDGE instrument seeks to limit this effect using a low-pressure diffusion chamber to enhance vapor deposition over particles collected onto silicon wafer substrates, while the DFPC instrument follows the methods of Langer and Rodgers (1975) to focus a flow of humid air over filter substrates, and using the best practices outlined by Bigg (1990). For both devices, attempts were made to limit particle collections to shorter times during FIN-02, in order to keep particle loading light on the substrates. An additional fundamental differences between FRIDGE and the DFPC is the use of the filter substrate in the latter case, which is placed on a paraffin layer that is heated to establish thermal contact with a cold plate prior to ice nucleation measurements. ~~For these two instruments, no limitation on condensing water and freezing particle populations is assumed for cases of light particle loading on substrates, as this limits reduction of saturation ratio over the substrates due to growth of some particles as ice. These instrument teams were allowed to evaluate possible influence of water vapor competition on limiting supersaturation over their substrates in each experiment, prior to entering data into comparisons shown herein. Attempts were made to limit particle collections to shorter times that would keep particle loading light on the substrates, but high aerosol concentrations generated for accessing ice active fraction over several orders of magnitude led to some uncertainty in defining appropriate collection times. When the influence of vapor competition on ice nucleation and growth were inferred, experimental results from these diffusion chambers were eliminated from comparisons.~~ The uncertain difference between condensation freezing and immersion freezing mechanisms (Vali et al., 2015) argues for an evaluation of results obtained near water saturation in this intercomparison as representative of proximal immersion freezing, for both instruments.

~~Wet suspension~~ Immersion freezing measurements of ~~immersion freezing~~ collected particles suspended in water are depicted in Fig. 1 by the blue arrows. These measurements fall along the water saturation line because collected particles are suspended in pure water whose final water activity is essentially 1. In some cases, the mass and surface area within liquid water volumes is varied over several orders of magnitude of weight percent, via adding purified water for dilution, in order to cover a range of activation temperatures ~~of activation~~. The various water ~~wet~~ suspension methods for immersion freezing used in FIN-02 are listed and referenced in Table 2. ~~Details on all of t~~The specific immersion freezing methods are also ~~given~~ described in the Supplement to this manuscript. The basic types of methods used involved: 1) cooling arrays of droplets of particle suspensions placed on a cold stage and within oil, as done with the Carnegie Mellon University Cold Stage (CMU-CS) and the Karlsruhe Institute of Technology Cold Stage (KIT-CS); 2) cooling of suspension aliquot volumes in array compartments, as done with the CSU Ice Spectrometer (IS) and the Bielefeld Ice Nucleation ARraY (BINARY); 3) creating and cooling emulsions of particle suspensions as done in the Vienna Optical Droplet Crystallization Analyzer (VODCA) instrument; 4) cooling of droplets containing particles that are pipetted directly onto a coated hydrophobic glass slide, as done with the University of Leeds Microliter Nucleation by Immersed Particles Instrument (μL-NIPI) and the North Carolina State University Cold Stage (NCSU-CS), and using similar droplet arrays on the FRIDGE substrates (referred to as FRIDGE-IMM in this case, for FRIDGE Immersion Freezing); 5) freezing of a droplet train within a microfluidic device WeIzmann

Supercooled Droplets Observation on Microarray (WISDOM); 6) and cooling of levitated particles as in the Mainz Acoustic Levitator (M-AL).

Most groups using ~~wet~~ liquid suspension freezing methods ~~groups~~ shared common samples from collections into liquid water (see discussion of sampling protocol in section 2.3), while in many cases the IS and FRIDGE-IMM measurements involved processing particles re-suspended from filters in pure water. Among these ~~wet suspension~~ measurements, only the µL-NIPI, hereafter simply NIPI, measurements were conducted immediately after collection at KIT, while others processed the samples at their home institutes.

~~2.3 AIDA chamber~~

~~Finally, in addition to besides the two basic methods for assessing ice nucleation activity, the 84 m^3 AIDA controlled expansion cloud chamber, denoted as AIDA hereafter, was used to perform experiments to form clouds via expansion cooling, serving as a cloud parcel comparison to other measurements. In this regard, we follow the example of the 2007 workshop, and a key recommendation from prior ice nucleation workshops prior to that time that an expansion cloud chamber be utilized to provide a simulation of cloud activation (DeMott et al., 2011). Schematic thermodynamic paths of the AIDA chamber experiments isare shown schematically by the yellow curves in Fig. 1. Of note in this regard is the fact that small supersaturations occur prior to cloud formation in AIDA, but once droplets are activated on all particles, then cooling follows at water saturation until a point where evacuation cannot sustain cooling against the surrounding warmer volume, and clouds begin to dissipate. In this regime at water saturation, it needs to be understood again that comparison to continuous flow chambers should not be made for those instruments at water saturation, but only for the higher values that assure more complete droplet activation within their sample lamina. For comparison to immersion freezing results by other methods, we have omitted AIDA experiments for which high ice nucleation rates were achieved at below water saturation (e.g., deposition nucleation regime), and wherein full subsequent activation of particles as CCN was not achieved due to rapid ice growth.~~

2.~~4~~3 Generation of varied INP types and general study procedures ~~Ice nucleating particles and aerosol generation~~

A variety of relevant aerosol particle types were produced for FIN-02 studies, as listed in Table 3. These types reflect key mineral compounds of atmospheric desert dust aerosols (illite NX) or their key components (K-feldspar), natural soil dust samples of varied arability collected from different regions of the world (Argentinian soil dust, erodible Tunisian soil dust, Saharan dust), and a biological (microbial, proteinaceous) INP type (Snomax®). These different INPs also span a range of activation temperatures that cover most of the mixed-phase cloud regime (i.e., 0 to -36°C). Thus, ~~so~~they provide a stringent examination of measurement capabilities and any biases that may occur.

Aerosol generation methods largely followed those presented in Hiranuma et al. (2015). Particles were independently provided to two different chambers, these being the AIDA chamber and a 4 m^3 holding chamber that will be referred to here as the aerosol particle chamber (APC). A total of 27 AIDA and 29 APC experiments were carried out during FIN-02. The particle types used for all 56 experiments are summarized in Table 3. Dry soil and

mineral dust particles were generated using a rotating brush disperser (PALAS, RBG1000) and were subsequently passed through a series of inertial cyclone impactor stages (with 50% cut-point diameters of about 5 and 1 μm) prior to introduction into each chamber. This was an important step in limiting the numbers of particles present at sizes above 1 μm and emphasizing ~~mode~~ sizes that could be efficiently sampled by all measurement systems, including continuous flow devices. While natural particle distributions may sometimes include INPs to much larger sizes, it was deemed important for this study to limit this factor that can lead to measurement discrepancies due to sampling limitations. Size distributions of dry particles were measured using a scanning mobility particle sizer (SMPS, TSI Inc., Model 3081 differential mobility analyzer, DMA, and Model 3010 condensation particle counter, CPC) and an aerodynamic particle sizer (APS, TSI Inc., Model 3321). Particles were assumed to be spheres, and dynamic shape factors and particle densities listed in Table 3 were used to obtain the geometric-based (volume equivalent) diameters from the SMPS and APS data (Hiranuma et al., 2014b; 2015). Total particle surface areas were calculated and tabulated as a function of time using lognormal fits to size distributions in each experiment, as shown for two exemplary soil dust experiments (one AIDA and one APC) in Fig. 2.

Aerosol generation from aqueous suspensions was used during FIN-02 to generate INPs from Snomax® ~~suspensions~~. The injection of Snomax® particles into the ventilated APC and AIDA vessels was achieved by atomization of a 5 g Snomax® suspension in 1 L of 18.2 MΩ ultrapure water followed by a diffusion dryer. The home-built atomizer used in Wex et al. (2015) was employed for all Snomax® particle generation. A total of eight polydisperse Snomax® injections were performed during FIN-02 (Table 3). Accordingly, aerosolized Snomax® particles were characterized for total number concentration and size distribution during each experiment.

Due to the efforts made to limit the generation of supermicron particles, the ~~online~~direct sampling ice nucleation instruments typically operated without special upstream impactors that would be used during atmospheric sampling to limit aerosol particles entering at sizes that could be mistaken as grown ice crystals (i.e., many CFDCs differentiate ice and aerosols by size alone). However, ~~it was the case~~ in a few experiments ~~that~~ some larger particles were present ~~and~~ that could contribute to size channels that typically demarcate only ice crystals. Redefinition of ice channels was done in some those cases to enable use of data from these experiments. An example of such corrections is given in Supplement Section S.1.2.

The daily protocol determined for aerosol generation and measurements is an aspect of these studies that bears strongly on the organization and discussion of results in this manuscript. Especially, sampling periods were organized to optimize the opportunities and conditions for all instruments to sample the variety of aerosols. Each day over the three-week workshop period typically began with fills of one INP type into the APC, and sampling of that aerosol into liquid and onto filters over a two-hour period for later assessment by the post-processing devices, as detailed below. This was followed by the direct samplers processing the same INP type from the APC over another two-hour period. This typically permitted direct measurement at a couple specific temperatures, with data at other temperatures being acquired on another day for the same INP type (from the APC or AIDA). Then, at midday, the AIDA chamber would be filled, typically with a different INP type than used in the morning APC experiments. Direct sampling from AIDA by the flow chambers would occur over a period of time just prior to the start of expansion cooling experiments. As well, collections onto filters or wafers used by the DFPC and FRIDGE device (standard method) would be made only

from the AIDA aerosol fill on each day, since these methods required very short sampling times in order to limit particle loading. For example, the DFPC-ISAC filters were collected for periods of 10's of seconds. Other collections into liquid or onto filters for immersion freezing post-processing would not occur from the AIDA chamber prior to expansions. A consequence of these procedures is that we will find it convenient to present results on different bases when discussing sampling from the APC and from AIDA. While we might ideally wish to present all data on the same basis as measurements are reported for atmospheric sampling, as number concentrations, we choose to do so only for the APC experiment period that offers the opportunity for comparing the most measurement systems. We describe how that is done next. For AIDA sampling, we will display results as active fractions and ice active site density, which then allows integrating APC results along with AIDA results for the same INP types over the course of the workshop.

An example of a timeline of APC aerosol particle properties at the start of an ~~typical~~ experimental day is shown in Fig. 3 to demonstrate a typical morning of activity that integrated sampling by post-processing and direct systems for subsequent analyses. ~~On most days, a first period involved generation of particles into the APC and the start of sampling for offline measurement systems.~~ The chamber was initially filled with a high concentration of aerosol particles to create appropriate sampling conditions for the ~~offline~~ systems for immersion freezing post-processing, which ~~typically require~~ can utilize high total particle concentration ($0.4 <$ mass concentration < 40 mg m^{-3}) in order to take advantage of the ability of some of these methods to assess the lower INP concentrations active at modest supercooling. Collection of particles into liquid suspensions for shared use by a suite of immersion freezing devices was performed by impinging a flow of particles from the APC into a glass bioaerosol sampler (SKC Inc.) (Hader et al., 2014; DeMott et al., 2017), referred to here as impinger samples. Two impinger samples were collected for ~120 min with a flow rate of 12.5 L min^{-1} from the APC. Flows were checked daily. Impingers were cleaned by wiping, rinsing with ultrapure water (18 MΩ-cm), and soaking in isopropyl alcohol overnight (2-propanol, ≥99.8%, ROTH). Before assembly the impingers were rinsed using ultrapure water water once more. Following the sampling of Snomax® particles, the impingers were baked overnight at 200°C instead of soaking in alcohol. This was done to eliminate the possibility of carryover by ice active due to these biological samples. During sampling the water was replenished every ~30 minutes to keep the water level near 20 mL. Due to evaporation, the final bottled volume was typically about half of the added water. The two impinger suspensions were combined into one sample and topped off to a total of ~36 mL. The sample was divided into 4 ml aliquots, bottled in pre-cleaned DNA free cryovials and stored locally in a freezer at -20°C. The same procedure was applied to the handling of blanks. At the end of the campaign, blanks and samples were placed on dry ice and shipped overnight to participating groups. Shipment to Israel was delayed by customs, allowing the sample to thaw en-route. After receiving the sample, each group decided on their own sample storage and handling strategies. Again, we note that the University of Leeds group performed NIPI measurements of these suspensions on-site in Karlsruhe immediately after collection (i.e., without freezing).

Filter collections from the APC were made for post-processing by the ~~total of s~~even ~~samplers devices (i.e., DFPC-ISAC filter,~~ NCSU CS ~~State particle into liquid impingers – one devoted to the Leeds group, NC State filter~~, FRIDGE ~~filters~~ (for immersion freezing), CSU IS ~~filter~~, and Leeds NIPI instruments. ~~, and STXM/NEXAFS grids for future study) were employed and~~ These filters (0.2 μm pore size polycarbonate) ran up to 100 min, aligned with ~~It was typical to for the NC State and CSU filters to operate over~~ the same time period as the impingers. ~~, while~~ The FRIDGE filters

were collected over multiple and shorter time periods (10 min) within this same time frame. Clean protocol for preparation of filters prior to sampling is discussed within the IS instrument description in the Supplement (Section S.2.3). ~~The DFPC-ISAC filters were only collected during sampling from the AIDA chamber, and over periods of 10's of seconds to limit particle loading for steady state chamber measurements.~~

In some cases, aerosol particle concentrations were sufficiently depleted that an additional APC fill was done to augment collections and suffice for the later sampling by direct sampling ~~(dry particle)~~ systems. ~~When this was done, the separate impinger samples for each period were combined prior to being divided for distribution and processing by different groups.~~ A smaller injection of aerosol mass and concentration was typically used during the second fills in order to optimize sampling conditions for the ~~online~~ direct sampling instruments (i.e., they would immediately begin sampling from the APC at that point). Other sampling was suspended for the direct sampling period. Such a two-stage injection period is highlighted in Fig. 3 by two regions of blue shading. Smoothed, interpolated aerosol curves are shown in Fig. 3. Exponential fits to decay periods were found to represent particle number concentrations with r^2 values exceeding 0.98, as expected for the first order loss processes occurring in the APC during sampling. These loss processes were dominated by the drawing of air from the APC by samplers, replenished in all cases by clean synthetic air. Curves are shown for total particle numbers, numbers of particles larger than 0.5 μm ~~(only for comparison)~~, and total particle surface area (spherical equivalency assumed for measured particle diameters). By integrating the exponential fit functions during sampling periods (blue shading), the integrated number concentrations and surface areas were determined for the combination of ~~offline~~ sample periods for post-processing. While we focus in the following discussion on quantifying the decay of total (CPC) particle numbers in order to correct INP number concentration data during the direct sampling periods ("online" used as shorthand in equations) for equivalency with the prior post-processing collection periods ("offline" used as shorthand in equations), we noted (not shown) differences ranging from only 10-30% in fractional loss rates when instead using particle numbers in the larger size range (>500 nm) to characterize particle number decay over time in the APC. These relatively minor differences, evident in Fig. 3, are consistent with the limited physical loss mechanisms existing for particles with mode sizes as shown in Fig. 2, and with limited numbers of supermicron particles that might be subject to sedimentation. ~~For example, w~~

With reference to Fig. 3 and the fit to the exponential decay in any period i with start and end times t_{0i} and t_{1i}, respectively, the period average total aerosol concentration ($\bar{n}_{\mathrm{CPC,offline,i}}$) is given by,

$$\bar{n}_{CPC,offline,i} = \int_{t_{0i}}^{t_{1i}} a_i \exp(b_i\, t) = \frac{a_i}{b_i}(\exp(b_i t_{1i}) - \exp(b_i t_{0i})) \quad (1)$$

Then for i = 1 to x periods of offline or post-processing sampling of aerosols from the APC for interval times Δt_i,

$$\bar{n}_{CPC,offline} = \sum_{i=1}^{x} \Delta t_i n_{CPC,offline,i} \,/\, \sum_{i=1}^{x} \Delta t_i \quad (2)$$

The APC sampling period offered the best opportunity to directly compare all ice nucleation instruments aside from the AIDA chamber, and to do so in the most straightforward manner (fewest assumptions) possible, as number

concentrations per volume of air. ~~Because it was desired as a first inspection to compare as many instruments as possible by INP number concentration measurement alone,~~ To allow such a comparison, INP concentrations measured by ~~online~~ direct sampling systems during the later period (green shaded area in Fig. 3) at any sample time *t* were corrected to give equivalence to the volumetric INP concentration measured by ~~offline~~ post-processing systems during their integrated sampling periods. That is,

$$n_{INP,online,corr}(t) = n_{INP,online}(t)\,\overline{n}_{CPC,offline}/n_{CPC}(t) \quad (3)$$

Correction factors for the online period were sometimes well in excess of 1 and up to 13 in a few experiments, since ~~online~~ sampling from the APC oftentimes continued for more than a few hours after the impinger and filter sampling period had been completed. ~~Comparing online and offline systems during APC sampling as number concentrations per volume of air is considered the most straightforward comparison of equivalence due to requiring no special assumptions~~. We may note that integrated (spherical equivalent) surface areas for the post-processing samples~~ystems~~ are determined in the same manner as reflected in Eqs. 1 to 3 for results shown in Section 3.2.

~~In addition to APC experiments, the online instruments and a few offline samplers also drew aerosol particles from the AIDA chamber during the afternoon periods of each day.~~ Direct sampling by flow chambers from AIDA was done in the time prior to the start of cloud expansions. ~~In addition to the aforementioned~~ DFPC-ISAC and FRIDGE filter collections, ~~the~~ and collection of particles onto wafer substrates for use in the standard (deposition/condensation freezing) FRIDGE instrument processing mode (see Supplement Section 2.10) was also performed from the AIDA chamber for limited time periods, with the previously stated ~~a similar~~ goal to limit total particle number loading for the diffusion chamber measurements. Aerosol number concentrations were typically much lower in AIDA, and since the total volume of AIDA is much larger, the decay of number concentrations due to sampling by other instruments prior to expansion was much slower than in the APC. Thus, in most cases, comparison measurement from other instruments to the AIDA ice crystal activation results could be made directly, with a small correction at times to account for the slightly higher ~~(in this case)~~ total particle (CPC) number concentrations at the time of sampling versus those during the subsequent AIDA expansion. We compare activated fractions and the deterministic active site density parameter in these experiments so that multiple AIDA sampling experiments of the same aerosol types performed on different days may be included. This also allows for comparison of selected APC results to AIDA chamber results for similar aerosol types across the entire workshop period. This type of comparison also allows evaluation of measurement consistency, and comparison to previously published parameterizations.

We use calculated geometric aerosol surface areas, under the assumption of spherical equivalent diameters, to compute and compare surface active site densities, $n_{s,geo}\ (T)$ (m^{-2}). Assuming a uniform distribution of $n_{s,geo}\ (T)$ over a given total aerosol surface area (S_{tot}) and its size independency, we follow Hiranuma et al. (2015) to approximate $n_{s,geo}\ (T)$ as,

$$n_{s,geo}(T) \approx \frac{n_{INPs}(T)}{S_{tot}} \quad (4)$$

Uncertainty in $n_{s,geo}$ *(T)* is computed in quadrature from the confidence interval data for each INP type and assuming a 25% uncertainty in S_{tot}. S_{tot} is computed by normalizing the integrated aerosol surface area (μm^2 cm^{-3}) by total particle number concentrations. Integrated surface areas listed in Table S1 of the Supplement are determined based on lognormal fits to the aerosol distribution merged over the full particle size range from aerodynamic and aerosol mobility measurements (Fig. 2). Values of $n_{s,geo}$ *(T)* will be listed and plotted in m^{-2} herein.

Finally, we note that no corrections for particle losses in sample lines are made for comparisons shown herein. This is due to the fact that these losses may be assumed to be negligible in comparison to other uncertainties as defined by confidence intervals for the measurements. As noted in Fig. 2, both particle number and surface area in these experiments were mainly from particles in the size range between 0.1 and 1 μm. Using the worst-case sampling scenario, which was for the PIMCA-PINC instrument sampling from the AIDA chamber (flow rate of 1.6 L min^{-1} through 5 m of 0.457 cm interior diameter stainless tubing, and assumed bulk particle density of 2.6 g cm^{-3}), calculations of estimated penetration efficiency through tubing versus particle size were made using equations from Baron and Willeke (2005). Calculations captured diffusional losses in tubing, inertial losses in a straight tube (i.e., incline was ignored), and impaction losses in tubing (four 90° bends assumed). This demonstrated that penetration efficiency likely exceeded 88% at all sizes below 1 μm, and even at a size of 2 μm, the proximal upper size generated in any experiments, ~60% of the particles should have reached all instruments. All investigators were given the ability to re-evaluate data quality and potential experimental issues after the original archive was produced. The amount of data contributed to final comparisons varied widely amongst the different instruments, in some cases due to operational issues that arose during the workshop.

3 Results and Discussion

3.1 APC sampling of INPs

As discussed in Section 2, the primary basis for comparison of methods for sampling different INP types from the APC was for the measured or calculated number concentrations of INPs. Four experiments in which the largest number of ~~most~~ measurement methods sampled from the APC are shown in Figures 4 to 7. These comparisons necessarily exclude the AIDA chamber data. Each figure assesses, 1) comparisons of direct sampling devices ~~online~~ (larger blue colored symbols of different types are for the CFDC-CSU, SPIN-TROPOS and SPIN-MIT, CIC-PNNL, INKA and PIMCA-PINC) versus collection and post-processing instruments (all other symbols of various types and colors); 2) comparison of different ~~offline~~ methods for immersion freezing post-processing, whether as droplet ~~immersion freezing~~ arrays on substrates or in aliquot wells (IS, BINARY, NIPI, KIT-CS, NCSU-CS, CMU-CS, VODCA, FRIDGE-IMM), in microfluidic devices (WISDOM), ~~or in diffusion chambers (FRIDGE STD)~~ or in an acoustic levitator ~~electrodynamic traps~~ (M-AL); 3) shared (most immersion freezing arrays or devices using the common impinger samples) versus individual samples (IS and FRIDGE-IMM); and 4) different collection methods (filters for IS and FRIDGE-IMM, except for Snomax®; impingers for others).

The comparisons obtained for sampling Argentinian soil dust particles (Fig. 4) were among the best in this study. A ~~most~~ striking feature of these results is the general correspondence betweenamongst ~~all~~ methods and sampling

techniques in ranges of overlap, as well as the apparent meshing of results from direct sampling and post-processing of immersion freezing to capture ~~mostly within one order of magnitude in INP number concentrations across the entire mixed phase temperature regime, which is good agreement when put in the perspective of INP number concentration increases of about~~ 7 or more orders of magnitude of INP activity in the~~is~~ temperature regime from -5 to -35°C. Direct overlap showing correspondence of the continuous flow methods with a minimum of four different bulk methods occurs over 3 orders of magnitude range at temperatures from -20 to -30°C. Good consistency is also seen amongst direct sampling methods as a group and ~~whether comparing~~ post-processing~~offline~~ methods taken together, ~~versus online in their temperature range of overlap~~, ~~within the online and offline two categories of measurement types~~, for shared impinger samples~~offline method~~s, and whether post-processed ~~offline~~ samples were ~~are~~ collected by impinger or separate polycarbonate filters (IS and FRIDGE-IMM) that were subsequently rinsed of particles. Recall ~~Note~~ that the IS filter was collected simultaneously with the impinger sample, while the FRIDGE-IMM filter was collected over a shorter time frame. ~~Greatest~~ The largest discrepancies, in consideration of measurement uncertainties (see Supplement for explanation of measurement uncertainties for each device~~al~~) occur at the coldest temperatures. In this region, data from the PIMCA-PINC instrument, which activates individually-grown droplets on particles prior to cooling, falls at the upper end of measured INP concentrations in comparison to the few other immersion methods that extended to the heterogeneous ice nucleation limit, just warmer than homogeneous freezing temperatures. We note again here that some scatter may occur in the direct processing methods due to investigators deciding in each case what ~~the imperfect understanding of what value for processing~~ RH_w above 100% to report data for as representing~~represents complete~~ immersion freezing. ~~No correction has been made for this issue, previously discussed by DeMott et al. (2015), Garimella et al. (2017) and Burkert-Kohn et al. (2017), which would drive the online flow chamber data to higher values. Nevertheless, overall, the inter-comparison represented in Fig. 4 is encouraging.~~

Measurements for a Tunisian desert dust sampling experiment in the APC are shown in Fig. 5. Fewer overall measurements are available for this comparison. Nevertheless, results are similar to those obtained for the Argentinian soil dust sample, albeit with a slightly higher than one order of magnitude overall range of values measured by all methods at any particular temperature. A somewhat steeper inflection in data near -20°C is noted in this case, which may exacerbate discrepancies between methods due to temperature uncertainties alone. Within the ~~offline~~ immersion freezing methods sharing the impinger sample, variance increases from a factor of a few to more than an order of magnitude at colder temperatures. Two FRIDGE-IMM samples were collected 15 minutes apart for this experiment, and demonstrate results that span the range of INP concentrations measured by all methods at temperatures near -20°C. The two FRIDGE-IMM filter samples also bracket the results from the IS filter collection that spanned the same time frame as the impinger sample. At the coldest temperatures examined, a separation develops between the directly sampled ~~online~~ (higher) and post-processed ~~offline~~ (lower) INP concentration ranges. And as for the Argentinian soil sample, the PIMCA-PINC data cap the ~~online~~ direct processing instrument measurements of Tunisian soil dust at the coldest temperatures, leading to nearly a two order of magnitude discrepancy of measured INP concentrations at below -32°C. Thus, this experiment is consistent with the experiment for Argentinian soil dust particles in showing good agreement amongst INP measurements, but with the largest uncertainties typically occurring at the very warmest and coldest ends of the temperature spectrum, where ice nucleation activity is lowest and highest, respectively.

Although both of the soil dust examples show a sigmoidal ice nucleation activation temperature spectrum, this is more pronounced for the less "desert-like" sample from Argentina. This likely reflects the activity of different sized particles and the presence of multiple INP types or ice active sites, with the warmest freezers possibly from proteinaceous and other heat labile organic INPs achieving a plateau of activation at temperatures warmer than -20°C (see, e.g., O'Sullivan et al., 2014; Hill et al., 2016; Beydoun et al., 2017). This sigmoidal behavior is also seen in the upper bound of precipitation water immersion freezing spectra (Petters and Wright, 2015) and in natural particle samples collected over arable soil regions, where it has been attributed to soil and plant emissions (Delort and Amato, 2018). The levelling-off of the ice nucleating activity at low temperatures is also similar to desert dust laden air observed around Cape Verde (Price et al., 2018).

For the conditions of overlap between directly sampled and post-processing~~online and offline~~ methods (<-20°C), neither of the soil dust examples tested show the types of discrepancies noted for the mineral illite NX (Emersic et al., 2015; Hiranuma et al., 2015; Beydoun et al., 2016). Co-location of instruments, limitation of the size range of particles collected, and sharing of common samples collected ~~at the same times~~ simultaneously onto filters or into liquid may have all contributed to the consistency of results for natural soil dusts in this study. If true, it does not mean that different methods will agree in atmospheric measurements, but rather that the differences that do occur are influenced by other sampling limitations (e.g., sizes of particles that can be assessed, etc.) (Burkert-Kohn et al., 2017; DeMott et al., 2017). This would also apply to intercomparisons in which laboratories in different places are free to dispense samples independently prior to comparison. ~~Alternatively, or i~~In addition, it may be the case that the soil dusts examined in this study have specific features for activation that differ from minerals or proxy dusts like illite NX, and these are less influenced by water immersion and storage either cool or frozen.

Results for illite NX as a test aerosol will be addressed below in the discussion of sampling experiments directly from AIDA and comparison of all results by active site density. K-feldspar was examined as an additional example of a mineral aerosol in this study. This K-feldspar sample is referred to as FS02, as described in Atkinson et al. (2013) and Peckhaus et al. (2016), and has similar ice nucleating activities to other K-feldspars with microtexture (Whale et al., 2017). A ~~C~~comparison of INP concentrations in Fig. 6 shows similar results as for the soil dust samples, but the INP activation curve of K-feldspar particles is much steeper with a pronounced levelling-off below about -25°C (i.e., it reaches a maximum and is only weakly dependent on temperature). This steepness is associated in this case with an up to two order of magnitude spread among ~~offline~~ bulk sample immersion freezing methods at around -25°C, greater than for the natural soil dusts at this temperature. This may be partly explained by temperature uncertainties, which range from ±0.2 to ±0.5°C for the immersion freezing methods (see specific Supplement sections for each device). Confidence intervals are also seen to be relatively large in this case, probably reflecting the high sensitivity of freezing to temperature. The leveling-off of INP concentrations below -25°C is consistent with previous measurements for K-feldspars summarized in Harrison et al. (2016) and Niedermeier et al. (2015). The separate filter sample (IS and FRIDGE-IMM) results are again consistent with those from instruments that shared the same impinger sample, although falling mostly to the upper side of these other measurements. A potential difference in this case is the time that particles may have spent stored in water, as the IS and FRIDGE-IMM results were presumably processed immediately after placing particles into liquid, thus minimizing time for flocculation of the clay. Most ~~online~~

~~samplers~~direct sampler results in Fig. 6 show ~~results~~ INP concentrations that are consistent with the upper bounds of ~~offline~~ post-processed immersion freezing measurements at below -20°C. Exceptions are the SPIN-MIT instrument data, elevated at -21.3°C, and the PIMCA-PINC data elevated at colder temperatures, as was seen for PIMCA-PINC data in the Argentinian and Tunisian soil dust experiments.

The experiments for soil dusts and minerals do not offer comprehensive comparisons of the consistency of all of the different measurement methods at cloud temperatures warmer than about -20°C. Using a more active INP type within this temperature regime, Snomax® bacterial INPs, offers the opportunity for such assessment, as shown in Fig. 7. The unique activation properties of these INPs suggest separating the discussion around two temperature regions of Fig. 7; for temperatures warmer and colder than about -9°C. Online measurements were only obtained at temperatures colder than -9°C, where the ice nucleation activity is found to be maximized and only weakly dependent on temperature~~, likely due to the fact that aggregates of only two to four proteins are predicted to be involved in freezing at -9°C (Govindarajan and Lindow, 1988) and single proteins of these bacteria are likely sufficient at somewhat colder temperatures~~. Thus, biases should be solely due to uncertainty in derived INP concentration in this colder temperature regime. The excellent agreement in INP concentrations between all direct and post-processed ~~online and offline~~ methods suggests biases of at most a factor of 5 in this case.

All bulk immersion freezing methods ~~(all results, including those for the IS, are from shared impinger samples in this case)~~ capture the strong rise in activation due to the presence of the most active biological ice nucleators, those within the realm of the Groups I and II as defined by Yankofsky et al. (1981). This is expressed~~, noted~~ as a pronounced shoulder in all freezing spectra at temperatures warmer than -8°C in Fig. 7. We may note here that all bulk freezing methods shared the same impinger sample in this case, including the IS. This warm temperature shoulder of ice nucleation activity has also been demonstrated by Wex et al. (2015), Budke and Koop (2015), and Polen et al. (2016). Nevertheless, discrepancies are most strongly apparent in this region where these larger and more fragile aggregates of ice nucleating proteins are responsible for the ice nucleation activity. Measurement discrepancies across all immersion freezing methods are seen to range from one to four orders of magnitude (up to 4°C equivalent difference), increasing toward the warmest temperatures in this temperature region in Fig. 7. This appears to result largely from a bifurcation of freezing behavior of the (warmest) first-freezers in multiple freezing scans of the thawed CMU-CS impinger sample, and a similarly strong increase in the activation of first freezers in a few NIPI scans that were processed without prior storage as a frozen sample (i.e., processed immediately after collection, the only group to do so), including following dilution of the sample performed in order to access colder freezing temperatures for droplet arrays. The CMU-CS results in two of four scans appear to reflect the instability of Group I freezers noted in previous studies, possibly dependent on the time delay involved in conducting a freezing experiment following thawing of the impinger sample (Polen et al., 2016). How the individual freezing assays were separated for averaging is described in the Section S.2.2. ~~upporting Information~~. In summary, the s~~ource of variations~~ strong variability in activity seen at ~~in~~ the warmest activation temperature regime for Snomax® particles brings into question the ability to utilize the warmest temperature (> -10°C) freezing behavior of Snomax® reliably for calibration purposes. This has been noted previously~~, as similarly noted~~ by Polen et al. (2016), and attributed to ~~(e.g., due to~~ batch-to-batch variability and the loss of activity following long-term ~~in~~ storage~~)~~. The freezing behaviors at colder than -10°C are quite stable, and a simple conclusion

from this experiment is that there is no fundamental limitation or apparent bias in the ability of any method ~~(online or offline)~~ to measure immersion freezing activation in the modestly supercooled temperature regime warmer than -15°C versus below -20°C, at least for detecting biological INPs in relatively high numbers. Hence, if disagreements occur between ~~online and offline~~direct and post-processing methods in this temperature regime, one possibility is that such disagreement relates to the impact of immersion in water on ice nucleation activity for certain particle types whose morphology can be altered in water (e.g., Grawe et al., 2016) and/or other differences in activation of single particles by ~~online~~ direct processing methods versus particle populations placed into bulk water, sometimes stored frozen for later processing.

3.2 Sampling of INPs from the AIDA chamber and comparison to subsequent AIDA freezing results

Data collected in coordination with AIDA experiments provided additional intercomparisons. These data were first analyzed as active fractions, which is the number fraction of all particles freezing when normalized to the total number concentrations of particles (potential INP)~~ types~~ present at the onset of expansions. Because of the large volume of the AIDA chamber, only modest differences in aerosol particle concentrations existed in the time prior to expansion start. Despite more limited participation, most ~~online~~ direct measurement systems and a few ~~offline~~ diffusion chamber systems (using collected filters or substrates) processed particles in these experiments. Generally lower INP number concentrations in AIDA limited any chance that INP number concentrations achieve values that might lead to vapor depletion in the continuous flow instruments (Levin et al., 2016). Use of active fraction allowed for inclusion and comparison of data from multiple AIDA experiments, and from APC experiments, to examine for consistency and repeatability. As discussed in Section 2.4, the active fraction data could be readily converted to active site density.

In Fig. 8, results are included for the illite NX, for which comprehensive experiments in the APC were not examined in Section 3.1. Figure 8a shows active fraction data from various ice nucleation instruments in multiple AIDA experiments (listed in Fig. 8 caption and Table S1), and from the ice concentrations measured in subsequent AIDA expansions. These results for illite NX show a scatter of INP active fraction at selected temperatures of more than two orders of magnitude, consistent with Hiranuma et al. (2015). Data from two FRIDGE-STD wafer collections demonstrate a variability factor of several fold despite collection of the particles in close temporal proximity. This could reflect the negative impacts of excess particle loading on causing water vapor depletion in the diffusion chamber as freezing ensues, limiting full activation at 1% supersaturation. Consistent with such an assumption, we note that sample 73 (lower set of FRIDGE-STD data points at -25 and -30°C) had four times the volume of sample 74 (higher active fraction data points at -25 and -30°C). The convergence of the FRIDGE-STD results toward the FRIDGE-IMM results is also noted for the latter sample. This issue of determining the suitable volume of air for collection for substrate ice nucleation studies given its dependence on the concentration of INPs has been recognized for many years. Nevertheless, correspondingly low active fractions at -25°C are also measured by PINC, a flow diffusion chamber that should have no issues with water vapor depletion. We may note, however, the strong sensitivity to processing supersaturation in flow diffusion chambers for sampling illite NX particles as reflected by the CFDC-CSU results at 105% and maximum RH_w prior to onset of water droplet breakthrough. We may further note that AIDA activated ice

number fractions for illite NX are bracketed by these CFDC-CSU results. These results are consistent with the findings of DeMott et al. (2015) for certain natural and desert dusts, suggesting that underestimates of INP concentrations active in the water supersaturated regime where immersion freezing sometimes dominates in CFDCs could be a general feature, also discussed by Garimella et al. (2017). A strong sensitivity of illite NX to RH_w may be partly responsible for the wider range of INP active fraction for diffusion chambers in this case, and the shorter residence time of the PINC instrument may contribute to its lower estimate in comparison to other continuous flow chambers at certain temperatures. Each continuous flow chamber also may stimulate different responses in regard to RH_w sensitivity, dependent on a variety of factors in addition to residence time that may include the evaporation section control. These things may require special study for the flow diffusion chambers as a group.

Data are plotted as $n_{s,geo}\ (T)$ values in Fig. 8b, and parameterizations developed from the study by Hiranuma et al. (2015) are overlain. This demonstrates that the single DFPC-ISAC chamber data point at -20°C and the upper bound values of FRIDGE-STD measurements are consistent with the $n_{s,geo}$ curve (log-space version shown as long-dashed curve) function found to represent immersion freezing measurement data by Hiranuma et al. (2015). A fair amount of the ~~online~~ direct sampling instrument data from AIDA sampling is also consistent with this function. Nevertheless, it is also the case that some portion of the ~~online~~ direct sampling instrument data, particularly the CIC, CFDC-CSU measurements at maximum water supersaturation, AIDA expansion results, and all lower temperature flow diffusion chamber data including the PIMCA-PINC, generally align with the Hiranuma et al. (2015) parameterization for results obtained from dry dispersion measurements in that study (short-dashed line in Fig. 8b). The FRIDGE-IMM results at warmer temperatures appear as the outlier, splitting the two parameterizations at the warm end of measurements.

When $n_{s,geo}\ (T)$ values derived from APC experimental results on illite NX particles are added in Fig. 8c, it becomes clear that most ~~offline~~ post-processed immersion freezing results in the present study align quite well with the parameterization of ~~offline~~ previous immersion freezing results from Hiranuma et al. (2015). Furthermore, it is seen that the DFPC-ISAC and FRIDGE-STD results, and the lower range of CFDC-type measurements (PINC, CFDC-TAMU) are most consistent with the immersion freezing data. However, we note the addition in Fig. 8c of CFDC-type measurements from APC experiments, including data from the CFDC-CSU, INKA, and SPIN-TROPOS instruments, which trend toward the dry suspension parameterization from Hiranuma et al. (2015). Most strikingly, these data, while limited to a few additional experiments, support the extension of this dry suspension relation to temperatures near -20°C, with the consequence that a three-order magnitude or more discrepancy occurs between direct and post-processed ~~online and offline~~ measurements at this temperature. The data noted in blue for CFDC-CSU and INKA were the only data collected in the March 13 experiment. Nothing peculiar stands out for the aerosol generated on that day, with sizes that did not reach close to ice crystal detection sizes. Hence, the bifurcation of INP behaviors of illite NX at different times and potentially by different methods are confirmed in the present study, and with no special new insights as yet into their source nor of the relevance of these discrepancies as a potential concern for atmospheric INP measurements. While proposed as an atmospheric dust surrogate, the ice nucleation behaviors of illite NX assessed by different methods contrast with the general equivalency of measurements of INP behaviors of natural soil dusts found in this study.

Agreement of methods for measuring the INP activity of Snomax® particles as shown in Fig. 7 is repeated in the AIDA experiments, as shown by $n_{s,geo}$ *(T)* calculations presented in Fig. 9a. Ice active site densities derived from fractional activation and particle surface areas in the AIDA experiments (listed in Fig. 9 caption) fall to the high side of other ~~online~~ direct processing measurements, but only by a modest factor of no more than a few, and within experimental uncertainties. Little difference is seen between CFDC-CSU results at 105% or the maximum RH_w achieved before water droplet breakthrough. As well, there is no discrepancy seen between the FRIDGE-STD and other results. This may be because Snomax® INPs have been observed to achieve their maximum activated fraction by 100% RH_w at temperatures below -10°C (DeMott et al., 2011), and so no strong artificial supersaturation dependence occurs. Prediction of $n_{s,geo}$ *(T)* on the basis of the n_m *(T)* (active site density per unit mass) determined in the Snomax® particle ice nucleation studies of Wex et al. (2015) is also presented in Fig. 9a. This conversion uses n_m *(T)* as given in Eq. 6 of Wex et al. (2015), divided by the surface area to mass concentration ratio, following Eq. 3 from Hiranuma et al. (2015). A surface area to mass concentration ratio value of 7.99 m^2 g^{-1} was derived from the Snomax® particle size distribution measurements made in association with the AIDA results reported in Wex et al. (2015). Particle generation methods for Snomax® used in the present AIDA experiments were identical to that prior study. It is seen that although the peak predicted $n_{s,geo}$ *(T)* values exceed the values measured by most methods in this study, it is by only a small amount. Since this demonstrates close consistency of the present experiments with past Snomax® experiments, we did not pursue the exercise of re-deriving the surface to mass concentration ratio particular to the FIN-02 studies. APC data were used to derive $n_{s,geo}$ *(T)* in Fig. 9b. This demonstrates repeatability during the FIN-02 studies for assessment of the ice nucleation activity of Snomax® INPs and a level of consistency with prior results that suggests the potential suitability of Snomax® as a bacterial INP calibrant surrogate, albeit with the mentioned caveats on the instability of detection of first freezers at the warmest temperatures.

AIDA experimental results converted to $n_{s,geo}$ *(T)* for Argentinian and Tunisian soil dusts are shown in Fig. 10a. As expected, the range of site density measured by the continuous flow chambers prior to expansion, and based on AIDA ice activation measurements during expansion, mimics a similar spread in INP number concentrations observed by all measuring systems in sampling from the APC. We also note the agreement between AIDA ice crystal activation in cloud parcel simulations and the INP measurements from the portable instruments in these two cases at near -25°C. The non-continuous-flow diffusion chamber results from these AIDA chamber experiments fall moderately to the low side of $n_{s,geo}$ *(T)* values for these dusts. The two dusts have similar activation properties at below -20°C, and the range of $n_{s,geo}$ *(T)* is at least partly consistent with multiple natural soil dust $n_{s,geo}$ *(T)* parameterizations, including O'Sullivan et al. (2014) for "fertile soil dust", Tobo et al. (2014) for "Wyoming soil dust" and Steinke et al. (2016) for "agricultural soil dust". Derived $n_{s,geo}$ *(T)* based on the APC experiments on Argentinian dust (Fig. 4) are overlain in panel b, and $n_{s,geo}$ *(T)* derived from APC Tunisian dust experimental data (Fig. 5) is overlain in panel c of Fig. 10. In contrast to larger discrepancies found for illite NX, $n_{s,geo}$ *(T)* results for both Argentinian and Tunisian dust shown in Fig. 10 demonstrate much greater consistency. Larger discrepancies occur only at the coldest temperatures, where the PIMCA-PINC measurements of direct freezing of single particles within droplets diverge to much higher values than most of the immersion freezing measurements. This is especially the case for the Tunisian dust results, where $n_{s,geo}$ *(T)* based on the maximum RH_w INP data from the CFDC-CSU do not clearly align with the PIMCA-PINC results in

the same manner that they do for Argentinian dust at colder temperatures. The WISDOM data also diverge strongly from other immersion freezing data at colder than -25°C. Finally, we may note that the $n_{s,geo}$ *(T)* results for the more loamy Argentinian dust align quite well with values predicted from previous studies of arable soil dusts in the studies of O'Sullivan et al. (2014) and Tobo et al. (2014), but not well with those predicted from Steinke et al. (2016). The Tunisian dust results in Fig. 10c show less consistency with the fertile soil dust parameterization, which may be expected due to the more arid nature of the Tunisian sample.

Finally, $n_{s,geo}$ *(T)* results for sampling K-feldspar particles from AIDA prior to expansions are shown in Fig. 11a, and the same data are overlain with APC data for K-feldspar in Fig. 11b. Additionally, an $n_{s,geo}$ *(T)* parameterization is added on the basis of the $n_{s,BET}$ *(T)* fit to immersion freezing ice nucleation data published by Atkinson et al. (2013), where the BET refers to the fact that the surface area employed is based on Brunauer–Emmett–Teller (BET) gas adsorption data rather than an estimate of geometric surface area. To convert the parameterization, we use the laser diffraction-based surface-to-mass conversion factor of 0.89 m^2 g^{-1} determined by Atkinson et al. (2013) and the specific BET surface area measured for the samples used in this study of 2.6 m^2 g^{-1}. Hence, the normalization factor is 2.6/0.89. While all of the data parallel the Atkinson et al. (2013) parameterization, agreement with it quantitatively is seen for selected ~~online~~ direct sampling instrument data and the limited AIDA data available for which water saturation was achieved in expansion tests for FS02. Exceptionally large spread in inferred $n_{s,geo}$ values occurs at -20°C. Note here that only the 105% RH_w data was usable for the CFDC-CSU and INKA instruments in this case because of an issue that was associated with and exacerbated by the steep activation curve of K-feldspar at this temperature. In particular, it was seen that very steep $n_{s,geo}$ *(T)* led to the appearance of small ice crystals in the optical particle counter spectra at just above the 3 μm size used to separate smaller liquid from larger ice particles. This is an unusual feature for this type of device, with nucleated ice crystals typically growing to larger optical channels (sizes), and it likely reflects the late freezing of liquid particles as they were evaporating and cooling upon entry into the evaporation region of the instruments. This possibility is unique to the present configuration of the CSU CFDC due to the adjustment of the walls in evaporation region to match the inner (cold) wall temperature. This issue could similarly be realized in any diffusion chamber if there is a "cold point" anywhere along the flow path. Consequently, the SPIN-MIT data shown were reprocessed to report their data at the coldest wall temperature measured in the instrument growth region. Further discussion of this issue is provided for the CFDC-CSU in the Supplement to this paper (Section S.1.2). An additional (red) data point is shown in Fig. 11 for the CFDC that is considered erroneously attributed to the activation temperature near -20°C, even though it aligns close to the AIDA chamber data. In this case, it was found that the rate of RH_w change during scanning from lower to higher values was too fast, and exacerbated the over-estimation of INPs on the basis of OPC particle size. We note that the INKA instrument used a larger channel (size) to count INPs, and at the reported water supersaturation 4%, smaller the ice crystals were not being counted. Hence, the ice size channel might have been redefined for the CSU instrument in order to report additional data, but we choose here to use the data instead to make a point about instrument design considerations. As a final note, it should be understood that scans of RH_w are not a typical operational practice when collecting atmospheric data. In this case, constant RH_w or step-wise values are used.

While the various $n_{s,geo}$ *(T)* data trend well overall with the previous parameterization for FS02 particles, correspondence amongst results in Fig. 11 is not as good as for the soil dust samples in the -20 to -25°C range, and more resemble the spread of results for illite NX, with separation of $n_{s,geo}$ *(T)* of up to three orders of magnitude. Again, the variance amongst measurements follows the steepness of the INP activity versus temperature. The steep ice activation function of K-feldspar in the region from -15 to -25°C has already been noted in Fig. 6. INP activity rises at least 10^6 times over the 10°C for K-feldspar in this range, whereas the steepest rise for the natural soil dusts is 10^3 to 10^4 units per 10°C. For illite NX the activity rises about 10^5 per 10°C. Thus, modest differences in temperature, or their control within instruments, equate to large differences in ice activation for K-feldspar.

4 Summary and Conclusions

Through careful coordination and collaboration in a laboratory setting, most of the objectives of the second phase of the Fifth Ice Nucleation Workshop were strongly advanced if not fully achieved, and the existence of the data set should continue to serve explorations of measurement consistencies and issues for applying different techniques in isolation or in tandem for making atmospheric ice nucleation measurements. Extensive comparisons involving a large number of teams and using multiple INP types were made within just a three-week workshop. Some operational issues occurred for investigators at times (obvious errors, measurement biases, inability to achieve comparative conditions for proximal immersion freezing) ~~We particularly note that some data were not added to this paper in circumstances where cases of clear error or measurement bias~~ and where these were recognized, data were either not entered into comparisons or in a few cases were revised. Some issues were investigated, such as the appearance of small ice in the CSU CFDC data for INPs with steep activation functions. ~~as noted in the manuscript above.~~ Others remain the subject of active investigation.

We may summarize the workshop results generally around the stated objectives as follows:

1) *Compare ice nucleation measurement systems for conditions considered to be equivalent as much as possible, across a wide dynamic temperature range, including temperatures warmer than -15°C.*

To simplify this first analysis of FIN-02 data, a focus was placed in this paper on immersion freezing nucleation and activation within continuous flow chambers in the water supersaturated regime, across a wide temperature range including temperatures warmer than -15°C through the use of bacterial INPs in selected experiments. ~~Excellent~~ The proximal behavior model for comparing immersion freezing by direct processing instruments versus bulk immersion freezing methods worked reasonably well, excepting cases noted later in this summary. Very good correspondence was obtained between many measurements for soil dusts and bacterial INPs, both ~~across~~ amongst instruments that directly-processed single particles and those that post-processed bulk aerosol collections~~online and offline methods~~ for assessing immersion freezing INP concentrations (Figures 4, 5, 7). Agreement of INP number concentrations and geometric active site density within less than about 1 order of magnitude was achieved under most circumstances analyzed herein for these three materials. This was strictly demonstrated for both direct and post-processed samples over a more limited temperature range, approximately -20 to -30°C for the soil dusts and -10 to -30°C for the bacterial INPs. For these atmospherically-relevant particle types ~~examined~~, no strong biases between ~~online and offline~~ the

two basic types of measurement systems were evident in thisir range of overlap. except primarily In the case of illite NX, where discrepancies seen in Hiranuma et al. (2015) were reproduced at temperatures warmer than -25°C.

The fact that agreements were much better quite good overall in this study may have been strongly assisted by the combination ofbe due to co-sampling the same aerosol particle sources in the same laboratory, sharing similar collected aerosol samples, and limiting the largest particle sizes assessed in workshop experiments to those that could readily be measured by all techniques. The nature of active sites for the various INPs examined may also have influenced comparability of direct particle sampling versus post-processed bulk collection online and offline methods across a major portion of the mixed-phase cloud temperature regime. Consequently, it appears that soil dust particles are much more equally assessed for INP content than some minerals and mineral mixtures, and may better serve as potential calibration INPs. This was supported by the worst agreement between methods, up to three orders of magnitude, for illite NX and the FS02 samples that have a very steep activation spectra versus temperature, which exacerbates disagreements that otherwise represent only a few degrees of temperature change. In the case of illite NX, where discrepancies seen in Hiranuma et al. (2015) were reproduced at temperatures warmer than -25°C. Productively, thisThe steep activation behavior of the FS02 also led to new the discovery of instrument behavior in the case of the finding that when sampling such INP types, CFDC cooling in the to achieve evaporation in the exit section of a CFDC can express "late" activation of ice crystals that remain at small sizes and should not be attributed to the set point temperature of the instrument growth regionCFDC instrument. It is worth noting thatThis may be an issue primarily for laboratory measurements of such INPs, since most natural INP T-spectral slopes are lower than for many of the samples tested, often only approximately 2 orders of magnitude per 10°C, rather than 5 orders or more per 10°C (DeMott et al., 2017; Price et al., 2018).

Assessment of agreement between direct processing of single particles and post-processing online and offline measurement systems was mostly only possible below -20°C since flow chamber online devices have a limit of detection which restricts measurements at warmer temperatures. The exception is in cases where the higher concentrations of bacterial INPs were assessed. Since biological/biogenic INPs are the most likely contributors to freezing at modest supercooling (e.g., Murray et al., 2012; Hoose and Möhler, 2012), it would seem valid that combining bulk aerosol sampling offline measurements to capture INPs at very modest supercooling with direct online measurements extending to colder temperatures within the same atmospheric study will lead to a reasonably valid representation of immersion freezing INPs (e.g., DeMott et al., 2017; Welti et al., 2018).

2) *Gain insights into how detection of ice nucleation is influenced by the specific configuration of similar measurement systems.*

Among offline measurements on samples collected for post-processing, there wasappears no particular or consistent bias between different approaches to bulk suspension measurements. Furthermore, there appears to be little discrepancy between measurements made with particles collected directly into liquid versus collection onto filters followed by resuspension into liquid. There also appear to be no discernable impacts of freezing samples versus processing them immediately, on the basis of the µl-NIPI versus other methods apart from impacts on the warmest temperature freezing of bacterial particles (e.g., results from Snomax® experiments). Factors affecting reproducibility, such as accuracy of temperature attributed to sample freezing and instability of the warmest bacterial INPs, are the

most important factors affecting the agreement between methods, which often spans an order of magnitude overall. Most ~~offline~~ measurement groups have likely performed careful assessments of their temperature measurements attributed to droplet volumes, but there is evidence that errors may occur due to the inability to perfectly assess temperature at the point of freezing (Beall et al., 2017).

For ~~offline~~ diffusion chamber measurements of collected particles, the need for awareness of volume effects on processed INPs remains as a requirement. Results in a few cases showed these measurements to fall to the low side in assessing immersion freezing nucleation. It may be necessary to collect varied volumes to assure that particle loading in different cases is not influencing accurate assessment of INP number concentrations.

Differences between INP measurements in the water-supersaturated regime by continuous flow chambers were seen, and ~~again~~ these differences likely relate to the ~~artificial~~ need of these systems to achieve higher than expected RH_w in order to fully activate aerosols to facilitate their subsequent immersion freezing on the full particle population within the diffusion chambers (DeMott et al., 2015; Garimella et al., 2017; Burkert-Kohn et al., 2017). These instruments may universally have an issue in focusing aerosol particles reliably into the center of the imposed RH_w field, among other factors that depend on particle types, including their hygroscopicity and ability to activate ice nucleation already in the sub-water saturated regime (not discussed in this paper). Solving the issue(s) involved could provide the ~~decision~~guidance on correcting these data for the RH_w-sensitivity factor present in the water supersaturated regime for all of these devices. Different systems have varied ability to achieve higher RH_w, depending on the different water breakthrough RH_w as imposed by device design (see Section 3 and Section S.1.2). For example, it was noted that the PINC instrument more commonly measured INP concentrations at the lower range of the flow chamber devices, which may be attributable to its shorter residence time. These systems will continue to be used in this manner to measure atmospheric INP activation, but will struggle to equivalent~~uniform~~ly capture activation to the same degree until issues are solved. Such solutions could involve redesign of how samples are introduced to the chambers. This is clearly deserving of a special study, which was beyond the scope of this workshop. Study of the use of different evaporation region temperatures also merits attention as it may impact detection of ice formation at higher RH_w. Limitations on assessing the impacts of larger aerosols as INPs in continuous flow instruments will remain, unless special inlets are developed.

Of note in this study is the agreement between most direct sampling and post-processing ~~online and offline~~ measurements at the colder temperatures in comparison to the large discrepancies found in a recent study comparing measurements of ambient particles (DeMott et al., 2017). We believe that this is attributable to assuring comparability of measurement methods in FIN-02 by restricting particle sizes, as mentioned above. This likewise implies that discrepancies between direct and post-processing methods can be expected to occur in ambient sampling when larger particles are present, although the source of those discrepancies as true impacts (i.e., of larger particles acting as individual INPs versus ~~de-agglomeration~~ breakup of INPs after time in bulk suspensions) must remain a topic of future research. Both bulk sample ~~offline~~ immersion freezing and proximal immersion freezing in the ~~online~~ flow diffusion chambers sometimes underestimate freezing in comparison to the PIMCA-PINC single particle immersion freezing method. For CFDC type instruments, this is partly understood as the need to achieve much higher RH_w, sometimes practically unachievable, to effectively simulate and capture immersion freezing (previous paragraph), requiring

corrections that were not applied in this study. Whether such corrections are the only reason for discrepancies with PIMCA-PINC require further investigations. Reasons why the ~~offline~~ bulk immersion freezing methods do not always agree with PIMCA-PINC may relate in some unresolved manners to factors at play during extended bulk immersion, such as breakup, sedimentation, and alteration of active sites. ~~of all particles into the same liquid volume.~~ It would be helpful if the PIMCA-PINC method could be extended to lower active fractions and INP concentrations, but this appears to be a fundamental limitation of the phase discrimination technique.

3) *Utilize different INP types to investigate if differences between instruments occur ~~vary~~ with these different types.*

The use of varied INP types was clearly vital in achieving the first two objectives summarized above. For example, the use of a highly active biological INP type clearly helped to demonstrate that there is no fundamental limit on INP detection by any method if limits of detection are met. It is not known if this conclusion is peculiar to the biological INPs, although these may be the most common and important type to detect in the warmer supercooled temperature regime. While the utility of Snomax® as a calibration INP was again demonstrated here, issues in achieving well-defined active fractions at temperatures above -9°C via post-processing of bulk collections for immersion freezing found in previous studies were repeated herein. Comparisons with direct processing methods was not obtained in this temperature regime, making this an important topic for future studies.

The use of both natural soils and mineral samples as INPs allowed for seeing that the soil INPs were more consistently measured within and across measurement methods compared to the mineral component K-feldspar and a material representing key mineral compounds of desert dust aerosols (illite NX). The steeper nucleation rate functions of the minerals were key to identifying the potential bias in production of ice nucleation in the evaporation sections of the CSU and INKA CFDC's, likely due to the additional cooling occurring there. Other devices that warm the airflow while reducing the relative humidity toward ice saturation to evaporate activated cloud droplets did not see small ice crystal production. Detection of the small ice crystals produced in this manner can be largely biased against through adjustment of the channel size used for ice detection in the optical particle counter, although mitigation through redesign may provide a more satisfactory long term solution. Further investigation of this issue is merited.

Through the use of multiple INP types, results from this workshop could also be compared versus previously published parameterizations. These comparisons were very encouraging for demonstrating reproducibility of laboratory study results in general, further supporting the picture of general consistency of present INP measurements within identified uncertainties.

The FIN-02 archive will remain for additional scientific investigations of topics explored, such as ~~at least limited~~ comparisons in the ice nucleation regime below water saturation (see below), analysis of experiments regarding homogeneous freezing and the role of particle pre-activation for ice formation. While the FIN-02 workshop objectives were generally achieved, a number of topical research needs remain and some recommendations are suggested.

- Although the coordinated sampling protocols during FIN-02 worked very well, and the possibility of establishing certain calibration standards was suggested, it is not practical for the majority of members of the international INP measurement community to gather with high frequency for such activities. It may be possible that similar correspondence of measurements can be obtained through the distribution of some

standards and the use of defined aerosol generation protocol. A basic attempt at such an exercise that restricts sample types to a natural dust and bacterial INPs is worth exploring, as a wide distribution exercise has only thus far occurred for illite NX. The general correspondence of present workshop data with n_s parameterizations derived in previous laboratory studies provides a positive outlook.

- Special investigation of detection of ice formation in the regime below water saturation remains as a need that will be only partially addressable with FIN-02 data due to somewhat limited range of temperatures assessed by most direct processing instruments. While the number of instruments involved in such an assessment is more limited, it is no less important for evaluation in regard to the use of ice nucleation instruments in the colder regions of the troposphere. For example, are similar results obtained or is there a wider discrepancy between shorter residence time diffusion chamber, substrate-based processing devices, and controlled expansion cloud chambers in this regime?
- Ice nucleation measurements are also needed for fundamental understanding of ice nucleation and of the nature of INPs, which an array of measurement devices can address better than a single technique. Questions remain on differences between condensation and immersion freezing (Vali et al., 2015; Burkert-Kohn et al., 2017), the nature of ice nucleation in the regime below water saturation (Higuchi and Fukuta, 1966; Marcolli, 2014), connecting practical measurements with molecular scale understanding and many other topics.
- Other focused studies involving instruments within direct and post-processing communities are recommended for addressing needs specific to these communities. For direct sampling, examples are a careful comparison of the operational characteristics of continuous flow instruments as a function of RH_w, and a rigorous comparison of use of optical size for detecting ice in CFDC-style instruments versus use of depolarization and machine learning methods. For post-processing methods, the role of sample storage aggregation and breakup as a function of particle loading and size in bulk immersion freezing studies deserves study.
- Establishing best practices for handling of bulk immersion freezing samples, and for limiting and correcting for the background freezing counts introduced in the water used for collection (for impingers) or for rinsing (of filters) is a topic that was not covered directly in FIN-02. Improvement and standardization of protocol would only help to improve the good results obtained across these methods in this study. This is a topic of a separate paper published in this special issue (Polen et al., 2018).
- The role of INP size and more careful quantification of biases involved in assessing this factor deserves more focused attention. The use of monodisperse aerosols in a workshop like FIN-02 would present logistical challenges, but would add an important dimension for study and greatly assist interpretation of results.
- The low INP concentration regime still presents a strong challenge for the measurement community, one that becomes critically important in atmospheric studies. Low INP concentrations are ubiquitous at modest supercooling, but can also occur at lower temperatures in the atmosphere. For existing direct sampling devices like flow chambers, no current comparisons have focused on their abilities to control and correct for background frost artifacts. While ambient measurement campaigns such as FIN-03 allow some focus on this topic, a laboratory campaign could do the same. Only post-processing methods for immersion freezing can

access the regime at modest supercooling. This limits temporal and spatial resolution, especially when sampling on aircraft. Can new methods be developed for directly assessing INP concentrations in larger sample volumes? Even modest improvement to direct methods to provide more overlap of measurement methods in the regime > -20°C would help to further evaluate the validity of meshing direct and post-processing methods to characterize INPs over the full mixed-phase temperature regime. Aerosol pre-concentration has been applied to extend the dynamic range of direct INP measurements in atmospheric studies (e.g., Tobo et al., 2013; Boose et al., 2016), but aerodynamic concentration methods bias against particle sizes much below 1 μm. Hence, it is worth investigating the possible use of other concentration methods applicable to the full aerosol size distribution, such as pre-condensation. Novel ideas are needed.

- Further comparisons for which the sampling groups are "blind" to the nature and concentrations of INPs being sampled could be useful toward giving confidence to the wider community that the INP measurement community is capable of recognizing issues and properly interpreting data. This will assist confidence and utility of larger global data sets. Such a comparison from FIN-02 will be reported on in a separate publication in preparation.
- Similar exercises as FIN-02 are also needed in sampling under ambient atmospheric conditions. This is the subject of the FIN-03 campaign that will be reported on separately.

Workshops such as FIN-02 will continue to play a large role in assessing measurement biases and ultimately improving the comparability of INP measurements made by a large community of researchers sampling on a global scale. The shared experience of these workshops is irreplaceable in providing special insights into the status of and issues involved in obtaining INP data in different scenarios that may be dominated by certain aerosol types. FIN-02 demonstrates that the INP measurement community remains on a progressive track towards assessing convergence between different methods used for INP quantification.

Data availability. Tables of all data used and plotted in this manuscript are included as Table S1 and Table S2 in the Supplement of this manuscript. These tables are also included with data archived in the KITopen data respository under doi:10.5445/IR/1000082906 (available upon publication). Other daa are available upon request.

Competing interests. The authors declare no competing interests.

Special issue statement. This article is part of the special issue "Fifth International Workshop on Ice Nucleation (FIN)". It is not associated with a conference

Acknowledgments. The FIN-02 campaign was partially-supported by U.S. National Science Foundation Grant # AGS-1339264, and by the U.S. Department of Energy's Atmospheric System Research, an Office of Science, Office of Biological and Environmental Research program, under Grant No. DE-SC0014487. P. J. DeMott, E. J. T. Levin, and K. J. Suski acknowledge additional support from NSF Grant # AGS-1358495. The following authors acknowledge

funding by the German Science Foundation (DFG) through the research unit FOR 1525 (INUIT): O. Möhler, N. Hiranuma, A. Peckhaus and A. Kiselev under MO 668/4-1, C. Budke and T. Koop under KO 2944/2-2, M. Szakáll and O. Eppers under SZ260/4-2, and H. Bingemer and D. Weber under BI 462/3-2. Y. Rudich acknowledges funding by the DFG Mercator fellowship. T.B. Kristensen acknowledges funding from the German Federal Ministry of Education and Research (BMBF) project 01LK1222B. A. Welti, P. Herenz, F. Belosi, G. Santachiara, J. Vergara-Temprado, H. Bingemer and J. Schrod acknowledge support funding for their research from the European Union's Seventh Framework Programme (FP7/2007-2013) project BACCHUS under grant agreement No. 603445. F. Belosi and G. Santachiara also acknowledge the Institute for Atmospheric and Environmental Sciences (Goethe-University Frankfurt) for support in filter collections. M. Burkert-Kohn was funded by grant no. ETH-17 12-1, ETH Zurich. H. Grothe, L. Felgitsch, and T. Seifried acknowledge funding from The Austrian Science Fund, FWF project number P26040. The University of Leeds team (T. F. Whale, H. P. Price, J. Vergara-Temprado, D. O'Sullivan, T. W. Wilson, and B. J. Murray) acknowledge support from the European Research Council (ERC, 240449 ICE; 632272 IceControl; 648661 MarineIce, 713664 CryoProtect) and the Natural Environment Research Council (NE/K004417/1, NE/I019057/1). S. D. Brooks, K. N. Collier, and J. Zenker acknowledge additional support from the U.S. National Science Foundation, Grant # ECS-1309854. M. J. Polen and R. C. Sullivan were supported by NSF Grants # CHE-1213718 and CHE-1554941, and M. J. Polen by an NSF Graduate Research Fellowship. M. D. Petters, S. S. Petters, and H. P. Taylor acknowledge additional support from NSF Grants # AGS-1010851 and # AGS-1450690. G. Kulkarni acknowledges support by the Office of Science of the U.S. Department of Energy (DOE) as part of the Atmospheric System Research Program. Pacific Northwest National Laboratory is operated for the U.S. DOE by Battelle Memorial Institute under contract DEAC05-76RL0 1830. Finally, all authors wish to acknowledge support from the AIDA team for preparing and operating the AIDA chamber, and supporting other operational logistics for this workshop.

References

Agresti, A. and Coull, B. A.: Approximate is better than "exact" for interval estimation of binomial proportions, The American Statistician, 52, 119-126, doi:10.1080/00031305.1998.10480550, 1998.

Archuleta, C. M., DeMott, P. J., and Kreidenweis, S. M.: Ice nucleation by surrogates for atmospheric mineral dust and mineral dust/sulfate particles at cirrus temperatures, Atmos. Chem. Phys., 5, 2617–2634, doi:10.5194/acp-5-2617-2005, 2005.

Ardon-Dryer, K. and Levin, Z.: Ground-based measurements of immersion freezing in the eastern Mediterranean, Atmos. Chem. Phys., 14, 5217-5231, doi:10.5194/acp-14-5217-2014, 2014.

Atkinson, J. D., Murray, B. J., Woodhouse, M. T., Whale, T. F., Baustian, K. J., Carslaw, K. S., Dobbie, S., O'Sullivan, D., and Malkin, T. L.: The importance of feldspar for ice nucleation by mineral dust inmixed-phase clouds, Nature, 498, 355-358, doi:10.1038/nature12278, 2013.

Baron, P. A., and Willeke, K., *Aerosol Measurement: Principles, Techniques, and Applications*, Second Edition, Wiley, 2005.

Beall, C. M., Stokes, M. D., Hill, T. C., DeMott, P. J., DeWald, J. T., and Prather, K. A., 2017: Automation and Heat Transfer Characterization of Immersion Mode Spectroscopy for Analysis of Ice Nucleating Particles, Atmos. Meas. Tech., 10, 2613-2626, https://doi.org/10.5194/amt-10-2613-2017.

Belosi, F., Santachiara, G., and Prodi, F.: Ice-forming nuclei in Antarctica: New and past measurements, Atmospheric Research 145–146, 105–11, doi:10.1016/j.atmosres.2014.03.030, 2014.

Benz, S., Megahed, K., Möhler, O., Saathoff, H., Wagner, R., and Schurath, U.: T-dependent rate measurements of homogeneous ice nucleation in cloud droplets using a large atmospheric simulation chamber, J. Photochem. Photobiol. A, 176, 208–217, doi:10.1016/j.jphotochem.2005.08.026, 2005.

Beydoun, H., Polen, M., and Sullivan, R. C.: Effect of particle surface area on ice active site densities retrieved from droplet freezing spectra. Atmos. Chem. Phys., 16, 13359–13378, doi:10.5194/acp-16-13359-2016, 2016.

Beydoun, H., Polen, M. and Sullivan, R. C.: A new multicomponent heterogeneous ice nucleation model and its application to Snomax bacterial particles and a Snomax–illite mineral particle mixture, Atmos. Chem. Phys., 17(22), 13545–13557, doi:10.5194/acp-17-13545-2017, 2017.

Boose, Y., Kanji, Z. A., Kohn, M., Sierau, B., Zipori, A., Crawford, I., Lloyd, G., Bukowiecki, N, Herrmann, E., Kupiszewski, P., Steinbacher, M. and U. Lohmann: Ice Nucleating Particle Measurements at 241K during Winter Months at 3580m MSL in the Swiss Alps, J. Atmos. Sci., 73, 2203-2228, 2016.

Buck, A.L.: New equations for computing vapour pressure and enhancement factor. J. Appl. Meteorol., 20, 1527–1532, doi:10.1175/1520-0450(1981)020<1527:NEFCVP>2.0.CO;2, 1981.

Budke, C. and Koop, T.: BINARY: an optical freezing array for assessing temperature and time dependence of heterogeneous ice nucleation, Atmos. Meas. Tech., 8, 689–703, doi:10.5194/amt-8-689-2015, 2015.

Burkert-Kohn, M., Wex, H., Welti, A., Hartmann, S., Grawe, S., Hellner, L., Herenz, P., Atkinson, J D., Stratmann, F., and Kanji, Z. A.: Leipzig Ice Nucleation chamber Comparison (LINC): intercomparison of four online ice nucleation counters. Atmos. Chem. Phys., 17, 11683–11705, https://doi.org/10.5194/acp-17-11683-2017, 2017.

Chou, C., Stetzer, O., Weingartner, E., Juranyi, Z., Kanji, Z. A. and Lohmann, U.: Ice nuclei properties within a Saharan dust event at the Jungfraujoch in the Swiss Alps, Atmos. Chem. Phys., 11(10), 4725-4738, doi:10.5194/acp-11-4725-2011, 2011.

Delort, A.-M., and Amato, P., Eds., *Microbiology of Aerosols*, John Wiley & Sons, Inc., 1st Edition, ISBN: 978-1119132288, 2018.

DeMott, P. J., Möhler, O., Stetzer, O., Vali, G., Levin, Z., Petters, M. D., Murakami, M., Leisner, T., Bundke, U., Klein, H., Kanji, Z., Cotton, R., Jones, H., Petters, M., Prenni, A., Benz, S., Brinkmann, M., Rzesanke, D., Saathoff, H., Nicolet, M., Gallavardin, S., Saito, A., Nillius, B., Bingemer, H., Abbatt, J., Ardon, K., Ganor, E., Georgakopoulos, D. G., and Saunders, C.: Resurgence in ice nucleation research. Bull. Amer. Meteor. Soc., 92, 1623-1635, doi:10.1175/2011BAMS3119.12011, 2011.

DeMott, P. J., Prenni, A. J., McMeeking, G. R., Tobo, Y., Sullivan, R. C. , Petters, M. D., Niemand, M., Möhler, O., and Kreidenweis, S. M.: Integrating laboratory and field data to quantify the immersion freezing ice nucleation activity of mineral dust particles, Atmos. Chem. Phys., 15, 393–409, doi:10.5194/acp-15-393-2015, 2015.

DeMott, P. J., Hill, T. C. J., Petters, M. D., Bertram, A. K., Tobo, Y., Mason, R, H., Suski, K. J., McCluskey, C. S., Levin, E. J. T., Schill1, G. P., Boose, Y., Rauker, A. M., Miller, A. J., Zaragoza, J., Rocci, K., Rothfuss, N. E., Taylor, H. P., Hader, J. D., Chou, C., Huffman, J. A., Pöschl, U., Prenni, A. J., and Kreidenweis, S. M.: Comparative measurements of ambient atmospheric concentrations of ice nucleating particles using multiple immersion freezing methods and a continuous flow diffusion chamber, Atmos. Chem. Phys., 17, 11227–11245, 2017.

Di Biagio, C., Formenti, P., Styler, S. A., Pangui, E. and Doussin, J.-F.: Laboratory chamber measurements of the longwave extinction spectra and complex refractive indices of African and Asian mineral dusts, Geophys. Res. Lett., 41, 6289–6297, doi:10.1002/2014GL060213, 2014.

Diehl, K., Debertshäuser, M., Eppers, O., Schmithüsen, H., Mitra, S. K., and Borrmann, S.: Particle surface area dependence of mineral dust in immersion freezing mode: investigations with freely suspended drops in an acoustic levitator and a vertical wind tunnel, Atmos. Chem. Phys., 14, 12343-12355, doi:10.5194/acp-14-12343-2014, 2014.

Eidhammer, T., DeMott, P. J., Prenni, A. J., Petters, M. D., Twohy, C. H., Rogers, D. C., Stith, J., Heymsfield, A., Wang, Z., Haimov, S., French, J., Pratt, K., Prather, K., Murphy, S., Seinfeld, J., Subramanian, R., and Kreidenweis, S. M.: Ice initiation by aerosol particles: Measured and predicted ice nuclei concentrations versus measured ice crystal concentrations in an orographic wave cloud, J. Atmos. Sci., 67, 2417–2436, doi:10.1175/2010JAS3266.1, 2010.

Emersic, C., Connolly, P. J., Boult, S., Campana, M., and Li, Z.: Investigating the discrepancy between wet-suspension- and dry dispersion-derived ice nucleation efficiency of mineral particles, Atmos. Chem. Phys., 15, 11311–11326, doi:10.5194/acp-15-11311-2015, 2015.

Fahey, D. W., Gao, R.-S., Möhler, O., Saathoff, H., Schiller, C., Ebert, V., Krämer, M., Peter, T., Amarouche, N., Avallone, L. M., Bauer, R., Bozóki, Z., Christensen, L. E., Davis, S. M., Durry, G., Dyroff, C., Herman, R. L., Hunsmann, S., Khaykin, S. M., Mackrodt, P., Meyer, J., Smith, J. B., Spelten, N., Troy, R. F., Vömel, H., Wagner, S., and Wienhold, F. G.: The AquaVIT-1 intercomparison of atmospheric water vapor measurement techniques, Atmos. Meas. Tech., 7, 3177-3213, doi:10.5194/amt-7-3177-2014, 2014.

Fan, J., Leung, L. R., Rosenfeld, D. and DeMott, P. J.: Effects of Cloud Condensation Nuclei and Ice Nucleating Particles on Precipitation Processes and Supercooled Liquid in Mixed-phase Orographic Clouds, Atmos. Chem. Phys., 17, 1017–1035, doi:10.5194/acp-17-1017-2017, 2017.

Friedman, B., Kulkarni, G., Beránek, J., A. Zelenyuk, A., Thornton, J. A., and D. J. Cziczo, D. J.: Ice nucleation and droplet formation by bare and coated soot particles, J. Geophys. Res., 116, D17203, doi:10.1029/2011JD015999, 2011.

Garimella, S., Kristensen, T. B., Ignatius, K., Welti, A., Voigtländer, J., Kulkarni, G. R., Sagan, F., Kok, G. L., Dorsey, J., Nichman, L., Rothenberg, D. A., Rösch, M., Kirchgäßner, A. C. R., Ladkin, R., Wex, H., Wilson, T. W., Ladino, L. A., Abbatt, J. P. D., Stetzer, O., Lohmann, U., Stratmann, F., and Cziczo, D. J.: The SPectrometer for Ice Nuclei (SPIN): an instrument to investigate ice nucleation, Atmos. Meas. Tech., 9, 2781-2795, doi:10.5194/amt-9-2781-2016, 2016.

Garimella, S., Rothenberg, D. A., Wolf, M. J., David, R. O., Kanji, Z. A., Wang, C., Rösch, M., and Cziczo1, D. J.: Uncertainty in counting ice nucleating particles with continuous diffusion flow chambers, Atmos. Chem. Phys. Discuss., doi:10.5194/acp-2016-1180, 2017.

Glen, A. and Brooks, S. D.: Single particle measurements of the optical properties of small ice crystals and heterogeneous ice nuclei, AS&T, 48:1, 1123-1132, doi:10.1080/02786826.2014.963023, 2014.

Grawe, S., Augustin-Bauditz, S., Hartmann, S., Hellner, L., Pettersson, J. B. C., Prager, A., Stratmann, F., and Wex, H.: The immersion freezing behavior of ash particles from wood and brown coal burning, Atmos. Chem. Phys., 16, 13911-13928, doi:10.5194/acp-16-13911-2016, 2016.

Govindarajan, A. G., and Lindow, S. E.: Size of bacterial icenucleation sites measured in situ by radiation inactivation analysis, Proc. Natl. Acad. Sci. U. S. A., 85(5), 1334–1338, 1988.

Hader, J. D., Wright, T. P., and Petters, M. D.: Contribution of pollen to atmospheric ice nuclei concentrations, Atmos. Chem. Phys., 14, 5433–5449, doi:10.5194/acp-14-5433-2014, 2014.

Harrison, A. D., Whale, T. F., Carpenter, M. A., Holden, M. A., Neve, L., O'Sullivan, D., Vergara Temprado, J. and Murray, B J.: Not all feldspars are equal: a survey of ice nucleating properties across the feldspar group of minerals, Atmos. Chem. Phys., 16, 10927–10940, doi:10.5194/acp-16-10927-2016, 2016.

Higuchi, K. and Fukuta, N.: Ice in the capillaries of solid particles and its effect on their nucleating ability, J. Atmos. Sci., 23, 187–190, doi:10.1175/1520-0469(1966)023<0187:IITCOS>2.0.CO;2, 1966.

Hill, T. C. J., Moffett, B. F., DeMott, P. J., Georgakopoulos, D. G., Stump, W. L., and Franc, G. D.: Measurement of ice nucleation-active bacteria on plants and in precipitation by quantitative PCR. Appl. Environ. Microbiol. 80(4):1256-1267, doi:10.1128/AEM.02967-13, 2014.

Hill, T. C. J., DeMott, P. J., Tobo, Y., Fröhlich-Nowoisky, J., Moffett, B. F., Franc, G. D., and Kreidenweis, S. M.: Sources of organic ice nucleating particles in soils, Atmos. Chem. Phys., 16, 7195–7211, doi:10.5194/acp-2016-1, 2016

Hiranuma, N., Paukert, M., Steinke, I., Zhang, K., Kulkarni, G., Hoose, C., Schnaiter, M., Saathoff, H., and Möhler, O.: A comprehensive parameterization of heterogeneous ice nucleation of dust surrogate: laboratory study with hematite particles and its application to atmospheric models, Atmos. Chem. Phys., 14, 13145–13158, doi:10.5194/acp-14-13145-2014, 2014a.

Hiranuma, N., Hoffmann, N., Kiselev, A., Dreyer, A., Zhang, K., Kulkarni, G., Koop, T., and Möhler, O.: Influence of surface morphology on the immersion mode ice nucleation efficiency of hematite particles, Atmos. Chem. Phys., 14, 2315–2324, doi:10.5194/acp-14-2315-2014, 2014b.

Hiranuma, N., Augustin-Bauditz, S., Bingemer, H., Budke, C., Curtius, J., Danielczok, A., Diehl, K., Dreischmeier, K., Ebert, M., Frank, F., Ho mann, N., Kandler, K., Kiselev, A., Koop, T., Leisner, T., Möhler, O., Nillius, B., Peckhaus, A., Rose, D., Weinbruch, S., Wex, H., Boose, Y., DeMott, P. J., Hader, J. D., Hill, T. C. J., Kanji, Z. A., Kulkarni, G., Levin, E. J. T., McCluskey, C. S., Murakami, M., Murray, B. J., Niedermeier, D., Petters, M. D., O'Sullivan, D., Saito, A., Schill, G. P., Tajiri, T., Tolbert, M. A., Welti, A., Whale, T. F., Wright, T. P., and Yamashita, K.: A comprehensive laboratory study on the immersion freezing behavior of illite NX particles: a

comparison of 17 ice nucleation measurement techniques, Atmos. Chem. Phys., 15, 2489–2518, doi:10.5194/acp-15-2489-2015, 2015.

Hoose, C., and Möhler, O.: Heterogeneous ice nucleation on atmospheric aerosols: a review of results from laboratory experiments, Atmos. Chem. Phys., 12, 9817–9854, doi:10.5194/acp-12-9817-2012, 2012.

Kanji, Z. A., Welti, A., Chou, C., Stetzer, O., and Lohmann, U.: Laboratory studies of immersion and deposition mode ice nucleation of ozone aged mineral dust particles, Atmos. Chem. Phys., 13(17), 9097-9118, doi:10.5194/acp-13-9097-2013, 2013.

Klein, H., Haunold, W., Bundke, U., Nillius, B., Wetter, T., Schallenberg, S., Bingemer, H.: A new method for sampling of atmospheric ice nuclei with subsequent analysis in a static diffusion chamber, Atmospheric Research, 96, 218-224, doi:10.1016/j.atmosres.2009.08.002, 2010.

Kohn, M., Lohmann, U., Welti, A., and Kanji, Z. A.: Immersion mode ice nucleation measurements with the new Portable Immersion Mode Cooling chAmber (PIMCA), J. Geophys. Res. Atmos., 121, 4713–4733, doi:10.1002/2016JD024761, 2016.

Kulkarni, G., China, S., Liu, S, Nandasiri, M., Sharma, N., Wilson, J., Aiken, A. C., Chand, D., Laskin, A., Mazzoleni, C., Pekour, M., Shilling, J., Shutthanandan, V., Zelenyuk, A., and Zaveri, R. A.: Ice nucleation activity of diesel soot particles at cirrus relevant temperature conditions: Effects of hydration, secondary organics coating, soot morphology, and coagulation, Geophys. Res. Lett., 43, 3580–3588, doi:10.1002/2016GL068707, 2016.

Kulkarni, G., and co-authors: A new method for operating a continuous flow diffusion chamber to investigate temperature and time dependence in immersion freezing study, in preparation for Atmospheric Measurement Technology Discussion, 2018.

Lafon, S., Sokolik, I. N., Rajot, J. L., Caquineau, S. and Gaudichet, A.: Characterization of iron oxides in mineral dust aerosols: Implications for light absorption, J. Geophys. Res., 111, D21207, doi:10.1029/2005JD007016, 2006.

Langer, G. and Rogers, J.: An Experimental Study of the Detection of Ice Nuclei on Membrane Filters and Other Substrata, J. Appl. Meteor., 14, 560-570, doi:10.1175/1520-0450(1975)014<0560:AESOTD>2.0.CO;2, 1975

Levin, E. J. T., McMeeking, G. R., DeMott, P. J., McCluskey, C. S., Carrico, C. M., Nakao, S., Stockwell, C. E., Yokelson, R. J., and Kreidenweis, S. M. (2016), Ice-nucleating particle emissions from biomass combustion and the potential importance of soot aerosol, *J. Geophys. Res. Atmos.*, 121, doi:10.1002/2016JD024879.

Lüönd, F., Stetzer, O., Welti, A., and Lohmann, U.: Experimental study on the ice nucleation ability of size-selected kaolinite particles in the immersion mode, J. Geophys. Res.-Atmos., 115(D14201), DOI:10.1029/2009jd012959, 2010.

Marcolli, C.: Deposition nucleation viewed as homogeneous or immersion freezing in pores and cavities, Atmos. Chem. Phys., 14, 2071–2104, doi:10.5194/acp-14-2071-2014, 2014.

McFarquhar, G. M., Ghan, S., Verlinde, J., Korolev, A., Strapp, J. W., Schmid, B., Tomlinson, J. M., Wolde, M., Brooks, S. D., Cziczo, D., Dubey, M. K., Fan, J., Flynn, C., Gultepe, I., Hubbe, J., Gilles, M. K., Laskin, A., Lawson, P., Leaitch, W. R., Liu, P., Liu, X., Lubin, D., Mazzoleni, C., Macdonald, A.-M., Moffet, R. C., Morrison, H., Ovchinnikov, M., Shupe, M. D., Turner, D. D., Xie, S., Zelenyuk, A., Bae, K., Freer, M., and Glen, A.: Indirect

and Semi-direct Aerosol Campaign, Bulletin of the American Meteorological Society, 92, 183-201, 10.1175/2010bams2935.1, 2011.

Möhler, O., Stetzer, O., Schaefers, S., Linke, C., Schnaiter, M., Tiede, R., Saathoff, H., Krämer, M., Mangold, A., Budz, P., Zink, P., Schreiner, J., Mauersberger, K., Haag, W., Kärcher, B., and Schurath, U.: Experimental investigation of homogeneous freezing of sulphuric acid particles in the aerosol chamber AIDA, Atmos. Chem. Phys., 3, 211–223, doi:10.5194/acp-3-211-2003, 2003.

Möhler, O., Büttner, S., Linke, C., Schnaiter, M., Saathoff, H., Stetzer, O., Wagner, R., Krämer, M., Mangold, A., Ebert, V., and Schurath, U.: Effect of sulphuric acid coating on heterogeneous ice nucleation by soot aerosol particles, J. Geophys. Res., 110, D11 210, doi:10.1029/2004JD005 169, 2005

Möhler, O., Field, P. R., Connolly, P., Benz, S., Saathoff, H., Schnaiter, M.,Wagner, R., Cotton, R., Krämer, M., Mangold, A., and Heymsfield, A. J.: Efficiency of the deposition mode ice nucleation on mineral dust particles, Atmos. Chem. Phys., 6, 3007–3021, doi:10.5194/acp-6-3007-2006, 2006.

Murray, B. J., O'Sullivan, D., Atkinson, J. D., and Webb, M. E.: Ice nucleation by particles immersed in supercooled cloud droplets, Chem. Soc. Rev., 41(19), 6519–6554, doi:10.1039/C2CS35200A, 2012.

Murphy, D. M. and Koop, T.: Review of the vapour pressures of ice and supercooled water for atmospheric applications, Q. J. Roy. Meteor. Soc., 131, 1539–1565, doi/10.1256/qj.04.942005.

Niedermeier, D., S. Augustin-Bauditz, S. Hartmann, H. Wex, K. Ignatius, and F. Stratmann (2015), Can we define an asymptotic value for the ice active surface site density for heterogeneous ice nucleation?, J. Geophys. Res. Atmos., 120, 5036–5046, doi:10.1002/2014JD022814.

Niemand, M., Möhler, O., Vogel, B., Vogel, H., Hoose, C., Connolly, P., Klein, H., Bingemer, H., DeMott, P., and Skrotzki, J.: A particle-surface-area-based parameterization of immersion freezing on desert dust particles, J. Atmos. Sci., 69, 3077–3092, doi:10.1175/Jas-D-11-0249.1, 2012.

O'Sullivan, D., Murray, B. J., Malkin, T. L., Whale, T. F., Umo, N. S., Atkinson, J. D., Price, H. C., Baustian, K. J., Browse, J., and Webb, M. E.: Ice nucleation by fertile soil dusts: relative importance of mineral and biogenic components, Atmos. Chem. Phys., 14, 1853-1867, 2014.

O′Sullivan, D., Murray, B. J., Ross, J. F., Whale, T. F., Price, H. C., Atkinson, J. D., Umo, N. S., and Webb, M. E.: The relevance of nanoscale biological fragments for ice nucleation in clouds, Sci. Rep., 5, 2015.

Peckhaus, A., Kiselev, A., Hiron, T., Ebert, M., and Leisner, T.: A comparative study of K-rich and Na/Ca-rich feldspar ice-nucleating particles in a nanoliter droplet freezing assay, Atmos. Chem. Phys., 16, 11477-11496, doi:10.5194/acp-16-11477-2016, 2016.

Petters, M. D., and Wright, T. P. (2015), Revisiting ice nucleation from precipitation samples, *Geophys. Res. Lett.*, **42**, 8758–8766, doi:10.1002/ 2015GL065733.

Polen, M., Lawlis, E. and Sullivan, R. C.: The unstable ice nucleation properties of Snomax® bacterial particles, J. Geophys. Res. Atmos., 121(19), 11,666-11,678, doi:10.1002/2016JD025251, 2016.

Polen, M., Brubaker, T., Somers, J., and Sullivan, R. C.: Cleaning up our water: reducing interferences from nonhomogeneous freezing of "pure" water in droplet freezing assays of ice-nucleating particles, Atmos. Meas. Tech., 11, 5315-5334, https://doi.org/10.5194/amt-11-5315-2018, 2018.

Prenni, A. J., P. J. DeMott, D. C. Rogers, S. M. Kreidenweis, G. M. McFarquhar, G. Zhang, and M. R. Poellot, 2009: Ice nuclei characteristics from M-PACE and their relation to ice formation in clouds. Tellus, 61B, DOI: 10.1111/j.1600-0889.2009.00415.x, 436-448.

Price, H. C., Baustian, K. J., McQuaid, J. B., Blyth, A., Bower, K. N., Choularton, T., Cotton, R. J., Cui, Z. Field, P. R., Gallagher, M., Hawker, R., Merrington, A., Miltenberger, A., Neely, R. R. III, Parker, S. T., Rosenberg, P. D., Taylor, J. W., Trembath, J., Vergara-Temprado, J., Whale, T. F., Wilson, T. W., Young, G., and Murray, B. J.: Atmospheric ice nucleating particles in the dusty tropical Atlantic. Journal of Geophysical Research: Atmospheres, 123. https://doi.org/10.1002/2017JD027560, 2018.

Pummer, B. G., Bauer, H., Bernardi, J., Bleicher, S., and Grothe, H.: Suspendable macromolecules are responsible for ice nucleation activity of birch and conifer pollen, Atmos. Chem. Phys., 12, 2541-2550, doi:10.5194/acp-12-2541-2012, 2012.

Reicher, N., Segev, L., and Rudich, Y., The WeIzmann Supercooled Droplets Observation on a Microarray (WISDOM), Atmospheric Measurement Techniques, 11, 233–248, 2018.

Rogers, D. C.: Development of a continuous flow thermal gradient diffusion chamber for ice nucleation studies, Atmospheric Research, *22*(2), 149-181, doi:10.1016/0169-8095(88)90005-1, 1988.

Rogers, D. C., DeMott, P. J., Kreidenweis S. M., and Chen, Y., A continuous flow diffusion chamber for airborne measurements of ice nuclei, J. Atmos. Oceanic Technol., 18, 725-741, doi:10.1175/1520-0426(2001)018<0725:ACFDCF>2.0.CO;2, 2001.

Santachiara, G., Di Matteo, L., Prodi, F., Belosi, F.: Atmospheric particles acting as Ice Forming Nuclei in different size ranges, Atmos. Res. 96, 266-272, 2010.

Schmitz, C. H. J., Rowat, A. C., Koster, S. and Weitz, D. A.: Dropspots: a picoliter array in a microfluidic device, Lab on a Chip, 9, 44–49, doi:10.1039/B809670H, 2009.

Schiebel, T., Höhler, K., Levin, E. J. T., Nadolny, J., Suski, K. J., Weber, I., DeMott, P. J., Leisner, T., and Möhler, O.: The new continuous flow diffusion chamber INKA for ice nucleation measurements, In preparation for submission to Atmos. Meas. Tech, Discuss., 2018.

Schill, G. P., Jathar, S. H., Kodros, J. K., Levin, E. J. T., Galang, A. M., Friedman, B., Link, M. F., Farmer, D. K., Pierce, J. R., Kreidenweis, S. M. and DeMott, P. J.: Ice-nucleating particle emissions from photochemically-aged diesel and biodiesel exhaust, Geophys. Res. Lett., 43, 5524–5531, doi:10.1002/2016GL069529, 2016.

Schnaiter, M., Büttner, S., Möhler, O., Skrotzki, J., Vragel, M., and Wagner, R.: Influence of particle size and shape on the backscattering linear depolarisation ratio of small ice crystals – cloud chamber measurements in the context of contrail and cirrus microphysics, Atmos. Chem. Phys., 12, 10465-10484, doi:10.5194/acp-12-10465-2012, 2012.

Schrod, J., Danielczok, A., Weber, D., Ebert, M., Thomson, E. S., and Bingemer, H. G.: Re-evaluating the Frankfurt isothermal static diffusion chamber for ice nucleation, Atmos. Meas. Tech., 9, 1313-1324, doi:10.5194/amt-9-1313-2016, 2016.

Steinke, I., Funk, R., Busse, J., Iturri, A., Kirchen, S., Leue, M., Möhler, O., Schwartz, T., Schnaiter, M., Sierau, B., Toprak, E., Ullrich, R., Ulrich, A., Hoose, C., and Leisner, T.: Ice nucleation activity of agricultural soil dust

aerosols from Mongolia, Argentina, and Germany, J. Geophys. Res. Atmos., 121, 13,559-13,576, doi:10.1002/2016JD025160, 2016.

Stetzer, O., Baschek, B., Löünd, F., and Lohmann, U.: The Zurich Ice Nucleation Chamber (ZINC)—A new instrument to investigate atmospheric ice formation, Aerosol Sci. Technol., 42(1), 64–74, doi:10.1080/02786820701787944, 2008.

Tan, I., T. Storelvmo, and M. D. Zelinka, 2016: Observational constraints on mixed-phase clouds imply higher climate sensitivity, Science, 352 (6282), 224-227, doi:10.1126/science.aad5300.

Tobo, Y., P. J. DeMott, T. C. J. Hill, A. J. Prenni, N. G. Swoboda-Colberg, G. D. Franc, and S. M. Kreidenweis, 2014: Organic matter matters for ice nuclei of agricultural soil origin. Atmos. Chem. Phys. Discuss., 14, 9705–9728.

Vali, G.: Quantitative evaluation of experimental results on the heterogeneous freezing nucleation of supercooled liquids. J. Atmos. Sci., 28, 402–409, doi:10.1175/1520-0469(1971)028<0402:QEOERA>2.0.CO;2, 1971.

Vali, G., DeMott, P. J., Möhler, O., and Whale, T. F., Technical Note: A proposal for ice nucleation terminology, Atmos. Chem. Phys., 15, 10263–10270, doi:10.5194/acp-15-10263-2015, 2015.

Wagner, R., Möhler, O., Saathoff, H., Schnaiter, M., and Leisner, T.: New cloud chamber experiments on the heterogeneous ice nucleation ability of oxalic acid in the immersion mode, Atmos. Chem. Phys., 11, 2083–2110, doi:10.5194/acp-11-2083-2011, 2011.

Welti, A., Müller, K., Fleming, Z. L., and Stratmann, F.: Concentration and variability of ice nuclei in the subtropical maritime boundary layer, Atmos. Chem. Phys., 18, 5307-5320, https://doi.org/10.5194/acp-18-5307-2018, 2018.

Wex, H., Augustin-Bauditz, S., Boose, Y., Budke, C., Curtius, J., Diehl, K., Dreyer, A., Frank, F., Hartmann, S., Hiranuma, N., Jantsch, E., Kanji, Z. A., Kiselev, A., Koop, T., Möhler, O., Niedermeier, D., Nillius, B., Rösch, M., Rose, D., Schmidt, C., Steinke, I., and Stratmann, F.: Intercomparing different devices for the investigation of ice nucleating particles using Snomax® as test substance, Atmos. Chem. Phys., 15, 1463-1485, doi:10.5194/acp-15-1463-2015, 2015.

Whale, T. F., Murray, B. J., O'Sullivan, D., Wilson, T. W., Umo, N. S., Baustian, K. J., Atkinson, J. D., Workneh, D. A., and Morris, G. J.: A technique for quantifying heterogeneous ice nucleation in microlitre supercooled water droplets, Atmos. Meas. Tech., 8, 2437-2447, 2015

Whale, T. F., Holden, M. A., Kulak, A. N., Kim, Y.-Y., Meldrum, F. C., Christenson, H. K., and Murray, B. J.: The role of phase separation and related topography in the exceptional ice-nucleating ability of alkali feldspars, Phys. Chem. Chem. Phys., , 19, 31186—31193, doi: 10.1039/c7cp04898j, 2017.

Wright, T. P. and Petters, M. D.: The role of time in heterogeneous freezing nucleation, J. Geophys. Res. Atmos., 118, 3731–3743, doi:10.1002/jgrd.50365, 2013.

Yankofsky, S. A., Levin, Z., Bertold, T. Sandlerman, N.: Some basic characteristics of bacterial freezing nuclei, J. Appl. Meteor., 20, 1013-1019, 1981.

Zenker, J., Collier, K. N., Xu, G., Yang, P., Levin, E. J. T., Suski, K. J., DeMott, P. J., and Brooks, S. D., Using depolarization to quantify ice nucleating particle concentrations: a new method, Atmos. Meas. Tech., 10, 4639–4657, https://doi.org/10.5194/amt-10-4639-0, 2017.

Table 1. Direct processing ~~ry aerosol based online~~ INP instruments

Instrument	Type	Institute	References
AIDA	Expansion cloud chamber	Karlsruhe Institute of Technology	Möhler et al. (2003); Möhler et al. (2005); Niemand et al. (2012)
CFDC-CSU	Continuous flow diffusion chamber (cylindrical)	Colorado State University	Rogers (1988); Rogers et al. (2001); Eidhammer et al. (2010)
CFDC-TAMU	Continuous flow diffusion chamber (cylindrical)	Texas A&M University	Glen and Brooks (2014); Zenker et al. (2017)
INKA	Continuous flow diffusion chamber (cylindrical)	Karlsruhe Institute of Technology	Schiebel (2017)
SPIN-MIT	Continuous flow diffusion chamber (parallel)	Massachusetts Institute of Technology	Garimella et al. (2016)
SPIN-TROPOS	Continuous flow diffusion chamber (parallel)	Institute for Tropospheric Research	Garimella et al. (2016)
CIC-PNNL	Continuous flow diffusion chamber (parallel)	Pacific Northwest National Laboratory	Friedman et al. (2011) and Kulkarni et al. (2016)
PINC PIMCA-PINC	Continuous flow diffusion chamber (parallel) Immersion mode adaptation	ETH-Zurich	Chou et al. (2011); Kanji et al. (2013); Kohn et al. (2016)

Table 2. ~~Dry and wet suspension offline~~ Post-processing INP instruments

Instrument	Type	Institute	References
NCSU-CS	Cold stage droplet freezing array	North Carolina State University	Wright and Petters (2013); Hader et al. (2014); Hiranuma et al. (2015).
CMU-CS	Cold stage droplet freezing array in oil	Carnegie Mellon University	Polen et al. (2016); Beydoun et al. (2017)
KIT-CS	Cold stage droplet freezing array in oil	Karlsruhe Institute of Technology	Peckhaus et al. (2016)
µL-NIPI	Cold stage droplet freezing array	University of Leeds	Whale et al. (2015)
BINARY	Cold stage droplet freezing array in compartments	Bielefeld University	Budke and Koop (2015)
IS	Aliquot array freezing	Colorado State University	Hiranuma et al. (2015); Hill et al. (2016)
VODCA	Cold stage emulsion freezing	Technical University of Vienna	Pummer et al. (2012)
WISDOM	Microfluidics droplet freezing train	Weizmann Institute	Reicher et al. (2017)
M-AL	Acoustic levitator	University of Mainz	Diehl et al. (2014)
FRIDGE-STD	Low pressure diffusion chamber (Si wafers)	Goethe University of Frankfurt	Klein et al. (2010); Schrod et al. (2016)
FRIDGE-IMM	Cold stage droplet freezing array (on wafers)	Goethe University of Frankfurt	Hiranuma et al. (2015)
DFPC-ISAC	Dynamic filter processing chamber	ISAC-CNR	Santachiara et al. (2010); Belosi et al. (2014)

Table 3. List of aerosol types, particle generation techniques and aerosol properties.

Aerosol type[†]	Generator	AIDA Expt. ID	APC Expt. ID	BET specific sfc. (m^2 g^{-1})[*]	Density (g cm^{-3})[**]	Dynamic Shape Factor[**]	Reference[§]
Illite NX (IS03)	Rotating brush (PALAS, RGB1000)	FIN02_4,10, 22,25	APC_1-4,7-8	124.4	2.6	1.3	Hiranuma et al. (2015)
Argentinian soil dust (SDAr01)	Rotating brush (PALAS, RGB1000)	FIN02_5,9,24,26	APC_9-10,20-21,29	13.1	2.6	1.2	Steinke et al. (2016)
Saharan desert dust (SD6)	Rotating brush (PALAS, RGB1000)	FIN02_3	APC_5-6	6.9	2.6	1.2	Niemand et al. (2012)
Tunisian soil dust (SDT01)	Rotating brush (PALAS, RGB1000)	FIN02_7,12	APC_11-12,27	7.0	2.6	1.2	Lafon et al. (2006); Di Biagio et al. (2014)
K-rich feldspar (FS02) BCS376	Rotating brush (PALAS, RGB1000)	FIN02_8,11, 14	APC_13-14	2.6	2.6	1.1	Atkinson et al. (2013); Peckaus et al. (2016)
Snomax (SM04)	Atomizer (TSI, 3076)	FIN02_6,13, 27	APC_15-16,18-19,28	N/A	1.4	1.1	Wex et al. (2015)

[†]IDs in parentheses represent the AIDA-INUIT code names.

[*]The BET method to measure specific surface area of bulk powder is described in Hiranuma et al. (2014a). Note that our measurements have ± 5% uncertainty.

[**]For our geometric surface area estimations, we used the optimized effective densities and dynamic shape factors provided in this table.

[§]Bulk composition data of aerosols are available in these references. For SD6 and SDT01, XRD data are available upon request.

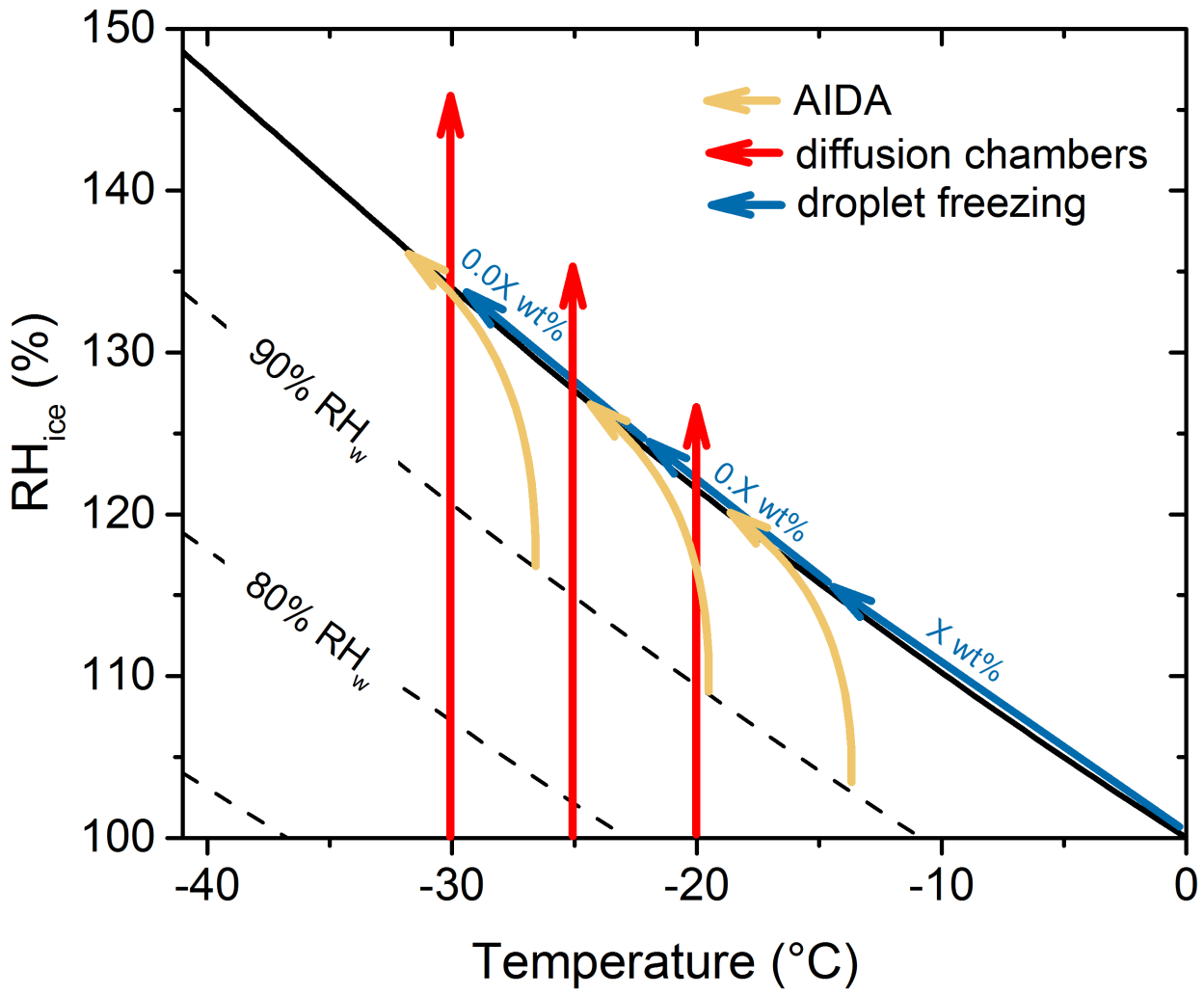

Figure 1. Schematic representation of different experiments conducted in the mixed-phase cloud temperature regime using different measurement systems during FIN-02. Yellow curves and arrows show the typical thermodynamic path of AIDA cloud chamber experiments. Red lines with arrows indicate the typical trajectory of ~~online~~ direct particle sampling, continuous flow instrument systems and ~~offline~~ systems that process substrate-collected initially dry particle populations under controlled humidity and temperature conditions. The blue arrow following the water saturation line in *T*-RH_w space shows the trajectory of subsequently diluted samples (generically and schematically referred to as X, 0.X an 0.0X weight percent suspensions) of collected aerosols measured by immersion freezing methods. Such dilution is required in many cases for the laboratory samples tested, but the need for dilution or not also depends on the droplet size/volume used. The PIMCA-PINC instrument follows the trajectory of the ~~offline~~ bulk aerosol immersion freezing devices, but does so for water droplets activated originally on single dry aerosol particles (and hence without the varied weight percent).

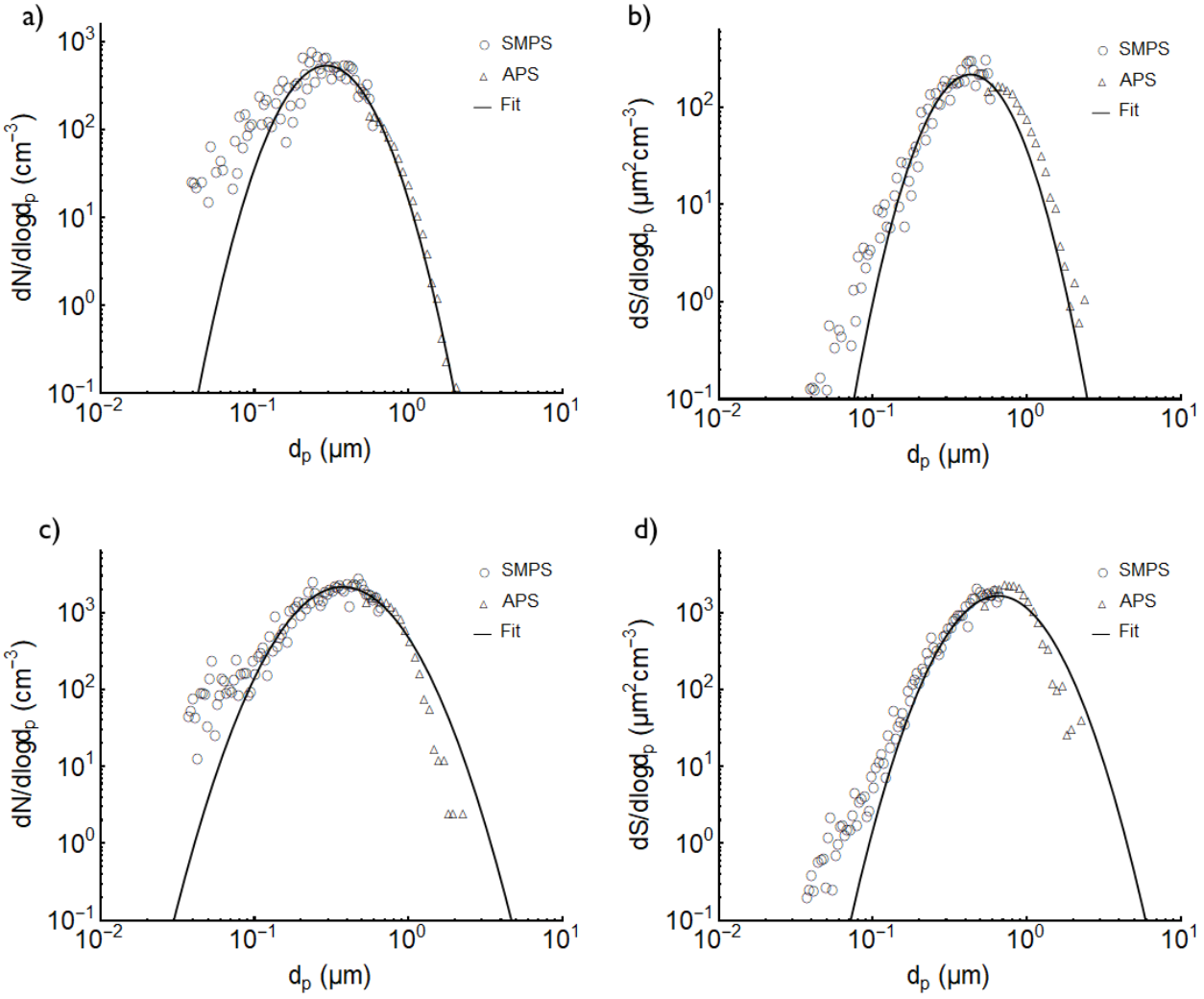

Figure 2. Number, in a), and surface area distribution, in b), of SDT01 dust particles generated into the AIDA chamber, measured with the SMPS and APS instruments, as well as the lognormal fits to the size distributions for exemplary AIDA experiment 12 on March 20, 2015, 648 s prior to expansion start. APS data have been converted based on assumed density (2.6 g cm^{-3}) and dynamic shape factor (1.2). The same data for SDT01 particles generated in APC experiment 12 on March 18, 2015, 785s following aerosol particle injection, are shown in panels c) and d). Lognormal fits are used to obtain total surface areas and these were tabulated as a function of time in each experiment.

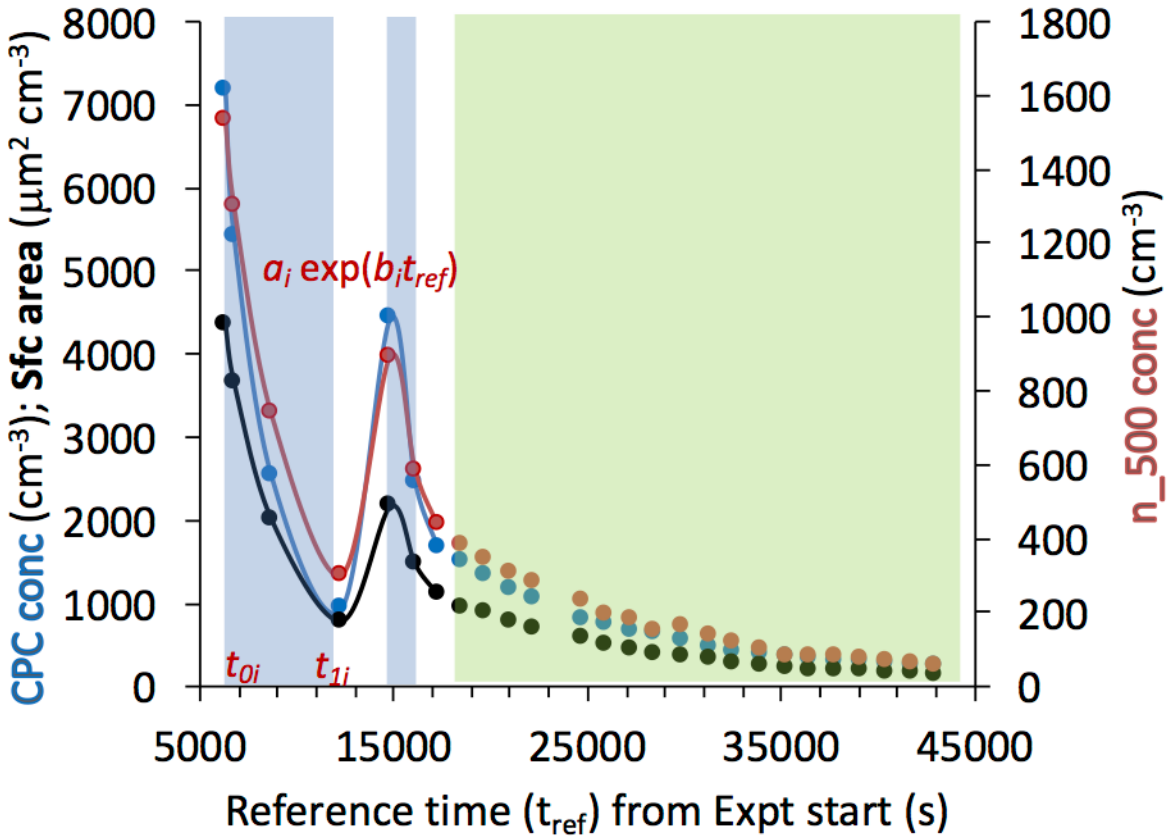

Figure 3. Data from the f~~F~~irst half of a daily experimental series, after an initial fill of Tunisian soil dust (Experiment 11 and 12 of the FIN-02 APC series on March 18, 2015) into the APC at a time (time 0) taken to be the experimental start time. Impinger and filter sample periods after two separate chamber ~~the~~ fills are highlighted in light blue shading ~~indicating that a refill was required on this day~~. To obtain a reference aerosol concentration (cm^{-3}) via the CPC (total particles) (blue points, left scale) or optical particle counter at sizes larger than 500 nm (n_500; brown points, right scale), as well as surface area (μm^2 cm^{-3}) (black points, left scale) for the ~~offline~~ impinger/filter sampling period, the time-weighted average of the two sampling periods was determined. This period-integrated concentration value could then be used to ratio versus the concentrations of particles present at later sampling times during the online sampling of aerosols from the APC (green shaded region) in order to back-correct the directly-sampled ~~online~~ INP number concentrations to those ~~interpret~~derived for the collections for post-processed ~~offline~~ samples.

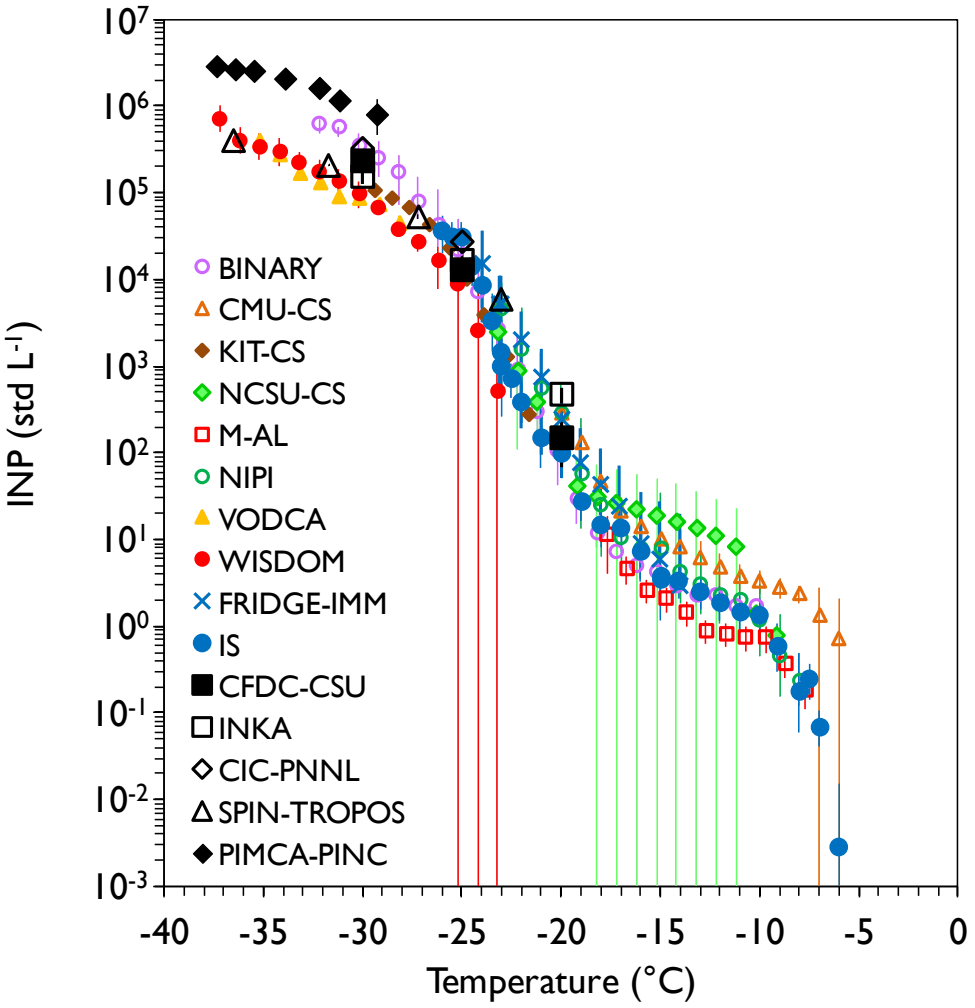

Figure 4. Combined results of all ~~online and offline~~ measurements of Argentinian soil dust sampled from the APC under conditions representative of those favoring immersion freezing nucleation in all devices. Note that most of the ~~offline~~ bulk immersion freezing data have been sub-sampled at ~1°C intervals. These ~~offline, bulk~~ immersion freezing methods are distinguishable here by their smaller data points (using different symbols and colors) over a broad range of temperatures, whereas ~~online~~ direct sampling devices ~~methods~~ using conditions supersaturated with respect to water (immersion freezing assumed as a major contributor) at specific temperatures are indicated by sparse (larger) blue data points. The KIT-CS, NCSU-CS, NIPI, VODCA, M-AL, BINARY and WISDOM instruments shared impinger samples, while the IS and FRIDGE-IMM used separate filter collections (distinguished here by black circle data points). As discussed in the text and Eqs. (1) - (3), corrections have been applied to real-time ~~online~~ instrument data depending on the time of sampling, constituting a ratio of total particle concentrations present at the time of ~~sampling offline~~ impingers/filter collections to those present at the time of specific flow chamber ~~online~~ measurements. Error bars represent 95% confidence intervals, unless stated otherwise in the Supplement for each specific instrument. When error bars are not present ~~on some points~~, they may be subsumed ~~buried~~ within the marker (i.e., small errors) or alternately the binned point represents a single observation. The data herein correspond to FIN-02 APC experiments 9 and 10 on March 17, 2015.

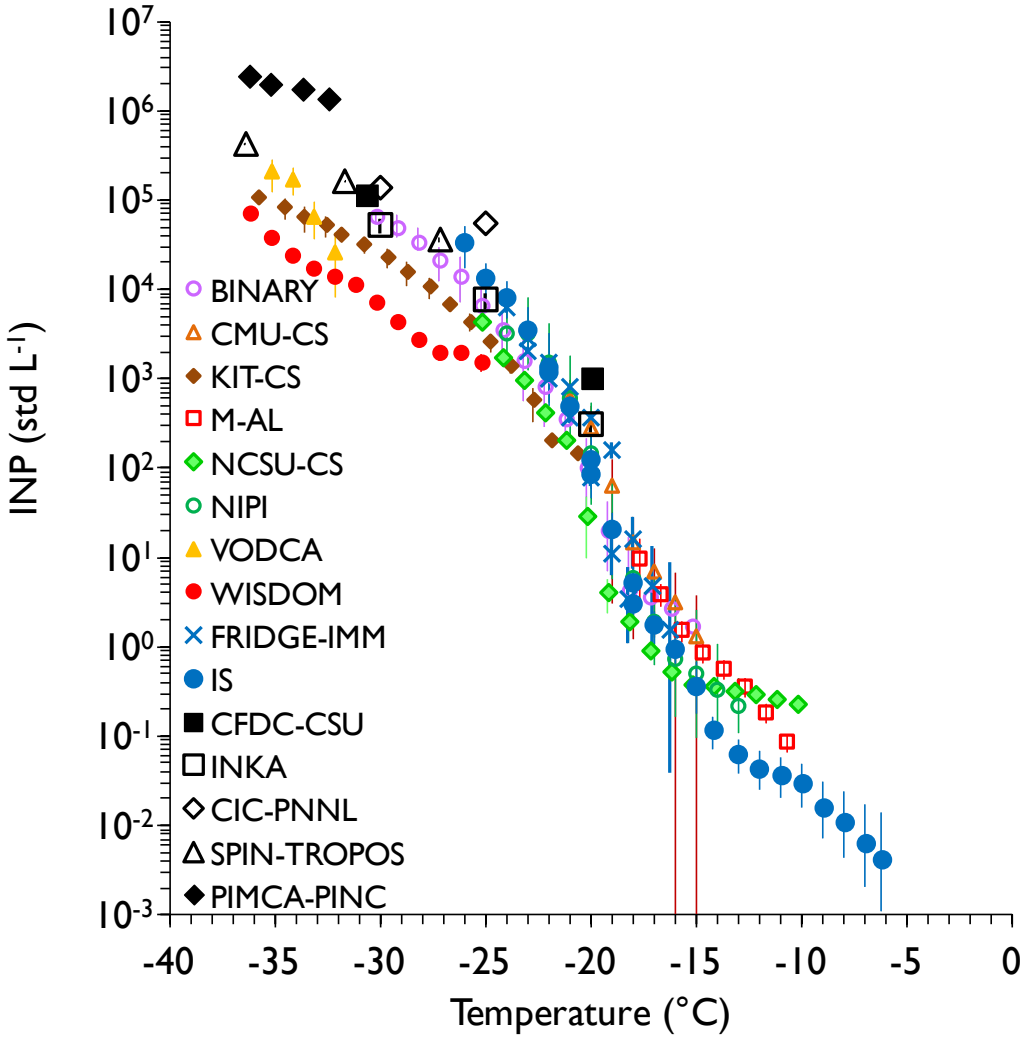

Figure 5. As in Fig. 4, but for sampling of Tunisian soil dust from the APC. All distinguishing features discussed with regard to Fig. 4 apply here as well. Note that two FRIDGE-IMM filter samples are represented here as two data points at a given temperature. The data herein correspond to FIN-02 APC experiments 11 and 12 on March 18, 2015.

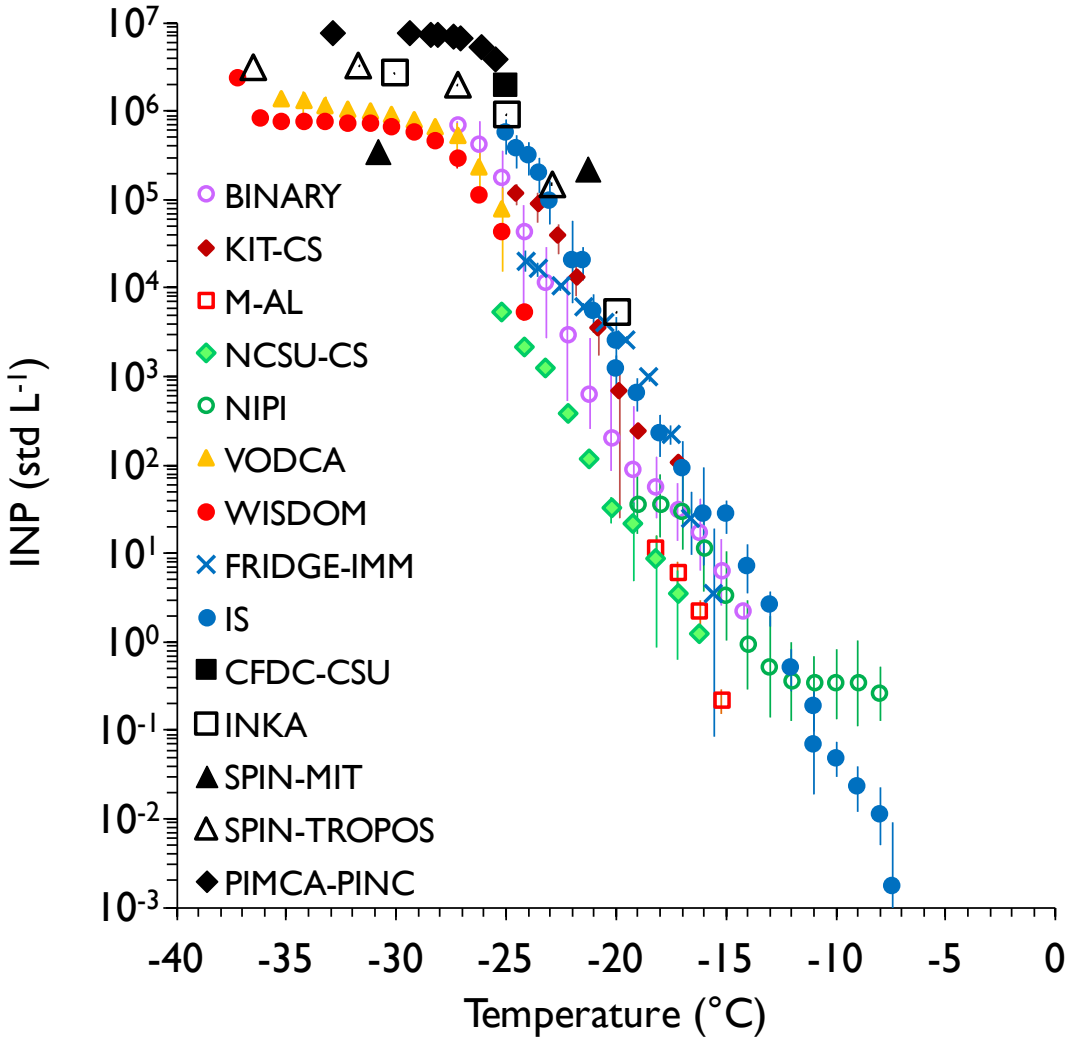

Figure 6. As in Fig. 4, but for sampling of K-feldspar particles from the APC. All distinguishing features discussed with regard to Fig. 4 apply here as well. The data herein correspond to FIN-02 APC experiments 13 and 14 on March 19, 2015.

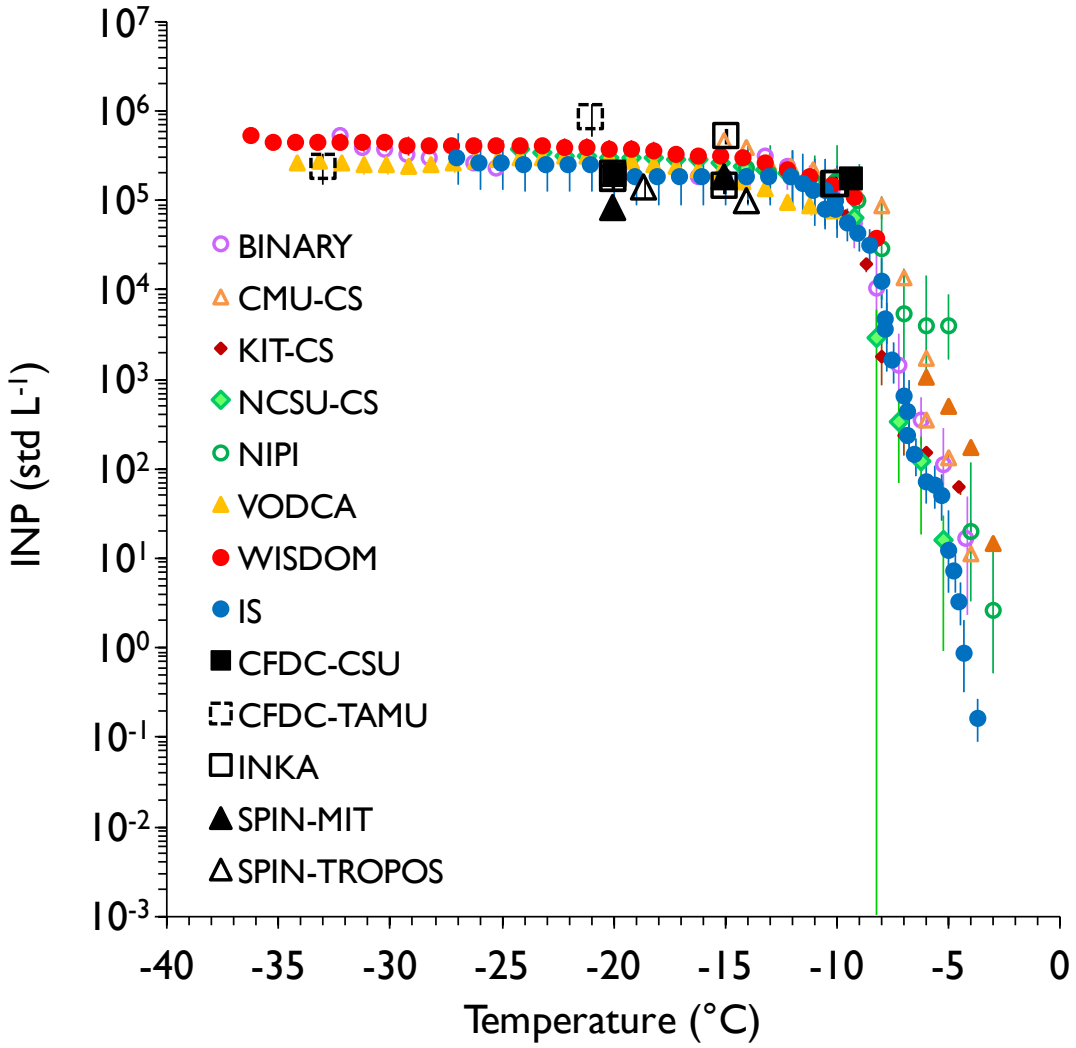

Figure 7. As in Fig. 4, but for sampling of aerosolized Snomax® particles from the APC. Two sets of measurements are plotted separately from the CMU-CS system (open and filled) due to variability observed between replicate samples as discussed in the text. The closed orange triangles are from experiments run immediately after the sample had thawed, while the open triangles are for runs that occurred within a few hours of thawing. ~~All~~ In this case, all ~~offline samplers~~ post-processed data are from the impinger samples ~~in this case~~. INKA data are included for all water supersaturated conditions not exceeding water breakthrough RH_w. The data herein correspond to FIN-02 APC experiments 15 and 16 on March 20, 2015.

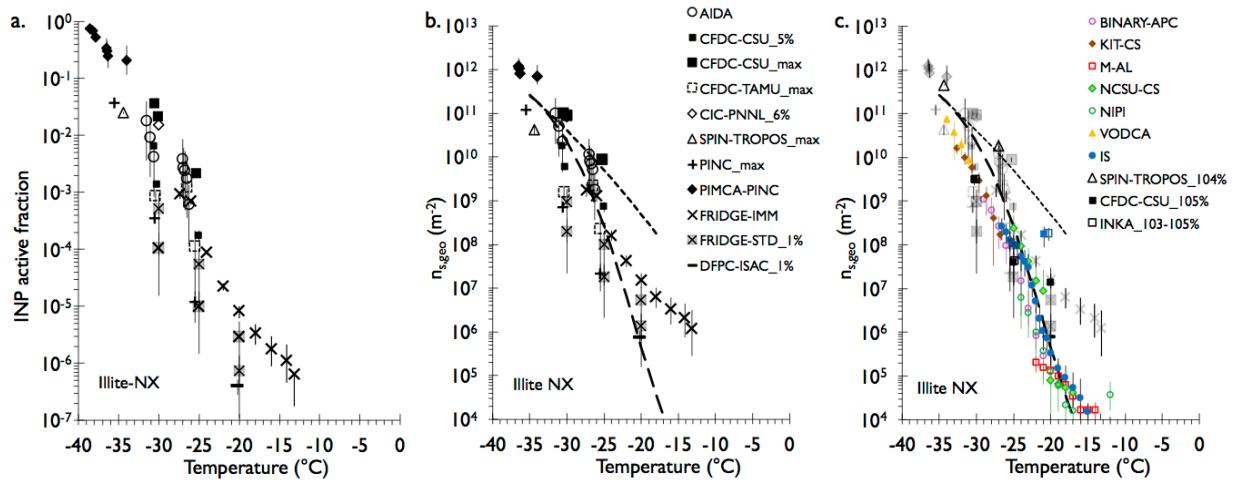

Figure 8. Panel a: Ice active fraction from multiple experiments performed on illite NX aerosols sampled directly from the AIDA chamber prior to expansion cloud experiments. In these cases, the subsequent AIDA measurements of activated ice crystal concentrations are included for comparison when water supersaturation was achieved during the expansion cycle. Instrument symbols are shown in Panel b. Panel b: Conversion of data to geometric surface active site density parameter, $n_{s,geo}$ using AIDA aerosol distribution data, and data within Table 3. Where specific instrument water supersaturations were selected for comparison, these are indicated after the instrument label (e.g., CIC-PNNL_6%, implies 106% RH_w). The term "max" means the highest RH_w achieved in a scan (102-110%), as listed in Table S1. FIN-02 AIDA experiments (unnumbered, March 11, 2015), 4 (March 16, 2015), 10 (March 19, 2015), 22 (March 26, 2015), and 25 (March 27, 2015) are represented. Gumbel cumulative distribution (log-space) fit curves for illite NX are from Hiranuma et al. (2015; cf., Table 3), representing wet suspension (long dash) and dry-dispersion experiments (short dash) in that study. Panel c: Wet suspension (colored points) and flow chamber (black points) $n_{s,geo}$ data derived from APC experiment 7 (March 16, 2015) for all instruments listed in the legend are overlain on greyed-out AIDA experiment points from Panel b. Additional CFDC-CSU and INKA data points from APC experiment 3 (March 13, 2015) are included as blue data points for these instruments

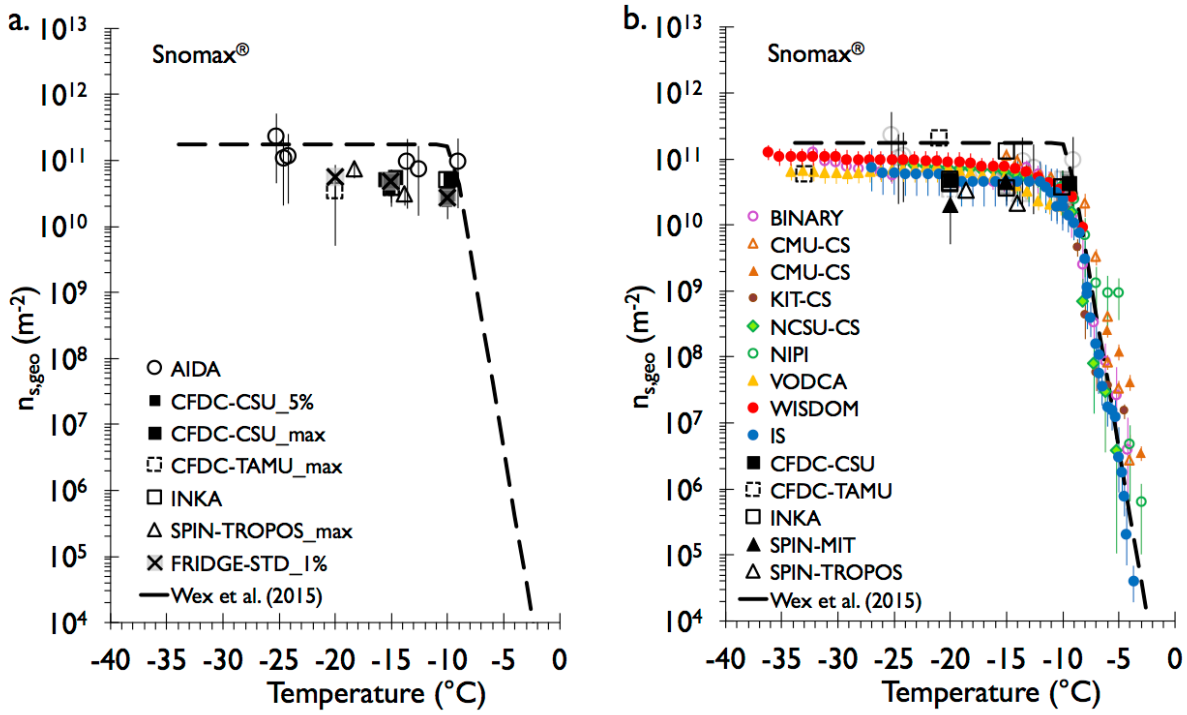

Figure 9. As in Fig. 8. Panel a: Ice active site density in multiple experiments performed on Snomax® aerosols sampled directly from the AIDA chamber. AIDA experiments 6 (March 17, 2015) and 13 (March 21, 2015) are represented, as listed for different instruments in Tables S1 and S2. The fit for $n_{s,geo}$ is derived from the Wex et al. (2015) fit for nm, the number of molecular INPs per dry mass of Snomax®, as explained in the text. Panel b: $n_{s,geo}$ derived from FIN-02 APC experiments 15 and 16 on March 20, 2015 (Fig. 7) are overlain on greyed-out AIDA experiment data points from Panel a.

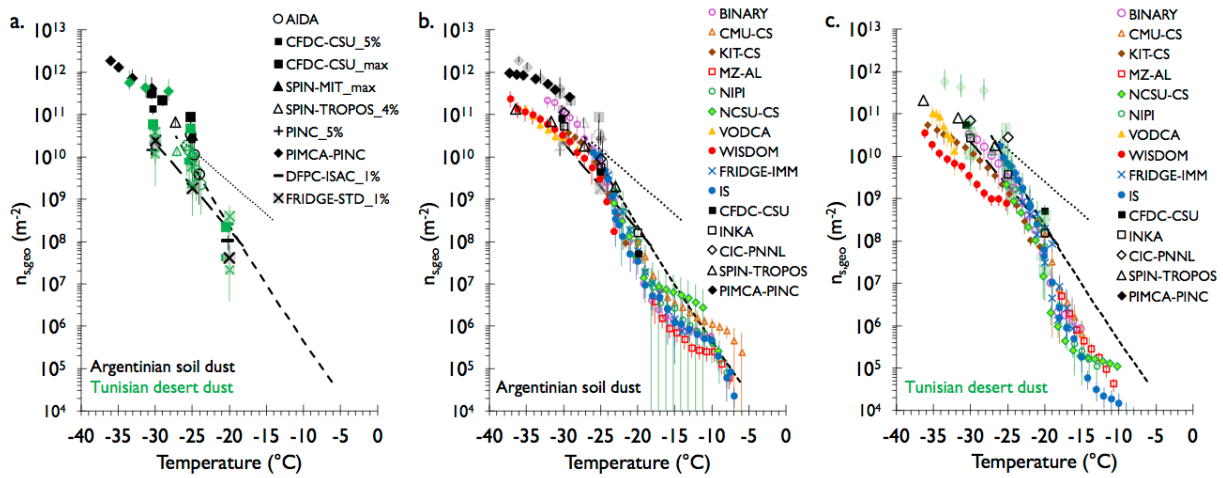

Figure 10. As in Figures 8 and 9, but for Argentinian soil dust and Tunisian soil dust sample experiments. Panel a: Data from FIN-02 AIDA experiments 5 (March 16, 2015), 9 (March 19, 2015), 24 (March 26, 2015), and 26 (March 27, 2015) are represented for Argentinian soil dust, and AIDA experiments 7 (March 18, 2015) and 12 (March 20, 2015) are represented for Tunisian soil dust, as listed for different instruments in Table S1. AIDA cloud expansion results are represented only for AIDA experiments 7 and 9, when mixed-phase clouds formed and persisted. Two fits of $n_{s,geo}$ *(T)* for previous surface soil dust particle types reported in the literature are from Tobo et al. (2014) ("Wyoming soil dust", long-dashed) and O'Sullivan et al. (2014) ("fertile soil dust", short-dashed), and Steinke et al. (2016) ("agricultural soil dust", dotted). APC data from Fig. 4 for Argentinian dust and Fig. 5 for Tunisian dust are overlain in panels b and c, respectively.

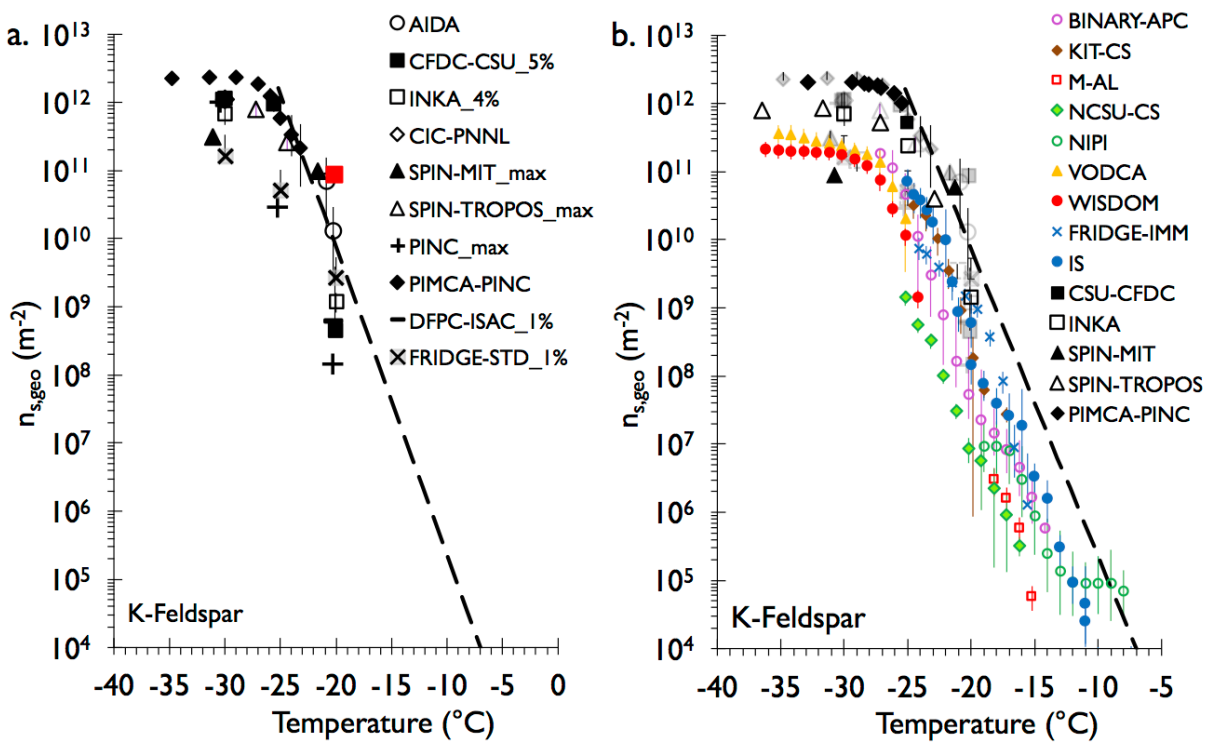

Figure 11. As in Fig. 9, but for K-feldspar aerosols sampled from the AIDA chamber prior to expansion-cooling experiments 8 (March 18, 2015), 11 (March 201, 2013), and 14 (March 23, 2013) for panel a, and overlay of data from APC experiments 13 and 14 on March 19, 2015 (Fig. 6) in panel b. The K-feldspar fit from Atkinson et al. (2013) is shown for comparison, after conversion from $n_{s,BET}$ to $n_{s,geo}$, as described in the text. The experiment represented by the red data point in panel a from the CFDC-CSU instrument is discussed in Supplement Section S.1.2 in relation to experimental detection issues.

S.1 Direct sampling ~~Online~~ instrument systems

Online INP measurement systems are cloud chambers or instruments using continuous flow systems to assess INPs. Most have been reported on in the literature or will be in the near future, and some have a record of reported data of more than 20 years. Most of these systems are documented to the extent that they could easily be reproduced, and in some cases certain ones have a legacy in an earlier version of one type. This will be noted in the descriptions below.

S.1.1 AIDA (Aerosol Interaction and Dynamics in the Atmosphere) cloud simulation chamber

The Aerosol Interaction and Dynamics in the Atmosphere (AIDA) cloud simulation chamber, which consists of an 84 m^3 isothermal aluminum vessel, is a comprehensive experimental facility that can be used for recreating supercooled clouds in the vessel (Möhler et al., 2003). More specifically, the chamber conditions are precisely controlled by mechanically pumping air in the vessel, inducing concurrent and homogeneous reduction of both gas temperature and pressure. The resulting so-called expansion cooling provides a wide range of simulated atmospheric in-cloud conditions, such as temperature (60 to -90°C with an uncertainty ± 0.3°C), pressure (~1000 to below 1 hPa) and relative humidity (from ~0% to above water saturation). In such cloud simulation experiments, spontaneous droplet activation and ice crystal formation occur in simulated supercooled clouds at or above saturation with respect to water and ice (e.g., Möhler et al., 2005; Niemand et al., 2012). Further, AIDA is unique since its cloud experiments are systematically performed with atmospherically relevant droplet sizes (i.e., a few to tens of micrometer diameter at the largest) as well as under atmospherically relevant cooling rate; i.e., an average cooling rate of 1.7 ± 0.1 (standard error) °C min^{-1}.

Besides its central function as a cloud emulator, the AIDA chamber can be also utilized as a platform for multiple instruments to investigate aerosol-cloud interactions and cloud microphysics in ice nucleation experiments (*DeMott et al*., 2011). During FIN-02, similar to previous AIDA studies (e.g., Wagner et al., 2011; Hiranuma et al., 2014a and 2014b), a combination of 6 online instruments, including (1) a condensation particle counter (CPC, TSI, Model 3076), (2) a scanning mobility particle sizer (SMPS, TSI, Model 3080 DMA and Model 3010 CPC), (3) an aerosol particle sizer (APS, TSI, Model 3321), (4) the white light aerosol spectrometer optical particle counters (Welas-OPCs, Palas, Sensor series 2300 and 2500; Benz et al., 2005), (5) a tunable diode laser (TDL) water vapor absorption spectroscopy (Fahey et al., 2014) and (6) a home-built device for scattering intensity measurement for the optical detection of ice (hereafter SIMONE - German abbreviation for Streulicht-Intensitätsmessungen zum optischen Nachweis von Eispartikeln; Schnaiter et al., 2012), used to characterize the physical properties of aerosol and hydrometeors (droplets and ice crystals) formed during the AIDA expansion experiments with a detection limit for number concentration of 0.1 cm^{-3}. It is noteworthy that, in dense supercooled liquid clouds, the AIDA-TDL data is offset by +5% in order to match the liquid-phase saturation (Murphy and Koop, 2005) conditions expected for the immersion freezing event. The reason for this systematic deviation of the TDL measurement from the expected saturation is unclear. More technical details on individual instruments and their applications at the AIDA facility are given in above listed publications.

S.1.2 CFDC-CSU (Continuous Flow Diffusion Chamber - Colorado State University)

The Colorado State University (CSU) Continuous Flow Diffusion Chamber (CFDC) operating principles are described in the earlier works of Rogers (1988), Rogers et al. (2001) and Eidhammer et al. (2010). The current versions of the CFDC-CSU used in ground based (CFDC-1F) and aircraft studies (CFDC-1H) are geometrically identical and composed of cylindrical walls that are coated with ice via flooding and expelling water from the chamber when the walls are set at a controlled temperature of ~-27°C before each experimental period. The plate separation is 1.12 cm prior to ice application, which has a typical thickness of 0.015 cm. The chamber is divided into two sections vertically, separated by a Delrin collar. A temperature gradient between the colder (inner) and warmer (outer) ice walls in the upper 50 cm "growth" section creates an ice supersaturated field into which an aerosol lamina is directed. Vapor pressure relations used within the analytical equations given in Rogers et al. (2001) are taken from Murphy and Koop (2005). The Delrin inlet manifold has a stainless-steel knife-edge ring threaded into it, so that aerosol flow is directed centrally between two sheath flows of clean and dry air. The ratio of aerosol and sheath flows can be varied, but typically the aerosol lamina represents 15% of the 10 L min^{-1} total flow. Ice crystals forming on INPs in the growth region of the chamber enter the lower 30 cm "evaporation" section of the chamber where the two walls are held equivalently to the cold (inner) wall temperature. As shown by DeMott et al. (2015), residence time in the growth region is approximately 5 s under conditions used in the present study, although residence at prescribed steady state conditions is probably on the order of 3s, followed by 2 s in the evaporation regime. When the temperature gradient in the growth section is adjusted for water supersaturated conditions that activate cloud droplets in the aerosol lamina, these will evaporate to haze sizes in the evaporation section, at least up to some water relative humidity (RH_w) where they survive, referred to by many as the droplet breakthrough RH_w. Until that high RH_w, only ice crystals and haze particles will exit the CFDC. Ice crystals and aerosols exiting the CFDC at sizes above approximately 500 nm are counted with an optical particle counter (OPC), where the two populations are distinguished in different size modes. For the data collected in this work, we count all particles in size bins above 3 μm as ice particles when not encountering droplet breakthrough. The cut-channel used for analysis of activated ice crystals at a calibrated 3 μm size was channel 50 for FIN-02. In usual operation, aerosol particles larger than 2.4 μm are removed by a set of inertial impactors prior to the chamber inlet to eliminate misidentification as ice crystals, but the impactors were removed for all data reported in this paper. Data archive files indicate times when impactors were used in selected experiments. Some experiments with the impactors in place will be reported in the paper summarizing blind inter-comparisons.

CFDC-1F measurements for FIN-02 were ideally made via slowly scanning RH_w (~1% min^{-1}) at single temperatures, including below and above water saturation to identify the maximum freezing activity prior to the point that water droplets "breakthrough" the lower evaporation section. The RH_w of droplet breakthrough was also identified whenever possible, but this higher RH_w was not always achieved. Figure S1 shows an example for which dRH_w/dt was kept to close to 0.5 % min^{-1}.

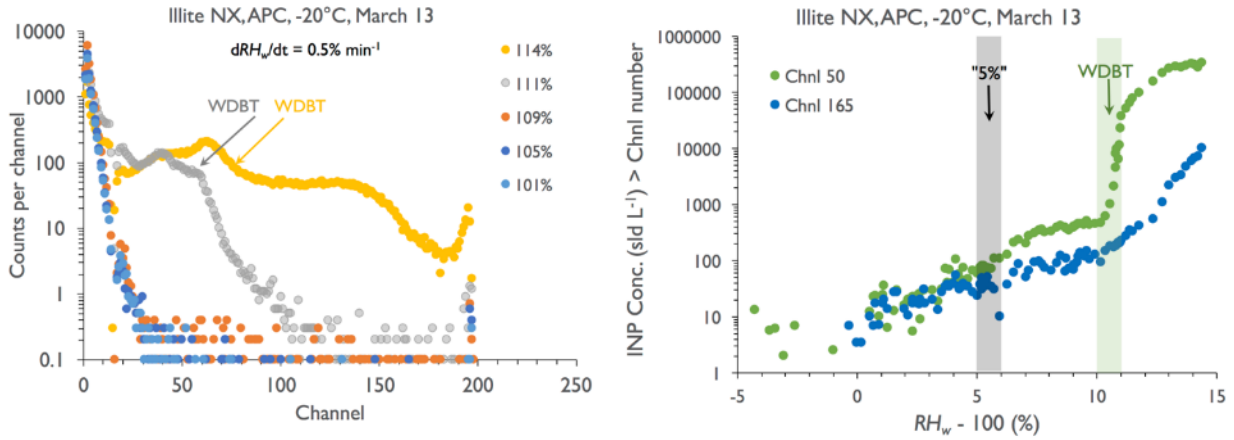

Fig. S.1. Example of data from a slow RH_w scan (~0.5% min^{-1}) with the CFDC-CSU instrument while sampling illite NX and processing it at a temperature of -20°C on March 13, 2015. Each OPC channel size spectra (at the RH_w values in the legend) in the left panel or single point in the right panel represents a 10 s interval. In the left panel, the spectra indicating water droplet breakthrough (WDBT) are indicated by the progressive appearance of a high concentration mode of particles becoming more prominent as RH_w is further increase from 111 to 114%. This point is clear also in the cumulative apparent INP concentration at sizes larger than the standard cut-point for ice at 3 μm (Chnl 50). INP concentrations are referenced for this study primarily at 105% RH_w, which is computed as an average over the range 105 to 106%. As previously reported (DeMott et al., 2015), the maximum INP concentration prior to WDBT is a factor three to four larger than values referenced to 105% RH_w in this case. The comparability of Chnl 50 and Chnl 165 data at RH_w up to 105% makes it clear that most of the first ice crystals nucleated grow to large sizes. This is the basis for using Chnl 165 in cases where aerosol particles were present already at sizes >3 μm before the start of an RH_w scan.

Higher ice cut-point sizes were applied in cases where sufficient large aerosol particles were present initially to "pollute" standard ice size channels. This was a peculiarity of the laboratory study that is not encountered in atmospheric sampling. A higher cut-size for ice was selected to derive INP concentrations from these data because it was expected that large aerosols might retain some water after liquid particle activation and thereby show up even at sizes between channel 50 and some larger channel in the OPC at the exit of the CFDC. The appropriateness of this procedure is demonstrated for a typical experiment Fig. S1. In all cases, the larger cut-size selected and reported is listed as channel 165 in the CFDC-CSU archive files. The cut size employed in each experiment is also noted in Table S1. Note that the channel size is not linearly related to particle size, but typically follows a square relationship to channel, and hence, channel 165 is likely in the range of 5 μm. This was not calibrated. An example of correction for aerosols polluting typical ice cut-size channels by using Chnl 165 for ice definition is shown in Fig. S2.

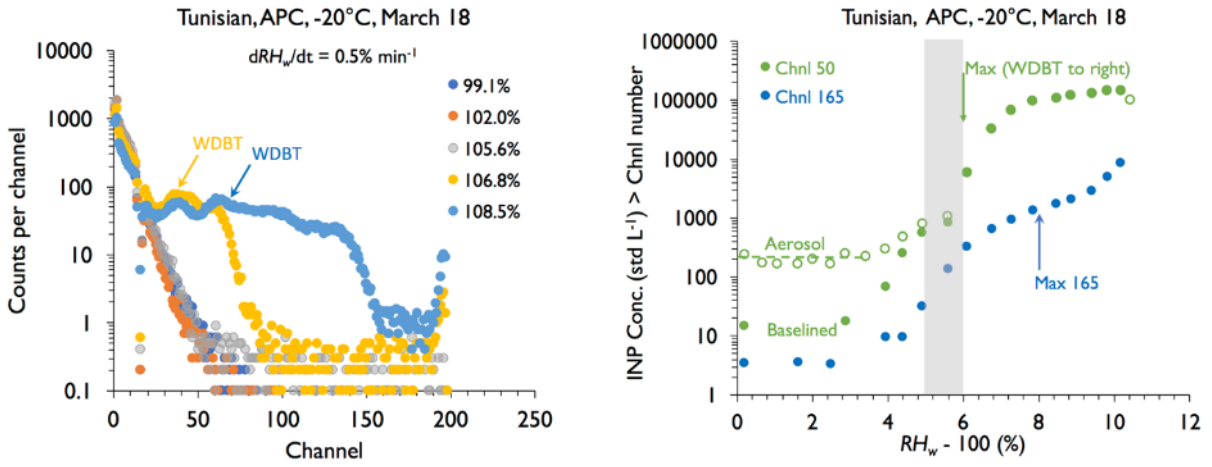

Fig. S2. As in Fig. S1, but for the Tunisian dust experiment on March 18 (Fig. 5) in which aerosols were already present at "ice" channel sizes in the APC when the RH_w scan was initiated in the CFD-CSU instrument (without the upstream impactor in place to remove >2.5 µm particles). In this case, WDBT occurs sooner, despite the slow dRH_w/dt scan. After subtracting the aerosol background, the Chnl 50 data (standard "ice" channel) resemble the Chnl 165 data. Nevertheless, to be conservative, the Chnl 165 data is used to define ice in these cases. It can be seen that the Chnl 165 data also allows definition of a maximum INP concentration in this case.

It was noted in a few experiments, most notably for K-feldspar, that what appeared similar to droplet breakthrough even in the absence of aerosol "pollution", occurred at low water supersaturations. We hypothesize this to be due to small ice crystal formation occurring for evaporating droplets in the lowered temperature region of the evaporation section of the CFDC-CSU instrument, a consequence of both exceeding desired dRH_w/dt rates and the steep activation function of K-feldspar versus temperature. This is demonstrated in Fig. S3, where OPC data from contrasting AIDA chamber sampling experiments on March 20 and March 23, the two days plotted in Fig. 11 of the manuscript, are shown. The discontinuous and strong rise in ice activation at moderate supersaturation, especially noted on March 23 when dRH_w/dt exceeded twice the desired rate for scanning, had not been seen in previous studies (DeMott et al., 2015), just as it is not evident in Fig. S1 or S2. That is, normally, INP freezing in the growth region of the instrument will grow to larger sizes, and not be present frozen at near to the size of activated cloud droplets in the CFDC growth section. While Fig. S3 shows that use of Chnl 165 may derive the most appropriate INP concentrations for relating to the CFDC processing temperature in these cases, Chnl 50 data is plotted in Fig. 11 to emphasize this discovered CFDC sampling issue for K-feldspar in the temperature region near -20°C. RH_w scan rates exceeded 1% min^{-1} in two other K-Feldspar experiments on March 18, one in the APC and one in the AIDA chamber, so these data are not included in Fig. 6 and Fig. 11. Although this situation is considered unusual, as scanning RH_w is not a practice that is often operationally practiced in the field (i.e., constant values or steps of RHw are used), these findings may motivate testing reconfiguration of the CFDC-CSU instrument so that the evaporation section presents warming instead of cooling. This could be accommodated simply by configuring the inner cylindrical wall to be the warmest wall instead of the coldest wall.

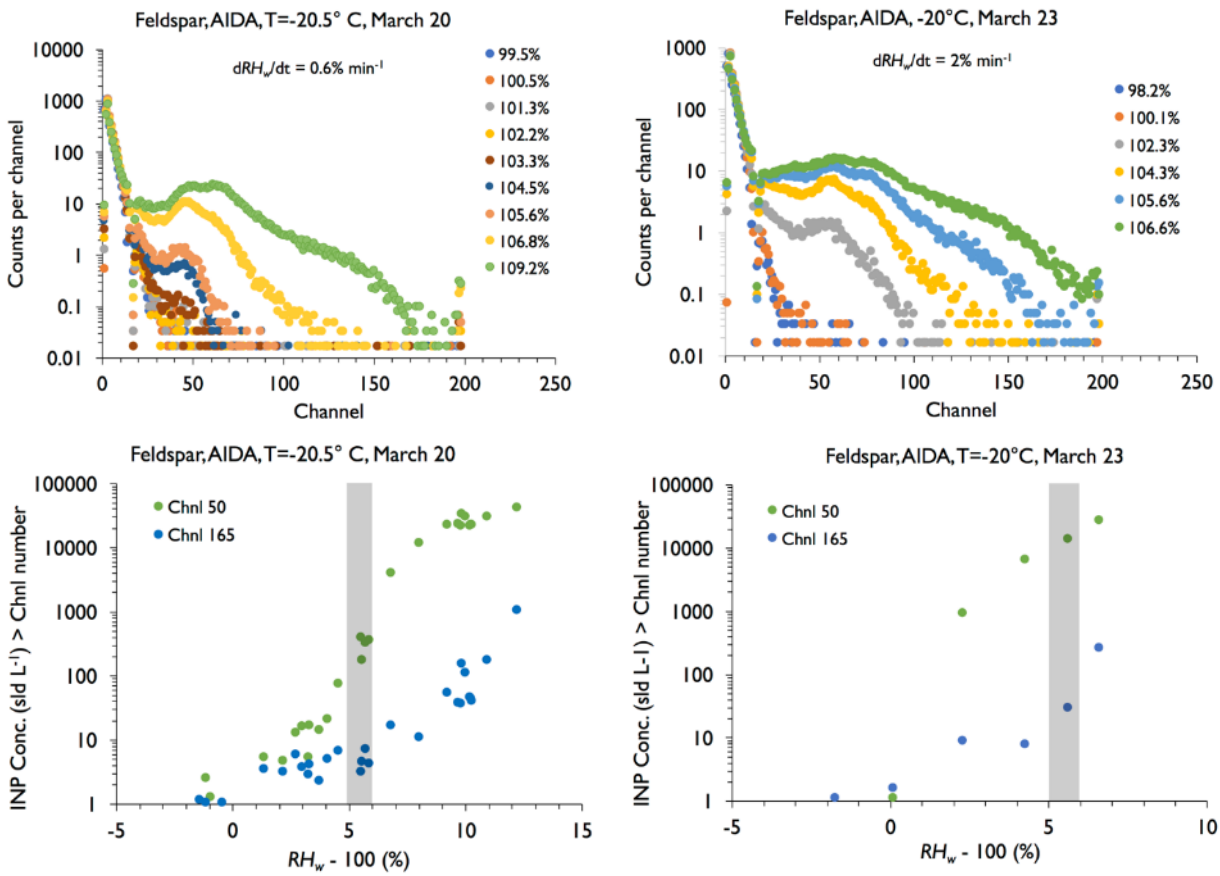

Fig. S3. Spectral and cumulative INP > specific channel plots as in Fig. S2, but for the K-feldspar experiments used to define the low (left panels, March 20, 2015) and high (right panels, March 23, 2015) CFDC-CSU INP concentration data points in Fig. 11 of the manuscript. The occurrence in these cases of "small ice" by 5% water supersaturation is distinct from Fig. S1 despite the absence of aerosol "pollution" of the initial spectra and similar dRH_w/dt rates. The unexpected population of small ice crystals are believed to result from "late" freezing as liquid particles cool before completely evaporating upon entering the evaporation section of this instrument. In the experiment on March 23, dRH_w/dt was three times faster, far above the desirable rates. Less steady control of RH_w led to even stronger growth of the small ice crystal mode and likely overestimation of INP (via the standard Chnl 50 ice point definition) attributable to the processing temperature of -20°C.

Interval periods occurred during RH_w scanning in which the aerosol sample was filtered in order to determine background frost influences on ice particle counts in the OPC, as described in prior publications (e.g., DeMott et al., 2015; Schill et al., 2016). Following Schill et al. (2016), sample period concentrations are those with the interpolated background concentrations of adjacent filter periods subtracted. The standard deviation derived from Poisson counting statistics from both the sample and the interpolated background concentrations were added in quadrature to obtain the INP concentration error. Concentrations are considered significant if they are 1.64 times larger than the INP concentration error, which corresponds to the Z statistic at 95% confidence for a one-tailed distribution.

Particle losses in the aerosol impactor and the inlet manifold of the CFDC have been previously estimated as 30% of total condensation nuclei when sampling ambient air (Rogers et al., 2001), but only 10% for aerosols in the 100 to 800 nm size range based on laboratory tests (Prenni et al., 2009). We apply the 10% correction to all CFDC data herein. Temperature uncertainty is ± 0.5°C at the reported CFDC lamina processing temperature (Hiranuma et al., 2015). RH_w uncertainty depends inversely on temperature, and has been estimated as ± 1.6, 2 and 2.4 % at -20, -25, and -30°C, respectively (Hiranuma et al., 2015).

S.1.3 CFDC-TAMU (Continuous Flow Diffusion Chamber - Texas A&M University)

The Texas A&M Continuous Flow Diffusion Chamber (CFDC-TAMU), including a Cloud Aerosol Spectrometer with Polarization (CASPOL) is an apparatus designed to measure the concentration, backscatter, and depolarization ratio of ice crystals nucleated under controlled conditions. The CFDC, built at Texas A&M University, measures the nucleation and growth of ice crystals under well-controlled temperature and supersaturation conditions (Rogers et al., 2001; Glen and Brooks, 2014; McFarquhar et al., 2011; Zenker et al., 2017). Leaving the CFDC, samples enter the CASPOL (Droplet Measurement Technologies, Inc.) which counts the ice crystals activated on INIPs and determines the optical properties of individual ice crystals at 680 nm (Glen and Brooks, 2014). An inlet at the top of the CFDC allows for an aerosol stream to enter into an annular chamber. Here, the sample air passes between two laminar flows of dry filtered air. The walls of the chamber are coated with ice and held at different temperatures in order to create a controlled supersaturation field between the walls. The aerosol sample has the potential to nucleate and form ice crystals as it travels through this controlled supersaturation region.

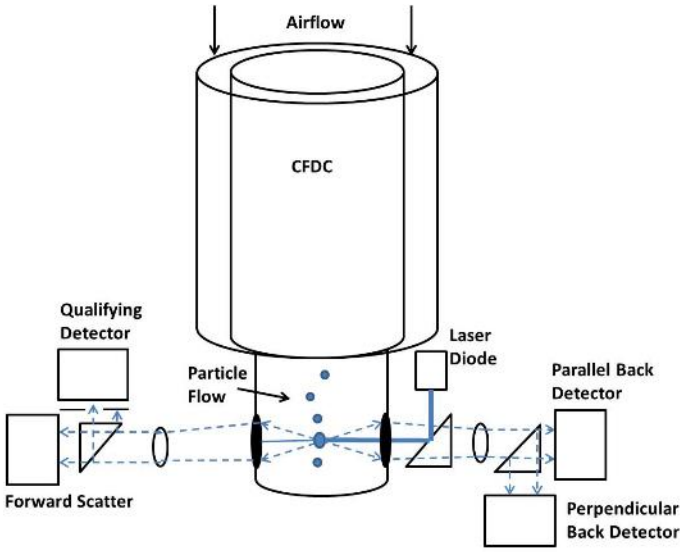

Figure S4: Schematic of the CFDC-TAMU with CASPOL illustrating how the particles are analyzed by the CASPOL after exiting the CFDC.

After nucleation and growth of ice crystals have occurred in the CFDC, the ice crystals are counted by the CASPOL based on size discrimination. The CASPOL employs 3 detectors which measure light scattered in the forward (4°-12°) and backward (168°-176°) directions. The concentration and size of IN are determined by the forward

scattering detector. Backscatter light is split between two detectors, which measure the parallel and perpendicularly polarized light, respectively. The back detectors are used to determine the backscattering intensity and the depolarization ratio of individual ice crystals (Fig. S4).

During FIN-02, TAMU CFDC experimental uncertainty in concentration was +/- 39% based on instrument uncertainties in sheath and total flow rates, particle losses within the CFDC and in the transition zone between the CFDC and CASPOL, background corrections, icing thickness, and CASPOL uncertainties (choice of bin size, coincidence of multiple particles). In FIN-02, uncertainty in supersaturation arose mainly from the possible separation of the hydrophobic material on the lower section of the warm (inner) wall (used to induce evaporation) by as much as 2 mm. Assuming laminar flow considerations and that the hydrodynamic flow is fully developed, this causes an uncertainty in SSw of +/- 1.75%. The use of spheres to calibrate the CASPOL may lead to uncertainties in particle sizing for aspherical particles. In an earlier version of the CFDC-TAMU, sample air flowing from the CFDC to the CASPOL was observed to warm, causing an estimated ice loss corresponding to a small decrease in radius of less than 1% below ~ -50°C and unquantified changes in the associated optical properties (Glen and Brooks, 2014). Prior to FIN0-2, the connection between the CFDC and CASPOL has been modified to eliminate this warming.

S.1.4 INKA (Ice Nucleation Instrument of the Karlsruhe Institute of Technology)

The new INKA (Ice Nucleation Instrument of the Karlsruhe Institute of Technology) is a continuous flow diffusion chamber that is based on the design of Rogers (1988) and was built in cooperation with Colorado State University. The INKA instrument is most specifically modeled after the Colorado State University "laboratory" CFDC (Archuleta et al., 2005) and is described in detail in Schiebel (2017). INKA is a longer column version of the CSU CFDC-1H, but with cooling baths for temperature control. INKA's ice nucleation chamber consists of concentrically aligned copper tubes that have been ebonized for wetting purpose and are individually cooled via external chillers to temperatures as low as -60°C. During operation, the side walls of the 1 cm annular gap between the copper tubes are coated with a 0.4 mm ice layer. A total flow of 12.5 L min^{-1}l passes through the chamber. This flow consists of 5% to 10% of sample flow encased in 90% to 95% of particle free sheath air. The sample to sheath flow ratio was adapted during the FIN-02 measurements according to available aerosol concentration and fresh synthetic air was used as for sheath flow.

The total length of the INKA chamber is 150 cm, with the upper 2/3 acting as so called "nucleation and growth section". Here, the sample is exposed to defined water vapor levels above ice saturation by setting both walls to different temperatures. Following Rogers (1988), the temperature and relative humidity in the sample lamina is calculated for the measured wall temperatures, flow velocity and sample to sheath ratio. Depending on the chosen conditions, deposition and/or immersion freezing mode nucleation can be studied. During FIN-02, we stepwise increased the relative humidity at the sample location while keeping the laminar mean temperature constant. For most samples, we studied a range from 90% to 110% RH_w with respect to liquid water. INP concentrations close to 105% RH_w were used for intercomparison with other immersion freezing methods. In between the investigated RH_w-plateaus, the chamber background was measured by effective filtering of aerosols from the sample flow.

The lower 1/3 of the outer wall can be cooled separately from the upper section. Here, a Delrin spacer inhibits thermal contact between the outer wall copper pieces. For the FIN-02 measurements, we chose to couple the cooling of the inner wall and the outer lower wall, thus setting those to equal temperatures (colder than the upper outer wall). With entry into this so called "droplet evaporation section", the ice particles, any existent droplets and interstitial aerosol particles quickly adapt to the abruptly lowered vapor pressure. As the sample is still held at ice saturation, the formed ice crystals are able to grow further while droplets will shrink due to evaporation, thus enabling the identification and counting of ice particles by an optical particle counter (Climet CI-3100) at the chamber outlet.

Although the air samples taken from AIDA or the APC were rather dry, we used silica gel equipped diffusion dryers to ensure consistent conditioning. To prevent the erroneous classification of large inactivated aerosol particles as ice particles by OPC counting, an impactor with a well-defined flow dependent cut-off size of about 2 µm was used in some experiments. To account for particle loss in the impactor, the particle number concentrations were measured with and without the impactor in place, at a position before the chamber inlet, using a condensation particle counter (TSI model 3772). Particle losses in the sampling line were found to be negligible.

A detailed description of the INKA instrument will be given in Schiebel (2017). This paper will also include a thorough analysis of measurement uncertainties. For the FIN-02 campaign we estimate an uncertainty in temperature of 1 K and an uncertainty in particle number concentrations of 20%.

S.1.5 PINC (Portable Ice Nucleation Chamber – ETH Zurich)

The Portable Ice Nucleation Chamber (PINC, Chou et al., 2011) is a parallel-plate vertical continuous flow diffusion chamber and the portable version of the Zurich Ice Nucleation Chamber (ZINC, Stetzer et al., 2008). The general operational principle follows that of Rogers (1988) as described in the previous sections. Prior to the ice nucleation experiments, an ice layer is applied to the chamber walls (568 x 300 mm) which have a distance of 1cm between them. A temperature gradient is set between the chamber walls that generates a parabolic supersaturation profile with a peak saturation close to the center plane. The sample aerosol is introduced with a flow rate of 1 $lmin^{-1}$ and layered between two particle-free sheath air flows of 4.5 $lmin^{-1}$ ensuring a narrow, centered sample lamina. Aerosol particles are introduced into the chamber and may nucleate and grow to ice crystals during a residence time of 4-5 s in the ice nucleation and growth section before entering the evaporation section, where both walls are isothermally set to the warm wall temperature. This creates a subsaturated environment with respect to water in which any formed droplets evaporate while ice crystals are maintained at the ice saturated conditions. Exiting aerosol particles and ice crystals are detected at the bottom of the chamber by an optical particle counter (Lighthouse R5104). In this study, particles larger than a set size threshold of 3 µm are counted as ice crystals and no impactor was used upstream of the chamber to limit larger aerosol particles from being sampled. Measurements were performed as RH_w scans (<2 % RH min^{-1}) at prescribed temperatures from ice saturation to above water saturation up to an RH_w at which ice crystals cannot be distinguished from droplets based on their size (droplet breakthrough). Above water saturation conditions condensation freezing and immersion freezing cannot be distinguished in this setup. Before and after each scan, background concentrations of ice crystals in the chamber are obtained by sampling filtered air. The background counts are linearly interpolated between two filter periods and subtracted from the sample signal and the INP concentration

is determined. The INP active fraction is calculated as the ratio of ice crystals detected with the OPC to the number of total aerosol particles measured with a CPC on the aerosol chambers (AIDA or APC).

The accuracy of the temperature sensors is ±0.1°C and the variation of the temperature across the theoretically defined sample lamina is ±0.4°C, which corresponds to an uncertainty in RH_w of ±2 % (Chou et al., 2011). The uncertainty in INP concentration is 10 % due to counting by the OPC and uncertainty in active fraction is 14% including an additional uncertainty of 10 % for the measurement of the total aerosol particle concentration. Chamber characterization experiments with PINC revealed particle losses below 5 % without the use of an impactor upstream of PINC (Boose et al., 2016).

S.1.6 PIMCA-PINC (Portable Immersion Mode Cooling Chamber - ETH Zurich)

PIMCA is a vertical extension of the PINC instrument and used to investigate the ice nucleating ability of aerosol particles explicitly in the immersion mode (Kohn et al., 2016). After entering PIMCA aerosol particles are activated to cloud droplets at 40°C in supersaturated conditions with respect to water (RH_w>115 %) by applying a temperature gradient of ΔT = 25°C between two chamber walls with constantly wetted filter paper. The droplets with single-immersed aerosol particles are then supercooled to the desired ice nucleation temperature prior to entering PINC, which is held at water saturation conditions. Typical flow rates in the PIMCA-PINC setup are 0.6 L min^{-1} sample flow and 2.2 L min^{-1} particle-free sheath air on either side of the aerosol lamina. A frozen fraction of entering cloud droplets is calculated by the ratio of ice crystals to the number of total particles (cloud droplets and ice crystals) in the sample volume using the Ice Optical DEpolarization detector (IODE, Nicolet et al., 2010), which is attached to PINC. Measurements with PIMCA-PINC are performed by scanning the temperature from homogeneous freezing conditions (e.g., T<233 K) until the detected frozen fraction is not distinguishable from the experimental background at water saturation conditions in the entire sample lamina.

Each reported data point consists of about 2-5 individual measurements at one temperature, which corresponds to more than 3000 measured single particle intensity peaks. The sample concentration is diluted upstream of the chamber to avoid coincidence errors for appropriate peak detection and the frozen fraction is the primary data set. For calculation of the INP concentration, the frozen fraction is multiplied by the total aerosol particle concentration in the aerosol chambers measured in parallel.

Temperature and RH uncertainties are equivalent to those for PINC. The uncertainties in frozen fraction are based on the uncertainty from the potential false classification of ice crystals as cloud droplets and vice-versa. Measurements with PIMCA-PINC were conducted on the same sample line as has been used for PINC and are discussed at the end of section 2.4.

S.1.7 CIC-PNNL (Compact Ice Chamber – Pacific Northwest National Laboratory)

The Pacific Northwest National Laboratory (PNNL) Cloud Ice Chamber (CIC) has been previously described by Friedman et al. (2011) and Kulkarni et al. (2016). This device is modeled after the ice nucleation chamber described by Stetzer et al. (2008), and is the predecessor design on which the SPectrometer for Ice Nucleation (see later sections) was modeled. The chamber consists of two parallel plates through which flow is directed in a downward, vertical

direction, with an evaporation section attached at the bottom of the chamber to remove water droplets (Stetzer et al., 2008). The chamber plates are coated with an ice layer ~0.5 mm thick and independently temperature controlled using two external cooling baths (Lauda Binkmann Inc.). Temperature data are logged using a National Instrument CompactRIO programmable automation controller at 1 Hz sampling rate. Cooling baths were operated such that a linear temperature gradient was developed across the chamber plates. The gradient was adjusted to produce the desired ice-supersaturated conditions inside the chamber, and relative humidity with respect to ice (RH_i) and liquid water was calculated using the Murphy and Koop (2005) vapor pressure formulations. The chamber design ensures that aerosol particles are placed between the layers of two sheath flows. The sheath and sample flows were 6 and 1 L min^{-1}, respectively, which resulted in a particle residence time of the sample stream to ~12 s within the chamber. For FIN-02, the CIC-PNNL instrument was operated for at least part of the time in scanning RH_w mode, wherein the thermal gradient between the chamber walls was slowly increased in a manner that also held the average temperature of the aerosol stream constant. Temperature and RH_i uncertainty limits are ±1.0°C and ±3%, respectively. Ice crystals that grew to sizes greater than ~1.5 μm were detected with an optical particle counter (OPC, CLiMET, Model CI-3100). Background INP counts were calculated by sampling only filtered dry air for at least 15 min at the beginning, middle, and at the end of the experiment. Background INP counts were subtracted from the measured INP counts in each experiment. INP concentrations reported are interquartile means.

S.1.8 SPIN-MIT (Spectrometer for Ice Nuclei – Massachusetts Institute of Technology)

The MIT SPectrometer for Ice Nuclei (SPIN) is a commercially-available ice nuclei counter manufactured by Droplet Measurement Technologies in Boulder, CO, technically described by Garimella et al. (2016). SPIN is a continuous flow diffusion chamber with parallel plate geometry similar to the Zurich Ice Nucleation Chamber (ZINC) (Stetzer et al., 2008) and the Portable Ice Nucleation Chamber (PINC) (Chou et al., 2011). Ice supersaturation conditions are created by coating two parallel plates with ice, holding them at different temperatures (both below 0°C), and owing an aerosol lamina in the center of a sheath flow between the walls. After flowing through the main chamber, the air stream enters an isothermal evaporation section to evaporate liquid droplets. It then passes through a linear depolarization optical particle counter (OPC) for particle, droplet, and ice counting. The instrument can be operated at aerosol temperatures as low as -55°C and ice supersaturations exceeding 60%.

SPIN was operated for FIN-02 in both a “static" mode, where the wall temperatures were controlled to provide constant aerosol temperature and supersaturation conditions, and in a “ramp" mode, also referred to as RH_w scan mode in this paper, where the wall temperatures were set to diverge from a starting temperature, resulting in increasing supersaturation at a relatively constant temperature. Ramps were generally performed such that dT/dt for each wall was 0.5°C min^{-1}. In all cases, the evaporation section is isothermal and held at the desired aerosol temperature.

The aerosol temperature and supersaturation in the lamina are calculated using the method in Rogers (1988). Uncertainties in the temperatures and supersaturations experienced by the aerosol arise from inhomogeneity in wall temperatures, uncertainties in flows, differences in conditions across the width of the aerosol lamina, and deviations from the analytical calculations in Rogers (1988). Below water saturation, aerosol particles and ice crystals are distinguishable by optical size and light depolarization. At certain conditions above water saturation, dependent on

temperature, droplets do not evaporate fully in the evaporation section and can enter the OPC. Size and depolarization signals are used to distinguish particles, droplets, and ice (Garimella et al., 2016).

S.1.9 SPIN-TROPOS (Spectrometer for Ice Nuclei – Leibniz Institute for Tropospheric Research)

The SPIN-TROPOS is nearly identical in configuration, operation, and uncertainties to the SPIN-MIT. A description of the chambers design and functionality can be found in Garimella et al. (2016). During an experiment, a continuous flow of aerosol particles is exposed for 10-12 s to controlled ice supersaturated conditions and temperatures, allowing ice nucleation to occur on the aerosol under investigation. Ice crystals grow subsequently on the fraction of particles acting as ice nuclei. The number of ice crystals formed at a specific condition is detected optically by an OPC measuring the intensity of light scattered by individual particles. The OPC signal of ice crystals is distinguished from the signal of aerosol particles by a higher intensity, caused by the larger size of ice crystals. Sequences of increasing ice saturation ramps up to above water saturation, at several constant temperatures were run during FIN-02. Experimental uncertainties in temperature and saturation, derived from the wall temperature inhomogeneity during each measurement are typically below +/-1K and +/-5%, respectively.

S.2 Instrument systems for post-processing of bulk particle collections ~~Offline instrument systems~~

All of these instrument systems employ cooled surfaces or wells holding particles exposed to water vapor, or water droplets/water volumes. Each are unique, and many are documented already in the literature, as noted herein.

S.2.1 NCSU-CS (North Carolina State University Cold Stage)

The design of the NC State cold stage-supported droplet freezing assay and data reduction methods are described in Wright and Petters (2013), Hader et al. (2014) and Hiranuma et al. (2015). For the experiments reported here, aqueous suspensions from impinger collections were distributed on the cold stage as follows. Approximately 64 drops of V = 1 µL, measured with an electronic micropipette, were placed directly on a hydrophobic glass slide. These drops are in contact with a gas-phase composed of dry nitrogen. Squalene oil to immerse the droplets, which was used in previous studies of the NC State CS was not applied. A constant cooling rate of 2°C min^{-1} was applied and the fraction of unfrozen drops was recorded using a microscope camera at incremental ΔT = 0.17°C resolution. Droplet frozen fractions versus temperature data were inverted to first determine the concentration of INPs using the method of Vali (1971):

$$c_{IN}(T) = -\frac{\ln\left(f_{unfrozen}(T)\right)}{V_{drop}} \quad \text{(S1)}$$

where $c_{IN}(T)$ is the concentration of INPs per unit volume of water (m^{-3}), $f_{unfrozen}$ is the fraction of unfrozen drops at T, and V_{drop} is the population-median drop volume.

Volumetric INP concentrations in air ($C_{INP}(T)$) were calculated via,

$$c_{INP}(T) = \frac{c_{IN}(T)\cdot f\cdot V_{imp}}{V_a} \quad \text{(S2)}$$

where V_{imp} is the total impinger water volume collected for distribution to other investigators, f accounts for the dilution of the impinger water (f = 1 for undiluted), and V_a is the air volume collected into liquid.

Samples were stored frozen at inside a -80°C freezer in Raleigh before the experiments, which were performed between April and September 2015. For each dilution, the experiment was repeated three times. In addition, experiments with diluted impinger water and on sample blanks for quality control were performed. This resulted in sample data from 4 to 9 individual experiments for a given collection. Results from these experiments were binned into 1°C temperature intervals; 95% confidence intervals for c_{INP} are reported for the binned data.

S.2.2 CMU-CS (Carnegie Mellon University Cold Stage)

The Carnegie Mellon University Cold Stage (CMU-CS) is composed of an air-cooled cascade 3-stage thermoelectric chiller (TEC) unit (TECA, AHP-1200CAS), topped with a custom-built aluminum stage described further by Polen et al. (2016) and Beydoun et al. (2017). The stage houses an external single-stage thermoelectric element (TE Technology Inc., VT-127-1.4-1.5-72P) and an associated thermistor (TE Technology Inc., MP-3176) placed beneath a removable aluminum sample dish. The thermistor provides temperature measurement for all experiments and is calibrated as described below. Droplet samples are placed on hydrophobically-coated coverslips (Hampton Research, HR3-231) in an inert squalene oil (VWR, H0097, ≥98.0% purity) environment to prevent contamination and droplet interaction. The chiller's plastic lid encloses the entire aluminum chamber that is placed on the cascade TEC to insulate it from ambient conditions. Dry air is flowed over the top of the plastic lid to prevent fogging, and a beaker of desiccant is used to dry the air inside the enclosure. The cooling ramp cycle is controlled by the TE Tech software. The single-stage element is held at 10°C until the experiment begins; it then begins to ramp to 0°C for 1 min. After this 1 min, the temperature is set to ramp down at 5°C intervals every 5 min to -40°C, producing a 1°C min^{-1} cooling rate. The cascade chiller that acts as the heat sink for the single-stage TEC is set to -45°C throughout the experiment.

Temperature calibration of the system was performed by attaching a thermistor to a hydrophobic coverslip, placing it into the sample dish, and covering it in oil. The temperature was ramped down at 1°C min^{-1} using the same program as a typical freezing experiment. The thermistor temperature was recorded at 1 Hz frequency. This was repeated multiple times to insure similar temperature ramp rates for all experiments. Following these ramps, a plot of the thermistor temperature measurement and the system measurement (using the same model thermistor, placed in its usual location in the aluminum stage under the sample dish) is generated. The linear relationship between the system temperature and the cover slip temperature is used to correct the measured system temperature to that of the cover slip during normal droplet freezing assays. Occasional tests of the cover slip temperature during a normal cooling cycle were performed to confirm that the relationship remained the same.

FIN-02 samples were kept frozen at ~ -10°C in their original containers until the droplet freezing experiment was run. Samples were thawed until no ice remained in the sample, but not completely to room temperature. A small volume of the stock sample was then poured into a sterile, unused secondary plastic vial to avoid contamination of the original sample. The original sample was then returned to the freezer. The secondary volume was used for that day's experiments exclusively and then disposed of. The secondary volume was not re-frozen between experiments to avoid repeated freezing and thawing of the sample. The secondary sample was hand shaken briefly to re-suspend any particles that may have settled out.

For Snomax® (FIN02-15-J) dilution experiments, the stock sample was poured into a second vial and returned to the freezer. From the second vial, 100 µL was pipetted into a third vial, which was immediately stored in the freezer until the experiment was performed. Shortly before the cooling experiment, the 100 µL sample was thawed completely and diluted to 50 mL (500X dilution) to examine the colder freezing temperature ice nucleants. The diluted sample was hand-mixed briefly, immediately generated into droplets, and the cooling cycle was started.

The secondary volumes of solutions were used exclusively for droplet generation to avoid contamination of the stock sample. A p2 variable electronic pipette (SEOH, 3824-1LC) was used to create 0.1 µL droplets in squalene oil on top of a hydrophobic glass coverslip. New sterile pipette tips were used between different droplet arrays to avoid contamination. Each droplet was placed on top of the oil and allowed to sink to the bottom to rest on the coverslip. Each array contained 40-60 droplets.

Pure water samples were from an in-house Milli-Q system (18.2 MΩ·cm) which is run for at least 5 min before obtaining a sample. Fourteen independent pure water arrays containing more than 600 droplets total were subjected to the standard droplet generation and temperature program. 10% of droplets had frozen by -25°C and 50% were frozen at ~ -30°C.

For uncertainty analysis, 2-3 replicate droplet arrays were measured for each sample, and their freezing temperature spectra were averaged to produce the averaged droplet freezing spectrum determined from Eqs. (S1) and (S2). A new droplet array was generated from the same secondary volume for each replicate run. The error bars are the 95% confidence intervals determined from the replicate runs for each sample. The Snomax® sample was separated into two different average spectra, due to differences observed between the replicates. The first freezing cycle, performed as soon as droplets were generated immediately after the sample had thawed, was separated from the second and third freezing cycles on new droplet arrays generated from the same secondary volume. The average spectrum from the diluted Snomax® sample was combined with the average of the 2^{nd} & 3^{rd} runs to produce the complete Snomax® spectrum. An additional first freezing cycle was also performed on a later day, by re-thawing out the Snomax® stock sample.

S.2.3 IS (Colorado State University Ice Spectrometer)

The Colorado State University Ice Spectrometer (IS) emanates from the developments of Hill et al. (2014; 2016) and is described in the approximate form used in this study by Hiranuma et al. (2015). Immersion freezing temperature spectra are obtained in the IS following dispensing 24 or 32 aliquots of 50 or 60 µL of suspensions of aerosols into sterile, 96-well PCR trays (Life Science Products Inc.) in a laminar flow cabinet. The IS is constructed using two 96-well aluminum incubation blocks (VWR), designed for cooling or heating PCR plates, placed end-to-end and encased on their sides and base by cold plates (Lytron). A ULT-80 low temperature bath (Thermo Neslab) circulating SYLTHERM XLT heat transfer fluid (Dow Corning Corporation) is used for cooling. Loaded PCR plates were placed in the blocks, the device covered with a plexiglass window and the headspace purged with 0.5-1.5 L min^{-1} of filtered (HEPA-CAP, Whatman) nitrogen. Temperature was lowered at 0.33°C min^{-1}, measured using a thermistor verification probe (Bio-Rad, Hercules, CA, VPT-0300) inserted into a side well. Frozen wells were counted at 0.2-1°C degree intervals to a limit of -27°C, and cumulative numbers of INPs mL^{-1} of suspension were estimated using Eq. (S1). INPs

per volume of air processed were calculated with Eq. (S2), where V_{imp} in this case was either of the impinger sample or of the filter suspension sample. For filter samples, filter blanks were processed in a similar manner as aerosol samples to obtain a mean background INP spectrum. Binomial sampling confidence intervals (95%) were derived using the formula recommended by Agresti and Coull (1998):

$$\mathrm{CI}_{95\%} = \left(\hat{p} + \frac{1.96^2}{2n} \pm 1.96\sqrt{\left[\hat{p}(1-\hat{p}) + {}^{1.96^2}/_{4n}\right]/n}\right) / \left(1 + {}^{1.96^2}/_{n}\right) \quad \text{(S3)}$$

where $\hat{p}$ is the proportion of droplets frozen and n is the total number of droplets. Using this formula, for a single well frozen out of 32 aliquots the $\mathrm{CI}_{95\%}$ ranges from 18% to 540% of the estimated INP concentration, while for 16/32 wells frozen it is 68-132% of the INP concentration.

Most results reported in this paper were from filter samples, rather than the shared impinger samples. APC air was typically filtered for 120-130 min at 15 L min^{-1} through a 47-mm diameter in-line aluminum filter holder (Pall) fitted with a 0.2 μm diameter pore Nuclepore polycarbonate membrane (Whatman). These were collected at the same position as impinger samples, and the collection times typically aligned. Dis-assembled filter holders were cleaned by soaking in 10% H_2O_2 for 60 min followed by rinses in deionized water (18 MΩ-cm and 0.2 μm diameter-pore filtered) and removal of excess water with a gas duster before drying. Filters were prepared in a laminar flow cabinet (<0.01 particles cc^{-1}) by soaking them in 10% H_2O_2 for 10 min followed by three rinses in deionized water, the last of which had been filtered through a 0.02 μm pore diameter filter (Anotop 25 mm syringe filter, Whatman) and drying on foil.

After particle collection, filters were transferred using clean, plastic forceps to a sterile, 60 mm petri dish (CELLTREAT) and stored frozen at -20°C. For re-suspension of particles, filters were placed in sterile 50 mL Falcon polypropylene tubes (Corning Life Sciences), 6-10 mL of suspension solution added and particles re-suspended by tumbling end-over-end on a Roto-Torque (Cole-Palmer) at 60 cycles min^{-1} for 20 min. The re-suspension solution was 2 mM KCl (to prevent any influence on the ice nucleation activity of K-Feldspar) filtered through a 0.02 μm pore diameter filter (which contained, on average, 1.6 INPs mL^{-1} at -25°C). A series of up to five 20-fold dilutions in 2 mM KCl were used to cover the full temperature range.

For the Snomax® comparison as well as for the blind studies (Hoose et al., 2017), the IS processed samples from the impingers. A sub-sample of the NCSU impinger water was melted and tested neat and after dilution in 20-fold steps in 0.02 μm pore filter deionized water.

S.2.4 μL-NIPI (Leeds Microliter Nucleation by Immersed Particles Instrument)

This instrument has been previously described in detail by Whale et al. (2015). Briefly, approximately 40 droplets of 1 μL volume are pipetted onto a hydrophobic glass slide (Hampton Research HR3-23) using an electronic pipette (Picus Biohit). The glass slide is placed onto an Asymptote EF600 Stirling cryocooler, which is used to control the temperature of the slide. The slide is enclosed within a Perspex chamber and a gentle flow of dry nitrogen is used to prevent water condensation during cooling. Freezing of droplets is monitored using a digital camera, allowing the fraction of droplets frozen at a given temperature to be determined. Samples were used for freezing experiments immediately following collection at the AIDA facility. All experiments presented here were conducted at a cooling rate of 1°C min^{-1}. Temperature error was calculated by taking the random error of the thermocouple used to measure

cold stage temperature, propagated with the melting point range observed for water, resulting in a maximum error of less than ± 0.4°C. Due to the ice nucleation induced by the slide and other sources of contamination there is a lower limit to the temperature at which this instrument can be used. In order to account for this effect a background freezing curve has been produced, which is subtracted from the cumulative nucleus spectrum for individual experiments. In this way freezing events which are not unambiguously caused by the heterogeneous nucleator under investigation are eliminated from the dataset. This process is described in O'Sullivan et al. (2015). Uncertainties in INP concentration for the binned data shown in this paper were derived from the experiment-to-experiment variability.

S.2.5 BINARY (Bielefeld Ice Nucleation ARraY)

A detailed description of the BINARY setup is given by Budke and Koop (2015). Briefly, the setup as it is used in this study consists of a compartment array for 36 droplets (V_{drop} = 0.6 µL) positioned on a Peltier cooling stage (Linkam LTS120). Each compartment is composed of a lower hydrophobic glass slide with contact to the drop, a polydimethylsiloxane (PDMS) spacer at the sides, and an upper acrylic glass. The drops are cooled down at a constant rate of 1 K min^{-1}. Freezing temperatures are determined optically based on the change in brightness when the transparent liquid drops become opaque during freezing. The temperature uncertainty is ±0.3 K.

The suspension droplets were positioned onto the hydrophobic glass slide using an electronic pipette (Brand Transferpette®, accuracy ≤ ±1.0%). To minimize sedimentation the drops were pipetted in rows of 3 x 12 drops and the suspension was stirred with a vortex mixer (VWR) at 1000 rpm in advance of each row placement.

Due to contact with the lower glass slide and dust contaminations the apparatus has an applicable temperature range from 273 K down to about 245 K (25^{th} percentile freezing temperature of "pure" water). Based on the background freezing temperatures experiments with significant overlap were excluded from further analysis. Additionally, single data points were excluded if they did not satisfy the following rules: 1.) number of INPs per litre of examined suspension (diluted) $[L^{-1}] > 10^{(51.24 - 0.186 \cdot (T\,[K]-1))}$, 2.) number of INPs per litre of examined suspension (diluted) $[L^{-1}] > 10^5$.

Data subsampling was done by temperature binning into 1 K intervals giving the midpoint of each bin. INP concentrations c_{IN} for each bin are shown in terms of median (50^{th} percentile) values. Error bars indicate the 5^{th} and 95^{th} percentile, respectively. Please note that especially for samples as Snomax® where INP concentrations increase strongly with decreasing temperature the large error bars do not stem from a significant spread of the data but rather from the steep increase in c_{IN} within a 1 K temperature bin.

S.2.6 M-AL (Mainz Acoustic Levitator)

For a detailed description of the Mainz Acoustic Levitator see Diehl et al. (2014). The M-AL consists of an ultrasonic trap (APOS BA 10, tec5 AG, Germany) in which single water droplets of 2 mm in diameter were levitated; the imaging digital video camera which served for determining the drop size; and an infrared thermometer (KT 19.82 II from Heitronics) which measured the drop surface temperature (ΔT (2σ) = 0.5 K) continuously. The M-AL was placed in the walk-in cold chamber of the Mainz vertical wind tunnel laboratory in which the air temperature was cooled down to –26±2°C, and monitored by a platinum resistance (Pt-100) thermometer. For each measurement, a

single drop was generated using a medical syringe and injected into the M-AL. Prior to injection the sample was hand shaken briefly in order to avoid any sedimentation. When injecting, the drop temperature was approximately +10°C which decayed continuously adapting to the ambient temperature. The onset of drop freezing in the M-AL is characterized by a rapid increase of the drop surface temperature ensuing from the latent heat release as the phase change is initiated. Thus, the freezing temperature could be determined in the experiments from the lowest surface temperature recorded by the infrared thermometer. For each collected impinger sample, 22 to 60 individual drops were measured without diluting the delivered FIN-02 suspensions, and the fraction of frozen drops, f_{ice}, was calculated. The only exception was the mystery sample M2-D used for blind studies (Hoose et al., 2017), which was diluted to 1:9 (i.e., 10%). Since the Snomax samples were also measured undiluted, i.e., the INPs were in high concentration, they initiated freezing at high temperatures (just below zero °C). It resulted in a very limited number of observed freezing events, and large freezing temperature uncertainties. Because of these insufficient statistics, the Snomax results from M-AL are not presented here.

FIN-02 samples were kept frozen inside a refrigerator until the freezing experiment was carried out. Samples were thawed at room temperature until no ice remained in the sample. The whole sample volume in the sample tube was used for that day's experiments exclusively.

The frozen fractions were binned into 1 °C temperature intervals giving the midpoint of each bin, and the concentration of active sites per liter water was calculated using Eq. (S1). The error of c_{IN}(T) was derived from,

$$\Delta c_{IN} = \sqrt{\left(\frac{3\cdot\ln(1-f_{ice})}{\frac{\pi}{6}d_t^4}\Delta d_t\right)^2 + \left(\frac{1}{1-f_{ice}}\cdot\frac{1}{\frac{\pi}{6}d_t^3}\Delta f_{ice}\right)^2} \quad \text{(S4)}$$

where Δf_{ice} represents the error originating from the temperature uncertainty (the error due to the drop volume uncertainty on Δf_{ice} was neglected), and was calculated from the number of drops frozen within a temperature interval of 0.5 ΔT (the factor 0.5 comes from the fact that the drops were continuously cooled down, thus, only one direction of temperature uncertainty was taken into account). Δd_t is the uncertainty of the drop size which was determined from the individual drop images, and represents a 2σ error.

The INP per liter air was calculated from Eq. (S3). Since no errors are assumed in the values of the V_{imp} or V_a, the error of INP (per liter) in air was derived from,

$$\Delta INP = \frac{\Delta c_{IN}\cdot V_{imp}}{V_a} \quad \text{(S5)}$$

where only the uncertainty from Δc_{IN} was taken into account.

S.2.7 KIT-CS (Karlsruhe Institute of Technology Cold Stage)

The central part of the experimental setup of the KIT-CS includes a Cold Stage (Linkham, Model MDBCS-196), which was used to carry out temperature ramp experiments with defined cooling rates. Cooling is achieved by pumping liquid nitrogen from a reservoir to the sample holder.

A silicon substrate (Plano GmbH, 10x10mm) for supporting droplets was first cleaned with high grade acetone (p.a.), then rinsed several times with NanoPure® water. Finally, the silicon wafer was purged with nitrogen to remove residual water. The cleaned silicon wafer was mounted into a copper basin on top of the sample holder.

A piezo injector (GeSIM, Model A010-006 SPIP) was filled with aqueous suspensions. Before printing, the substrate was cooled to the ambient dew point to reduce the evaporation of droplets. Up to one thousand identical suspension droplets (0.5 nL) were printed onto the silicon wafer, resulting in 100µm drops in spherical cap geometry. After printing, the droplets were covered with silicone oil (VWR, Rhodorsil® 47 V 1000,) to prevent any interaction between supercooled and frozen droplets. Typical ramp experiments started from 0°C to -40°C with the cooling rate of -1K min^{-1} and followed by heating the sample up to +1°C.

To accurately determine the temperature of the droplets a calibrated thin film platinum resistance sensor (Pt-100) was directly fixed on the surface of silicon substrate by applying the small amount of heat conducting paste. The Pt-100 was calibrated in the temperature range from -40°C to +30°C prior to the experiment.

A charge-coupled device (CCD)-camera (EO® progressive) with a wide field objective (DiCon fiberoptics Inc.) was used to visualize the droplets. The substrate was illuminated by a circular light emitting array installed around the objective lens. Two polarizers (one in front of the light emitting diode and one in front of the objective) were used to detect the frozen droplets. A video (AVI) and temperature file were recorded, allowing for identification of individual freezing events with 0.125s temporal resolution and 0.1K temperature accuracy. Subsequent data processing with a LabView® routine allowed for calculation of a fraction frozen curve.

For data processing, the number of INP per liter water was calculated according to Eq. (S1). The initial concentration of impurities was obtained from experiments with NanoPure® water. To estimate the background prior to homogenous freeing limit a 3rd degree polynomial was applied to pure water data. Equation (S2) was used to calculate the number of IN per liter air. The scaling factors were calculated by dividing the volumes of the impingers and the added water during operation through the sample volume. For the impingers, a sampling efficiency of 100% was assumed.

S.2.8 VODCA (Vienna Optical Droplet Crystallization Analyzer)

The Vienna Optical Droplet Crystallization Analyzer (VODCA) device has at its core a cryo-microscope cell that consists of a single-stage Peltier element (Quick-cool QC-31-1.4-3.7M) mounted on a copper cooling block on ice water sewage, placed in an airtight cell, that can be flushed with dry nitrogen between measurements (Pummer et al., 2012). A glass window in the cover of the cell allows observation of the sample via a light microscope (Olympus BX51M) and an attached camera (Hengtech MDC320), linked to a computer. The temperature measurement has a standard deviation of 0.5 K. Samples were measured as emulsion with 90 wt% paraffin and 10 wt% lanolin (water-free grade) as oil phase. The emulsion was created directly on a thin glass slide with the help of a pipette tip. We use slightly more oil than liquid phase. Droplets diameters ranged from 20-41 µm. Prepared samples were placed on a glass slide and set onto the Peltier stage, where they were chilled with a cooling rate of approx. 10 K min^{-1}. Each slide was measured at four different positions with all measured droplets being summed up to one freezing curve. This was done twice for each sample. Droplet sizes were divided in three groups regarding their diameter to minimize the error of their non-uniformity (20-26 µm, 26-35 µm, 35-41 µm). Calculations of INP concentrations in air were made following the procedures used by other investigators.

S.2.9 WISDOM

The **We**I**z**mann **S**upercooled **D**roplets **O**bservation on **M**icroarray (**WISDOM**) is an instrument designed to study immersion freezing down to the homogeneous freezing temperature region, which combines a cryo-optic-stage with microfluidics techniques for fast generation of static picoliter to nanoliter droplet arrays (Reicher et al., 2018). The droplets are generated in a flow-focusing junction, and trapped in chamber arrays following their generation. In this study, the microfluidic device was based on a design by Schmitz et al. (2009). Each experiment contained about 500 droplets with diameter of 30-40µm, suspended in an oil phase, and a cooling rate of 1 K min^{-1} was applied. Temperature uncertainty of ±0.3 K was estimated. The suspension was sonicated for 5 min prior to droplet generation process. After droplet production, the microfluidic device, which contained the droplets, was placed in a cooling stage (Linkam, THMS 600), and the experiments were monitored using an optical microscope (Olympus, BX-51, transmitted mode) and a CCD camera. Freezing events were determined automatically based on the optical difference of frozen and unfrozen droplets. The microfluidic devices were fabricated in our laboratory using polydimethylsiloxane (PDMS) and a 1-mm thick microscope slide. For each material processed, same microfluidic device was recycled, each time with a new freshly prepared array.

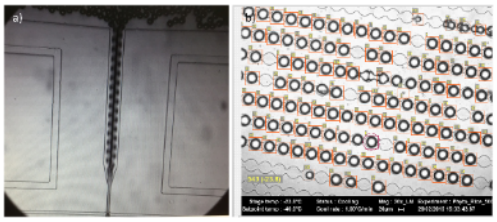

Figure S5. a) Generation process of monodispersed droplets by the microfluidic device. b) Example of an array filled with ~40 µm diameter droplets, which are trapped inside the microfluidic device chambers, before cooling applied. The orange squares present the automatic online identification of the droplets.

S.2.10 FRIDGE (FRankfurt Ice nucleation Deposition freezinG Experiment)

The FRIDGE methods address either,

a) deposition/condensation freezing INP or

b) immersion freezing INP number concentration

Both approaches work offline: aerosol particles are first collected on substrates, and the samples are then processed in the FRIDGE INP counter (Klein et al., 2010; Schrod et al., 2016). The ice nucleus counter FRIDGE itself is a 500 ml thermostated vessel with a cold table inside that carries the sample. A CCD camera records images of the sample through a window on top of the chamber.

a) Deposition/Condensation mode operation (standard mode: FRIDGE-STD)

For this measurement aerosol is collected from the atmosphere by electrostatic precipitation of the particles onto the surface of a silicon wafer of 45mm diameter Klein et al., 2010). For sampling of aerosol particles air is pumped through the central tube of a cylindrical sampler that carries 12 electrodes of gold wire. The electrodes are arranged concentrically around the inlet, and are at 12 kV voltage against the grounded substrate at the bottom of the sampler. Aerosol particles are charged by emitted electrons and are deposited downstream on the substrate. Usually 30-100 L

of air sample volume are collected. In an effort to limit the depletion of water vapor during analysis by the presence of too many particles (volume effect) the sample volume was adjusted according to the estimated particle number concentration.

After collection, the substrates are stored in at room temperature in petri dishes until analysis. During FIN-02 samples were stored at room temperature. Most samples were analyzed on-site within a couple of days. For some cases the storage ranged between 10 to 47 days. For analysis, a wafer is placed on the cold table inside the FRIDGE INP counter. The chamber is evacuated, and the temperature of the cold table is adjusted to the desired temperature. Operational temperatures may range between 0 and -35°C. For practical reasons (sample volume, detection limit, occurrence of blank counts) samples are routinely analyzed at -20°C, -25°C and -30°C, and at up to 1% water supersaturation. When the chamber is inflated with water vapor ice grows on the activated INPs to become macroscopic crystals. The vapor pressure is regulated to the desired value. The water vapor saturation is calculated from the pressure inside the chamber and from the temperature of the substrate. The substrate is photographed by a CCD camera. During the first 100 seconds of crystal growth one image is stored every 10 seconds. The image at 100 seconds is usually taken as the final image for counting. The ice crystals are counted automatically. It is assumed that one crystal represents one INP. Only bright objects (i.e., ice crystals) that grow during the 100 seconds to sizes larger than 30 Pixels (*~600µm) are counted. The operating parameters of the chamber, as well as the image processing and the counting of crystals, are controlled by LabView software.

After analysis, the sampling cell is evacuated, the temperature and vapor pressure may be set to new conditions, and the sample may be processed again. The substrates carry a coordinate system (3 laser-marked crosses) that allows to identify from the images the positions of the ice crystals on the substrate. Using this information, the morphology and composition of individual particles at the sites of crystal growth (i.e., the INPs) can be analyzed subsequently by electron microscopical analysis (with EDX) of the substrate.

b) immersion freezing mode operation (FRIDGE-IMM)

The measurement of immersion freezing INPs combines membrane filter sampling of aerosol particles with analysis of droplet freezing temperatures of aqueous filter extracts on the cold stage of FRIDGE. Aerosol is sampled on Teflon membrane filters (Fluoropore PTFE, 47 mm, 0.2µm, Merck Millipore Ltd.). Air sample volumes range between a few to 200 liters, the maximum during FIN-02. The particles are extracted into 5 or 10 ml of DIW by agitating. Around 150 drops of 0.5 µl each are taken with a pipette from the washing solution and placed randomly on a silicon plate on the cold stage of FRIDGE. With the chamber almost closed, but at ambient atmospheric pressure the temperature of the cold stage is lowered by 1°C min^{-1}. The number of drops that freeze as function of temperature is recorded by the CCD camera and is counted. This process is repeated several times with fresh droplets. A total number of 1000 droplets at minimum is exposed. The INP number concentration is derived following Eqs. (S1) and (S2).

The uncertainty in the measurement is ± 0.2°C for T, and is estimated at around 40% for INP number concentrations at -20°C for Illite NX, but may become lower with decreasing temperature.

S.2.11 DFPC-ISAC (Dynamic Filter Processing Chamber – Institute of Atmospheric Sciences and Climate (CNR Bologna))

The Dynamic Filter Processing Chamber (DFPC) (Santachiara et al., 2010; Belosi et al., 2014) is a replica of the Langer dynamic developing chamber (Langer and Rogers, 1975). Concentrations of INPs are detected by the membrane filter technique. Aerosol particles are sampled onto nitrocellulose black gridded membrane filters (0.45 μm porosity Millipore). At the FIN-02 workshop sampling flow rate was 2 L min^{-1} and the volume sampled was about 20 L. After collection, the filters are stored in Petri dishes. Before being processed the sampled filter is inserted onto a metal plate, previously covered with a smooth surface of paraffin, in order to assure good thermal contact of the filter with the supporting substrate. Subsequently the paraffin is slightly heated and rapidly cooled in order to fill the filter pores.

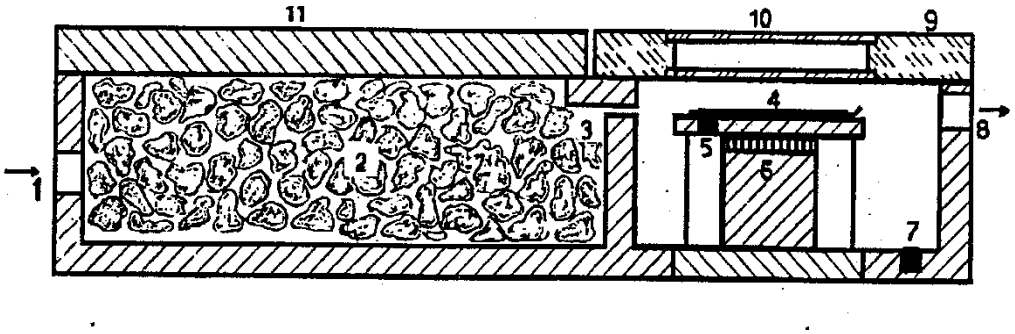

Figure S6. 1: air inlet; 2: minced ice; 3: slit and air temperature thermocouple; 4: filter; 5: filter temperature thermocouple; 6: Peltier cooling device; 7: thermocouple; 8: air outlet; 9: plexiglass cover; 10: observation slit; 11: aluminium plate.

Figure S6 shows the schematic of the chamber, which is housed in a refrigerator. Filtered air is forced by a pump to flow through the chamber in a closed loop. Air enters the chamber through a perforated plate (1), spreads into the ice bed (2) and becomes saturated with respect to ice, which is cooled by the base plate. The temperature of the air is measured just in front of the nozzle (3) aiming the air at the metal plate supporting the sampled filter (4), placed on a top of the Peltier cooled surface (6). The temperatures of the air and of the Peltier device (7) are measured with resistance temperature sensors (PT 100). By controlling the temperatures of the filter and of the air, saturated with respect to finely minced ice and flowing continuously grazing the filter, it is possible to obtain different supersaturations with respect to ice and water, SS_{ice} and SS_w, respectively. Therefore, deposition and condensation freezing ice nucleation modes can be investigated. Measurement uncertainties in consideration of T and SS_w uncertainties are estimated as 30% in all cases. Limit of detection is estimated as 0.025 L^{-1} on the basis of contaminant background of 0.5 per filter (Belosi et al., 2014) and the sample volumes used in this study.

Supersaturations are calculated theoretically from vapour pressures of ice and water (Buck, 1981) at the considered temperatures. The exposure time of the filter is 20 min, long enough to grow sizeable ice crystals on INPs at the considered relative humidity and temperature. Use of the dynamic chamber circumvents some of the problems arising with the static chamber, e.g. that the moisture supply under static conditions may be rather inadequate at the filter

surface, both in overcoming the effect of hygroscopic particles and in activating all potential INPs. Fig. S7 shows a picture of the DFPC with the top cover removed (minced ice is visible) and a filter with ice crystals.

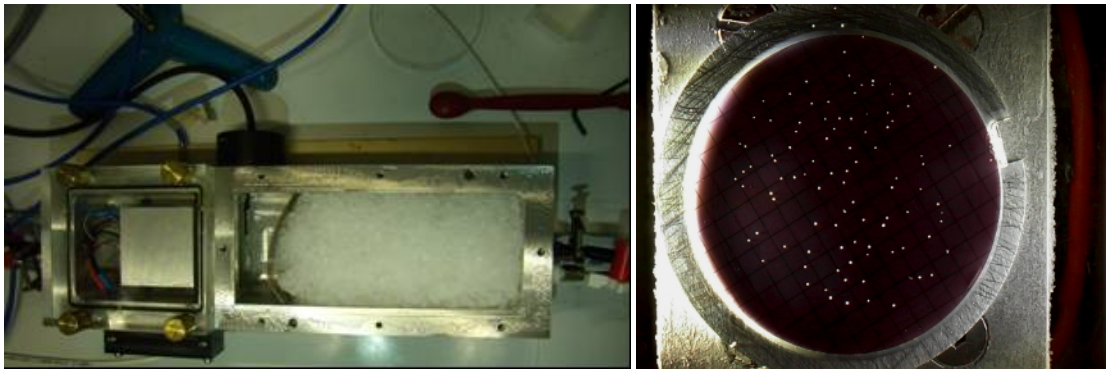

Figure S7. DFPC housed in a refrigerator (on the left). Ice crystal growth (on the right).

Table S1. Direct processing (online) instrument data used in the manuscript figures. Listed are the date, experiment identifier, aerosol particle sample type, sample number if applicable, instrument, relative humidity, temperature, correction factor (*: see footnote), INP concentration in air (#: see footnote), positive INP concentration uncertainty defined by confidence interval, negative INP uncertainty, total particle number of reference to INP concentration, surface area concentration, INP active fraction, positive uncertainty in active fraction defined by confidence interval, negative uncertainty in active fraction, active site density, positive uncertainty in active site density, negative uncertainty in active site density, threshold size or optical particle counter channel for defining ice crystals versus aerosol particles ("depol" refers to depolarization detection of ice), and evaporation section temperature (&: see footnote).

Date	Expt	Aerosol	Instrument	Sample	RHw	Temp	Corr fact*	INP Conc.#	ci INP+	ci INP-	total particles	Sfc area	frac	frac_ci+	frac_ci-	$n_{s,geo}$	$n_{s,geo}$ ci+	$n_{s,geo}$ ci-	Ice threshold	Evap T&
					%	°C		m^{-3}	m^{-3}	m^{-3}	cm^{-3}	$\mu m^2 cm^{-3}$				m^{-2}	m^{-2}	m^{-2}		
11-Mar-15	APC-01	IS03	SPIN-TROPOS		101.3	-34.4	1.0	9750000.0	390000.0	390000.0	390.0	230.0	2.50E-02	1.00E-03	1.00E-03	4.24E+10	1.07E+10	1.07E+10	3 µm	lamina T
13-Mar-15	APC-03	IS03	CFDC-CSU		105.5	-20.9	1.0	70900.0	10500.0	10500.0	2000.0	430.0	3.55E-05	5.25E-06	5.25E-06	1.74E+08	8.58E+07	8.58E+07	3 µm	cold wall
13-Mar-15			INKA		105.5	-20.3	1.0	75753.7	15150.7	15150.7	1800.0	414.0	4.21E-05	8.42E-06	8.42E-06	3.08E+09	7.80E+08	3.29E+09	>4 µm	cold wall
16-Mar-15	APC-08	IS03	CFDC-CSU		105.5	-30.3	4.0	18107847.8	680412.3	171600.0	18636.0	5569.0	9.72E-04	3.65E-05	3.65E-05	3.08E+09	7.80E+08	3.29E+09	Chnl 165	cold wall
					105.4	-25.0	12.2	234774.7	148406.8	12227.0	18636.0	5569.0	1.26E-05	7.96E-06	7.96E-06	4.00E+07	2.72E+07	8.37E+08	Chnl 165	cold wall
					105.5	-20.0	10.8	79853.2	93881.4	7392.0	18636.0	5569.0	4.28E-06	5.04E-06	5.04E-06	1.36E+07	1.64E+07	1.86E+08	Chnl 165	cold wall
		IS03	SPIN-TROPOS		103.7	-34.4	1.8	181542633.7	2648820.8	2648820.8	18636.0	5569.0	1.04E-01	1.51E-03	1.51E-03	4.51E+11	6.58E+09	6.58E+09	3 µm	lamina T
					103.6	-27.0	3.3	4853838.9	616796.0	616796.0	18636.0	5569.0	4.26E-03	5.41E-04	5.41E-04	1.85E+10	2.35E+09	2.35E+09	3 µm	lamina T
		IS03	INKA		105.1	-25.0	5.0	196000.0	39200.0	39200.0	18636.0	5569.0	1.06E-05	2.12E-06	2.12E-06	4.41E+07	8.83E+06	8.83E+06	>4 µm	cold wall
					104.7	-30.1	12.1	20449000.0	4089800.0	4089800.0	18636.0	5569.0	7.35E-04	1.47E-04	1.47E-04	3.19E+09	6.39E+08	6.39E+08	>4 µm	cold wall
16-Mar-15	AIDA-04	IS03	AIDA		101.7	-30.6	1.0	1569810.0	1883770.0	1255850.0	484.0	86.0	4.18E-03	5.02E-03	3.35E-03	2.35E+10	2.84E+10	1.90E+10	N/A	N/A
					101.3	-31.1	1.0	3459500.0	4151400.0	2767600.0	484.0	86.0	9.34E-03	1.12E-02	7.47E-03	5.26E+10	6.33E+10	4.24E+10	N/A	N/A
					101.1	-31.6	1.0	6587250.0	7904700.0	5269800.0	484.0	86.0	1.81E-02	2.17E-02	1.45E-02	1.02E+11	1.23E+11	8.21E+10	N/A	N/A
			CFDC-CSU		105.5	-25.0	1.0	68778.0	16326.0	16326.0	394.0	93.0	1.75E-04	4.14E-05	4.14E-05	7.40E+08	1.90E+08	1.90E+08	3 µm	cold wall
					105.6	-30.2	1.0	584341.0	68601.0	68601.0	421.0	97.2	1.39E-03	1.63E-04	1.63E-04	6.01E+09	9.27E+08	9.27E+08	3 µm	cold wall
					109.4	-25.3	1.0	828162.0	59964.0	59964.0	394.0	93.0	2.10E-03	1.52E-04	1.52E-04	8.90E+09	1.10E+09	1.10E+09	3 µm	cold wall
					111.5	-30.0	1.0	8946137.0	193338.0	193338.0	421.0	97.2	2.12E-02	4.59E-04	4.59E-04	9.20E+10	9.42E+09	9.42E+09	3 µm	cold wall
			CIC-PNNL		106.0	-30.0	1.0	17160000.0	-	-	550.0	99.0	1.50E-02	-	-	8.33E+10	2.08E+10	2.08E+10	3 µm	lamina T
19-Mar-15	AIDA-10	IS03	AIDA		101.1	-26.3	1.0	192448.0	230938.0	153958.0	400.0	132.0	6.17E-04	7.40E-04	4.93E-04	1.87E+09	2.25E+09	1.51E+09	N/A	N/A
					101.2	-26.5	1.0	543041.0	651649.0	434433.0	400.0	132.0	1.76E-03	2.12E-03	1.41E-03	5.34E+09	6.44E+09	4.31E+09	N/A	N/A
					102.5	-26.7	1.0	732475.0	878970.0	585980.0	400.0	132.0	2.41E-03	2.89E-03	1.93E-03	7.30E+09	8.79E+09	5.89E+09	N/A	N/A
					102.2	-26.9	1.0	823390.0	988068.0	658712.0	400.0	132.0	2.74E-03	3.29E-03	2.19E-03	8.31E+09	1.00E+10	6.70E+09	N/A	N/A
					100.8	-27.0	1.0	1162000.0	1394400.0	929600.0	400.0	132.0	3.92E-03	4.70E-03	3.13E-03	1.19E+10	1.43E+10	9.57E+09	N/A	N/A
			CFDC-CSU		105.5	-30.6	1.0	2413879.0	120848.0	120848.0	378.0	134.0	6.39E-03	3.20E-04	3.20E-04	1.80E+10	2.01E+09	2.01E+09	3 µm	cold wall
			PIMCA-PINC		N/A	-38.5	1.0	299061333.2	33953807.2	38404474.0	400.0	134.0	7.48E-01	8.49E-02	9.60E-02	2.23E+12	6.13E+11	1.72E+11	depol	N/A
					N/A	-38.2	1.0	276145333.2	36848323.2	34481656.8	400.0	134.0	6.90E-01	9.21E-02	8.62E-02	2.06E+12	5.84E+11	1.63E+11	depol	N/A
					N/A	-37.8	1.0	212377000.0	48921000.0	38201000.0	400.0	134.0	5.31E-01	1.22E-01	9.55E-02	1.58E+12	5.39E+11	1.66E+11	depol	N/A
					N/A	-36.5	1.0	134644000.0	68755168.4	47004502.0	400.0	134.0	3.37E-01	1.72E-01	1.18E-01	1.00E+12	5.71E+11	2.45E+11	depol	N/A
					N/A	-36.4	1.0	120190000.0	62093168.8	40477168.8	400.0	134.0	3.00E-01	1.55E-01	1.01E-01	8.97E+11	5.15E+11	2.16E+11	depol	N/A
					N/A	-36.3	1.0	97368000.0	54838768.0	36028768.0	400.0	134.0	2.43E-01	1.37E-01	9.01E-02	7.27E+11	4.48E+11	2.00E+11	depol	N/A
					N/A	-34.0	1.0	83825333.2	67323007.2	37000340.8	400.0	134.0	2.10E-01	1.68E-01	9.25E-02	6.26E+11	5.26E+11	2.67E+11	depol	N/A
26-Mar-15	AIDA-22	IS03	CFDC-TAMU		103.0	-25.5	1.0	171540.1129	148194.826	148194.826	1850.0	890.0	9.27E-05	8.01E-05	8.01E-05	1.93E+08	1.67E+08	1.67E+08	2 µm	~lamina T@
					101.7	-26.5	1.0	1865311.781	287731.3033	287731.3033	1600.0	870.0	1.17E-03	1.80E-04	1.80E-04	2.14E+09	3.31E+08	3.31E+08	2 µm	~lamina T@
					104.0	-30.4	1.0	1302200.052	287731.3033	287731.3033	1507.0	802.0	8.64E-04	1.91E-04	1.91E-04	1.62E+09	3.59E+08	3.59E+08	2 µm	~lamina T@
			FRIDGE-STD	73	101.0	-20.0	1.0	4390.0	3740.0	3740.0	1500.0	852.0	2.93E-06	2.49E-06	2.49E-06	5.15E+06	4.39E+06	4.39E+06	N/A	N/A
					101.0	-25.0	1.0	14800.0	12600.0	12600.0	1500.0	852.0	9.87E-06	8.40E-06	8.40E-06	1.74E+07	1.48E+07	1.48E+07	N/A	N/A
					101.0	-30.0	1.0	159000.0	136000.0	136000.0	1500.0	852.0	1.06E-04	9.07E-05	9.07E-05	1.87E+08	1.60E+08	1.60E+08	N/A	N/A
			FRIDGE-STD	74	101.0	-20.0	1.0	1100.0	936.0	936.0	1500.0	852.0	7.33E-07	6.24E-07	6.24E-07	1.39E+06	1.23E+06	1.23E+06	N/A	N/A

					101.0	-25.0	1.0	82300.0	70200.0	70200.0	1500.0	852.0	5.49E-05	4.68E-05	4.68E-05	1.04E+08	9.23E+07	9.23E+07	N/A	N/A
					101.0	-30.0	1.0	777000.0	663000.0	663000.0	1500.0	852.0	5.18E-04	4.42E-04	4.42E-04	9.80E+08	8.72E+08	8.72E+08	N/A	N/A
			PINC		112.4	-30.5	1.0	521000.0	50000.0	50000	1500.0	901.0	3.47E-04	3.33E-05	3.33E-05	7.32E+08	1.96E+08	1.96E+08	3 μm	warm wall
					109.8	-25.5	1.0	17700.0	10000.0	10000	1500.0	892.0	1.18E-05	6.67E-06	6.67E-06	2.23E+07	1.38E+07	1.38E+07	3 μm	warm wall
			DFPC-ISAC		101.0	-20.2	1.0	600.0	180.0	180.0	1600.0	850.0	4.00E-07	1.20E-07	1.20E-07	7.53E+05	2.94E+05	2.94E+05	N/A	N/A
27-Mar-15	AIDA-25	IS03	PINC		101.9	-35.5	1.0	7500000.0	200000.0	200000.0	973.0	303.0	3.75E-02	1.00E-03	1.00E-03	1.20E+11	3.03E+10	3.03E+10	3 μm	warm wall
18-Mar-15	AIDA-08	FS02	CFDC-CSU		105.5	-30.0	1.0	175974148.0	1175834.0	1175834.0	380.0	155.0	4.78E-01	3.19E-03	3.19E-03	1.17E+12	2.93E+11	2.93E+11	3 μm	cold wall
			DFPC-ISAC		101.0	-20.2	1.0	87.0	26.1	26.1	380.0	155.0	2.49E-04	7.46E-05	7.46E-05	6.09E+08	2.38E+08	2.38E+08	N/A	N/A
			FRIDGE-STD	21	101.0	-20	1.0	48300.0	47800.0	47800.0	380.0	155.0	1.27E-04	1.26E-04	1.26E-04	3.12E+08	3.18E+08	3.18E+08	N/A	N/A
					101.0	-25	1.0	677000.0	669000.0	669000.0	380.0	155.0	1.78E-03	1.76E-03	1.76E-03	4.37E+09	4.45E+09	4.45E+09	N/A	N/A
			PIMCA-PINC		N/A	-34.8	1.0	358134800.0	9184517.9	11168117.9	380.0	155.0	9.42E-01	2.42E-02	2.94E-02	2.31E+12	5.81E+11	1.46E+11	depol	N/A
					N/A	-31.4	1.0	365743666.5	4440032.5	4448899.4	380.0	155.0	9.62E-01	1.17E-02	1.17E-02	2.36E+12	5.91E+11	1.48E+11	depol	N/A
					N/A	-29.0	1.0	361282466.5	7665231.2	7829898.1	380.0	155.0	9.51E-01	2.02E-02	2.06E-02	2.33E+12	5.85E+11	1.47E+11	depol	N/A
					N/A	-27.0	1.0	288390866.5	23884327.0	20018460.4	380.0	155.0	7.59E-01	6.29E-02	5.27E-02	1.86E+12	4.90E+11	1.27E+11	depol	N/A
					N/A	-25.9	1.0	193612533.5	32959764.4	24299564.4	380.0	155.0	5.10E-01	8.67E-02	6.39E-02	1.25E+12	3.78E+11	1.06E+11	depol	N/A
					N/A	-25.0	1.0	92454000.0	46089619.0	30184085.5	380.0	155.0	2.43E-01	1.21E-01	7.94E-02	5.96E+11	3.33E+11	1.37E+11	depol	N/A
					N/A	-24.0	1.0	52326000.0	47028852.4	26026252.4	380.0	155.0	1.38E-01	1.24E-01	6.85E-02	3.38E+11	3.15E+11	1.75E+11	depol	N/A
					N/A	-23.2	1.0	34250666.5	39367891.7	19691491.7	380.0	155.0	9.01E-02	1.04E-01	5.18E-02	2.21E+11	2.60E+11	1.63E+11	depol	N/A
19-Mar-15	APC-14	FS02	CFDC-CSU		105.0	-25.0	15.1	1927241005.9	7604512.7	7604512.7	7750.2	3703.1	2.49E-01	9.81E-04	5.80E-04	5.20E+11	1.30E+11	1.30E+11	3 μm	cold wall
			INKA		104.1	-20.0	4.1	5378173.7	114153.8	114153.8	7750.2	3703.1	6.94E-04	1.47E-05	1.47E-05	1.45E+09	3.64E+08	3.64E+08	>4 μm	cold wall
					104.7	-25.0	5.7	903242700.7	2460189.4	2460189.4	7750.2	3703.1	1.17E-01	3.17E-04	3.17E-04	2.44E+11	6.10E+10	6.10E+10	>4 μm	cold wall
					104.7	-30.1	8.6	2670340000.0	18051988.9	18051988.9	7750.2	3703.1	3.45E-01	2.33E-03	2.33E-03	7.21E+11	1.80E+11	1.80E+11	>4 μm	cold wall
			PIMCA-PINC		N/A	-32.9	1.0	7575532413.6	48408615.5	78324372.0	7750.2	3703.1	9.77E-01	6.25E-03	1.01E-02	2.05E+12	5.12E+11	5.12E+11	depol	N/A
					N/A	-29.4	1.0	7558494901.9	44331121.1	86995950.1	7750.2	3703.1	9.75E-01	5.72E-03	1.12E-02	2.04E+12	5.10E+11	5.11E+11	depol	N/A
					N/A	-28.4	1.0	7299031259.4	135528351.7	202877555.0	7750.2	3703.1	9.42E-01	1.75E-02	2.62E-02	1.97E+12	4.94E+11	4.96E+11	depol	N/A
					N/A	-28.1	1.0	7097371159.5	219962614.0	194154461.4	7750.2	3703.1	9.16E-01	2.84E-02	2.51E-02	1.92E+12	4.83E+11	4.82E+11	depol	N/A
					N/A	-27.4	1.0	6882354883.3	244974891.3	305633094.6	7750.2	3703.1	8.88E-01	3.16E-02	3.94E-02	1.86E+12	4.69E+11	4.72E+11	depol	N/A
					N/A	-27.1	1.0	6434755232.9	380252656.0	427838859.4	7750.2	3703.1	8.30E-01	4.91E-02	5.52E-02	1.74E+12	4.46E+11	4.50E+11	depol	N/A
					N/A	-26.1	1.0	5234714884.3	554639769.7	479643711.5	7750.2	3703.1	6.75E-01	7.16E-02	6.19E-02	1.41E+12	3.84E+11	3.76E+11	depol	N/A
					N/A	-25.5	1.0	3817694879.0	599085113.2	434806789.4	7750.2	3703.1	4.93E-01	7.73E-02	5.61E-02	1.03E+12	3.04E+11	2.83E+11	depol	N/A
			SPIN-TROPOS		105.7	-36.5	6.6	3013418082.5	17131132.6	17131132.6	7750.2	3703.1	3.89E-01	2.21E-03	1.43E-03	8.14E+11	2.03E+11	2.03E+11	3 μm	lamina T
					105.1	-31.7	8.0	3235505258.5	19002992.0	19002992.0	7750.2	3703.1	4.17E-01	2.45E-03	1.59E-03	8.74E+11	2.18E+11	2.18E+11	3 μm	lamina T
					103.9	-27.2	7.5	1965720157.0	16199258.7	16199258.7	7750.2	3703.1	2.54E-01	2.09E-03	1.94E-03	5.31E+11	1.33E+11	1.33E+11	3 μm	lamina T
					102.8	-22.9	9.5	147317204.7	5739492.3	5739492.3	7750.2	3703.1	1.90E-02	7.41E-04	7.55E-04	3.98E+10	1.01E+10	1.01E+10	3 μm	lamina T
			SPIN-MIT		105.0	-30.8	4.8	331363861.3	-	-	7750.2	3703.1	4.28E-02	-	-	8.95E+10	2.24E+10	2.24E+10	depol	lamina T[%]
					105.0	-21.3	6.2	217900313.9	-	-	7750.2	3703.1	2.81E-02	-	-	5.88E+10	1.47E+10	1.47E+10	depol	lamina T[%]
20-Mar-15	AIDA-11	FS02	CFDC-CSU		105.7	-20.1	1.0	67556.0	7422.0	7422.0	389.0	151.0	1.80E-04	9.00E-05	9.00E-05	4.64E+08	3.43E+09	3.43E+09	3 μm	cold wall
			CIC-PNNL		106.0	-30.0	1.0	171000000.0	-	-	380.0	151.0	4.50E-01	-	-	1.13E+12	2.83E+11	2.83E+11	3 μm	lamina T
			FRIDGE-STD	28	101.0	-20.0	1.0	411000.0	406000.0	406000.0	380.0	155.0	1.08E-03	1.07E-03	1.07E-03	2.65E+09	2.70E+09	2.70E+09	N/A	N/A
					99.0	-25.0	1.0	7880000.0	7800000.0	7800000.0	380.0	155.0	2.07E-02	2.05E-02	2.05E-02	5.08E+10	5.19E+10	5.19E+10	N/A	N/A
					99.0	-30.0	1.0	25800000.0	25500000.0	25500000.0	380.0	155.0	6.79E-02	6.71E-02	6.71E-02	1.66E+11	1.70E+11	1.70E+11	N/A	N/A
			SPIN-MIT		103.0	-31.1	1.0	80000.0	79.0	79.0	405.0	252.0	1.98E-01	9.88E-04	9.88E-04	3.17E+11	7.94E+10	7.94E+10	depol	lamina T[%]
					106.0	-21.7	1.0	15000.0	6.8	6.8	382.0	151.0	3.93E-02	4.53E-04	4.53E-04	9.93E+10	2.49E+10	2.49E+10	depol	lamina T[%]
			SPIN-TROPOS		104.1	-27.2	1.0	120590.0	448.7	448.7	389.0	151.0	3.10E-01	3.72E-03	3.72E-03	7.99E+11	2.00E+11	2.00E+11	3 μm	lamina T
					103.3	-24.4	1.0	37500.0	94.8	94.8	375.0	145.0	1.00E-01	2.53E-03	2.53E-03	2.59E+11	6.50E+10	6.50E+10	3 μm	lamina T
23-Mar-15	AIDA-14	FS02	AIDA		101.6	-20.3	1.0	1332420.0	1598900.0	1065940.0	300.0	114.0	5.03E-03	6.04E-03	4.03E-03	1.32E+10	1.60E+10	1.07E+10	N/A	N/A
					100.8	-20.9	1.0	6922620.0	8307140.0	5538100.0	300.0	114.0	2.66E-02	3.19E-02	2.13E-02	7.00E+10	8.43E+10	5.64E+10	N/A	N/A

			CFDC-CSU		105.6	-20.2	1.0	9917338.0	150739.0	150739.0	300.0	114.0	3.41E-02	5.19E-04	5.19E-04	8.98E+10	2.40E+10	2.40E+10	3 μm	cold wall
					105.5	-25.6	1.0	105206098.0	751115.0	751115.0	268.0	102.0	3.69E-01	2.63E-03	2.63E-03	9.69E+11	2.42E+11	2.42E+11	3 μm	cold wall
					105.5	-30.2	1.0	121683497.0	1277222.0	1277222.0	270.0	107.0	4.51E-01	4.73E-03	4.73E-03	1.14E+12	2.84E+11	2.84E+11	3 μm	cold wall
			INKA		104.0	-20.0	1.0	139424.0	27884.9	27884.9	290.0	115.0	4.81E-04	9.62E-05	9.62E-05	1.21E+09	3.88E+08	3.88E+08	>4 μm	cold wall
					103.3	-30.0	1.0	70256300.0	14051300.0	14051300.0	290.0	102.0	2.42E-01	4.85E-02	4.85E-02	6.89E+11	2.21E+11	2.21E+11	>4 μm	cold wall
			PINC		110.9	-30.5	1.0	98000.0	700.0	700.0	300.0	114.0	3.92E-01	2.80E-03	2.80E-03	1.03E+12	2.58E+11	2.58E+11	3 μm	warm wall
					104.7	-25.3	1.0	2840.0	140.0	140.0	268.0	102.0	1.14E-02	5.60E-04	5.60E-04	2.98E+10	7.61E+09	7.61E+09	3 μm	warm wall
					106.6	-20.3	1.0	14.7	20.0	20.0	270.0	107.0	5.88E-05	8.00E-05	8.00E-05	1.48E+08	2.05E+08	2.05E+08	3 μm	warm wall
17-Mar-15	APC-16	SM04	CFDC-CSU		105.2	-9.3	12.9	169686600.0	3096.0	3096.0	27802.0	4028.0	6.10E-03	1.11E-04	1.11E-04	4.21E+10	1.06E+10	1.06E+10	2 μm	cold wall
					101.8	-19.9	5.0	186550000.0	2205.0	2205.0	27802.0	4028.0	6.71E-03	7.93E-05	7.93E-05	4.63E+10	1.16E+10	1.16E+10	3 μm	cold wall
			CFDC-TAMU		109.3	-33.0	2.8	242718750.0	94660312.0	94660312.0	27802.0	4028.0	8.73E-03	3.40E-03	3.40E-03	6.03E+10	2.79E+10	2.79E+10	2 μm	~lamina T[@]
					101.0	-21.0	5.3	847058824.0	330352941.0	330352941.0	27802.0	4028.0	3.05E-02	1.19E-02	1.19E-02	2.10E+11	9.74E+10	9.74E+10	2 μm	~lamina T[@]
			INKA		104.3	-10.1	3.8	151875000.0	30375000.0	30375000.0	27802.0	4028.0	4.98E-03	1.13E-03	1.13E-03	3.44E+10	1.16E+10	1.16E+10	>4 μm	cold wall
					104.4	-10.1	4.0	156246400.0	31249320.0	31249320.0	27802.0	4028.0	3.16E-03	1.14E-04	1.14E-04	2.18E+10	5.51E+09	5.51E+09	>4 μm	cold wall
					104.9	-15.0	5.7	149797834.4	29959509.6	29959509.6	27802.0	4028.0	5.39E-03	1.08E-03	1.11E-04	3.72E+10	1.19E+10	9.33E+09	>4 μm	cold wall
					109.8	-15.0	5.9	530290657.9	106057894.7	106057894.7	27802.0	4028.0	1.91E-02	3.81E-03	1.11E-04	1.32E+11	4.21E+10	3.29E+10	>4 μm	cold wall
					104.2	-20.1	8.5	175567924.5	35113584.9	35113584.9	27802.0	4028.0	6.31E-03	1.26E-03	1.11E-04	4.36E+10	1.40E+10	1.09E+10	>4 μm	cold wall
					104.2	-20.1	8.6	171373714.3	34274742.9	34274742.9	27802.0	4028.0	6.16E-03	1.23E-03	1.11E-04	4.25E+10	1.36E+10	1.07E+10	>4 μm	cold wall
					110.2	-20.0	10.5	202632907.0	40526476.7	40526476.7	27802.0	4028.0	7.29E-03	1.46E-03	1.11E-04	5.03E+10	1.61E+10	1.26E+10	>4 μm	cold wall
			SPIN-MIT		105.0	-20.0	3.4	82127547.2	-	-	27802.0	4028.0	2.95E-03	-	-	2.04E+10	5.10E+09	5.10E+09	depol	lamina T[%]
					105.0	-15.0	4.1	180294545.5	-	-	27802.0	4028.0	6.48E-03	-	-	4.48E+10	1.12E+10	1.12E+10	depol	lamina T[%]
			SPIN-TROPOS		101.3	-18.6	3.5	138461538.5	31475769.2	31475769.2	27802.0	4028.0	4.98E-03	1.13E-03	1.13E-03	3.44E+10	1.16E+10	1.16E+10	3 μm	lamina T
					100.9	-14.0	4.4	87804878.0	3165365.9	3165365.9	27802.0	4028.0	3.16E-03	1.14E-04	1.14E-04	2.18E+10	5.51E+09	5.51E+09	3 μm	lamina T
17-Mar-15	AIDA-06	SM04	AIDA		101.6	-24.2	1.0	2505730.0	3006880.0	2004580.0	241.0	23.3	1.11E-02	1.33E-02	8.85E-03	1.14E+11	1.38E+11	9.23E+10	N/A	N/A
					101.6	-24.6	1.0	2316010.0	2779210.0	1852810.0	241.0	23.3	1.04E-02	1.24E-02	8.30E-03	1.07E+11	1.29E+11	8.65E+10	N/A	N/A
					101.8	-25.2	1.0	4938950.0	5926740.0	3951160.0	241.0	23.3	2.26E-02	2.71E-02	1.80E-02	2.33E+11	2.81E+11	1.88E+11	N/A	N/A
			CFDC-CSU		105.5	-10.0	1.0	552972.0	59028.0	59028.0	259.0	24.0	2.14E-03	2.28E-04	2.28E-04	2.30E+10	3.37E+09	3.37E+09	3 μm	cold wall
					105.5	-15.0	1.0	799823.0	73751.0	73751.0	241.0	23.0	3.24E-03	2.99E-04	2.99E-04	3.48E+10	4.73E+09	4.73E+09	3 μm	cold wall
					108.4	-9.9	1.0	733245.0	32036.0	32036.0	259.0	24.0	2.83E-03	1.24E-04	1.24E-04	3.06E+10	3.33E+09	3.33E+09	3 μm	cold wall
					124.4	-15.4	1.0	1140013.0	115665.0	115665.0	241.0	23.0	4.62E-03	4.68E-04	4.68E-04	4.96E+10	7.06E+09	7.06E+09	3 μm	cold wall
			FRIDGE-STD	6	101.0	-10.0	1.0	648000.0	297000.0	297000.0	260.0	25.0	2.59E-03	1.19E-03	1.19E-03	2.70E+10	1.41E+10	1.41E+10	N/A	N/A
					101.0	-15.0	1.0	1150000.0	530000.0	530000.0	260.0	25.0	4.60E-03	2.12E-03	2.12E-03	4.78E+10	2.51E+10	2.51E+10	N/A	N/A
					101.0	-20.0	1.0	1350000.0	621000.0	621000.0	260.0	25.0	5.40E-03	2.48E-03	2.48E-03	5.62E+10	2.94E+10	2.94E+10	N/A	N/A
			SPIN-TROPOS		102.0	-18.3	1.0	1912.5	215.0	215.0	255.0	26.0	7.50E-03	8.43E-04	8.43E-04	7.36E+10	2.02E+10	2.02E+10	3 μm	lamina T
					101.2	-13.8	1.0	725.2	139.1	139.1	259.0	24.0	2.80E-03	5.37E-04	5.37E-04	3.02E+10	9.52E+09	9.52E+09	3 μm	lamina T
21-Mar-15	AIDA-13	SM04	AIDA		101.1	-9.1	1.0	2215550.0	2658660.0	1772440.0	229.0	23.0	9.81E-03	1.18E-02	7.85E-03	1.18E+11	7.88E+10	7.88E+10	N/A	N/A
			CFDC-CSU		105.5	-9.5	1.0	1135824.0	44125.0	44125.0	229.0	23.0	4.53E-03	1.76E-04	1.76E-04	4.94E+10	5.30E+09	5.30E+09	3 μm	cold wall
					105.5	-14.9	1.0	1128809.0	73599.0	73599.0	229.0	23.0	4.50E-03	2.93E-04	2.93E-04	4.91E+10	5.86E+09	5.86E+09	3 μm	cold wall
					106.0	-9.6	1.0	733245.0	32036.0	32036.0	229.0	23.0	4.57E-03	1.73E-04	1.73E-04	4.99E+10	5.34E+09	5.34E+09	3 μm	cold wall
					109.4	-14.5	1.0	1148100.0	43328.0	115665.0	229.0	23.0	4.82E-03	3.11E-04	3.11E-04	5.26E+10	6.26E+09	6.26E+09	3 μm	cold wall
			CFDC-TAMU		102.4	-15.0	1.0	984751.9	406643.9	406643.9	75.0	8.0	4.10E-03	1.69E-03	1.69E-03	3.85E+10	1.86E+10	1.86E+10	2 μm	~lamina T[@]
					101.2	-20.0	1.0	839963.3	685955.4	685955.4	230.0	23.0	3.50E-03	2.86E-03	2.86E-03	3.50E+10	2.99E+10	2.99E+10	2 μm	~lamina T[@]
			INKA		104.6	-10.0	1.0	1210537.0	77950.0	216243.0	279.0	24.9	4.51E-03	9.01E-04	9.01E-04	5.05E+10	1.62E+10	1.62E+10	>4 μm	cold wall
					104.6	-15.0	1.0	866660.0	173332.0	173332.0	250.0	23.0	3.61E-03	7.22E-04	7.22E-04	3.93E+10	1.26E+10	1.26E+10	>4 μm	cold wall
27-Mar-15	AIDA-27	SM04	AIDA		99.5	-12.6	1.0	1953930.0	2344720.0	1563140.0	236.0	28.3	9.01E-03	1.08E-02	7.21E-03	9.05E+10	6.06E+10	6.06E+10	N/A	N/A
					101.3	-13.6	1.0	2453210.0	2943850.0	1962570.0	236.0	28.3	1.15E-02	1.38E-02	9.22E-03	1.16E+11	7.75E+10	7.75E+10	N/A	N/A
16-Mar-15	AIDA-05	SDAr01	CFDC-CSU		105.5	-25.0	1.0	4403989.0	215519.0	215519.0	370.0	185.0	1.26E-02	6.15E-04	6.15E-04	2.51E+10	6.36E+09	6.36E+09	3 μm	cold wall

					105.4	-30.1	1.0	9803125.0	135193.0	135193.0	370.0	185.0	2.93E-02	4.04E-04	4.04E-04	5.86E+10	1.47E+10	1.47E+10	3 μm	cold wall
					105.5	-30.3	1.0	21252577.0	448727.0	448727.0	370.0	185.0	6.61E-02	1.40E-03	1.40E-03	1.32E+11	3.31E+10	3.31E+10	3 μm	cold wall
					109.6	-25.2	1.0	14823835.0	366291.0	366291.0	370.0	185.0	4.23E-02	1.04E-03	1.04E-03	8.45E+10	2.11E+10	2.11E+10	3 μm	cold wall
					110.5	-29.0	1.0	35103544.0	542065.0	542065.0	370.0	185.0	1.05E-01	1.61E-03	1.61E-03	2.09E+11	5.24E+10	5.24E+10	3 μm	cold wall
					110.5	-30.5	1.0	48786312.0	599960.0	599960.0	370.0	185.0	1.52E-01	1.87E-03	1.87E-03	3.03E+11	7.59E+10	7.59E+10	3 μm	cold wall
			PIMCA-PINC		N/A	-36.1	1.0	223032300.0	50843550.0	32954050.0	370.0	185.0	6.03E-01	1.37E-01	8.91E-02	1.21E+12	4.08E+11	1.18E+11	depol	N/A
					N/A	-34.9	1.0	174525300.0	73737127.2	44798194.0	370.0	185.0	4.72E-01	1.99E-01	1.21E-01	9.43E+11	4.63E+11	1.66E+11	depol	N/A
					N/A	-33.1	1.0	108551833.2	60830879.0	29242745.4	370.0	185.0	2.93E-01	1.64E-01	7.90E-02	5.87E+11	3.60E+11	1.32E+11	depol	N/A
					N/A	-30.5	1.0	67196933.2	61870305.9	21883172.7	370.0	185.0	1.82E-01	1.67E-01	5.91E-02	3.63E+11	3.47E+11	1.42E+11	depol	N/A
17-Mar-15	APC-10	SDAr01	CFDC-CSU		105.4	-19.9	5.2	151304.3	83478.3	83478.3	3439.0	3038.0	4.40E-05	2.43E-05	2.43E-05	4.98E+07	3.02E+07	3.02E+07	Chnl 165	cold wall
					105.5	-25.0	5.5	12992727.3	681818.2	681818.2	3439.0	3038.0	3.78E-03	1.98E-04	1.98E-04	4.28E+09	1.09E+09	1.09E+09	Chnl 165	cold wall
					105.5	-30.2	6.3	235515789.5	3448421.1	3448421.1	3439.0	3038.0	6.85E-02	1.00E-03	1.00E-03	7.75E+10	1.94E+10	1.94E+10	Chnl 165	cold wall
			INKA		104.2	-20.0	1.9	474285.7	95238.1	95238.1	3439.0	3038.0	1.38E-04	2.77E-05	2.43E-05	1.56E+08	5.01E+07	4.77E+07	>4 μm	cold wall
					104.9	-25.0	3.0	16350000.0	3270000.0	3270000.0	3439.0	3038.0	4.75E-03	9.51E-04	1.98E-04	5.38E+09	1.72E+09	1.36E+09	>4 μm	cold wall
					104.8	-30.0	4.6	156073846.2	31213846.2	31213846.2	3439.0	3038.0	4.54E-02	9.08E-03	1.00E-03	5.14E+10	1.64E+10	1.29E+10	>4 μm	cold wall
			CIC-PNNL		106.0	-25.0	2.4	26860800.0	-	-	3439.0	3038.0	7.81E-03	-	-	8.84E+09	2.21E+09	2.21E+09	3 μm	lamina T
					106.0	-30.0	3.4	328097142.9	-	-	3439.0	3038.0	9.54E-02	-	-	1.08E+11	2.70E+10	2.70E+10	3 μm	lamina T
			SPIN-TROPOS		106.2	-36.5	3.5	402185792.3	5434754.1	5434754.1	3439.0	3038.0	1.17E-01	1.58E-03	2.43E-05	1.32E+11	3.31E+10	3.31E+10	3 μm	lamina T
					105.6	-31.7	4.3	209066666.7	4462933.3	4462933.3	3439.0	3038.0	6.08E-02	1.30E-03	2.43E-05	6.88E+10	1.73E+10	1.72E+10	3 μm	lamina T
					104.3	-27.2	5.3	53333333.3	2602666.7	2602666.7	3439.0	3038.0	1.55E-02	7.57E-04	2.43E-05	1.76E+10	4.47E+09	4.39E+09	3 μm	lamina T
					102.9	-23.0	5.6	5861052.6	887017.5	887017.5	3439.0	3038.0	1.70E-03	2.58E-04	2.43E-05	1.93E+09	5.64E+08	4.83E+08	3 μm	lamina T
			PIMCA-PINC		N/A	-37.4	1.0	2866688000.0	137243683.2	136539683.2	3439.0	3038.0	8.34E-01	3.99E-02	3.97E-02	9.44E+11	2.40E+11	2.40E+11	depol	N/A
					N/A	-36.4	1.0	2634869334.4	243020144.0	213569475.2	3439.0	3038.0	7.66E-01	7.07E-02	6.21E-02	8.67E+11	2.31E+11	2.28E+11	depol	N/A
					N/A	-35.5	1.0	2523424000.0	278050764.8	253282764.8	3439.0	3038.0	7.34E-01	8.08E-02	7.36E-02	8.31E+11	2.27E+11	2.24E+11	depol	N/A
					N/A	-33.9	1.0	2056736000.0	407975027.2	304839027.2	3439.0	3038.0	5.98E-01	1.19E-01	8.86E-02	6.77E+11	2.16E+11	1.97E+11	depol	N/A
					N/A	-32.2	1.0	1574480000.0	456975712.0	305167712.0	3439.0	3038.0	4.58E-01	1.33E-01	8.87E-02	5.18E+11	1.99E+11	1.64E+11	depol	N/A
					N/A	-31.2	1.0	1151029334.4	537707110.4	306197776.0	3439.0	3038.0	3.35E-01	1.56E-01	8.90E-02	3.79E+11	2.01E+11	1.38E+11	depol	N/A
					N/A	-29.3	1.0	775477334.4	513819776.0	226929107.2	3439.0	3038.0	2.25E-01	1.49E-01	6.60E-02	2.55E+11	1.81E+11	9.82E+10	depol	N/A
19-Mar-15	AIDA-09	SDAr01	AIDA		101.4	-24.1	1.0	609000.0	731000.0	487000.0	310.0	172.0	2.12E-03	1.70E-03	2.54E-03	3.82E+09	4.60E+09	3.08E+09	N/A	N/A
					101.1	-24.8	1.0	1730000.0	2070000.0	1380000.0	310.0	172.0	6.10E-03	4.88E-03	7.32E-03	1.10E+10	1.32E+10	8.86E+09	N/A	N/A
					100.9	-25.3	1.0	5180000.0	6210000.0	4140000.0	310.0	172.0	1.86E-02	1.49E-02	2.23E-02	3.36E+10	4.04E+10	2.71E+10	N/A	N/A
			DFPC-ISAC		101.0	-20.2	1.0	11300.0	3390.0	3390.0	310.0	172.0	5.65E-05	1.70E-05	1.70E-05	1.02E+08	3.98E+07	3.98E+07	N/A	N/A
			FRIDGE-STD	23	101.0	-20.0	1.0	6590.0	7060.0	7060.0	310.0	172.0	2.21E-05	2.37E-05	2.37E-05	3.99E+07	4.38E+07	4.38E+07	N/A	N/A
					101.0	-25.0	1.0	292000.0	313000.0	313000.0	310.0	172.0	9.80E-04	1.05E-03	1.05E-03	1.77E+09	1.94E+09	1.94E+09	N/A	N/A
					101.0	-30.0	1.0	3920000.0	4200000.0	4200000.0	310.0	172.0	1.32E-02	1.41E-02	1.41E-02	2.37E+10	2.61E+10	2.61E+10	N/A	N/A
			SPIN-MIT		108.0	-30.0	1.0	4840000.0	96234.2	96234.2	310.0	172.0	1.53E-02	3.10E-04	3.10E-04	2.79E+10	7.00E+09	7.00E+09	depol	lamina T[%]
					104.0	-25.0	1.0	5500000.0	108825.5	108825.5	310.0	172.0	1.84E-02	3.51E-04	3.51E-04	3.21E+10	8.05E+09	8.05E+09	depol	lamina T[%]
			SPIN-TROPOS		104.4	-27.3	1.0	10850000.0	500000.4	500.4	310.0	172.0	3.50E-02	1.63E-03	1.63E-03	6.31E+10	1.60E+10	1.60E+10	3 μm	warm wall
26-Mar-15	AIDA-24	SDAr01	PINC		105.1	-30.5	1.0	2040000.0	101957.0	101957.0	177.0	105.0	8.33E-03	5.76E-04	1.00E-06	1.40E+10	3.51E+09	3.51E+09	3 μm	warm wall
18-Mar-15	APC-12	SDT01	CFDC-CSU		105.3	-19.9	6.0	980255.2	214538.4	214538.4	3001.0	2010.0	3.27E-04	7.15E-05	7.15E-05	4.88E+08	1.62E+08	1.62E+08	Chnl 165	cold wall
					105.6	-30.6	2.8	107772733.3	621116.7	621116.7	3001.0	2010.0	3.59E-02	2.07E-04	2.07E-04	5.36E+10	1.34E+10	1.34E+10	Chnl 165	cold wall
			INKA		103.8	-20.0	2.2	307368.5	61517.6	61517.6	3001.0	2010.0	1.02E-04	2.05E-05	2.05E-05	1.53E+08	4.90E+07	4.90E+07	>4 μm	cold wall
					104.8	-25.0	3.5	7555123.3	1511372.1	1511372.1	3001.0	2010.0	2.52E-03	5.04E-04	5.04E-04	3.76E+09	1.20E+09	1.20E+09	>4 μm	cold wall
					104.8	-30.0	5.0	52200360.0	10438080.0	10438080.0	3001.0	2010.0	1.74E-02	3.48E-03	3.48E-03	2.60E+10	8.31E+09	8.31E+09	>4 μm	cold wall
			CIC-PNNL		106.0	-25.0	2.4	54370689.7	-	-	3001.0	2010.0	1.81E-02	0.00E+00	-	-	6.76E+09	6.76E+09	3 μm	lamina T
					106.0	-30.0	5.6	137950400.0	-	-	3001.0	2010.0	4.60E-02	0.00E+00	-	-	1.72E+10	1.72E+10	3 μm	lamina T
			SPIN-TROPOS		105.0	-36.4	2.6	407329565.2	4763478.3	4763478.3	3001.0	2010.0	1.36E-01	1.59E-03	1.59E-03	2.03E+11	5.07E+10	5.07E+10	3 μm	lamina T
					105.0	-31.7	3.5	157894736.8	3600000.0	3600000.0	3001.0	2010.0	5.26E-02	1.20E-03	1.20E-03	7.86E+10	1.97E+10	1.97E+10	3 μm	lamina T

					103.1	-26.7	4.4	35912408.8	1927007.3	1927007.3	3001.0	2010.0	1.20E-02	6.42E-04	6.42E-04	1.79E+10	4.57E+09	4.57E+09	3 μm	lamina T
			PIMCA-PINC		N/A	-36.2	1.0	2380899999.0	177632439.0	181722438.0	3001.0	2010.0	7.93E-01	5.92E-02	6.06E-02	1.51E-02	3.95E-03	3.96E-03	depol	N/A
					N/A	-35.2	1.0	1967649999.0	232633491.0	195113490.0	3001.0	2010.0	6.56E-01	6.76E-02	6.50E-02	1.63E-02	4.40E-03	4.37E-03	depol	N/A
					N/A	-33.7	1.0	1732509999.0	306133458.0	262643457.0	3001.0	2010.0	5.77E-01	8.90E-02	8.75E-02	2.19E-02	6.43E-03	6.40E-03	depol	N/A
					N/A	-32.4	1.0	1299159999.0	236006148.0	165046149.0	3001.0	2010.0	4.33E-01	6.86E-02	5.50E-02	1.37E-02	4.07E-03	3.86E-03	depol	N/A
					N/A	-28.9	1.0	803850000.0	244168851.0	152658852.0	3001.0	2010.0	2.68E-01	7.10E-02	5.09E-02	1.27E-02	4.63E-03	3.99E-03	depol	N/A
18-Mar-15	AIDA-07	SDT01	AIDA		102.3	-23.8	1.0	259237.0	311084.0	207390.0	270.0	131.0	1.08E-03	8.62E-04	1.29E-03	2.22E+09	2.67E+09	1.79E+09	N/A	N/A
					102.3	-24.5	1.0	537809.0	645371.0	430247.0	270.0	131.0	2.27E-03	1.82E-03	2.73E-03	4.68E+09	5.64E+09	3.78E+09	N/A	N/A
					102.2	-25.0	1.0	1093630.0	1312360.0	874904.0	270.0	131.0	4.69E-03	3.75E-03	5.62E-03	9.66E+09	1.16E+10	7.79E+09	N/A	N/A
					101.6	-25.4	1.0	1567560.0	1881070.0	1254050.0	270.0	131.0	6.81E-03	5.44E-03	8.17E-03	1.40E+10	1.69E+10	1.13E+10	N/A	N/A
					100.7	-25.7	1.0	2011470.0	2413760.0	1609180.0	270.0	131.0	8.85E-03	7.08E-03	1.06E-02	1.82E+10	2.20E+10	1.47E+10	N/A	N/A
			CFDC-CSU		105.5	-25.6	1.0	923063.0	33533.0	33533.0	270.0	131.0	3.76E-03	1.37E-04	1.37E-04	7.76E+09	7.74E+09	1.94E+09	3 μm	cold wall
					105.6	-30.3	1.0	5842154.0	203342.0	203342.0	270.0	131.0	2.43E-02	8.47E-04	8.47E-04	5.08E+10	5.01E+10	1.25E+10	3 μm	cold wall
					112.0	-25.2	1.0	5273442.0	113137.0	113137.0	270.0	131.0	2.16E-02	4.64E-04	4.64E-04	4.50E+10	4.46E+10	1.13E+10	3 μm	cold wall
					106.5	-30.3	1.0	6523451.0	234653.0	234653.0	270.0	131.0	2.72E-02	9.78E-04	9.78E-04	5.68E+10	5.60E+10	1.40E+10	3 μm	cold wall
			FRIDGE-STD	16	101.0	-20.0	1.0	1330.0	1030.0	1030.0	270.0	131.0	1.02E-05	7.86E-06	7.86E-06	2.09E+07	1.70E+07	1.70E+07	N/A	N/A
					101.0	-25.0	1.0	146000.0	115000.0	115000.0	270.0	131.0	1.11E-03	8.78E-04	8.78E-04	2.30E+09	1.90E+09	1.90E+09	N/A	N/A
					101.0	-30.0	1.0	733000.0	576000.0	576000.0	270.0	131.0	5.60E-03	4.40E-03	4.40E-03	1.15E+10	9.51E+09	9.51E+09	N/A	N/A
			SPIN-TROPOS		104.1	-27.1	1.0	1781000.0	194000.0	194000.0	270.0	131.0	6.50E-03	7.98E-04	7.98E-04	1.36E+10	3.79E+09	3.79E+09	3 μm	lamina T
20-Mar-15	AIDA-12	SDT01	CFDC-CSU		105.6	-20.6	1.0	4400.0	4575.0	4399.0	285.0	118.0	1.69E-05	1.76E-05	1.68E-05	4.09E+07	1.02E+07	1.02E+07	3 μm	cold wall
					110.8	-20.4	1.0	22400.0	18153.0	18153.0	285.0	118.0	8.60E-05	6.97E-05	6.97E-05	2.08E+08	5.19E+07	5.19E+07	3 μm	cold wall
			DFPC-ISAC		101.0	-20.2	1.0	25000.0	7500.0	7500.0	290.0	116.0	1.00E-04	3.00E-05	3.00E-05	2.50E+08	9.76E+07	9.76E+07	N/A	N/A
			FRIDGE-STD	31	101.0	-20.0	1.0	46100.0	36200.0	36200.0	291.0	119.0	1.58E-04	1.24E-04	1.24E-04	3.87E+08	3.19E+08	3.19E+08	N/A	N/A
					101.0	-25.0	1.0	698000.0	548000.0	548000.0	291.0	119.0	2.40E-03	1.88E-03	1.88E-03	5.87E+09	4.83E+09	4.83E+09	N/A	N/A
					101.0	-30.0	1.0	4380000.0	3440000.0	3440000.0	291.0	119.0	1.51E-02	1.18E-02	1.18E-02	3.68E+10	3.03E+10	3.03E+10	N/A	N/A
			SPIN-TROPOS		105.8	-36.3	1.0	7275000.0	401209.0	401209.0	291.0	120.0	2.50E-02	1.48E-03	1.48E-03	6.06E+10	1.56E+10	1.56E+10	3 μm	lamina T
			PIMCA-PINC		N/A	-33.5	1.0	59357899.9	37332147.2	18606697.0	285.0	118.0	2.08E-01	1.31E-01	6.53E-02	5.03E+11	3.40E+11	1.37E+11	depol	N/A
					N/A	-31.3	1.0	45349200.0	44806043.0	18488193.1	285.0	118.0	1.59E-01	1.57E-01	6.49E-02	3.84E+11	3.92E+11	1.87E+11	depol	N/A
					N/A	-28.2	1.0	37908799.9	47585575.1	18572575.1	285.0	118.0	1.33E-01	1.67E-01	6.52E-02	3.21E+11	4.11E+11	2.26E+11	depol	N/A

*: correction factor refers to the particle number concentration ratio in Eq. (3) of the manuscript, the ratio between the integrated average particle concentration during offline sampling to the total particle concentration at the time of online sampling.

#: INP concentration is the actual INP concentration at the time of sampling when the correction factor is 1, but is equal to $n_{INP,online,corr}$ (sample time) when the correction factor exceeds 1.

&: evaporation section temperature refers to the temperature of the online flow chamber walls within the evaporation region of the instruments. Cold wall means that the ice surfaces on both walls are adjusted to the cold wall temperature to induce evaporation. Warm wall is just the opposite. Lamina T means that the walls are adjusted to the aerosol lamina temperature to induce evaporation without a change in temperature.

@: For the CFDC-TAMU, wall temperatures are maintained in the evaporation section, but the warm wall is covered by a hydrophobic material to actively stimulate evaporation, rather than wall temperature control alone. It is not known the extent to which this limits heat transfer from the warm wall, and thereby leads to cooling in the evaporation region.

%: The SPIN-MIT evaporation region temperature was 0 to 5°C warmer than the lamina temperature.

Table S2. Post-processed (offline) instrument data used in the manuscript figures. Listed are the date, experiment identifier, aerosol particle sample type, instrument, sample identifier (shared, or separate filter and number if applicable), temperature, INP concentration in air, positive INP concentration uncertainty defined by confidence interval, negative INP uncertainty, total particle number of reference to INP concentration, surface area concentration, INP active fraction, positive uncertainty in active fraction defined by confidence interval, negative uncertainty in active fraction, active site density, positive uncertainty in active site density, negative uncertainty in active site density, droplet or aliquot volumes used, and and notes regarding the data point ("binned" if multiple experiments are combined, and "selected points" if not all temperature points are shown.

Date	Expt	aerosol	Instrument	Sample	Temp	INP Conc	ci INP+	ci INP-	total particles	Sfc area	frac	frac_ci+	frac_ci-	ns,geo	ns,geo ci+	ns,geo ci-	Drop/aliquot volume	Notes
					°C	m^{-3}	m^{-3}	m^{-3}	cm^{-3}	$\mu m^2 cm^{-3}$				m^{-2}	m^{-2}	m^{-2}	µL	
16-Mar-15	APC-07	IS03	BINARY	Shared impinger	-21.0	1630.0	0.0	0.0	18636.2	5568.6	8.75E-08	0.00E+00	0.00E+00	2.93E+05	7.32E+04	7.32E+04	0.6	binned data
					-22.0	4710.0	17400.0	2500.0	18636.2	5568.6	2.53E-07	9.34E-07	1.34E-07	8.46E+05	3.13E+06	4.96E+05	0.6	binned data
					-23.0	19900.0	48600.0	12300.0	18636.2	5568.6	1.07E-06	2.61E-06	6.60E-07	3.57E+06	8.77E+06	2.38E+06	0.6	binned data
					-24.0	84000.0	205000.0	53300.0	18636.2	5568.6	4.51E-06	1.10E-05	2.86E-06	1.51E+07	3.70E+07	1.03E+07	0.6	binned data
					-25.0	260000.0	350000.0	119000.0	18636.2	5568.6	1.40E-05	1.88E-05	6.39E-06	4.67E+07	6.39E+07	2.44E+07	0.6	binned data
					-26.0	542000.0	416000.0	336000.0	18636.2	5568.6	2.91E-05	2.23E-05	1.80E-05	9.73E+07	7.86E+07	6.51E+07	0.6	binned data
					-27.0	1520000.0	1080000.0	1050000.0	18636.2	5568.6	8.16E-05	5.80E-05	5.63E-05	2.73E+08	2.06E+08	2.01E+08	0.6	binned data
					-28.0	3510000.0	3170000.0	1290000.0	18636.2	5568.6	1.88E-04	1.70E-04	6.92E-05	6.30E+08	5.91E+08	2.80E+08	0.6	binned data
					-29.0	6070000.0	650000.0	650000.0	18636.2	5568.6	3.26E-04	3.49E-05	3.49E-05	1.09E+09	2.96E+08	2.96E+08	0.6	binned data
			IS	Filter	-8.9	2.8	12.1	2.3	18636.2	5568.6	1.48E-10	4.95E+02	6.50E-10	1.22E-10	2.18E+03	4.27E+02	50	selected points
					-9.0	5.6	13.9	4.1	18636.2	5568.6	3.01E-10	1.01E+03	7.47E-10	2.19E-10	2.51E+03	7.76E+02	50	selected points
					-9.5	5.6	13.9	4.1	18636.2	5568.6	3.01E-10	1.01E+03	7.47E-10	2.19E-10	2.51E+03	7.76E+02	50	selected points
					-10.0	18.0	19.8	9.9	18636.2	5568.6	9.67E-10	3.24E+03	1.06E-09	5.34E-10	3.64E+03	1.96E+03	50	selected points
					-11.0	18.0	19.8	9.9	18636.2	5568.6	9.67E-10	3.24E+03	1.06E-09	5.34E-10	3.64E+03	1.96E+03	50	selected points
					-12.0	36.6	26.6	16.7	18636.2	5568.6	1.96E-09	6.57E+03	1.43E-09	8.99E-10	5.05E+03	3.43E+03	50	selected points
					-13.3	45.3	29.5	19.7	18636.2	5568.6	2.43E-09	8.13E+03	1.58E-09	1.06E-09	5.68E+03	4.08E+03	50	selected points
					14.0	45.3	29.5	19.7	18636.2	5568.6	2.43E-09	8.13E+03	1.58E-09	1.06E-09	5.68E+03	4.08E+03	50	selected points
					-15.0	85.1	42.7	32.8	18636.2	5568.6	4.57E-09	1.53E+04	2.29E-09	1.76E-09	8.57E+03	7.03E+03	50	selected points
					-16.0	170.9	310.5	113.7	18636.2	5568.6	9.17E-09	3.07E+04	1.67E-08	6.10E-09	5.63E+04	2.18E+04	50	selected points
					-17.0	295.0	368.3	171.5	18636.2	5568.6	1.58E-08	5.30E+04	1.98E-08	9.20E-09	6.75E+04	3.35E+04	50	selected points
					-18.0	499.4	449.5	252.6	18636.2	5568.6	2.68E-08	8.97E+04	2.41E-08	1.36E-08	8.38E+04	5.06E+04	50	selected points
					-19.0	816.0	560.5	363.7	18636.2	5568.6	4.38E-08	1.47E+05	3.01E-08	1.95E-08	1.07E+05	7.49E+04	50	selected points
					-20.0	1853.9	905.0	708.2	18636.2	5568.6	9.95E-08	3.33E+05	4.86E-08	3.80E-08	1.83E+05	1.52E+05	50	selected points
					-20.5	4109.6	1844.5	1647.7	18636.2	5568.6	2.21E-07	7.38E+05	9.90E-08	8.84E-08	3.79E+05	3.49E+05	50	selected points
					-21.0	5899.3	7366.7	3430.1	18636.2	5568.6	3.17E-07	1.06E+06	3.95E-07	1.84E-07	1.35E+06	6.70E+05	50	selected points
					-21.5	11466.7	9529.0	5592.4	18636.2	5568.6	6.15E-07	2.06E+06	5.11E-07	3.00E-07	1.79E+06	1.13E+06	50	selected points
					-22.0	28704.1	15292.0	11355.4	18636.2	5568.6	1.54E-06	5.15E+06	8.21E-07	6.09E-07	3.03E+06	2.41E+06	50	selected points
					-22.5	64454.8	28560.3	24623.7	18636.2	5568.6	3.46E-06	1.16E+07	1.53E-06	1.32E-06	5.89E+06	5.28E+06	50	selected points
					-23.0	171430.6	169050.9	90319.4	18636.2	5568.6	9.20E-06	3.08E+07	9.07E-06	4.85E-06	3.13E+07	1.80E+07	50	selected points
					-23.5	229334.5	190579.1	111847.6	18636.2	5568.6	1.23E-05	4.12E+07	1.02E-05	6.00E-06	3.57E+07	2.26E+07	50	selected points
					-24.0	292509.4	212709.8	133978.3	18636.2	5568.6	1.57E-05	5.25E+07	1.14E-05	7.19E-06	4.04E+07	2.74E+07	50	selected points
					-24.5	526170.6	290088.8	211357.3	18636.2	5568.6	2.82E-05	9.45E+07	1.56E-05	1.13E-05	5.72E+07	4.47E+07	50	selected points
					-25.0	574082.3	305839.2	227107.8	18636.2	5568.6	3.08E-05	1.03E+08	1.64E-05	1.22E-05	6.07E+07	4.82E+07	50	selected points
					-25.5	719508.3	360434.7	279306.3	18636.2	5568.6	3.86E-05	1.29E+08	1.93E-05	1.50E-05	7.23E+07	5.97E+07	50	selected points
					-26.0	1094122.5	515677.1	429288.1	18636.2	5568.6	5.87E-05	1.96E+08	2.77E-05	2.30E-05	1.05E+08	9.14E+07	50	selected points
					-26.6	1444056.6	733940.5	630831.2	18636.2	5568.6	7.75E-05	2.59E+08	3.94E-05	3.38E-05	1.47E+08	1.31E+08	50	selected points

			KIT-CS	Shared impinger	-26.8	938469.4	0.0	0.0	18636.2	5568.6	5.04E-05	0.00E+00	0.00E+00	1.69E+08	4.21E+07	4.21E+07	4.2	
					-27.7	2303457.9	2039358.3	2039358.3	18636.2	5568.6	1.24E-04	1.09E-04	1.09E-04	4.14E+08	3.81E+08	3.81E+08	4.2	
					-28.7	7287660.4	4318310.9	4318310.9	18636.2	5568.6	3.91E-04	2.32E-04	2.32E-04	1.31E+09	8.42E+08	8.42E+08	4.2	
					-29.7	16616677.8	7473340.4	7473340.4	18636.2	5568.6	8.92E-04	4.01E-04	4.01E-04	2.98E+09	1.54E+09	1.54E+09	4.2	
					-30.6	32222547.3	10854765.2	10854765.2	18636.2	5568.6	1.73E-03	5.82E-04	5.82E-04	5.79E+09	2.43E+09	2.43E+09	4.2	
					-31.6	55556777.0	11227616.0	11227616.0	18636.2	5568.6	2.98E-03	6.02E-04	6.02E-04	9.98E+09	3.21E+09	3.21E+09	4.2	
					-32.7	90103941.6	5543139.6	5543139.6	18636.2	5568.6	4.83E-03	2.97E-04	2.97E-04	1.62E+10	4.17E+09	4.17E+09	4.2	
			M-AL	Shared impinger	-22.0	1124.2	346.7	346.7	18636.2	5568.6	6.03E-08	1.86E-08	1.86E-08	2.02E+05	8.01E+04	8.01E+04	4.2	
					-21.0	860.8	262.0	262.0	18636.2	5568.6	4.62E-08	1.41E-08	1.41E-08	1.55E+05	6.09E+04	6.09E+04	4.2	
					-20.0	737.8	227.5	227.5	18636.2	5568.6	3.96E-08	1.22E-08	1.22E-08	1.32E+05	5.26E+04	5.26E+04	4.2	
					-19.0	562.7	179.2	179.2	18636.2	5568.6	3.02E-08	9.62E-09	9.62E-09	1.01E+05	4.09E+04	4.09E+04	4.2	
					-18.0	344.9	111.4	111.4	18636.2	5568.6	1.85E-08	5.98E-09	5.98E-09	6.19E+04	2.53E+04	2.53E+04	4.2	
					-17.0	191.9	63.1	63.1	18636.2	5568.6	1.03E-08	3.39E-09	3.39E-09	3.45E+04	1.42E+04	1.42E+04	4.2	
					-16.0	94.3	28.5	28.5	18636.2	5568.6	5.06E-09	1.53E-09	1.53E-09	1.69E+04	6.64E+03	6.64E+03	4.2	
					-15.0	94.3	28.5	28.5	18636.2	5568.6	5.06E-09	1.53E-09	1.53E-09	1.69E+04	6.64E+03	6.64E+03	4.2	
					-14.0	94.3	37.3	37.3	18636.2	5568.6	5.06E-09	2.00E-09	2.00E-09	1.69E+04	7.92E+03	7.92E+03	4.2	
			NCSU-CS	Shared impinger	-17.0	233.5	0.0	0.0	18636.2	5568.6	1.25E-08	0.00E+00	0.00E+00	4.19E+04	1.05E+04	1.05E+04	1	binned data
					-18.0	297.1	0.0	0.0	18636.2	5568.6	1.59E-08	0.00E+00	0.00E+00	5.34E+04	1.33E+04	1.33E+04	1	binned data
					-19.0	360.8	0.0	0.0	18636.2	5568.6	1.94E-08	0.00E+00	0.00E+00	6.48E+04	1.62E+04	1.62E+04	1	binned data
					-20.0	439.3	0.0	0.0	18636.2	5568.6	2.36E-08	0.00E+00	0.00E+00	7.89E+04	1.97E+04	1.97E+04	1	binned data
					-21.0	49167.9	95188.9	49167.0	18636.2	5568.6	2.64E-06	5.11E-06	2.64E-06	8.83E+06	1.72E+07	9.10E+06	1	binned data
					-22.0	83620.9	97537.7	83620.0	18636.2	5568.6	4.49E-06	5.23E-06	4.49E-06	1.50E+07	1.79E+07	1.55E+07	1	binned data
					-23.0	232405.8	229532.0	229532.0	18636.2	5568.6	1.25E-05	1.23E-05	1.23E-05	4.17E+07	4.25E+07	4.25E+07	1	binned data
					-24.0	525003.8	501473.1	501473.1	18636.2	5568.6	2.82E-05	2.69E-05	2.69E-05	9.43E+07	9.31E+07	9.31E+07	1	binned data
					-25.0	1315450.4	1284452.0	1284452.0	18636.2	5568.6	7.06E-05	6.89E-05	6.89E-05	2.36E+08	2.38E+08	2.38E+08	1	binned data
			NIPI	Shared impinger	-24.0	35300.0	47900.0	20400.0	18636.2	5568.6	1.89E-06	2.57E-06	1.09E-06	6.34E+06	8.75E+06	3.99E+06	1	binned data
					-23.0	15400.0	33700.0	10580.0	18636.2	5568.6	8.26E-07	1.81E-06	5.68E-07	2.77E+06	6.09E+06	2.02E+06	1	binned data
					-22.0	5600.0	15000.0	4080.0	18636.2	5568.6	3.00E-07	8.05E-07	2.19E-07	1.01E+06	2.71E+06	7.75E+05	1	binned data
					-21.0	2100.0	8000.0	1665.0	18636.2	5568.6	1.13E-07	4.29E-07	8.93E-08	3.77E+05	1.44E+06	3.14E+05	1	binned data
					-20.0	701.0	3979.0	596.0	18636.2	5568.6	3.76E-08	2.14E-07	3.20E-08	1.26E+05	7.15E+05	1.12E+05	1	binned data
					-19.0	342.0	838.0	242.6	18636.2	5568.6	1.84E-08	4.50E-08	1.30E-08	6.14E+04	1.51E+05	4.62E+04	1	binned data
					-18.0	119.0	393.0	91.5	18636.2	5568.6	6.39E-09	2.11E-08	4.91E-09	2.14E+04	7.08E+04	1.73E+04	1	binned data
					-17.0	89.4	89.6	44.7	18636.2	5568.6	4.80E-09	4.81E-09	2.40E-09	1.61E+04	1.66E+04	8.97E+03	1	binned data
					-12.0	205.0	205.0	103.0	18636.2	5568.6	1.10E-08	1.10E-08	5.53E-09	3.68E+04	3.79E+04	2.07E+04	1	binned data
			VODCA	Shared impinger	-34.0	410000000.0	39513400.3	39513400.3	18636.2	5568.6	2.20E-02	2.12E-03	2.12E-03	7.36E+10	1.97E+10	1.97E+10	0.000004 - 0.000036	selected points
					-33.0	205000000.0	144781645.5	144781645.5	18636.2	5568.6	1.10E-02	7.77E-03	7.77E-03	3.68E+10	2.76E+10	2.76E+10	0.000004 - 0.000036	selected points
					-32.0	110000000.0	45533430.3	45533430.3	18636.2	5568.6	5.90E-03	2.44E-03	2.44E-03	1.98E+10	9.55E+09	9.55E+09	0.000004 - 0.000036	selected points
					-31.0	48000000.0	5213291.1	5213291.1	18636.2	5568.6	2.58E-03	2.80E-04	2.80E-04	8.62E+09	2.35E+09	2.35E+09	0.000004 - 0.000036	selected points
26-Mar-15	AIDA-22		FRIDGE-IMM	Filter 17	-13.2	1090.0	1700.0	793.0	1688	892	6.46E-07	1.01E-06	4.70E-07	1.22E+06	1.93E+06	9.40E+05	0.5	selected points
					-14.1	1910.0	2030.0	1141.0	1688	892	1.13E-06	1.20E-06	6.76E-07	2.14E+06	2.34E+06	1.39E+06	0.5	selected points
					-16.0	3010.0	2380.0	1510.0	1688	892	1.78E-06	1.41E-06	8.95E-07	3.37E+06	2.80E+06	1.89E+06	0.5	selected points
					-18.0	5780.0	3050.0	2200.0	1688	892	3.42E-06	1.81E-06	1.30E-06	6.48E+06	3.78E+06	2.95E+06	0.5	selected points
					-20.0	14000.0	4400.0	3600.0	1688	892	8.29E-06	2.61E-06	2.13E-06	1.57E+07	6.30E+06	5.63E+06	0.5	selected points
					-22.0	38500.0	7200.0	6300.0	1688	892	2.28E-05	4.27E-06	3.73E-06	4.32E+07	1.35E+07	1.29E+07	0.5	selected points
					-24.0	149000.0	15000.0	14000.0	1688	892	8.83E-05	8.89E-06	8.29E-06	1.67E+08	4.50E+07	4.46E+07	0.5	selected points
					-26.0	826000.0	80000.0	74000.0	1688	892	6.99E-04	9.48E-05	8.89E-05	1.32E+09	3.76E+08	3.71E+08	0.5	selected points
					-27.4	1600000.0	430000.0	300000.0	1688	892	9.48E-04	2.55E-04	1.78E-04	1.79E+09	6.58E+08	5.61E+08	0.5	selected points
17-Mar-15	APC-09	SDAr01	BINARY	Shared impinger	-10.2	1720.0	0.0	0.0	3439.3	3038.1	5.00E-07	0.00E+00	0.00E+00	5.66E+05	1.42E+05	1.42E+05	0.6	binned data
					-11.2	1720.0	0.0	0.0	3439.3	3038.1	5.00E-07	0.00E+00	0.00E+00	5.66E+05	1.42E+05	1.42E+05	0.6	binned data

					-12.2	2330.0	0.0	0.0	3439.3	3038.1	6.77E-07	0.00E+00	0.00E+00	7.67E+05	1.92E+05	1.92E+05	0.6	binned data
					-13.2	2330.0	630.0	610.0	3439.3	3038.1	6.77E-07	1.83E-07	1.77E-07	7.67E+05	2.82E+05	2.78E+05	0.6	binned data
					-14.2	2960.0	650.0	0.0	3439.3	3038.1	8.61E-07	1.89E-07	0.00E+00	9.74E+05	3.24E+05	2.44E+05	0.6	binned data
					-15.2	4280.0	700.0	670.0	3439.3	3038.1	1.24E-06	2.04E-07	1.95E-07	1.41E+06	4.21E+05	4.16E+05	0.6	binned data
					-16.2	4980.0	720.0	700.0	3439.3	3038.1	1.45E-06	2.09E-07	2.04E-07	1.64E+06	4.73E+05	4.70E+05	0.6	binned data
					-17.2	7220.0	9980.0	1520.0	3439.3	3038.1	2.10E-06	2.90E-06	4.42E-07	2.38E+06	3.34E+06	7.77E+05	0.6	binned data
					-18.2	12200.0	5150.0	4120.0	3439.3	3038.1	3.55E-06	1.50E-06	1.20E-06	4.02E+06	1.97E+06	1.69E+06	0.6	binned data
					-19.2	29800.0	27400.0	14900.0	3439.3	3038.1	8.66E-06	7.97E-06	4.33E-06	9.81E+06	9.35E+06	5.48E+06	0.6	binned data
					-20.2	107000.0	95000.0	64200.0	3439.3	3038.1	3.11E-05	2.76E-05	1.87E-05	3.52E+07	3.25E+07	2.29E+07	0.6	binned data
					-21.2	298000.0	412000.0	137000.0	3439.3	3038.1	8.66E-05	1.20E-04	3.98E-05	9.81E+07	1.38E+08	5.13E+07	0.6	binned data
					-22.2	931000.0	1400000.0	503000.0	3439.3	3038.1	2.71E-04	4.07E-04	1.46E-04	3.06E+08	4.67E+08	1.82E+08	0.6	binned data
					-23.2	2750000.0	3690000.0	1260000.0	3439.3	3038.1	8.00E-04	1.07E-03	3.66E-04	9.05E+08	1.24E+09	4.72E+08	0.6	binned data
					-24.2	7220000.0	6480000.0	3670000.0	3439.3	3038.1	2.10E-03	1.88E-03	1.07E-03	2.38E+09	2.21E+09	1.35E+09	0.6	binned data
					-25.2	21800000.0	28000000.0	10200000.0	3439.3	3038.1	6.34E-03	8.14E-03	2.97E-03	7.18E+09	9.39E+09	3.81E+09	0.6	binned data
					-26.2	43500000.0	63500000.0	20000000.0	3439.3	3038.1	1.26E-02	1.85E-02	5.82E-03	1.43E+10	2.12E+10	7.49E+09	0.6	binned data
					-27.2	80300000.0	68700000.0	31100000.0	3439.3	3038.1	2.33E-02	2.00E-02	9.04E-03	2.64E+10	2.36E+10	1.22E+10	0.6	binned data
					-28.2	173000000.0	102000000.0	102000000.0	3439.3	3038.1	5.03E-02	2.97E-02	2.97E-02	5.69E+10	3.65E+10	3.65E+10	0.6	binned data
					-29.2	254000000.0	137000000.0	105000000.0	3439.3	3038.1	7.39E-02	3.98E-02	3.05E-02	8.36E+10	4.97E+10	4.04E+10	0.6	binned data
					-30.2	355000000.0	137000000.0	137000000.0	3439.3	3038.1	1.03E-01	3.98E-02	3.98E-02	1.17E+11	5.37E+10	5.37E+10	0.6	binned data
					-31.2	572000000.0	0.0	137000000.0	3439.3	3038.1	1.66E-01	0.00E+00	3.98E-02	1.88E+11	4.71E+10	6.52E+10	0.6	binned data
					-32.2	641000000.0	69000000.0	149000000.0	3439.3	3038.1	1.86E-01	2.01E-02	4.33E-02	2.11E+11	5.74E+10	7.20E+10	0.6	binned data
			CMU-CS	Shared impinger	-20.0	288560.0	32308.6	32308.6	3439.3	3038.1	8.39E-05	9.39E-06	9.39E-06	9.50E+07	2.60E+07	2.60E+07	0.1	binned data
					-6.0	717.4	1406.1	717.3	3439.3	3038.1	2.09E-07	4.09E-07	2.09E-07	2.36E+05	4.67E+05	2.36E+05	0.1	binned data
					-7.0	1330.0	1410.8	1329.0	3439.3	3038.1	3.87E-07	4.10E-07	3.86E-07	4.38E+05	4.77E+05	4.38E+05	0.1	binned data
					-8.0	2382.1	571.2	571.2	3439.3	3038.1	6.93E-07	1.66E-07	1.66E-07	7.84E+05	2.72E+05	2.72E+05	0.1	binned data
					-9.0	2875.7	756.7	756.7	3439.3	3038.1	8.36E-07	2.20E-07	2.20E-07	9.47E+05	3.44E+05	3.44E+05	0.1	binned data
					-10.0	3358.4	1016.5	1016.5	3439.3	3038.1	9.76E-07	2.96E-07	2.96E-07	1.11E+06	4.34E+05	4.34E+05	0.1	binned data
					-11.0	3843.7	1312.9	1312.9	3439.3	3038.1	1.12E-06	3.82E-07	3.82E-07	1.27E+06	5.36E+05	5.36E+05	0.1	binned data
					-12.0	4783.2	2100.3	2100.3	3439.3	3038.1	1.39E-06	6.11E-07	6.11E-07	1.57E+06	7.96E+05	7.96E+05	0.1	binned data
					-13.0	6232.0	3426.1	3426.1	3439.3	3038.1	1.81E-06	9.96E-07	9.96E-07	2.05E+06	1.24E+06	1.24E+06	0.1	binned data
					-13.2	3010.0	13790.0	2933.8	4747.0	4117.0	6.34E-07	2.90E-06	6.18E-07	7.31E+05	3.35E+06	7.36E+05	0.1	binned data
					-14.0	8142.2	4925.1	4925.1	3439.3	3038.1	2.37E-06	1.43E-06	1.43E-06	2.68E+06	1.75E+06	1.75E+06	0.1	binned data
					-15.0	10344.4	6119.4	6119.4	3439.3	3038.1	3.01E-06	1.78E-06	1.78E-06	3.40E+06	2.19E+06	2.19E+06	0.1	binned data
					-16.0	14318.2	4593.9	4593.9	3439.3	3038.1	4.16E-06	1.34E-06	1.34E-06	4.71E+06	1.92E+06	1.92E+06	0.1	binned data
					-17.0	21726.3	8777.4	8777.4	3439.3	3038.1	6.32E-06	2.55E-06	2.55E-06	7.15E+06	3.40E+06	3.40E+06	0.1	binned data
					-18.0	46312.1	13612.2	13612.2	3439.3	3038.1	1.35E-05	3.96E-06	3.96E-06	1.52E+07	5.88E+06	5.88E+06	0.1	binned data
			FRIDGE-IMM	Filter 3	-19.0	131096.0	51909.2	51909.2	3439.3	3038.1	3.81E-05	1.51E-05	1.51E-05	4.32E+07	2.02E+07	2.02E+07	0.5	selected points
					-14.0	3010.0	13790.0	2933.8	4747.0	4117.0	6.34E-07	2.90E-06	6.18E-07	7.31E+05	3.35E+06	7.36E+05	0.5	selected points
					-15.0	6020.0	15780.0	5291.0	4747.0	4117.0	1.27E-06	3.32E-06	1.11E-06	1.46E+06	3.85E+06	1.34E+06	0.5	selected points
					-16.0	9040.0	17360.0	7180.0	4747.0	4117.0	1.90E-06	3.66E-06	1.51E-06	2.20E+06	4.25E+06	1.83E+06	0.5	selected points
					-17.1	24200.0	23400.0	13800.0	4747.0	4117.0	5.10E-06	4.93E-06	2.91E-06	5.88E+06	5.87E+06	3.66E+06	0.5	selected points
					-18.0	42500.0	28800.0	19300.0	4747.0	4117.0	8.95E-06	6.07E-06	4.07E-06	1.03E+07	7.46E+06	5.35E+06	0.5	selected points
					-19.0	76300.0	36700.0	26900.0	4747.0	4117.0	1.61E-05	7.73E-06	5.67E-06	1.85E+07	1.00E+07	8.01E+06	0.5	selected points
					-20.0	243000.0	61000.0	51000.0	4747.0	4117.0	5.12E-05	1.29E-05	1.07E-05	5.90E+07	2.09E+07	1.93E+07	0.5	selected points
					-21.1	751000.0	108000.0	97000.0	4747.0	4117.0	1.58E-04	2.28E-05	2.04E-05	1.82E+08	5.26E+07	5.13E+07	0.5	selected points
					-22.0	2050000.0	200000.0	190000.0	4747.0	4117.0	4.32E-04	4.21E-05	4.00E-05	4.98E+08	1.34E+08	1.33E+08	0.5	selected points
					-23.0	5170000.0	480000.0	440000.0	4747.0	4117.0	1.09E-03	1.01E-04	9.27E-05	1.26E+09	3.35E+08	3.32E+08	0.5	selected points
					-24.0	15200000.0	5400000.0	3200000.0	4747.0	4117.0	3.20E-03	1.14E-03	6.74E-04	3.69E+09	1.60E+09	1.21E+09	0.5	selected points
			IS	Filter	-6.0	2.8	12.5	2.3	3439.3	3038.1	9.92E-10	8.25E-10	3.63E-09	9.34E+02	4.11E+03	8.06E+02	50	selected points

					-7.0	67.7	37.4	27.2	3439.3	3038.1	2.37E-08	1.97E-08	1.09E-08	2.23E+04	1.35E+04	1.06E+04	50	selected points
					-7.5	247.9	114.8	104.7	3439.3	3038.1	8.66E-08	7.21E-08	3.34E-08	8.16E+04	4.29E+04	4.00E+04	50	selected points
					-8.0	176.0	319.9	117.1	3439.3	3038.1	6.15E-08	5.12E-08	9.30E-08	5.79E+04	1.06E+05	4.12E+04	50	selected points
					-9.1	590.6	490.8	288.0	3439.3	3038.1	2.06E-07	1.72E-07	1.43E-07	1.94E+05	1.69E+05	1.07E+05	50	selected points
					-10.0	1354.9	747.0	544.3	3439.3	3038.1	4.73E-07	3.94E-07	2.17E-07	4.46E+05	2.70E+05	2.11E+05	50	selected points
					-11.0	1478.3	787.6	584.8	3439.3	3038.1	5.16E-07	4.30E-07	2.29E-07	4.87E+05	2.86E+05	2.28E+05	50	selected points
					-12.0	1909.6	932.2	729.5	3439.3	3038.1	6.67E-07	5.55E-07	2.71E-07	6.29E+05	3.45E+05	2.87E+05	50	selected points
					-13.0	2479.1	1135.0	932.3	3439.3	3038.1	8.66E-07	7.21E-07	3.30E-07	8.16E+05	4.26E+05	3.68E+05	50	selected points
					-14.1	3319.6	1470.9	1268.2	3439.3	3038.1	1.16E-06	9.65E-07	4.28E-07	1.09E+06	5.56E+05	4.99E+05	50	selected points
					-15.0	3718.6	1649.3	1446.6	3439.3	3038.1	1.30E-06	1.08E-06	4.80E-07	1.22E+06	6.23E+05	5.66E+05	50	selected points
					-15.0	3520.7	6397.6	2342.7	3439.3	3038.1	1.23E-06	1.02E-06	1.86E-06	1.16E+06	2.13E+06	8.24E+05	50	selected points
					-16.0	7426.3	8151.5	4096.7	3439.3	3038.1	2.59E-06	2.16E-06	2.37E-06	2.44E+06	2.75E+06	1.48E+06	50	selected points
					-17.0	13401.1	10379.0	6324.2	3439.3	3038.1	4.68E-06	3.90E-06	3.02E-06	4.41E+06	3.59E+06	2.36E+06	50	selected points
					-18.0	15064.9	10955.0	6900.2	3439.3	3038.1	5.26E-06	4.38E-06	3.19E-06	4.96E+06	3.81E+06	2.59E+06	50	selected points
					-19.0	27098.9	14940.2	10885.4	3439.3	3038.1	9.47E-06	7.88E-06	4.34E-06	8.92E+06	5.40E+06	4.22E+06	50	selected points
					-20.0	99162.7	45918.1	41863.3	3439.3	3038.1	3.46E-05	2.88E-05	1.34E-05	3.26E+07	1.72E+07	1.60E+07	50	selected points
					-21.0	148526.0	163030.3	81933.5	3439.3	3038.1	5.19E-05	4.32E-05	4.74E-05	4.89E+07	5.50E+07	2.96E+07	50	selected points
					-22.0	388852.3	253009.5	169443.7	3439.3	3038.1	1.36E-04	1.13E-04	7.36E-05	1.28E+08	8.92E+07	6.43E+07	50	selected points
					-22.5	717669.6	369515.7	283325.9	3439.3	3038.1	2.51E-04	2.09E-04	1.07E-04	2.36E+08	1.35E+08	1.10E+08	50	selected points
					-23.0	1441275.4	658624.0	572434.2	3439.3	3038.1	5.03E-04	4.19E-04	1.91E-04	4.74E+08	2.47E+08	2.23E+08	50	selected points
					-23.0	987022.5	2444017.8	720220.5	3439.3	3038.1	3.45E-04	2.87E-04	7.11E-04	3.25E+08	8.09E+08	2.51E+08	50	selected points
					-23.5	3316189.0	3613041.9	1833354.1	3439.3	3038.1	1.16E-03	9.64E-04	1.05E-03	1.09E+09	1.22E+09	6.62E+08	50	selected points
					-24.0	8507970.1	5505748.7	3726060.9	3439.3	3038.1	2.97E-03	2.47E-03	1.60E-03	2.80E+09	1.94E+09	1.41E+09	50	selected points
					-24.5	13868391.4	7352539.1	5572851.3	3439.3	3038.1	4.84E-03	4.03E-03	2.14E-03	4.56E+09	2.68E+09	2.16E+09	50	selected points
					-25.0	31433828.0	15155397.1	13252284.6	3439.3	3038.1	1.10E-02	9.14E-03	4.41E-03	1.03E+10	5.62E+09	5.07E+09	50	selected points
					-25.5	30893909.1	15144476.9	13172991.1	3439.3	3038.1	1.08E-02	8.98E-03	4.40E-03	1.02E+10	5.60E+09	5.03E+09	50	selected points
					-26.0	36694554.5	18333861.4	16362375.7	3439.3	3038.1	1.28E-02	1.07E-02	5.33E-03	1.21E+10	6.75E+09	6.17E+09	50	selected points
			KIT-CS	Shared impinger	-21.7	279.5			3439.3	3038.1	8.13E-05			9.20E+07	2.30E+07	2.30E+07	5.00E-04	
					-22.7	1278.4			3439.3	3038.1	3.72E-04			4.21E+08	1.05E+08	1.05E+08	5.00E-04	
					-23.9	3885.2			3439.3	3038.1	1.13E-03			1.28E+09	3.20E+08	3.20E+08	5.00E-04	
					-24.8	10341.1			3439.3	3038.1	3.01E-03			3.40E+09	8.51E+08	8.51E+08	5.00E-04	
					-25.6	23074.2			3439.3	3038.1	6.71E-03			7.60E+09	1.90E+09	1.90E+09	5.00E-04	
					-26.7	42851.0			3439.3	3038.1	1.25E-02			1.41E+10	3.53E+09	3.53E+09	5.00E-04	
					-27.7	66387.9			3439.3	3038.1	1.93E-02			2.19E+10	5.46E+09	5.46E+09	5.00E-04	
					-28.5	85979.9			3439.3	3038.1	2.50E-02			2.83E+10	7.08E+09	7.08E+09	5.00E-04	
					-29.4	108076.6			3439.3	3038.1	3.14E-02			3.56E+10	8.89E+09	8.89E+09	5.00E-04	
			M-AL	Shared impinger	-7.7	185.0	73.8	73.8	3439.3	3038.1	5.38E-08	2.15E-08	2.15E-08	6.09E+04	2.87E+04	2.87E+04	4.2	
					-8.7	382.5	127.1	127.1	3439.3	3038.1	1.11E-07	3.69E-08	3.69E-08	1.26E+05	5.23E+04	5.23E+04	4.2	
					-9.7	744.6	246.1	246.1	3439.3	3038.1	2.16E-07	7.16E-08	7.16E-08	2.45E+05	1.02E+05	1.02E+05	4.2	
					-10.7	744.6	226.4	226.4	3439.3	3038.1	2.16E-07	6.58E-08	6.58E-08	2.45E+05	9.65E+04	9.65E+04	4.2	
					-11.7	822.7	251.0	251.0	3439.3	3038.1	2.39E-07	7.30E-08	7.30E-08	2.71E+05	1.07E+05	1.07E+05	4.2	
					-12.7	902.9	275.4	275.4	3439.3	3038.1	2.63E-07	8.01E-08	8.01E-08	2.97E+05	1.17E+05	1.17E+05	4.2	
					-13.7	1436.9	460.9	460.9	3439.3	3038.1	4.18E-07	1.34E-07	1.34E-07	4.73E+05	1.92E+05	1.92E+05	4.2	
					-14.7	2090.4	661.6	661.6	3439.3	3038.1	6.08E-07	1.92E-07	1.92E-07	6.88E+05	2.78E+05	2.78E+05	4.2	
					-15.7	2624.4	811.5	811.5	3439.3	3038.1	7.63E-07	2.36E-07	2.36E-07	8.64E+05	3.43E+05	3.43E+05	4.2	
					-16.7	4654.4	1593.7	1593.7	3439.3	3038.1	1.35E-06	4.63E-07	4.63E-07	1.53E+06	6.50E+05	6.50E+05	4.2	
					-17.7	11398.0	7445.7	7445.7	3439.3	3038.1	3.31E-06	2.16E-06	2.16E-06	3.75E+06	2.62E+06	2.62E+06	4.2	
			NCSU-CS	Shared impinger	-9.2	790.8	0.0	0.0	3439.3	3038.1	2.30E-07	0.00E+00	0.00E+00	2.60E+05	6.51E+04	6.51E+04	1	binned
					-10.2	1419.0	0.0	0.0	3439.3	3038.1	4.13E-07	0.00E+00	0.00E+00	4.67E+05	1.17E+05	1.17E+05	1	binned

					-11.2	8420.5	14269.0	8420.5	3439.3	3038.1	2.45E-06	4.15E-06	2.45E-06	2.77E+06	4.75E+06	2.86E+06	1	binned
					-12.2	11034.6	18648.1	11034.0	3439.3	3038.1	3.21E-06	5.42E-06	3.21E-06	3.63E+06	6.20E+06	3.74E+06	1	binned
					-13.2	13600.5	23048.8	13600.4	3439.3	3038.1	3.95E-06	6.70E-06	3.95E-06	4.48E+06	7.67E+06	4.61E+06	1	binned
					-14.2	16098.7	27525.5	16098.0	3439.3	3038.1	4.68E-06	8.00E-06	4.68E-06	5.30E+06	9.16E+06	5.46E+06	1	binned
					-15.2	18907.9	31698.3	18907.0	3439.3	3038.1	5.50E-06	9.22E-06	5.50E-06	6.22E+06	1.05E+07	6.41E+06	1	binned
					-16.2	22044.2	35573.3	22044.0	3439.3	3038.1	6.41E-06	1.03E-05	6.41E-06	7.26E+06	1.18E+07	7.48E+06	1	binned
					-17.2	25962.5	39037.5	25962.4	3439.3	3038.1	7.55E-06	1.14E-05	7.55E-06	8.55E+06	1.30E+07	8.81E+06	1	binned
					-18.2	31815.5	41449.8	31815.5	3439.3	3038.1	9.25E-06	1.21E-05	9.25E-06	1.05E+07	1.39E+07	1.08E+07	1	binned
					-19.2	40835.8	40746.1	89.7	3439.3	3038.1	1.19E-05	1.18E-05	2.61E-08	1.34E+07	1.38E+07	3.36E+06	1	binned
					-20.2	131163.7	84126.8	47036.9	3439.3	3038.1	3.81E-05	2.45E-05	1.37E-05	4.32E+07	2.97E+07	1.89E+07	1	binned
					-21.2	387421.4	145078.4	242343.0	3439.3	3038.1	1.13E-04	4.22E-05	7.05E-05	1.28E+08	5.74E+07	8.59E+07	1	binned
					-22.2	883621.2	111642.9	771978.3	3439.3	3038.1	2.57E-04	3.25E-05	2.24E-04	2.91E+08	8.15E+07	2.64E+08	1	binned
					-23.2	2439642.4	0.0	0.0	3439.3	3038.1	7.09E-04	0.00E+00	0.00E+00	8.03E+08	2.01E+08	2.01E+08	1	binned
			NIPI	Shared impinger	-8.0	243.0	243.0	121.0	3439.3	3038.1	7.07E-08	7.07E-08	3.52E-08	8.00E+04	8.24E+04	4.46E+04	1	binned
					-9.0	464.0	926.0	309.0	3439.3	3038.1	1.35E-07	2.69E-07	8.98E-08	1.53E+05	3.07E+05	1.09E+05	1	binned
					-10.0	1180.0	1830.0	720.0	3439.3	3038.1	3.43E-07	5.32E-07	2.09E-07	3.88E+05	6.10E+05	2.56E+05	1	binned
					-11.0	2040.0	2510.0	1127.0	3439.3	3038.1	5.93E-07	7.30E-07	3.28E-07	6.71E+05	8.43E+05	4.07E+05	1	binned
					-12.0	2300.0	2610.0	1220.0	3439.3	3038.1	6.69E-07	7.59E-07	3.55E-07	7.57E+05	8.80E+05	4.44E+05	1	binned
					-13.0	3110.0	3970.0	1740.0	3439.3	3038.1	9.04E-07	1.15E-06	5.06E-07	1.02E+06	1.33E+06	6.27E+05	1	binned
					-14.0	4320.0	5780.0	2470.0	3439.3	3038.1	1.26E-06	1.68E-06	7.18E-07	1.42E+06	1.94E+06	8.87E+05	1	binned
					-15.0	8040.0	26560.0	6170.0	3439.3	3038.1	2.34E-06	7.72E-06	1.79E-06	2.65E+06	8.77E+06	2.14E+06	1	binned
					-16.0	8040.0	10360.0	4520.0	3439.3	3038.1	2.34E-06	3.01E-06	1.31E-06	2.65E+06	3.47E+06	1.63E+06	1	binned
					-17.0	10600.0	12700.0	5750.0	3439.3	3038.1	3.08E-06	3.69E-06	1.67E-06	3.49E+06	4.27E+06	2.08E+06	1	binned
					-18.0	24900.0	74800.0	18670.0	3439.3	3038.1	7.24E-06	2.17E-05	5.43E-06	8.20E+06	2.47E+07	6.48E+06	1	binned
					-19.0	57700.0	196300.0	44600.0	3439.3	3038.1	1.68E-05	5.71E-05	1.30E-05	1.90E+07	6.48E+07	1.54E+07	1	binned
					-20.0	293000.0	356000.0	160000.0	3439.3	3038.1	8.52E-05	1.04E-04	4.65E-05	9.64E+07	1.20E+08	5.79E+07	1	binned
					-21.0	554000.0	876000.0	339000.0	3439.3	3038.1	1.61E-04	2.55E-04	9.86E-05	1.82E+08	2.92E+08	1.21E+08	1	binned
					-22.0	1550000.0	3150000.0	1036000.0	3439.3	3038.1	4.51E-04	9.16E-04	3.01E-04	5.10E+08	1.04E+09	3.64E+08	1	binned
					-23.0	4560000.0	4550000.0	2280000.0	3439.3	3038.1	1.33E-03	1.32E-03	6.63E-04	1.50E+09	1.54E+09	8.39E+08	1	binned
			VODCA	Shared impinger	-28.2	44256043.6	9052157.0	9052157.0	3439.3	3038.1	1.29E-02	2.63E-03	2.63E-03	1.46E+10	4.71E+09	4.71E+09	0.000004 - 0.000036	selected points
					-29.2	72460652.7	5781348.2	5781348.2	3439.3	3038.1	2.11E-02	1.68E-03	1.68E-03	2.39E+10	6.26E+09	6.26E+09	0.000004 - 0.000036	selected points
					-30.2	85924020.0	5379733.4	5379733.4	3439.3	3038.1	2.50E-02	1.56E-03	1.56E-03	2.83E+10	7.29E+09	7.29E+09	0.000004 - 0.000036	selected points
					-31.2	89119003.3	8459165.1	8459165.1	3439.3	3038.1	2.59E-02	2.46E-03	2.46E-03	2.93E+10	7.84E+09	7.84E+09	0.000004 - 0.000036	selected points
					-32.2	128910268.6	8536962.3	8536962.3	3439.3	3038.1	3.75E-02	2.48E-03	2.48E-03	4.24E+10	1.10E+10	1.10E+10	0.000004 - 0.000036	selected points
					-33.2	166819951.3	8950755.3	8950755.3	3439.3	3038.1	4.85E-02	2.60E-03	2.60E-03	5.49E+10	1.40E+10	1.40E+10	0.000004 - 0.000036	selected points
					-34.2	272951854.4	43641504.0	43641504.0	3439.3	3038.1	7.94E-02	1.27E-02	1.27E-02	8.98E+10	2.67E+10	2.67E+10	0.000004 - 0.000036	selected points
					-35.2	403858245.0	4248181.3	4248181.3	3439.3	3038.1	1.17E-01	1.24E-03	1.24E-03	1.33E+11	3.33E+10	3.33E+10	0.000004 - 0.000036	selected points
			WISDOM	Shared impinger	-23.2	513132.7	1007231.9	513132.7	3439.3	3038.1	1.49E-04	2.93E-04	1.49E-04	1.69E+08	3.34E+08	1.74E+08	0.000014 - 0.000034	binned
					-24.2	2570813.1	4563101.7	2570813.1	3439.3	3038.1	7.47E-04	1.33E-03	7.47E-04	8.46E+08	1.52E+09	8.72E+08	0.000014 - 0.000034	binned
					-25.2	8793855.6	8674513.8	8793855.5	3439.3	3038.1	2.56E-03	2.52E-03	2.56E-03	2.89E+09	2.95E+09	2.98E+09	0.000014 - 0.000034	binned
					-26.2	16680368.7	7099952.2	9089337.5	3439.3	3038.1	4.85E-03	2.06E-03	2.64E-03	5.49E+09	2.71E+09	3.29E+09	0.000014 - 0.000034	binned
					-27.2	27387983.7	5391155.5	6404778.5	3439.3	3038.1	7.96E-03	1.57E-03	1.86E-03	9.01E+09	2.87E+09	3.09E+09	0.000014 - 0.000034	binned
					-28.2	38323923.2	6044116.8	5244841.7	3439.3	3038.1	1.11E-02	1.76E-03	1.52E-03	1.26E+10	3.73E+09	3.60E+09	0.000014 - 0.000034	binned
					-29.2	69071543.3	14032422.5	13277624.1	3439.3	3038.1	2.01E-02	4.08E-03	3.86E-03	2.27E+10	7.32E+09	7.17E+09	0.000014 - 0.000034	binned
					-30.2	98662951.9	33486521.3	31043537.2	3439.3	3038.1	2.87E-02	9.74E-03	9.03E-03	3.25E+10	1.37E+10	1.31E+10	0.000014 - 0.000034	binned
					-31.2	136049870.3	52189404.6	44512630.2	3439.3	3038.1	3.96E-02	1.52E-02	1.29E-02	4.48E+10	2.05E+10	1.84E+10	0.000014 - 0.000034	binned
					-32.2	178552717.2	61531625.3	53190537.8	3439.3	3038.1	5.19E-02	1.79E-02	1.55E-02	5.88E+10	2.50E+10	2.29E+10	0.000014 - 0.000034	binned
					-33.2	228089258.6	64815788.3	55146372.3	3439.3	3038.1	6.63E-02	1.88E-02	1.60E-02	7.51E+10	2.84E+10	2.61E+10	0.000014 - 0.000034	binned
					-34.2	294634848.7	124283866.9	95950524.2	3439.3	3038.1	8.57E-02	3.61E-02	2.79E-02	9.70E+10	4.76E+10	3.98E+10	0.000014 - 0.000034	binned

					-35.2	346348975.4	137283550.9	105460755.9	3439.3	3038.1	1.01E-01	3.99E-02	3.07E-02	1.14E+11	5.34E+10	4.49E+10	0.000014 - 0.000034	binned
					-36.2	403868339.9	165903706.7	123383389.2	3439.3	3038.1	1.17E-01	4.82E-02	3.59E-02	1.33E+11	6.39E+10	5.25E+10	0.000014 - 0.000034	binned
					-37.2	706910603.2	318719021.1	195083065.3	3439.3	3038.1	2.06E-01	9.27E-02	5.67E-02	2.33E+11	1.20E+11	8.66E+10	0.000014 - 0.000034	binned
18-Mar-15	APC-11	SDT01	BINARY	Shared impinger	-15.2	1690.0	0.0	0.0	3000.6	2009.7	5.63E-07	0.00E+00	0.00E+00	8.41E+05	2.10E+05	2.10E+05	0.6	binned
					-16.2	2600.0	310.0	310.0	3000.6	2009.7	8.67E-07	1.03E-07	1.03E-07	1.29E+06	3.58E+05	3.58E+05	0.6	binned
					-17.2	3550.0	0.0	0.0	3000.6	2009.7	1.18E-06	0.00E+00	0.00E+00	1.77E+06	4.42E+05	4.42E+05	0.6	binned
					-18.2	4210.0	12700.0	2520.0	3000.6	2009.7	1.40E-06	4.23E-06	8.40E-07	2.09E+06	6.34E+06	1.36E+06	0.6	binned
					-19.2	19800.0	23000.0	12700.0	3000.6	2009.7	6.60E-06	7.67E-06	4.23E-06	9.85E+06	1.17E+07	6.78E+06	0.6	binned
					-20.2	100000.0	114000.0	65000.0	3000.6	2009.7	3.33E-05	3.80E-05	2.17E-05	4.98E+07	5.81E+07	3.47E+07	0.6	binned
					-21.2	352000.0	358000.0	154000.0	3000.6	2009.7	1.17E-04	1.19E-04	5.13E-05	1.75E+08	1.83E+08	8.83E+07	0.6	binned
					-22.2	790000.0	900000.0	499000.0	3000.6	2009.7	2.63E-04	3.00E-04	1.66E-04	3.93E+08	4.59E+08	2.67E+08	0.6	binned
					-23.2	1580000.0	1610000.0	1020000.0	3000.6	2009.7	5.27E-04	5.37E-04	3.40E-04	7.86E+08	8.25E+08	5.44E+08	0.6	binned
					-24.2	3490000.0	2140000.0	1780000.0	3000.6	2009.7	1.16E-03	7.13E-04	5.93E-04	1.74E+09	1.15E+09	9.87E+08	0.6	binned
					-25.2	6340000.0	4160000.0	2060000.0	3000.6	2009.7	2.11E-03	1.39E-03	6.87E-04	3.16E+09	2.22E+09	1.29E+09	0.6	binned
					-26.2	13500000.0	9600000.0	6400000.0	3000.6	2009.7	4.50E-03	3.20E-03	2.13E-03	6.73E+09	5.07E+09	3.61E+09	0.6	binned
					-27.2	20600000.0	8700000.0	8200000.0	3000.6	2009.7	6.87E-03	2.90E-03	2.73E-03	1.03E+10	5.05E+09	4.83E+09	0.6	binned
					-28.2	33400000.0	15000000.0	6400000.0	3000.6	2009.7	1.11E-02	5.00E-03	2.13E-03	1.67E+10	8.59E+09	5.26E+09	0.6	binned
					-29.2	48400000.0	21400000.0	9900000.0	3000.6	2009.7	1.61E-02	7.13E-03	3.30E-03	2.43E+10	1.23E+10	7.84E+09	0.6	binned
					-30.2	63100000.0	6750000.0	6750000.0	3000.6	2009.7	2.10E-02	2.25E-03	2.25E-03	3.17E+10	8.63E+09	8.63E+09	0.6	binned
			CMU-CS	Shared impinger	-15.0	1292.1	2532.6	1292.0	3000.6	2009.7	4.31E-07	4.31E-07	8.44E-07	6.43E+05	6.63E+05	1.27E+06	0.1	binned
					-16.0	3114.6	3518.7	3114.0	3000.6	2009.7	1.04E-06	1.04E-06	1.17E-06	1.55E+06	1.60E+06	1.79E+06	0.1	binned
					-17.0	6979.7	5726.3	5726.3	3000.6	2009.7	2.33E-06	1.91E-06	1.91E-06	3.47E+06	2.98E+06	2.98E+06	0.1	binned
					-18.0	14464.7	13234.0	13234.0	3000.6	2009.7	4.82E-06	4.41E-06	4.41E-06	7.20E+06	6.83E+06	6.83E+06	0.1	binned
					-19.0	63275.1	60178.8	60178.8	3000.6	2009.7	2.11E-05	2.01E-05	2.01E-05	3.15E+07	3.10E+07	3.10E+07	0.1	binned
					-20.0	278445.0	210245.0	210245.0	3000.6	2009.7	9.28E-05	7.01E-05	7.01E-05	1.39E+08	1.10E+08	1.10E+08	0.1	binned
					-21.0	589866.0	390655.0	390655.0	3000.6	2009.7	1.97E-04	1.30E-04	1.30E-04	2.94E+08	2.08E+08	2.08E+08	0.1	binned
			FRIDGE-IMM	Filter 5	-16.3	1560.0	7140.0	1520.5	2368.0	1884.0	6.59E-07	3.02E-06	6.42E-07	8.28E+05	3.79E+06	8.33E+05	0.5	selected points
					-17.1	4690.0	9010.0	3724.0	2368.0	1884.0	1.98E-06	3.81E-06	1.57E-06	2.49E+06	4.82E+06	2.07E+06	0.5	selected points
					-18.0	15700.0	13100.0	8190.0	2368.0	1884.0	6.63E-06	5.53E-06	3.46E-06	8.33E+06	7.26E+06	4.82E+06	0.5	selected points
					-19.0	157000.0	35000.0	30000.0	2368.0	1884.0	6.63E-05	1.48E-05	1.27E-05	8.33E+07	2.79E+07	2.62E+07	0.5	selected points
					-20.0	357000.0	52000.0	47000.0	2368.0	1884.0	1.51E-04	2.20E-05	1.98E-05	1.89E+08	5.48E+07	5.35E+07	0.5	selected points
					-21.0	787000.0	82000.0	77000.0	2368.0	1884.0	3.32E-04	3.46E-05	3.25E-05	4.18E+08	1.13E+08	1.12E+08	0.5	selected points
					-22.0	1530000.0	130000.0	120000.0	2368.0	1884.0	6.46E-04	5.49E-05	5.07E-05	8.12E+08	2.14E+08	2.13E+08	0.5	selected points
					-23.0	2830000.0	230000.0	210000.0	2368.0	1884.0	1.20E-03	9.71E-05	8.87E-05	1.50E+09	3.95E+08	3.92E+08	0.5	selected points
					-24.0	6180000.0	760000.0	670000.0	2368.0	1884.0	2.61E-03	3.21E-04	2.83E-04	3.28E+09	9.14E+08	8.94E+08	0.5	selected points
				Filter 4	-18.2	3380.0	4510.0	2280.0	3402.0	2509.0	9.93E-07	0.00E+00	1.33E-06	1.35E+06	3.37E+05	1.83E+06	0.5	selected points
					-19.0	10900.0	6800.0	4690.0	3402.0	2509.0	3.20E-06	0.00E+00	2.00E-06	4.34E+06	1.09E+06	2.92E+06	0.5	selected points
					-20.0	77300.0	16100.0	13900.0	3402.0	2509.0	2.27E-05	0.00E+00	4.73E-06	3.08E+07	7.70E+06	1.00E+07	0.5	selected points
					-21.0	357000.0	37000.0	35000.0	3402.0	2509.0	1.05E-04	0.00E+00	1.09E-05	1.42E+08	3.56E+07	3.85E+07	0.5	selected points
					-22.1	998000.0	80000.0	82000.0	3402.0	2509.0	3.00E-04	0.00E+00	2.35E-05	4.07E+08	1.02E+08	1.07E+08	0.5	selected points
					-23.0	2040000.0	210000.0	200000.0	3402.0	2509.0	6.00E-04	0.00E+00	6.17E-05	8.13E+08	2.03E+08	2.20E+08	0.5	selected points
			IS	Filter	-6.2	4.0	10.0	2.9	3000.6	2009.7	1.33E-09	3.32E-09	9.73E-10	1.99E+03	4.98E+03	1.54E+03	50	selected points
					-6.5	6.1	11.1	4.1	3000.6	2009.7	2.03E-09	3.70E-09	1.35E-09	3.04E+03	5.57E+03	2.16E+03	50	selected points
					-7.0	6.1	11.1	4.1	3000.6	2009.7	2.03E-09	3.70E-09	1.35E-09	3.04E+03	5.57E+03	2.16E+03	50	selected points
					-8.0	10.5	13.2	6.1	3000.6	2009.7	3.51E-09	4.38E-09	2.04E-09	5.24E+03	6.68E+03	3.32E+03	50	selected points
					-9.0	15.3	15.1	8.1	3000.6	2009.7	5.10E-09	5.03E-09	2.69E-09	7.62E+03	7.75E+03	4.44E+03	50	selected points
					-10.0	29.1	20.0	13.0	3000.6	2009.7	9.71E-09	6.67E-09	4.33E-09	1.45E+04	1.06E+04	7.41E+03	50	selected points
					-11.0	35.7	22.2	15.2	3000.6	2009.7	1.19E-08	7.40E-09	5.05E-09	1.78E+04	1.19E+04	8.76E+03	50	selected points
					-12.0	43.0	24.6	17.6	3000.6	2009.7	1.43E-08	8.20E-09	5.85E-09	2.14E+04	1.34E+04	1.02E+04	50	selected points

					-13.0	60.8	30.5	23.5	3000.6	2009.7	2.03E-08	1.02E-08	7.82E-09	3.03E+04	1.70E+04	1.39E+04	50	selected points
					-14.2	115.1	51.0	44.0	3000.6	2009.7	3.84E-08	1.70E-08	1.47E-08	5.73E+04	2.91E+04	2.62E+04	50	selected points
					-15.0	356.8	321.1	180.5	3000.6	2009.7	1.19E-07	1.07E-07	6.02E-08	1.78E+05	1.66E+05	1.00E+05	50	selected points
					-16.0	939.8	518.1	377.5	3000.6	2009.7	3.13E-07	1.73E-07	1.26E-07	4.68E+05	2.83E+05	2.21E+05	50	selected points
					-17.0	1719.4	787.2	646.6	3000.6	2009.7	5.73E-07	2.62E-07	2.15E-07	8.56E+05	4.46E+05	3.86E+05	50	selected points
					-18.0	2936.0	1317.8	1177.1	3000.6	2009.7	9.78E-07	4.39E-07	3.92E-07	1.46E+06	7.51E+05	6.90E+05	50	selected points
					-18.0	5150.7	5653.7	2841.4	3000.6	2009.7	1.72E-06	1.88E-06	9.47E-07	2.56E+06	2.89E+06	1.55E+06	50	selected points
					-19.0	20506.8	10924.9	8112.5	3000.6	2009.7	6.83E-06	3.64E-06	2.70E-06	1.02E+07	6.00E+06	4.78E+06	50	selected points
					-20.0	85971.7	42925.6	40113.2	3000.6	2009.7	2.87E-05	1.43E-05	1.34E-05	4.28E+07	2.39E+07	2.26E+07	50	selected points
					-20.0	122473.2	120773.1	64525.9	3000.6	2009.7	4.08E-05	4.03E-05	2.15E-05	6.09E+07	6.20E+07	3.55E+07	50	selected points
					-21.0	486613.0	243961.5	187714.3	3000.6	2009.7	1.62E-04	8.13E-05	6.26E-05	2.42E+08	1.36E+08	1.11E+08	50	selected points
					-22.0	1174386.9	527103.8	470856.5	3000.6	2009.7	3.91E-04	1.76E-04	1.57E-04	5.84E+08	3.00E+08	2.76E+08	50	selected points
					-22.0	1324962.7	1944077.9	819133.2	3000.6	2009.7	4.42E-04	6.48E-04	2.73E-04	6.59E+08	9.81E+08	4.40E+08	50	selected points
					-23.0	3402862.6	2820735.4	1661542.9	3000.6	2009.7	1.13E-03	9.40E-04	5.54E-04	1.69E+09	1.47E+09	9.29E+08	50	selected points
					-23.5	5394013.7	3509653.0	2350460.5	3000.6	2009.7	1.80E-03	1.17E-03	7.83E-04	2.68E+09	1.87E+09	1.35E+09	50	selected points
					-24.0	7887676.3	4340009.2	3180816.7	3000.6	2009.7	2.63E-03	1.45E-03	1.06E-03	3.92E+09	2.37E+09	1.86E+09	50	selected points
					-24.5	11226315.5	5479810.2	4320617.7	3000.6	2009.7	3.74E-03	1.83E-03	1.44E-03	5.59E+09	3.06E+09	2.56E+09	50	selected points
					-25.0	13115096.7	6265112.3	5069518.5	3000.6	2009.7	4.37E-03	2.09E-03	1.69E-03	6.53E+09	3.52E+09	3.00E+09	50	selected points
					-25.5	17778698.6	8141968.8	6946375.0	3000.6	2009.7	5.93E-03	2.71E-03	2.32E-03	8.85E+09	4.62E+09	4.10E+09	50	selected points
					-26.0	33411927.6	17166214.3	15931856.0	3000.6	2009.7	1.11E-02	5.72E-03	5.31E-03	1.66E+10	9.50E+09	8.95E+09	50	selected points
			KIT-CS	Shared impinger	-20.6	142930.1	0.0	0.0	3000.6	2009.7	4.76E-05	0.00E+00	0.00E+00	7.11E+07	1.78E+07	1.78E+07	5.00E-04	
					-21.9	201932.9	0.0	0.0	3000.6	2009.7	6.73E-05	0.00E+00	0.00E+00	1.00E+08	2.51E+07	2.51E+07	5.00E-04	
					-22.7	564378.5	235338.5	235338.5	3000.6	2009.7	1.88E-04	7.84E-05	7.84E-05	2.81E+08	1.37E+08	1.37E+08	5.00E-04	
					-23.8	1375568.2	238940.4	238940.4	3000.6	2009.7	4.58E-04	7.96E-05	7.96E-05	6.84E+08	2.08E+08	2.08E+08	5.00E-04	
					-24.8	2580960.6	580850.2	580850.2	3000.6	2009.7	8.60E-04	1.94E-04	1.94E-04	1.28E+09	4.32E+08	4.32E+08	5.00E-04	
					-25.7	4346273.4	999157.3	999157.3	3000.6	2009.7	1.45E-03	3.33E-04	3.33E-04	2.16E+09	7.34E+08	7.34E+08	5.00E-04	
					-26.7	6865523.5	1235295.4	1235295.4	3000.6	2009.7	2.29E-03	4.12E-04	4.12E-04	3.42E+09	1.05E+09	1.05E+09	5.00E-04	
					-27.7	10527824.9	2689349.5	2689349.5	3000.6	2009.7	3.51E-03	8.96E-04	8.96E-04	5.24E+09	1.87E+09	1.87E+09	5.00E-04	
					-28.7	15716374.5	4737031.5	4737031.5	3000.6	2009.7	5.24E-03	1.58E-03	1.58E-03	7.82E+09	3.06E+09	3.06E+09	5.00E-04	
					-29.7	22620297.1	5589395.1	5589395.1	3000.6	2009.7	7.54E-03	1.86E-03	1.86E-03	1.13E+10	3.96E+09	3.96E+09	5.00E-04	
					-30.8	31271034.1	5782433.8	5782433.8	3000.6	2009.7	1.04E-02	1.93E-03	1.93E-03	1.56E+10	4.84E+09	4.84E+09	5.00E-04	
					-31.9	41190182.6	7950271.1	7950271.1	3000.6	2009.7	1.37E-02	2.65E-03	2.65E-03	2.05E+10	6.47E+09	6.47E+09	5.00E-04	
					-32.6	52574730.2	13702445.5	13702445.5	3000.6	2009.7	1.75E-02	4.57E-03	4.57E-03	2.62E+10	9.45E+09	9.45E+09	5.00E-04	
					-33.6	63428467.5	19670944.1	19670944.1	3000.6	2009.7	2.11E-02	6.56E-03	6.56E-03	3.16E+10	1.26E+10	1.26E+10	5.00E-04	
					-34.5	83140508.4	21883261.0	21883261.0	3000.6	2009.7	2.77E-02	7.29E-03	7.29E-03	4.14E+10	1.50E+10	1.50E+10	5.00E-04	
					-35.8	105887447.1	0.0	0.0	3000.6	2009.7	3.53E-02	0.00E+00	0.00E+00	5.27E+10	1.32E+10	1.32E+10	5.00E-04	
			M-AL	Shared impinger	-10.7	84.8	19.7	19.7	3000.6	2009.7	2.83E-08	6.57E-09	6.57E-09	4.22E+04	1.44E+04	1.44E+04	4.2	
					-11.7	182.8	43.6	43.6	3000.6	2009.7	6.09E-08	1.45E-08	1.45E-08	9.09E+04	3.14E+04	3.14E+04	4.2	
					-12.7	353.9	86.9	86.9	3000.6	2009.7	1.18E-07	2.90E-08	2.90E-08	1.76E+05	6.17E+04	6.17E+04	4.2	
					-13.7	568.2	132.0	132.0	3000.6	2009.7	1.89E-07	4.40E-08	4.40E-08	2.83E+05	9.65E+04	9.65E+04	4.2	
					-14.7	859.2	220.7	220.7	3000.6	2009.7	2.86E-07	7.36E-08	7.36E-08	4.28E+05	1.53E+05	1.53E+05	4.2	
					-15.7	1548.2	407.3	407.3	3000.6	2009.7	5.16E-07	1.36E-07	1.36E-07	7.70E+05	2.80E+05	2.80E+05	4.2	
					-16.7	3907.1	1137.8	1137.8	3000.6	2009.7	1.30E-06	3.79E-07	3.79E-07	1.94E+06	7.46E+05	7.46E+05	4.2	
					-17.7	9810.2	6567.6	6567.6	3000.6	2009.7	3.27E-06	2.19E-06	2.19E-06	4.88E+06	3.49E+06	3.49E+06	4.2	
			NCSU-CS	Shared impinger	-10.2	221.4	0.0	0.0	3000.6	2009.7	7.38E-08	0.00E+00	0.00E+00	1.10E+05	2.75E+04	2.75E+04	1	binned
					-11.2	253.4	0.0	0.0	3000.6	2009.7	8.44E-08	0.00E+00	0.00E+00	1.26E+05	3.15E+04	3.15E+04	1	binned
					-12.2	285.4	0.0	0.0	3000.6	2009.7	9.51E-08	0.00E+00	0.00E+00	1.42E+05	3.55E+04	3.55E+04	1	binned
					-13.2	317.4	0.0	0.0	3000.6	2009.7	1.06E-07	0.00E+00	0.00E+00	1.58E+05	3.95E+04	3.95E+04	1	binned
					-14.2	349.4	0.0	0.0	3000.6	2009.7	1.16E-07	0.00E+00	0.00E+00	1.74E+05	4.35E+04	4.35E+04	1	binned

					-15.2	375.0	12.5	12.5	3000.6	2009.7	1.25E-07	4.17E-09	4.17E-09	1.87E+05	4.71E+04	4.71E+04	1	binned
					-16.2	513.9	102.1	102.1	3000.6	2009.7	1.71E-07	3.40E-08	3.40E-08	2.56E+05	8.17E+04	8.17E+04	1	binned
					-17.2	872.1	145.9	145.9	3000.6	2009.7	2.91E-07	4.86E-08	4.86E-08	4.34E+05	1.31E+05	1.31E+05	1	binned
					-18.2	1918.2	738.6	738.6	3000.6	2009.7	6.39E-07	2.46E-07	2.46E-07	9.54E+05	4.38E+05	4.38E+05	1	binned
					-19.2	3979.6	1621.4	1621.4	3000.6	2009.7	1.33E-06	5.40E-07	5.40E-07	1.98E+06	9.47E+05	9.47E+05	1	binned
					-20.2	28784.8	18985.6	18985.6	3000.6	2009.7	9.59E-06	6.33E-06	6.33E-06	1.43E+07	1.01E+07	1.01E+07	1	binned
					-21.2	202251.8	0.0	0.0	3000.6	2009.7	6.74E-05	0.00E+00	0.00E+00	1.01E+08	2.52E+07	2.52E+07	1	binned
					-22.2	417740.3	0.0	0.0	3000.6	2009.7	1.39E-04	0.00E+00	0.00E+00	2.08E+08	5.20E+07	5.20E+07	1	binned
					-23.2	934105.7	0.0	0.0	3000.6	2009.7	3.11E-04	0.00E+00	0.00E+00	4.65E+08	1.16E+08	1.16E+08	1	binned
					-24.2	1708670.7	0.0	0.0	3000.6	2009.7	5.69E-04	0.00E+00	0.00E+00	8.50E+08	2.13E+08	2.13E+08	1	binned
					-25.2	4228140.8	0.0	0.0	3000.6	2009.7	1.41E-03	0.00E+00	0.00E+00	2.10E+09	5.26E+08	5.26E+08	1	binned
			NIPI	Shared impinger	-13.0	219.6	219.6	109.8	3000.6	2009.7	7.32E-08	7.32E-08	3.66E-08	1.09E+05	1.13E+05	6.11E+04	1	binned
					-14.0	328.8	730.4	226.7	3000.6	2009.7	1.10E-07	2.43E-07	7.56E-08	1.64E+05	3.66E+05	1.20E+05	1	binned
					-15.0	492.3	2062.4	397.5	3000.6	2009.7	1.64E-07	6.87E-07	1.32E-07	2.45E+05	1.03E+06	2.07E+05	1	binned
					-16.0	731.3	2571.3	569.3	3000.6	2009.7	2.44E-07	8.57E-07	1.90E-07	3.64E+05	1.28E+06	2.98E+05	1	binned
					-17.0	1879.7	3850.8	1263.1	3000.6	2009.7	6.26E-07	1.28E-06	4.21E-07	9.35E+05	1.93E+06	6.71E+05	1	binned
					-18.0	5788.7	13113.1	4015.9	3000.6	2009.7	1.93E-06	4.37E-06	1.34E-06	2.88E+06	6.56E+06	2.12E+06	1	binned
					-19.0	20307.2	53212.5	14698.1	3000.6	2009.7	6.77E-06	1.77E-05	4.90E-06	1.01E+07	2.66E+07	7.74E+06	1	binned
					-20.0	143624.5	391800.7	105098.1	3000.6	2009.7	4.79E-05	1.31E-04	3.50E-05	7.15E+07	1.96E+08	5.53E+07	1	binned
					-21.0	602343.1	1183357.8	399163.9	3000.6	2009.7	2.01E-04	3.94E-04	1.33E-04	3.00E+08	5.94E+08	2.12E+08	1	binned
					-22.0	1503195.9	2672706.6	962091.8	3000.6	2009.7	5.01E-04	8.91E-04	3.21E-04	7.48E+08	1.34E+09	5.14E+08	1	binned
					-23.0	3183939.9	4825696.8	1918280.3	3000.6	2009.7	1.06E-03	1.61E-03	6.39E-04	1.58E+09	2.43E+09	1.03E+09	1	binned
					-24.0	3183939.9	3957796.8	1764471.0	3000.6	2009.7	1.06E-03	1.32E-03	5.88E-04	1.58E+09	2.01E+09	9.63E+08	1	binned
			VODCA	Shared impinger	-35.2	204207501.3	81975685.0	81975685.0	3000.6	2009.7	6.81E-02	2.73E-02	2.73E-02	1.02E+11	4.81E+10	4.81E+10	0.000004 - 0.000036	selected points
					-34.7	191370025.1	52055718.2	52055718.2	3000.6	2009.7	6.38E-02	1.73E-02	1.73E-02	9.52E+10	3.52E+10	3.52E+10	0.000004 - 0.000036	selected points
					-34.2	169471282.2	58495479.5	58495479.5	3000.6	2009.7	5.65E-02	1.95E-02	1.95E-02	8.43E+10	3.59E+10	3.59E+10	0.000004 - 0.000036	selected points
					-33.7	101481161.1	34437457.1	34437457.1	3000.6	2009.7	3.38E-02	1.15E-02	1.15E-02	5.05E+10	2.13E+10	2.13E+10	0.000004 - 0.000036	selected points
					-33.2	64805529.4	28924211.8	28924211.8	3000.6	2009.7	2.16E-02	9.64E-03	9.64E-03	3.22E+10	1.65E+10	1.65E+10	0.000004 - 0.000036	selected points
					-32.7	50157669.8	26749088.8	26749088.8	3000.6	2009.7	1.67E-02	8.91E-03	8.91E-03	2.50E+10	1.47E+10	1.47E+10	0.000004 - 0.000036	selected points
					-32.2	25881469.4	17620409.9	17620409.9	3000.6	2009.7	8.63E-03	5.87E-03	5.87E-03	1.29E+10	9.34E+09	9.34E+09	0.000004 - 0.000036	selected points
			WISDOM	Shared impinger	-25.2	1528997.7	336379.5	336379.5	3000.6	2009.7	5.10E-04	1.12E-04	1.12E-04	7.61E+08	2.53E+08	2.53E+08	0.000014 - 0.000034	binned
					-26.2	1912206.6	305953.1	305953.1	3000.6	2009.7	6.37E-04	1.02E-04	1.02E-04	9.51E+08	2.82E+08	2.82E+08	0.000014 - 0.000034	binned
					-27.2	1912206.6	305953.1	305953.1	3000.6	2009.7	6.37E-04	1.02E-04	1.02E-04	9.51E+08	2.82E+08	2.82E+08	0.000014 - 0.000034	binned
					-28.2	2679781.2	321573.7	321573.7	3000.6	2009.7	8.93E-04	1.07E-04	1.07E-04	1.33E+09	3.70E+08	3.70E+08	0.000014 - 0.000034	binned
					-29.2	4219579.1	632936.9	632936.9	3000.6	2009.7	1.41E-03	2.11E-04	2.11E-04	2.10E+09	6.12E+08	6.12E+08	0.000014 - 0.000034	binned
					-30.2	6929271.9	485049.0	485049.0	3000.6	2009.7	2.31E-03	1.62E-04	1.62E-04	3.45E+09	8.95E+08	8.95E+08	0.000014 - 0.000034	binned
					-31.2	11226632.9	336799.0	336799.0	3000.6	2009.7	3.74E-03	1.12E-04	1.12E-04	5.59E+09	1.41E+09	1.41E+09	0.000014 - 0.000034	binned
					-32.2	13591213.4	951384.9	951384.9	3000.6	2009.7	4.53E-03	3.17E-04	3.17E-04	6.76E+09	1.76E+09	1.76E+09	0.000014 - 0.000034	binned
					-33.2	17165794.2	686631.8	686631.8	3000.6	2009.7	5.72E-03	2.29E-04	2.29E-04	8.54E+09	2.16E+09	2.16E+09	0.000014 - 0.000034	binned
					-34.2	23604502.8	472090.1	472090.1	3000.6	2009.7	7.87E-03	1.57E-04	1.57E-04	1.17E+10	2.95E+09	2.95E+09	0.000014 - 0.000034	binned
					-35.2	36817405.3	2209044.3	2209044.3	3000.6	2009.7	1.23E-02	7.36E-04	7.36E-04	1.83E+10	4.71E+09	4.71E+09	0.000014 - 0.000034	binned
					-36.2	70163698.0	2104910.9	2104910.9	3000.6	2009.7	2.34E-02	7.02E-04	7.02E-04	3.49E+10	8.79E+09	8.79E+09	0.000014 - 0.000034	binned
19-Mar-15	APC-13	FS02	BINARY	Shared impinger	-14.2	2190.0	330.0	330.0	7750.2	3703.1	2.83E-07	4.26E-08	4.26E-08	5.91E+05	8.91E+04	8.91E+04	0.6	binned
					-15.2	6150.0	8650.0	3630.0	7750.2	3703.1	7.94E-07	1.12E-06	4.68E-07	1.66E+06	2.34E+06	9.80E+05	0.6	binned
					-16.2	17300.0	24900.0	10900.0	7750.2	3703.1	2.23E-06	3.21E-06	1.41E-06	4.67E+06	6.72E+06	2.94E+06	0.6	binned
					-17.2	30900.0	31000.0	17000.0	7750.2	3703.1	3.99E-06	4.00E-06	2.19E-06	8.34E+06	8.37E+06	4.59E+06	0.6	binned
					-18.2	54800.0	69200.0	29600.0	7750.2	3703.1	7.07E-06	8.93E-06	3.82E-06	1.48E+07	1.87E+07	7.99E+06	0.6	binned
					-19.2	86700.0	375000.0	61500.0	7750.2	3703.1	1.12E-05	4.84E-05	7.94E-06	2.34E+07	1.01E+08	1.66E+07	0.6	binned
					-20.2	202000.0	1170000.0	115000.0	7750.2	3703.1	2.61E-05	1.51E-04	1.48E-05	5.45E+07	3.16E+08	3.11E+07	0.6	binned

					-21.2	615000.0	2130000.0	362000.0	7750.2	3703.1	7.94E-05	2.75E-04	4.67E-05	1.66E+08	5.75E+08	9.78E+07	0.6	binned
					-22.2	2960000.0	10700000.0	2420000.0	7750.2	3703.1	3.82E-04	1.38E-03	3.12E-04	7.99E+08	2.89E+09	6.54E+08	0.6	binned
					-23.2	11500000.0	18100000.0	8760000.0	7750.2	3703.1	1.48E-03	2.34E-03	1.13E-03	3.11E+09	4.89E+09	2.37E+09	0.6	binned
					-24.2	42200000.0	44500000.0	36900000.0	7750.2	3703.1	5.45E-03	5.74E-03	4.76E-03	1.14E+10	1.20E+10	9.96E+09	0.6	binned
					-25.2	173000000.0	177000000.0	103000000.0	7750.2	3703.1	2.23E-02	2.28E-02	1.33E-02	4.67E+10	4.78E+10	2.78E+10	0.6	binned
					-26.2	422000000.0	344000000.0	169000000.0	7750.2	3703.1	5.45E-02	4.44E-02	2.18E-02	1.14E+11	9.29E+10	4.56E+10	0.6	binned
					-27.2	692000000.0	74000000.0	74000000.0	7750.2	3703.1	8.93E-02	9.55E-03	9.55E-03	1.87E+11	2.00E+10	2.00E+10	0.6	binned
			FRIDGE-IMM	Filter 6	-15.6	3420.0	15680.0	3333.5	6535.1	2613.9	5.23E-07	2.40E-06	5.10E-07	1.31E+06	6.01E+06	1.32E+06	0.5	selected points
					-16.6	24000.0	25500.0	14350.0	6535.1	2613.9	3.67E-06	3.90E-06	2.20E-06	9.18E+06	1.00E+07	5.95E+06	0.5	selected points
					-17.5	219000.0	62000.0	51000.0	6535.1	2613.9	3.35E-05	9.49E-06	7.80E-06	8.38E+07	3.16E+07	2.86E+07	0.5	selected points
					-18.5	981000.0	129000.0	119000.0	6535.1	2613.9	1.50E-04	1.97E-05	1.82E-05	3.75E+08	1.06E+08	1.04E+08	0.5	selected points
					-19.5	2560000.0	240000.0	220000.0	6535.1	2613.9	3.92E-04	3.67E-05	3.37E-05	9.79E+08	2.61E+08	2.59E+08	0.5	selected points
					-20.5	3970000.0	340000.0	310000.0	6535.1	2613.9	6.07E-04	5.20E-05	4.74E-05	1.52E+09	4.01E+08	3.98E+08	0.5	selected points
					-21.5	6140000.0	530000.0	490000.0	6535.1	2613.9	9.40E-04	8.11E-05	7.50E-05	2.35E+09	6.21E+08	6.16E+08	0.5	selected points
					-22.5	10300000.0	1100000.0	1030000.0	6535.1	2613.9	1.58E-03	1.68E-04	1.58E-04	3.94E+09	1.07E+09	1.06E+09	0.5	selected points
					-23.5	16100000.0	3100000.0	2500000.0	6535.1	2613.9	2.46E-03	4.74E-04	3.83E-04	6.16E+09	1.94E+09	1.81E+09	0.5	selected points
					-24.1	19500000.0	6800000.0	4000000.0	6535.1	2613.9	2.98E-03	1.04E-03	6.12E-04	7.46E+09	3.20E+09	2.41E+09	0.5	selected points
			IS	Filter	-7.4	1.7	7.4	1.4	7750.2	3703.1	2.18E-10	9.58E-10	1.80E-10	2.01E+03	8.83E+03	1.73E+03	50	selected points
					-8.0	11.1	12.1	6.1	7750.2	3703.1	1.43E-09	1.57E-09	7.87E-10	3.28E+03	3.69E+03	1.98E+03	50	selected points
					-9.0	22.4	16.3	10.3	7750.2	3703.1	2.89E-09	2.10E-09	1.32E-09	4.40E+03	3.39E+03	2.30E+03	50	selected points
					-10.0	47.9	24.7	18.7	7750.2	3703.1	6.19E-09	3.19E-09	2.41E-09	6.68E+03	3.83E+03	3.10E+03	50	selected points
					-11.0	184.4	92.1	86.1	7750.2	3703.1	2.38E-08	1.19E-08	1.11E-08	2.49E+04	1.39E+04	1.32E+04	50	selected points
					-11.0	68.7	170.8	50.1	7750.2	3703.1	8.86E-09	2.20E-08	6.47E-09	4.61E+04	1.15E+05	3.56E+04	50	selected points
					-12.0	500.3	343.7	223.0	7750.2	3703.1	6.45E-08	4.43E-08	2.88E-08	9.28E+04	6.78E+04	4.74E+04	50	selected points
					-13.0	2519.6	1130.9	1010.2	7750.2	3703.1	3.25E-07	1.46E-07	1.30E-07	3.05E+05	1.57E+05	1.44E+05	50	selected points
					-14.0	7030.2	5842.1	3428.6	7750.2	3703.1	9.07E-07	7.54E-07	4.42E-07	1.58E+06	1.37E+06	8.65E+05	50	selected points
					-15.0	27004.0	12595.5	10182.0	7750.2	3703.1	3.48E-06	1.63E-06	1.31E-06	3.40E+06	1.80E+06	1.54E+06	50	selected points
					-16.0	27477.8	68313.0	20043.3	7750.2	3703.1	3.55E-06	8.81E-06	2.59E-06	1.84E+07	4.61E+07	1.42E+07	50	selected points
					-17.0	88404.2	97037.3	48767.7	7750.2	3703.1	1.14E-05	1.25E-05	6.29E-06	2.62E+07	2.95E+07	1.59E+07	50	selected points
					-18.0	221946.5	144774.3	96504.7	7750.2	3703.1	2.86E-05	1.87E-05	1.25E-05	3.91E+07	2.73E+07	1.96E+07	50	selected points
					-19.0	647078.6	291771.0	243501.4	7750.2	3703.1	8.35E-05	3.76E-05	3.14E-05	7.88E+07	4.06E+07	3.56E+07	50	selected points
					-20.0	1180452.9	546618.6	498349.0	7750.2	3703.1	1.52E-04	7.05E-05	6.43E-05	1.48E+08	7.77E+07	7.24E+07	50	selected points
					-20.0	2449661.1	2204489.7	1239096.9	7750.2	3703.1	3.16E-04	2.84E-04	1.60E-04	5.95E+08	5.56E+08	3.36E+08	50	selected points
					-21.0	5386035.6	3207894.2	2242501.3	7750.2	3703.1	6.95E-04	4.14E-04	2.89E-04	8.66E+08	5.60E+08	4.21E+08	50	selected points
					-21.5	20156454.4	9046884.8	8081491.9	7750.2	3703.1	2.60E-03	1.17E-03	1.04E-03	2.44E+09	1.26E+09	1.15E+09	50	selected points
					-22.0	20117609.3	36555799.6	13386370.3	7750.2	3703.1	2.60E-03	4.72E-03	1.73E-03	9.87E+09	1.81E+10	7.02E+09	50	selected points
					-23.0	96051832.7	65983680.5	42814251.2	7750.2	3703.1	1.24E-02	8.51E-03	5.52E-03	1.78E+10	1.30E+10	9.11E+09	50	selected points
					-23.5	193957920.7	99980683.9	76105883.3	7750.2	3703.1	2.50E-02	1.29E-02	9.82E-03	2.70E+10	1.55E+10	1.26E+10	50	selected points
					-24.0	304109414.2	139768480.5	115893679.9	7750.2	3703.1	3.92E-02	1.80E-02	1.50E-02	3.77E+10	1.97E+10	1.72E+10	50	selected points
					-24.5	372872234.2	167901435.2	144026634.6	7750.2	3703.1	4.81E-02	2.17E-02	1.86E-02	4.53E+10	2.34E+10	2.09E+10	50	selected points
					-25.0	560129094.8	262310481.4	238435680.8	7750.2	3703.1	7.23E-02	3.38E-02	3.08E-02	7.08E+10	3.76E+10	3.50E+10	50	selected points
			KIT-CS	Shared impinger	-17.2	103041.9	0.0	0.0	7750.2	3703.1	1.33E-05	0.00E+00	0.00E+00	2.78E+07	6.96E+06	6.96E+06	5.00E-04	
					-19.0	236433.9	0.0	0.0	7750.2	3703.1	3.05E-05	0.00E+00	0.00E+00	6.38E+07	1.60E+07	1.60E+07	5.00E-04	
					-19.9	694568.6	669207.1	669207.1	7750.2	3703.1	8.96E-05	8.63E-05	8.63E-05	1.88E+08	1.87E+08	1.87E+08	5.00E-04	
					-20.8	3430083.6	1683764.0	1683764.0	7750.2	3703.1	4.43E-04	2.17E-04	2.17E-04	9.26E+08	5.10E+08	5.10E+08	5.00E-04	
					-21.8	13193135.0	5221145.2	5221145.2	7750.2	3703.1	1.70E-03	6.74E-04	6.74E-04	3.56E+09	1.67E+09	1.67E+09	5.00E-04	
					-22.6	38530923.3	13869037.5	13869037.5	7750.2	3703.1	4.97E-03	1.79E-03	1.79E-03	1.04E+10	4.56E+09	4.56E+09	5.00E-04	
					-23.6	86551949.0	30485073.2	30485073.2	7750.2	3703.1	1.12E-02	3.93E-03	3.93E-03	2.34E+10	1.01E+10	1.01E+10	5.00E-04	
					-24.6	117883563.8	30916919.7	30916919.7	7750.2	3703.1	1.52E-02	3.99E-03	3.99E-03	3.18E+10	1.15E+10	1.15E+10	5.00E-04	

			M-AL	Shared impinger	-15.2	219.1	66.8	66.8	7750.2	3703.1	2.83E-08	8.62E-09	8.62E-09	5.92E+04	2.33E+04	2.33E+04	4.2	
					-16.2	2171.3	768.6	768.6	7750.2	3703.1	2.80E-07	9.92E-08	9.92E-08	5.86E+05	2.54E+05	2.54E+05	4.2	
					-17.2	5966.8	2121.4	2121.4	7750.2	3703.1	7.70E-07	2.74E-07	2.74E-07	1.61E+06	7.00E+05	7.00E+05	4.2	
					-18.2	11395.2	4204.5	4204.5	7750.2	3703.1	1.47E-06	5.43E-07	5.43E-07	3.08E+06	1.37E+06	1.37E+06	4.2	
			NCSU-CS	Shared impinger	-16.2	1222.0	235.3	235.3	7750.2	3703.1	1.58E-07	3.04E-08	3.04E-08	3.30E+05	1.04E+05	1.04E+05	1	binned
					-17.2	3456.8	2837.0	2837.0	7750.2	3703.1	4.46E-07	3.66E-07	3.66E-07	9.33E+05	8.01E+05	8.01E+05	1	binned
					-18.2	8477.1	7615.8	7615.8	7750.2	3703.1	1.09E-06	9.83E-07	9.83E-07	2.29E+06	2.13E+06	2.13E+06	1	binned
					-19.2	21362.7	16532.9	16532.9	7750.2	3703.1	2.76E-06	2.13E-06	2.13E-06	5.77E+06	4.69E+06	4.69E+06	1	binned
					-20.2	32641.4	10277.6	10277.6	7750.2	3703.1	4.21E-06	1.33E-06	1.33E-06	8.81E+06	3.54E+06	3.54E+06	1	binned
					-21.2	115375.4	0.0	0.0	7750.2	3703.1	1.49E-05	0.00E+00	0.00E+00	3.12E+07	7.79E+06	7.79E+06	1	binned
					-22.2	379011.2	0.0	0.0	7750.2	3703.1	4.89E-05	0.00E+00	0.00E+00	1.02E+08	2.56E+07	2.56E+07	1	binned
					-23.2	1236963.3	0.0	0.0	7750.2	3703.1	1.60E-04	0.00E+00	0.00E+00	3.34E+08	8.35E+07	8.35E+07	1	binned
					-24.2	2119253.1	0.0	0.0	7750.2	3703.1	2.73E-04	0.00E+00	0.00E+00	5.72E+08	1.43E+08	1.43E+08	1	binned
					-25.2	5306940.2	0.0	0.0	7750.2	3703.1	6.85E-04	0.00E+00	0.00E+00	1.43E+09	3.58E+08	3.58E+08	1	binned
			NIPI	Shared impinger	-8.0	257.2	257.2	128.6	7750.2	3703.1	3.32E-08	3.32E-08	1.66E-08	6.94E+04	7.16E+04	3.88E+04	1	binned
					-9.0	337.0	702.1	227.7	7750.2	3703.1	4.35E-08	9.06E-08	2.94E-08	9.10E+04	1.91E+05	6.56E+04	1	binned
					-10.0	337.0	499.9	201.3	7750.2	3703.1	4.35E-08	6.45E-08	2.60E-08	9.10E+04	1.37E+05	5.89E+04	1	binned
					-11.0	337.0	337.0	168.5	7750.2	3703.1	4.35E-08	4.35E-08	2.17E-08	9.10E+04	9.38E+04	5.09E+04	1	binned
					-12.0	353.6	622.3	225.5	7750.2	3703.1	4.56E-08	8.03E-08	2.91E-08	9.55E+04	1.70E+05	6.54E+04	1	binned
					-13.0	522.4	1467.4	385.2	7750.2	3703.1	6.74E-08	1.89E-07	4.97E-08	1.41E+05	3.98E+05	1.10E+05	1	binned
					-14.0	928.6	2041.1	638.2	7750.2	3703.1	1.20E-07	2.63E-07	8.24E-08	2.51E+05	5.55E+05	1.83E+05	1	binned
					-15.0	3310.9	7374.6	2285.0	7750.2	3703.1	4.27E-07	9.52E-07	2.95E-07	8.94E+05	2.00E+06	6.56E+05	1	binned
					-16.0	11201.5	23195.1	7553.7	7750.2	3703.1	1.45E-06	2.99E-06	9.75E-07	3.02E+06	6.31E+06	2.18E+06	1	binned
					-17.0	30031.1	51565.6	18978.4	7750.2	3703.1	3.87E-06	6.65E-06	2.45E-06	8.11E+06	1.41E+07	5.51E+06	1	binned
					-18.0	34878.9	44023.2	19460.6	7750.2	3703.1	4.50E-06	5.68E-06	2.51E-06	9.42E+06	1.21E+07	5.76E+06	1	binned
					-19.0	34878.9	39310.3	18481.1	7750.2	3703.1	4.50E-06	5.07E-06	2.38E-06	9.42E+06	1.09E+07	5.52E+06	1	binned
			VODCA	Shared impinger	-25.2	77000000.0	61600000.0	61600000.0	7750.2	3703.1	9.94E-03	7.95E-03	7.95E-03	2.08E+10	1.74E+10	1.74E+10	0.000004 - 0.000036	selected points
					-26.2	228000000.0	123000000.0	123000000.0	7750.2	3703.1	2.94E-02	1.59E-02	1.59E-02	6.16E+10	3.66E+10	3.66E+10	0.000004 - 0.000036	selected points
					-27.2	522000000.0	200000000.0	200000000.0	7750.2	3703.1	6.74E-02	2.58E-02	2.58E-02	1.41E+11	6.45E+10	6.45E+10	0.000004 - 0.000036	selected points
					-28.2	667000000.0	117000000.0	117000000.0	7750.2	3703.1	8.61E-02	1.51E-02	1.51E-02	1.80E+11	5.50E+10	5.50E+10	0.000004 - 0.000036	selected points
					-29.2	769000000.0	102000000.0	102000000.0	7750.2	3703.1	9.92E-02	1.32E-02	1.32E-02	2.08E+11	5.88E+10	5.88E+10	0.000004 - 0.000036	selected points
					-30.2	900000000.0	96700000.0	96700000.0	7750.2	3703.1	1.16E-01	1.25E-02	1.25E-02	2.43E+11	6.61E+10	6.61E+10	0.000004 - 0.000036	selected points
					-31.2	979000000.0	175000000.0	175000000.0	7750.2	3703.1	1.26E-01	2.26E-02	2.26E-02	2.64E+11	8.13E+10	8.13E+10	0.000004 - 0.000036	selected points
					-32.2	1050000000.0	234000000.0	234000000.0	7750.2	3703.1	1.35E-01	3.02E-02	3.02E-02	2.84E+11	9.50E+10	9.50E+10	0.000004 - 0.000036	selected points
					-33.2	1150000000.0	320000000.0	320000000.0	7750.2	3703.1	1.48E-01	4.13E-02	4.13E-02	3.11E+11	1.16E+11	1.16E+11	0.000004 - 0.000036	selected points
					-34.2	1290000000.0	381000000.0	381000000.0	7750.2	3703.1	1.66E-01	4.92E-02	4.92E-02	3.48E+11	1.35E+11	1.35E+11	0.000004 - 0.000036	selected points
					-35.2	1380000000.0	199000000.0	199000000.0	7750.2	3703.1	1.78E-01	2.57E-02	2.57E-02	3.73E+11	1.08E+11	1.08E+11	0.000004 - 0.000036	selected points
			WISDOM	Shared impinger	-24.2	5365858.9	173650.0	1072052.0	7750.2	3703.1	6.92E-04	2.24E-05	1.38E-04	1.45E+09	3.65E+08	4.64E+08	0.000014 - 0.000034	binned
					-25.2	42895869.5	1134923.6	6952817.1	7750.2	3703.1	5.53E-03	1.46E-04	8.97E-04	1.16E+10	2.91E+09	3.45E+09	0.000014 - 0.000034	binned
					-26.2	108726562.1	1866015.9	11365519.9	7750.2	3703.1	1.40E-02	2.41E-04	1.47E-03	2.94E+10	7.36E+09	7.96E+09	0.000014 - 0.000034	binned
					-27.2	283021580.9	10001570.3	57286533.6	7750.2	3703.1	3.65E-02	1.29E-03	7.39E-03	7.64E+10	1.93E+10	2.46E+10	0.000014 - 0.000034	binned
					-28.2	460306250.1	3638784.2	21857829.3	7750.2	3703.1	5.94E-02	4.70E-04	2.82E-03	1.24E+11	3.11E+10	3.16E+10	0.000014 - 0.000034	binned
					-29.2	580311767.4	2857494.3	17269331.7	7750.2	3703.1	7.49E-02	3.69E-04	2.23E-03	1.57E+11	3.92E+10	3.95E+10	0.000014 - 0.000034	binned
					-30.2	662990737.3	36833803.3	5681290.6	7750.2	3703.1	8.55E-02	4.75E-03	7.33E-04	1.79E+11	4.59E+10	4.48E+10	0.000014 - 0.000034	binned
					-31.2	724320788.1	16535423.1	2617775.9	7750.2	3703.1	9.35E-02	2.13E-03	3.38E-04	1.96E+11	4.91E+10	4.89E+10	0.000014 - 0.000034	binned
					-32.2	731176449.7	13953352.0	2216390.4	7750.2	3703.1	9.43E-02	1.80E-03	2.86E-04	1.97E+11	4.95E+10	4.94E+10	0.000014 - 0.000034	binned
					-33.2	742842908.9	8542736.6	1366508.9	7750.2	3703.1	9.58E-02	1.10E-03	1.76E-04	2.01E+11	5.02E+10	5.02E+10	0.000014 - 0.000034	binned
					-34.2	747596607.4	5738312.7	921263.2	7750.2	3703.1	9.65E-02	7.40E-04	1.19E-04	2.02E+11	5.05E+10	5.05E+10	0.000014 - 0.000034	binned
					-35.2	764646731.0	27492783.8	4291489.1	7750.2	3703.1	9.87E-02	3.55E-03	5.54E-04	2.06E+11	5.22E+10	5.16E+10	0.000014 - 0.000034	binned

					-36.2	808999815.5	6594769.2	1057584.4	7750.2	3703.1	1.04E-01	8.51E-04	1.36E-04	2.18E+11	5.46E+10	5.46E+10	0.000014 - 0.000034	binned
					-37.2	2354924984.2	35702856.9	173403670.6	7750.2	3703.1	3.04E-01	4.61E-03	2.24E-02	6.36E+11	1.59E+11	1.66E+11	0.000014 - 0.000034	binned
20-Mar-15	APC-15	SM04	BINARY	Shared impinger	-4.2	16300.0	31900.0	14000.0	27802.0	4028.0	5.86E-07	1.15E-06	5.04E-07	4.05E+06	7.98E+06	3.62E+06	0.6	binned
					-5.2	110000.0	170000.0	67600.0	27802.0	4028.0	3.96E-06	6.11E-06	2.43E-06	2.73E+07	4.28E+07	1.81E+07	0.6	binned
					-6.2	348000.0	283000.0	165000.0	27802.0	4028.0	1.25E-05	1.02E-05	5.93E-06	8.64E+07	7.35E+07	4.63E+07	0.6	binned
					-7.2	1400000.0	1820000.0	804000.0	27802.0	4028.0	5.04E-05	6.55E-05	2.89E-05	3.48E+08	4.60E+08	2.18E+08	0.6	binned
					-8.2	10500000.0	31400000.0	7810000.0	27802.0	4028.0	3.78E-04	1.13E-03	2.81E-04	2.61E+09	7.82E+09	2.05E+09	0.6	binned
					-9.2	56000000.0	49100000.0	26800000.0	27802.0	4028.0	2.01E-03	1.77E-03	9.64E-04	1.39E+10	1.27E+10	7.51E+09	0.6	binned
					-10.2	129000000.0	69000000.0	50300000.0	27802.0	4028.0	4.64E-03	2.48E-03	1.81E-03	3.20E+10	1.89E+10	1.48E+10	0.6	binned
					-11.2	177000000.0	71500000.0	62500000.0	27802.0	4028.0	6.37E-03	2.57E-03	2.25E-03	4.39E+10	2.09E+10	1.90E+10	0.6	binned
					-12.2	239000000.0	53000000.0	105000000.0	27802.0	4028.0	8.60E-03	1.91E-03	3.78E-03	5.93E+10	1.98E+10	3.00E+10	0.6	binned
					-13.2	305000000.0	13000000.0	159000000.0	27802.0	4028.0	1.10E-02	4.68E-04	5.72E-03	7.57E+10	1.92E+10	4.38E+10	0.6	binned
					-14.2	157000000.0	0.0	0.0	27802.0	4028.0	5.65E-03	0.00E+00	0.00E+00	3.90E+10	9.74E+09	9.74E+09	0.6	binned
					-15.2	170000000.0	0.0	0.0	27802.0	4028.0	6.11E-03	0.00E+00	0.00E+00	4.22E+10	1.06E+10	1.06E+10	0.6	binned
					-16.2	183000000.0	0.0	0.0	27802.0	4028.0	6.58E-03	0.00E+00	0.00E+00	4.54E+10	1.14E+10	1.14E+10	0.6	binned
					-19.2	198000000.0	0.0	0.0	27802.0	4028.0	7.12E-03	0.00E+00	0.00E+00	4.92E+10	1.23E+10	1.23E+10	0.6	binned
					-25.2	230000000.0	118000000.0	17000000.0	27802.0	4028.0	8.27E-03	4.24E-03	6.11E-04	5.71E+10	3.26E+10	1.49E+10	0.6	binned
					-26.2	259000000.0	10500000.0	10500000.0	27802.0	4028.0	9.32E-03	3.78E-04	3.78E-04	6.43E+10	1.63E+10	1.63E+10	0.6	binned
					-28.2	292000000.0	0.0	0.0	27802.0	4028.0	1.05E-02	0.00E+00	0.00E+00	7.25E+10	1.81E+10	1.81E+10	0.6	binned
					-29.2	318000000.0	0.0	0.0	27802.0	4028.0	1.14E-02	0.00E+00	0.00E+00	7.89E+10	1.97E+10	1.97E+10	0.6	binned
					-30.2	366000000.0	17500000.0	17500000.0	27802.0	4028.0	1.32E-02	6.29E-04	6.29E-04	9.09E+10	2.31E+10	2.31E+10	0.6	binned
					-31.2	383000000.0	43000000.0	35000000.0	27802.0	4028.0	1.38E-02	1.55E-03	1.26E-03	9.51E+10	2.61E+10	2.53E+10	0.6	binned
					-32.2	522000000.0	39500000.0	39500000.0	27802.0	4028.0	1.88E-02	1.42E-03	1.42E-03	1.30E+11	3.38E+10	3.38E+10	0.6	binned
			CMU-CS	Shared impinger	-4.0	11174.5	15143.2	15143.2	27802.0	4028.0	4.01929E-07	5.44677E-07	5.45E-07	2.77E+06	3.82E+06	3.82E+06	0.1	binned, scan1
					-5.0	134214.0	23188.9	23188.9	27802.0	4028.0	4.82746E-06	8.34068E-07	8.34E-07	3.33E+07	1.01E+07	1.01E+07	0.1	binned, scan1
					-6.0	343715.0	12007.2	12007.2	27802.0	4028.0	1.23629E-05	4.3188E-07	4.32E-07	8.53E+07	2.15E+07	2.15E+07	0.1	binned, scan1
					-6.0	1671760.0	0.0	0.0	27802.0	4028.0	6.01306E-05	0	0.00E+00	4.15E+08	1.04E+08	1.04E+08	0.1	binned, scan2
					-7.0	13561700.0	1620220.0	1620220.0	27802.0	4028.0	0.000487793	5.82767E-05	5.83E-05	3.37E+09	9.33E+08	9.33E+08	0.1	binned, scan2
					-8.0	86400900.0	25160200.0	25160200.0	27802.0	4028.0	0.003107703	0.000904972	9.05E-04	2.15E+10	8.23E+09	8.23E+09	0.1	binned, scan2
					-9.0	118748000.0	24566400.0	24566400.0	27802.0	4028.0	0.004271177	0.000883614	8.84E-04	2.95E+10	9.57E+09	9.57E+09	0.1	binned, scan2
					-10.0	178996000.0	17619000.0	17619000.0	27802.0	4028.0	0.006438202	0.000633727	6.34E-04	4.44E+10	1.19E+10	1.19E+10	0.1	binned, scan2
					-11.0	213774000.0	37345300.0	37345300.0	27802.0	4028.0	0.007689111	0.001343251	1.34E-03	5.31E+10	1.62E+10	1.62E+10	0.1	binned, scan2
					-12.0	234104000.0	0.0	0.0	27802.0	4028.0	0.008420349	0	0.00E+00	5.81E+10	1.45E+10	1.45E+10	0.1	binned, scan2
					-13.0	264820000.0	0.0	0.0	27802.0	4028.0	0.009525155	0	0.00E+00	6.57E+10	1.64E+10	1.64E+10	0.1	binned, scan2
					-14.0	382300000.0	0.0	0.0	27802.0	4028.0	0.013750724	0	0.00E+00	9.49E+10	2.37E+10	2.37E+10	0.1	binned, scan2
					-15.0	460110000.0	0.0	0.0	27802.0	4028.0	0.016549426	0	0.00E+00	1.14E+11	2.86E+10	2.86E+10	0.1	binned, scan2
					-3.0	14278.2	0.0	0.0	27802.0	4028.0	5.13564E-07	0	0.00E+00	3.54E+06	8.86E+05	8.86E+05	0.1	binned, first freeze
					-4.0	169419.0	18058.5	18058.5	27802.0	4028.0	6.09373E-06	6.49536E-07	6.50E-07	4.21E+07	1.14E+07	1.14E+07	0.1	binned, first freeze
					-5.0	490146.0	51065.3	51065.3	27802.0	4028.0	1.76298E-05	1.83674E-06	1.84E-06	1.22E+08	3.30E+07	3.30E+07	0.1	binned, first freeze
					-6.0	1055580.0	0.0	0.0	27802.0	4028.0	3.79675E-05	0	0.00E+00	2.62E+08	6.55E+07	6.55E+07	0.1	binned, first freeze
			IS	Shared impinger	-3.7	161.3	73.5	108.1	27802.0	4028.0	5.80E-09	3.89E-09	2.64E-09	4.01E+04	2.86E+04	2.08E+04	50	
					-4.3	848.8	527.0	1218.2	27802.0	4028.0	3.05E-08	4.38E-08	1.90E-08	2.11E+05	3.07E+05	1.41E+05	50	
					-4.5	3227.0	1470.6	2161.8	27802.0	4028.0	1.16E-07	7.78E-08	5.29E-08	8.01E+05	5.73E+05	4.16E+05	50	

					-4.7	7302.7	3091.4	3782.6	27802.0	4028.0	2.63E-07	1.36E-07	1.11E-07	1.81E+06	1.04E+06	8.91E+05	50	
					-5.0	12433.2	8297.7	22122.5	27802.0	4028.0	4.47E-07	7.96E-07	2.98E-07	3.09E+06	5.55E+06	2.20E+06	50	
					-5.3	50186.2	24058.9	37883.7	27802.0	4028.0	1.81E-06	1.36E-06	8.65E-07	1.25E+07	9.91E+06	6.74E+06	50	
					-5.6	64539.2	29411.1	43235.9	27802.0	4028.0	2.32E-06	1.56E-06	1.06E-06	1.60E+07	1.15E+07	8.33E+06	50	
					-6.0	72640.9	32423.6	46248.4	27802.0	4028.0	2.61E-06	1.66E-06	1.17E-06	1.80E+07	1.23E+07	9.23E+06	50	
					-6.5	146054.4	61827.9	75652.6	27802.0	4028.0	5.25E-06	2.72E-06	2.22E-06	3.63E+07	2.09E+07	1.78E+07	50	
					-6.8	231370.6	105402.5	119227.3	27802.0	4028.0	8.32E-06	4.29E-06	3.79E-06	5.74E+07	3.29E+07	2.98E+07	50	
					-6.8	435039.3	254399.2	530895.1	27802.0	4028.0	1.56E-05	1.91E-05	9.15E-06	1.08E+08	1.35E+08	6.87E+07	50	
					-7.0	642164.5	341393.6	617889.5	27802.0	4028.0	2.31E-05	2.22E-05	1.23E-05	1.59E+08	1.58E+08	9.37E+07	50	
					-7.5	1630304.3	714872.6	991368.4	27802.0	4028.0	5.86E-05	3.57E-05	2.57E-05	4.05E+08	2.66E+08	2.04E+08	50	
					-7.8	4627411.4	2108049.8	2384545.7	27802.0	4028.0	1.66E-04	8.58E-05	7.58E-05	1.15E+09	6.58E+08	5.97E+08	50	
					-7.8	3666316.6	2439587.6	6662080.5	27802.0	4028.0	1.32E-04	2.40E-04	8.77E-05	9.10E+08	1.67E+09	6.47E+08	50	
					-8.0	12299570.0	5998562.2	10221055.1	27802.0	4028.0	4.42E-04	3.68E-04	2.16E-04	3.05E+09	2.65E+09	1.67E+09	50	
					-8.5	30788938.4	12180145.7	16402638.5	27802.0	4028.0	1.11E-03	5.90E-04	4.38E-04	7.64E+09	4.50E+09	3.58E+09	50	
					-9.0	43320559.9	16421872.1	20644364.9	27802.0	4028.0	1.56E-03	7.43E-04	5.91E-04	1.08E+10	5.79E+09	4.88E+09	50	
					-9.5	56604614.0	21300817.3	25523310.1	27802.0	4028.0	2.04E-03	9.18E-04	7.66E-04	1.41E+10	7.25E+09	6.35E+09	50	
					-10.0	77447026.8	30127708.5	34350201.3	27802.0	4028.0	2.79E-03	1.24E-03	1.08E-03	1.92E+10	9.79E+09	8.89E+09	50	
					-10.5	77447026.8	30127708.5	34350201.3	27802.0	4028.0	2.79E-03	1.24E-03	1.08E-03	1.92E+10	9.79E+09	8.89E+09	50	
					-10.0	99465256.7	61492523.7	145942381.3	27802.0	4028.0	3.58E-03	5.25E-03	2.21E-03	2.47E+10	3.68E+10	1.65E+10	50	
					-10.5	126554894.6	73584166.6	158034024.3	27802.0	4028.0	4.55E-03	5.68E-03	2.65E-03	3.14E+10	4.00E+10	1.99E+10	50	
					-11.0	126554894.6	73584166.6	158034024.3	27802.0	4028.0	4.55E-03	5.68E-03	2.65E-03	3.14E+10	4.00E+10	1.99E+10	50	
					-11.5	154667021.1	85321178.5	169771036.1	27802.0	4028.0	5.56E-03	6.11E-03	3.07E-03	3.84E+10	4.32E+10	2.33E+10	50	
					-12.0	183881861.4	96879452.2	181329309.8	27802.0	4028.0	6.61E-03	6.52E-03	3.48E-03	4.57E+10	4.64E+10	2.66E+10	50	
					-13.0	183881861.4	96879452.2	181329309.8	27802.0	4028.0	6.61E-03	6.52E-03	3.48E-03	4.57E+10	4.64E+10	2.66E+10	50	
					-14.0	183881861.4	96879452.2	181329309.8	27802.0	4028.0	6.61E-03	6.52E-03	3.48E-03	4.57E+10	4.64E+10	2.66E+10	50	
					-15.0	183881861.4	96879452.2	181329309.8	27802.0	4028.0	6.61E-03	6.52E-03	3.48E-03	4.57E+10	4.64E+10	2.66E+10	50	
					-16.0	183881861.4	96879452.2	181329309.8	27802.0	4028.0	6.61E-03	6.52E-03	3.48E-03	4.57E+10	4.64E+10	2.66E+10	50	
					-17.0	183881861.4	96879452.2	181329309.8	27802.0	4028.0	6.61E-03	6.52E-03	3.48E-03	4.57E+10	4.64E+10	2.66E+10	50	
					-18.0	183881861.4	96879452.2	181329309.8	27802.0	4028.0	6.61E-03	6.52E-03	3.48E-03	4.57E+10	4.64E+10	2.66E+10	50	
					-19.0	183881861.4	96879452.2	181329309.8	27802.0	4028.0	6.61E-03	6.52E-03	3.48E-03	4.57E+10	4.64E+10	2.66E+10	50	
					-20.0	214289468.8	108392712.4	192842570.0	27802.0	4028.0	7.71E-03	6.94E-03	3.90E-03	5.32E+10	4.97E+10	3.00E+10	50	
					-21.0	245991399.7	119971244.2	204421101.8	27802.0	4028.0	8.85E-03	7.35E-03	4.32E-03	6.11E+10	5.30E+10	3.35E+10	50	
					-22.0	245991399.7	119971244.2	204421101.8	27802.0	4028.0	8.85E-03	7.35E-03	4.32E-03	6.11E+10	5.30E+10	3.35E+10	50	
					-23.0	245991399.7	119971244.2	204421101.8	27802.0	4028.0	8.85E-03	7.35E-03	4.32E-03	6.11E+10	5.30E+10	3.35E+10	50	
					-24.0	245991399.7	119971244.2	204421101.8	27802.0	4028.0	8.85E-03	7.35E-03	4.32E-03	6.11E+10	5.30E+10	3.35E+10	50	
					-25.0	255453695.6	124732417.0	211753270.4	27802.0	4028.0	9.19E-03	7.62E-03	4.49E-03	6.34E+10	5.49E+10	3.48E+10	50	
					-26.0	255453695.6	124732417.0	211753270.4	27802.0	4028.0	9.19E-03	7.62E-03	4.49E-03	6.34E+10	5.49E+10	3.48E+10	50	
					-27.0	302024043.1	154455824.1	265054162.5	27802.0	4028.0	1.09E-02	9.53E-03	5.56E-03	7.50E+10	6.84E+10	4.27E+10	50	
			KIT-CS	Shared impinger	-4.5	61593.2	0.0	0.0	27802.0	4028.0	2.22E-06	0.00E+00	0.00E+00	1.53E+07	3.82E+06	3.82E+06	5.00E-04	
					-6.0	152162.0	0.0	0.0	27802.0	4028.0	5.47E-06	0.00E+00	0.00E+00	3.78E+07	9.44E+06	9.44E+06	5.00E-04	
					-7.0	238969.7	100093.8	100093.8	27802.0	4028.0	8.60E-06	3.60E-06	3.60E-06	5.93E+07	2.89E+07	2.89E+07	5.00E-04	
					-8.0	1749105.9	897594.5	897594.5	27802.0	4028.0	6.29E-05	3.23E-05	3.23E-05	4.34E+08	2.48E+08	2.48E+08	5.00E-04	
					-8.7	18916879.2	2942698.3	2942698.3	27802.0	4028.0	6.80E-04	1.06E-04	1.06E-04	4.70E+09	1.38E+09	1.38E+09	5.00E-04	
					-9.6	67659429.6	4210943.9	4210943.9	27802.0	4028.0	2.43E-03	1.51E-04	1.51E-04	1.68E+10	4.33E+09	4.33E+09	5.00E-04	
					-10.5	125300935.4	10843885.1	10843885.1	27802.0	4028.0	4.51E-03	3.90E-04	3.90E-04	3.11E+10	8.23E+09	8.23E+09	5.00E-04	
			NCSU-CS	Shared impinger	-5.2	15611.4	14676.3	14676.3	27802.0	4028.0	5.62E-07	5.28E-07	5.28E-07	3.88E+06	3.77E+06	3.77E+06	1	binned
					-6.2	121527.3	102695.9	102695.9	27802.0	4028.0	4.37E-06	3.69E-06	3.69E-06	3.02E+07	2.66E+07	2.66E+07	1	binned
					-7.2	326734.6	258366.4	258366.4	27802.0	4028.0	1.18E-05	9.29E-06	9.29E-06	8.11E+07	6.73E+07	6.73E+07	1	binned
					-8.2	2843331.0	2843330.0	3240235.0	27802.0	4028.0	1.02E-04	1.17E-04	1.02E-04	7.06E+08	8.24E+08	7.28E+08	1	binned

					-9.2	64464901.3	19194131.3	19194131.3	27802.0	4028.0	2.32E-03	6.90E-04	6.90E-04	1.60E+10	6.22E+09	6.22E+09	1	binned
					-10.2	145302193.0	39137536.4	39137536.4	27802.0	4028.0	5.23E-03	1.41E-03	1.41E-03	3.61E+10	1.33E+10	1.33E+10	1	binned
					-11.2	178558020.6	18673608.4	18673608.4	27802.0	4028.0	6.42E-03	6.72E-04	6.72E-04	4.43E+10	1.20E+10	1.20E+10	1	binned
					-12.2	196487719.5	7985649.3	7985649.3	27802.0	4028.0	7.07E-03	2.87E-04	2.87E-04	4.88E+10	1.24E+10	1.24E+10	1	binned
					-13.2	217005649.5	5940382.1	5940382.1	27802.0	4028.0	7.81E-03	2.14E-04	2.14E-04	5.39E+10	1.35E+10	1.35E+10	1	binned
					-14.2	243388759.6	20119427.8	20119427.8	27802.0	4028.0	8.75E-03	7.24E-04	7.24E-04	6.04E+10	1.59E+10	1.59E+10	1	binned
					-15.2	263478270.2	36340286.2	36340286.2	27802.0	4028.0	9.48E-03	1.31E-03	1.31E-03	6.54E+10	1.87E+10	1.87E+10	1	binned
					-16.2	278572841.2	31995682.1	31995682.1	27802.0	4028.0	1.00E-02	1.15E-03	1.15E-03	6.92E+10	1.90E+10	1.90E+10	1	binned
					-17.2	285888521.3	39605092.2	39605092.2	27802.0	4028.0	1.03E-02	1.42E-03	1.42E-03	7.10E+10	2.03E+10	2.03E+10	1	binned
					-18.2	291147767.1	43183891.1	43183891.1	27802.0	4028.0	1.05E-02	1.55E-03	1.55E-03	7.23E+10	2.10E+10	2.10E+10	1	binned
					-19.2	296407012.9	46762689.9	46762689.9	27802.0	4028.0	1.07E-02	1.68E-03	1.68E-03	7.36E+10	2.18E+10	2.18E+10	1	binned
					-20.2	301666258.7	50341488.7	50341488.7	27802.0	4028.0	1.09E-02	1.81E-03	1.81E-03	7.49E+10	2.25E+10	2.25E+10	1	binned
					-21.2	306925504.5	53920287.6	53920287.6	27802.0	4028.0	1.10E-02	1.94E-03	1.94E-03	7.62E+10	2.33E+10	2.33E+10	1	binned
					-22.2	316369189.6	61887263.0	61887263.0	27802.0	4028.0	1.14E-02	2.23E-03	2.23E-03	7.85E+10	2.49E+10	2.49E+10	1	binned
					-23.2	333245685.2	64402593.1	64402593.1	27802.0	4028.0	1.20E-02	2.32E-03	2.32E-03	8.27E+10	2.61E+10	2.61E+10	1	binned
					-24.2	368610535.1	30680748.6	30680748.7	27802.0	4028.0	1.33E-02	1.10E-03	1.10E-03	9.15E+10	2.41E+10	2.41E+10	1	binned
			NIPI	Shared impinger	-3.0	2.6	10777.9	2104.5	27802.0	4028.0	9.41E-08	3.88E-07	7.57E-08	6.49E+05	5.47E+05	5.47E+05	1	binned
					-4.0	19.9	98536.9	16560.0	27802.0	4028.0	7.16E-07	3.54E-06	5.96E-07	4.94E+06	4.29E+06	4.29E+06	1	binned
					-5.0	3856.7	5094304.0	2194974.3	27802.0	4028.0	1.39E-04	1.83E-04	7.89E-05	9.57E+08	5.95E+08	5.95E+08	1	binned
					-6.0	3856.7	10442819.4	2816519.7	27802.0	4028.0	1.39E-04	3.76E-04	1.01E-04	9.57E+08	7.39E+08	7.39E+08	1	binned
					-7.0	5371.5	12079489.3	3718112.4	27802.0	4028.0	1.93E-04	4.34E-04	1.34E-04	1.33E+09	9.81E+08	9.81E+08	1	binned
					-8.0	28888.9	79343201.5	21177976.9	27802.0	4028.0	1.04E-03	2.85E-03	7.62E-04	7.17E+09	5.56E+09	5.56E+09	1	binned
					-9.0	100054.5	154602061.8	60743095.7	27802.0	4028.0	3.60E-03	5.56E-03	2.18E-03	2.48E+10	1.63E+10	1.63E+10	1	binned
					-10.0	161682.8	246889543.2	97700677.1	27802.0	4028.0	5.82E-03	8.88E-03	3.51E-03	4.01E+10	2.62E+10	2.62E+10	1	binned
					-11.0	161682.8	161682812.9	80841406.5	27802.0	4028.0	5.82E-03	5.82E-03	2.91E-03	4.01E+10	2.24E+10	2.24E+10	1	binned
					-12.0	183655.8	183655794.1	91827897.0	27802.0	4028.0	6.61E-03	6.61E-03	3.30E-03	4.56E+10	2.55E+10	2.55E+10	1	binned
					-13.0	202787.8	202787800.4	101393900.2	27802.0	4028.0	7.29E-03	7.29E-03	3.65E-03	5.03E+10	2.81E+10	2.81E+10	1	binned
					-14.0	223912.8	223912848.5	111956424.3	27802.0	4028.0	8.05E-03	8.05E-03	4.03E-03	5.56E+10	3.11E+10	3.11E+10	1	binned
			VODCA	Shared impinger	-10.2	76704112.5	7478069.5	7478069.5	27802.0	4028.0	2.76E-03	2.69E-04	2.69E-04	1.90E+10	5.11E+09	5.11E+09	0.000004 - 0.000036	selected points
					-11.2	84512762.3	15771703.5	15771703.5	27802.0	4028.0	3.04E-03	5.67E-04	5.67E-04	2.10E+10	6.55E+09	6.55E+09	0.000004 - 0.000036	selected points
					-12.2	95141425.5	15379330.1	15379330.1	27802.0	4028.0	3.42E-03	5.53E-04	5.53E-04	2.36E+10	7.03E+09	7.03E+09	0.000004 - 0.000036	selected points
					-13.2	131549740.0	2422324.1	2422324.1	27802.0	4028.0	4.73E-03	8.71E-05	8.71E-05	3.27E+10	8.19E+09	8.19E+09	0.000004 - 0.000036	selected points
					-14.2	160878067.6	7707190.2	7707190.2	27802.0	4028.0	5.79E-03	2.77E-04	2.77E-04	3.99E+10	1.02E+10	1.02E+10	0.000004 - 0.000036	selected points
					-15.2	205659593.9	19651144.4	19651144.4	27802.0	4028.0	7.40E-03	7.07E-04	7.07E-04	5.11E+10	1.37E+10	1.37E+10	0.000004 - 0.000036	selected points
					-16.2	215581389.0	28008951.3	28008951.3	27802.0	4028.0	7.75E-03	1.01E-03	1.01E-03	5.35E+10	1.51E+10	1.51E+10	0.000004 - 0.000036	selected points
					-17.2	233260669.0	42968859.6	42968859.6	27802.0	4028.0	8.39E-03	1.55E-03	1.55E-03	5.79E+10	1.80E+10	1.80E+10	0.000004 - 0.000036	selected points
					-18.2	248696385.5	56112968.0	56112968.0	27802.0	4028.0	8.95E-03	2.02E-03	2.02E-03	6.17E+10	2.08E+10	2.08E+10	0.000004 - 0.000036	selected points
					-19.2	275384883.8	79119616.9	79119616.9	27802.0	4028.0	9.91E-03	2.85E-03	2.85E-03	6.84E+10	2.60E+10	2.60E+10	0.000004 - 0.000036	selected points
					-20.2	295377656.5	96475374.6	96475374.6	27802.0	4028.0	1.06E-02	3.47E-03	3.47E-03	7.33E+10	3.02E+10	3.02E+10	0.000004 - 0.000036	selected points
					-21.2	314595379.9	113015724.0	113015724.0	27802.0	4028.0	1.13E-02	4.06E-03	4.06E-03	7.81E+10	3.42E+10	3.42E+10	0.000004 - 0.000036	selected points
					-22.2	306109465.4	104824512.7	104824512.7	27802.0	4028.0	1.10E-02	3.77E-03	3.77E-03	7.60E+10	3.22E+10	3.22E+10	0.000004 - 0.000036	selected points
					-23.2	295743619.5	93346341.9	93346341.9	27802.0	4028.0	1.06E-02	3.36E-03	3.36E-03	7.34E+10	2.96E+10	2.96E+10	0.000004 - 0.000036	selected points
					-24.2	290769318.9	82749566.4	82749566.4	27802.0	4028.0	1.05E-02	2.98E-03	2.98E-03	7.22E+10	2.73E+10	2.73E+10	0.000004 - 0.000036	selected points
					-25.2	282853327.8	69869168.6	69869168.6	27802.0	4028.0	1.02E-02	2.51E-03	2.51E-03	7.02E+10	2.47E+10	2.47E+10	0.000004 - 0.000036	selected points
					-26.2	273283509.9	63141047.8	63141047.8	27802.0	4028.0	9.83E-03	2.27E-03	2.27E-03	6.78E+10	2.31E+10	2.31E+10	0.000004 - 0.000036	selected points
					-27.2	263713692.0	56536059.0	56536059.0	27802.0	4028.0	9.49E-03	2.03E-03	2.03E-03	6.55E+10	2.16E+10	2.16E+10	0.000004 - 0.000036	selected points
					-28.2	250955100.3	47935618.1	47935618.1	27802.0	4028.0	9.03E-03	1.72E-03	1.72E-03	6.23E+10	1.96E+10	1.96E+10	0.000004 - 0.000036	selected points
					-29.2	241385282.4	41651089.0	41651089.0	27802.0	4028.0	8.68E-03	1.50E-03	1.50E-03	5.99E+10	1.82E+10	1.82E+10	0.000004 - 0.000036	selected points
					-30.2	247815276.9	48691126.5	48691126.5	27802.0	4028.0	8.91E-03	1.75E-03	1.75E-03	6.15E+10	1.96E+10	1.96E+10	0.000004 - 0.000036	selected points

					-31.2	250009889.9	50565122.2	50565122.2	27802.0	4028.0	8.99E-03	1.82E-03	1.82E-03	6.21E+10	2.00E+10	2.00E+10	0.000004 - 0.000036	selected points
					-32.2	264433963.2	44950395.9	44950395.9	27802.0	4028.0	9.51E-03	1.62E-03	1.62E-03	6.56E+10	1.98E+10	1.98E+10	0.000004 - 0.000036	selected points
					-33.2	275252018.3	40689482.0	40689482.0	27802.0	4028.0	9.90E-03	1.46E-03	1.46E-03	6.83E+10	1.98E+10	1.98E+10	0.000004 - 0.000036	selected points
					-34.2	262942139.2	32674451.3	32674451.3	27802.0	4028.0	9.46E-03	1.18E-03	1.18E-03	6.53E+10	1.82E+10	1.82E+10	0.000004 - 0.000036	selected points
			WISDOM	Shared impinger	-8.2	37870409.8	354694.0	86729.6	27802.0	4028.0	1.36E-03	1.28E-05	3.12E-06	9.40E+09	2.35E+09	2.35E+09	0.000014 - 0.000034	binned
					-9.2	109349118.6	23004923.3	24533815.0	27802.0	4028.0	3.93E-03	8.27E-04	8.82E-04	2.71E+10	8.87E+09	9.12E+09	0.000014 - 0.000034	binned
					-10.2	143767561.7	23555829.2	24807570.7	27802.0	4028.0	5.17E-03	8.47E-04	8.92E-04	3.57E+10	1.07E+10	1.08E+10	0.000014 - 0.000034	binned
					-11.2	180821284.2	30846117.9	31125827.6	27802.0	4028.0	6.50E-03	1.11E-03	1.12E-03	4.49E+10	1.36E+10	1.36E+10	0.000014 - 0.000034	binned
					-12.2	217327717.8	28167395.2	28202110.5	27802.0	4028.0	7.82E-03	1.01E-03	1.01E-03	5.40E+10	1.52E+10	1.52E+10	0.000014 - 0.000034	binned
					-13.2	256612873.3	15327839.3	16980741.1	27802.0	4028.0	9.23E-03	5.51E-04	6.11E-04	6.37E+10	1.64E+10	1.65E+10	0.000014 - 0.000034	binned
					-14.2	298180888.9	28421498.9	29738879.5	27802.0	4028.0	1.07E-02	1.02E-03	1.07E-03	7.40E+10	1.98E+10	1.99E+10	0.000014 - 0.000034	binned
					-15.2	315743875.0	61855536.7	55785715.6	27802.0	4028.0	1.14E-02	2.22E-03	2.01E-03	7.84E+10	2.49E+10	2.40E+10	0.000014 - 0.000034	binned
					-16.2	315743875.0	61855536.7	55785715.6	27802.0	4028.0	1.14E-02	2.22E-03	2.01E-03	7.84E+10	2.49E+10	2.40E+10	0.000014 - 0.000034	binned
					-17.2	321289842.4	50550458.8	46693172.2	27802.0	4028.0	1.16E-02	1.82E-03	1.68E-03	7.98E+10	2.36E+10	2.31E+10	0.000014 - 0.000034	binned
					-18.2	348078692.9	111585496.0	84792013.3	27802.0	4028.0	1.25E-02	4.01E-03	3.05E-03	8.64E+10	3.51E+10	3.02E+10	0.000014 - 0.000034	binned
					-19.2	363326211.9	116195545.9	88164997.0	27802.0	4028.0	1.31E-02	4.18E-03	3.17E-03	9.02E+10	3.66E+10	3.14E+10	0.000014 - 0.000034	binned
					-20.2	370188828.5	99778696.5	78250798.5	27802.0	4028.0	1.33E-02	3.59E-03	2.81E-03	9.19E+10	3.38E+10	3.01E+10	0.000014 - 0.000034	binned
					-21.2	387059852.7	103733430.2	81596947.2	27802.0	4028.0	1.39E-02	3.73E-03	2.93E-03	9.61E+10	3.52E+10	3.14E+10	0.000014 - 0.000034	binned
					-22.2	387059852.7	103733430.2	81596947.2	27802.0	4028.0	1.39E-02	3.73E-03	2.93E-03	9.61E+10	3.52E+10	3.14E+10	0.000014 - 0.000034	binned
					-23.2	395991394.2	84770704.3	71244549.6	27802.0	4028.0	1.42E-02	3.05E-03	2.56E-03	9.83E+10	3.24E+10	3.03E+10	0.000014 - 0.000034	binned
					-24.2	395991394.2	84770704.3	71244549.6	27802.0	4028.0	1.42E-02	3.05E-03	2.56E-03	9.83E+10	3.24E+10	3.03E+10	0.000014 - 0.000034	binned
					-25.2	395991394.2	84770704.3	71244549.6	27802.0	4028.0	1.42E-02	3.05E-03	2.56E-03	9.83E+10	3.24E+10	3.03E+10	0.000014 - 0.000034	binned
					-26.2	395991394.2	84770704.3	71244549.6	27802.0	4028.0	1.42E-02	3.05E-03	2.56E-03	9.83E+10	3.24E+10	3.03E+10	0.000014 - 0.000034	binned
					-27.2	395991394.2	84770704.3	71244549.6	27802.0	4028.0	1.42E-02	3.05E-03	2.56E-03	9.83E+10	3.24E+10	3.03E+10	0.000014 - 0.000034	binned
					-28.2	395991394.2	84770704.3	71244549.6	27802.0	4028.0	1.42E-02	3.05E-03	2.56E-03	9.83E+10	3.24E+10	3.03E+10	0.000014 - 0.000034	binned
					-29.2	403937789.2	109084045.3	82856140.1	27802.0	4028.0	1.45E-02	3.92E-03	2.98E-03	1.00E+11	3.69E+10	3.24E+10	0.000014 - 0.000034	binned
					-30.2	443612583.2	71560768.7	61752108.7	27802.0	4028.0	1.60E-02	2.57E-03	2.22E-03	1.10E+11	3.28E+10	3.15E+10	0.000014 - 0.000034	binned
					-31.2	443612583.2	71560768.7	61752108.7	27802.0	4028.0	1.60E-02	2.57E-03	2.22E-03	1.10E+11	3.28E+10	3.15E+10	0.000014 - 0.000034	binned
					-32.2	443612583.2	71560768.7	61752108.7	27802.0	4028.0	1.60E-02	2.57E-03	2.22E-03	1.10E+11	3.28E+10	3.15E+10	0.000014 - 0.000034	binned
					-33.2	443612583.2	71560768.7	61752108.7	27802.0	4028.0	1.60E-02	2.57E-03	2.22E-03	1.10E+11	3.28E+10	3.15E+10	0.000014 - 0.000034	binned
					-34.2	443612583.2	71560768.7	61752108.7	27802.0	4028.0	1.60E-02	2.57E-03	2.22E-03	1.10E+11	3.28E+10	3.15E+10	0.000014 - 0.000034	binned
					-35.2	443612583.2	71560768.7	61752108.7	27802.0	4028.0	1.60E-02	2.57E-03	2.22E-03	1.10E+11	3.28E+10	3.15E+10	0.000014 - 0.000034	binned
					-36.2	519164891.9	24140515.5	23840216.5	27802.0	4028.0	1.87E-02	8.68E-04	8.57E-04	1.29E+11	3.28E+10	3.28E+10	0.000014 - 0.000034	binned